



HAL
open science

Electrical properties of film-forming polymer/graphene nanocomposites : Elaboration through latex route and characterization

Amélie Noël

► **To cite this version:**

Amélie Noël. Electrical properties of film-forming polymer/graphene nanocomposites: Elaboration through latex route and characterization. Other. Ecole Nationale Supérieure des Mines de Saint-Etienne, 2014. English. NNT : 2014EMSE0767 . tel-01146803

HAL Id: tel-01146803

<https://theses.hal.science/tel-01146803>

Submitted on 29 Apr 2015

HAL is a multi-disciplinary open access archive for the deposit and dissemination of scientific research documents, whether they are published or not. The documents may come from teaching and research institutions in France or abroad, or from public or private research centers.

L'archive ouverte pluridisciplinaire **HAL**, est destinée au dépôt et à la diffusion de documents scientifiques de niveau recherche, publiés ou non, émanant des établissements d'enseignement et de recherche français ou étrangers, des laboratoires publics ou privés.



NNT : 2014 EMSE 0767

THÈSE

présentée par

Amélie NOËL

pour obtenir le grade de
Docteur de l'École Nationale Supérieure des Mines de Saint-Étienne

Spécialité : Science et Génie des Matériaux

Propriétés électriques de nanocomposites souples polymère/graphène :
Élaboration par voie latex et caractérisation

Electrical properties of film-forming polymer/graphene nanocomposites:
Elaboration through latex route and characterization

soutenue à Saint Etienne, le 27 Novembre 2014

Membres du jury

Président :	Didier CHAUSSY	Professeur, Laboratoire de Génie des procédés papetiers-UMR 5518, Grenoble
Rapporteurs :	Stefan BON Alain PENICAUD	Professeur, University of Warwick, Coventry Professeur, Centre de Recherche Paul Pascal, Pessac
Directeur de thèse :	Jean-Paul VIRICELLE	Professeur, ENSM-SE, Saint Etienne
Co-Directrice de thèse :	Elodie BOURGEAT-LAMI	Professeur, Laboratoire C2P2-CPE Lyon, Lyon
Co-Encadrante :	Jenny FAUCHEU	Enseignant-chercheur, ENSM-SE, Saint Etienne
Invité :	Philippe HAJJI	Docteur, Arkema, Pierre-bénite

Spécialités doctorales	Responsables :	Spécialités doctorales	Responsables
SCIENCES ET GENIE DES MATERIAUX MECANIQUE ET INGENIERIE GENIE DES PROCÉDES SCIENCES DE LA TERRE SCIENCES ET GENIE DE L'ENVIRONNEMENT	K. Wolski Directeur de recherche S. Drapier, professeur F. Gruy, Maître de recherche B. Guy, Directeur de recherche D. Grailot, Directeur de recherche	MATHEMATIQUES APPLIQUEES INFORMATIQUE IMAGE, VISION, SIGNAL GENIE INDUSTRIEL MICROELECTRONIQUE	O. Roustant, Maître-assistant O. Boissier, Professeur J.C. Pinoli, Professeur A. Dolgui, Professeur S. Dauzere Peres, Professeur

EMSE : Enseignants-chercheurs et chercheurs autorisés à diriger des thèses de doctorat (titulaires d'un doctorat d'État ou d'une HDR)

ABSI	Nabil	CR		CMP
AVRIL	Stéphane	PR2	Mécanique et ingénierie	CIS
BALBO	Flavien	PR2		FAYOL
BASSEREAU	Jean-François	PR		SMS
BATTON-HUBERT	Mireille	PR2	Sciences et génie de l'environnement	FAYOL
BERGER DOUCE	Sandrine	PR2		FAYOL
BERNACHE-ASSOLLANT	Didier	PR0	Génie des Procédés	CIS
BIGOT	Jean Pierre	MR,(DR2)	Génie des Procédés	SPIN
BILAL	Essaid	DR	Sciences de la Terre	SPIN
BOISSIER	Olivier	PR1	Informatique	FAYOL
BORBELY	Andras	MR,(DR2)	Sciences et génie des matériaux	SMS
BOUCHER	Xavier	PR2	Génie Industriel	FAYOL
BRODHAG	Christian	DR	Sciences et génie de l'environnement	FAYOL
BRUCHON	Julien	MA,(MDC)	Mécanique et ingénierie	SMS
BURLAT	Patrick	PR2	Génie Industriel	FAYOL
COURNIL	Michel	PR0	Génie des Procédés	DIR
DARRIEULAT	Michel	IGM	Sciences et génie des matériaux	SMS
DAUZERE-PERES	Stéphane	PR1	Génie Industriel	CMP
DEBAYLE	Johan	CR	Image Vision Signal	CIS
DELAFOSSÉ	David	PR1	Sciences et génie des matériaux	SMS
DESRAYAUD	Christophe	PR2	Mécanique et ingénierie	SMS
DOLGUI	Alexandre	PR0	Génie Industriel	FAYOL
DRAPIER	Sylvain	PR1	Mécanique et ingénierie	SMS
FEILLET	Dominique	PR2	Génie Industriel	CMP
FEVOTTE	Gilles	PR1	Génie des Procédés	SPIN
FRACZKIEWICZ	Anna	DR	Sciences et génie des matériaux	SMS
GARCIA	Daniel	MR,(DR2)	Génie des Procédés	SPIN
GERINGER	Jean	MA,(MDC)	Sciences et génie des matériaux	CIS
GOEURIOT	Dominique	DR	Sciences et génie des matériaux	SMS
GRAILLOT	Didier	DR	Sciences et génie de l'environnement	SPIN
GROSSEAU	Philippe	DR	Génie des Procédés	SPIN
GRUY	Frédéric	PR1	Génie des Procédés	SPIN
GUY	Bernard	DR	Sciences de la Terre	SPIN
HAN	Woo-Suck	CR	Mécanique et ingénierie	SMS
HERRI	Jean Michel	PR1	Génie des Procédés	SPIN
KERMOUCHE	Guillaume	PR2	Mécanique et Ingénierie	SMS
KLOCKER	Helmut	DR	Sciences et génie des matériaux	SMS
LAFOREST	Valérie	MR,(DR2)	Sciences et génie de l'environnement	FAYOL
LERICHE	Rodolphe	CR	Mécanique et ingénierie	FAYOL
LI	Jean-Michel		Microélectronique	CMP
MALLIARAS	Georges	PR1	Microélectronique	CMP
MOLIMARD	Jérôme	PR2	Mécanique et ingénierie	CIS
MONTHAILLET	Frank	DR	Sciences et génie des matériaux	SMS
MOUTTE	Jacques	CR	Génie des Procédés	SPIN
NEUBERT	Gilles			FAYOL
NIKOLOVSKI	Jean-Pierre			CMP
NORTIER	Patrice	PR1		SPIN
PIJOLAT	Christophe	PR0	Génie des Procédés	SPIN
PIJOLAT	Michèle	PR1	Génie des Procédés	SPIN
PINOLI	Jean Charles	PR0	Image Vision Signal	CIS
POURCHEZ	Jérémy	CR	Génie des Procédés	CIS
ROBISSON	Bruno			CMP
ROUSSY	Agnès	MA,(MDC)		CMP
ROUSTANT	Olivier	MA,(MDC)		FAYOL
ROUX	Christian	PR		CIS
STOLARZ	Jacques	CR	Sciences et génie des matériaux	SMS
TRIA	Assia	Ingénieur de recherche	Microélectronique	CMP
VALDIVIESO	François	MA,(MDC)	Sciences et génie des matériaux	SMS
VIRICELLE	Jean Paul	MR,(DR2)	Génie des Procédés	SPIN
WOLSKI	Krzysztof	DR	Sciences et génie des matériaux	SMS
XIE	Xiaolan	PR1	Génie industriel	CIS
YUGMA	Gallian	CR	Génie industriel	CMP

ENISE : Enseignants-chercheurs et chercheurs autorisés à diriger des thèses de doctorat (titulaires d'un doctorat d'État ou d'une HDR)

BERGHEAU	Jean-Michel	PU	Mécanique et Ingénierie	ENISE
BERTRAND	Philippe	MCF	Génie des procédés	ENISE
DUBUJET	Philippe	PU	Mécanique et Ingénierie	ENISE
FEULVARCH	Eric	MCF	Mécanique et Ingénierie	ENISE
FORTUNIER	Roland	PR	Sciences et Génie des matériaux	ENISE
GUSSAROV	Andrey	Enseignant contractuel	Génie des procédés	ENISE
HAMDI	Hédi	MCF	Mécanique et Ingénierie	ENISE
LYONNET	Patrick	PU	Mécanique et Ingénierie	ENISE
RECH	Joël	PU	Mécanique et Ingénierie	ENISE
SMUROV	Igor	PU	Mécanique et Ingénierie	ENISE
TOSCANO	Rosario	PU	Mécanique et Ingénierie	ENISE
ZAHOUANI	Hassan	PU	Mécanique et Ingénierie	ENISE

Aknowlegments

Cette thèse a été réalisée en co-tutelle entre plusieurs institutions, les départements SMS et SPIN à l'école des Mines de Saint Etienne et le laboratoire C2P2 à CPE Lyon. Ce projet de thèse a été élaboré par Jenny Faucheu, puis encadré par Elodie Bourgeat-Lami et Jean-Paul Viricelle. Je tiens à remercier particulièrement ces trois encadrants, sans qui cette thèse n'aurait pas pu avoir lieu. Jenny, merci tout d'abord d'avoir créé ce projet, de m'avoir choisie comme thésarde et de m'avoir fait confiance pendant ces trois années. Je tiens à te remercier tout particulièrement pour tes conseils, ton soutien, toutes nos discussions autour de cette thèse mais également pour tout le reste. Ton encadrement m'a beaucoup appris et m'a fait grandir durant ces trois années. Je tiens aussi à remercier Elodie, cette dernière année que j'ai passée au C2P2 a été très enrichissante pour moi. Je tiens également à te dire merci de m'avoir accordé du temps pour toutes les discussions que nous avons pu avoir. Merci pour tous ces échanges qui m'ont beaucoup appris. Enfin je tiens également à remercier Jean-Paul viricelle et Mathilde Rieu pour leur aide sur la partie mesures électriques et l'impression jet d'encre.

Merci à tous les techniciens et personnels techniques de l'école des Mines pour leur aide, Maryline et Sergio en Microscopie, Yoann et Vincent pour l'AFM (je sais bien que j'y ai passé beaucoup de temps et je vous remercie pour votre patience), Barroudi, Christophe et Dominique pour la partie attrition (je me suis tellement battue avec cette machine, j'espère qu'elle survivra à mon passage), Olivier breuil pour la partie informatique. Et bien sûr, Max Boudes, pour toute l'installation du labo, son aide au quotidien et surtout son soutien (^).

Merci également à Jean-Marc Chenal, sans qui aucune mesure mécanique n'aurait été possible. Merci pour ta patience et ton investissement, je sais que j'ai été envahissante pendant quelques mois. Un grand merci à Pierre-Yves Dugas, déjà pour la partie informatique, pour la mise en place des manips et ton aide pour les plans du mini-réacteur. Merci d'avoir réussi à me supporter dans ton bureau quelques temps et merci aussi pour la partie microscopie (ces longues heures en MEB, cryo-MEB, Cryo-TEM et HR-TEM n'ont pas toujours été faciles mais heureusement que ta bonne humeur était là).

J'en viens à toutes les personnes, thésards et post-doc, qui ont été à mes côtés durant cette thèse. Tout d'abord mes co-bureaux stéphanois : Loic et Aly, sans qui cette thèse n'aurait pas été pareille ^^merci beaucoup pour nos discussions et nos fous rires, c'était génial de pouvoir partager ce bureau avec vous. Je n'oublie pas non plus mes co-bureaux lyonnais : Emilie G. avec qui nous avons beaucoup échangé et Guilhem, merci beaucoup c'était vraiment super de finir ma thèse en ta compagnie et toujours en musique :)

Merci aussi à tout le K4 : Fred, Greg, Tanguy, Mélanie, Alix, Flavien, My-thu, Fiona, Amevi, Ameth, Vincent, Etienne, Lisa, Robin et les conjoints respectifs pour toutes les soirées, les

mariages, les weekends et toutes les sorties que je n'oublierai jamais, merci pour l'ambiance géniale que vous avez apporté à ce couloir.

Merci également aux lyonnais : Laura, Jennifer, Benoit (merci de m'avoir supporté dans ton bureau régulièrement, toujours pour me plaindre, pour les parties de Catane et toutes nos discussions), Seb, Vincent, Fabrice, Arthur (pour tes fentes et tes répliques exceptionnelles), Sandra, Emilie V., Ana et Nathalie (merci pour ta bonne humeur et nos discussions de « filles » dans ton bureau ^^). Merci pour les parties de cartes, les pauses café, les repas à la mezzanine mais aussi les bars et les soirées. Sans oublier le paintball, les sorties bowling et les restos. Céline et Leyla, je suis très heureuse d'avoir pu vous rencontrer, merci pour tout (les potins, les fous rires et les après-midi Calicéo).

Un peu mot à Claire à Jiminy qui ont été super pendant ces trois ans et que je remercie particulièrement pour leur amitié.

Arrive maintenant ma famille, tout d'abord mes parents qui m'ont toujours soutenue et aidée et sans qui je n'aurais pas pu arriver jusque là mais également mon frère Benjamin qui malgré nos différences a toujours été là, même si ce n'était pas toujours facile avec la distance. Merci pour votre amour et votre soutien quotidien.

Et enfin Pierre, je tiens à te remercier tout d'abord pour avoir réussi à me supporter, la rédaction n'a pas été un moment très facile et malgré mon caractère de cochon tu m'as toujours soutenue. Merci pour tout mais surtout merci d'être là tous les jours.

Table of contents

Abbreviations.....	VII
Resumé en français.....	IX
General Introduction.....	XXV

CHAPTER 1: State-of-the-art..... 1

Introduction	2
I. Context	2
1. Functional textiles	2
2. Conductive inks.....	4
II. Nanosize Multilayer Graphene (NMG).....	8
1. Description	8
2. Production of NMG.....	10
III. Latex routes to elaborate graphene/polymer Nanocomposites	17
1. Advantages of latex routes over other elaboration routes	17
2. Percolation description of latex-based composites	21
3. Synthesis of polymer latexes.....	23
4. Nanocomposites via latex blending.....	27
5. Nanocomposites via <i>in situ</i> latex synthesis in the presence of GO or rGO particles	32
Conclusions	40
References	41

CHAPTER 2: Nanosize Multilayered Graphene (NMG): preparation and characterization.....50

Introduction	50
I. Experimental procedures: wet-grinding of graphite suspensions.....	50
1. Description of the apparatus.....	51
2. Characterization of the graphite-NMG phase	53
3. Description of the surfactant phase	55
II. Influence of processing parameters.....	59
1. Influence of the size of the grinding beads	61
2. Surfactant: SDS vs. SDBS	64

3. Effect of delamination time	66
4. Effect of sonication and combination of sonication and wet grinding.....	67
5. Repeatability.....	69
6. Stability of the suspensions	70
III. Influence of the nature and concentration of stabilizer on NMG characteristics	71
1. Description of the experimental procedure	71
2. Effect of the type and concentration of stabilizers	72
Conclusions	85
References	86

CHAPTER 3: Film-forming conductive inks obtained by physical blending.....90

Introduction	90
I. State of the art on percolation theory	91
1. General considerations	91
2. Geometrical percolation	92
3. Percolation approach for electrical properties.....	93
4. Percolation approach for mechanical properties	94
II. Experimental part: physical blends preparation.....	95
1. NMG suspensions	95
2. Synthesis of surfactant-free latexes	96
3. Preparation of the physical blending.....	101
III. Morphological characterization of the NMG/latex nanocomposites	102
IV. Electrical conductivity of the nanocomposites	104
1. Effect of the NMG delamination process.....	104
2. Effect of the latex beads diameter	105
V. Thermo-mechanical properties of the nanocomposites	109
1. Comparison of T_{α} and T_g	110
2. Thermo-mechanical measurements	111
Conclusions	114
References	115

CHAPTER 4: *In situ* polymerization with Nanosize Multilayered Graphene (NMG)...117

Introduction	118
I. <i>In situ</i> polymerization in the presence of graphene	119

1.	<i>In situ</i> polymerization with graphene	119
2.	Reactivity of graphene platelets	119
3.	Characterization techniques	121
II.	Emulsion polymerization in the presence of NMG suspensions.....	126
1.	Emulsion polymerization mechanisms and impact of NMG	126
2.	Experimental procedure for <i>in situ</i> emulsion polymerization with NMG suspensions.....	128
3.	<i>In situ</i> emulsion polymerization with NMG/SDBS suspensions	131
4.	<i>In situ</i> emulsion polymerization with NMG/PSSNa suspensions	139
5.	<i>In situ</i> emulsion polymerization with NMG/PS <i>b</i> PEO 1030 suspensions	144
6.	Conclusions	149
III.	Miniemulsion polymerization in the presence of NMG.....	149
1.	Generalities on miniemulsion polymerization	149
2.	Experimental part	151
3.	<i>In situ</i> miniemulsion polymerization with NMG/SDBS suspensions.....	152
4.	<i>In situ</i> miniemulsion with NMG/PS <i>b</i> PEO 1030 suspensions	157
5.	Conclusions	161
IV.	Dispersion polymerization in the presence of NMG.....	162
1.	Generalities on dispersion polymerization	162
2.	Preliminary study	164
3.	NMG suspensions stabilized by PVPk30.....	168
4.	Conclusions	177
V.	Electrical properties of the nanocomposites synthesized by <i>in situ</i> polymerization ...	178
	Conclusions	181
	References	181
	General conclusion.....	186
	Appendix I.....	189
	Appendix II	197

Abbreviations

2D	Two-dimensional
3D	Three-dimensional
AFM	Atomic Force Microscopy
AIBN	2,2'-Azobisisobutyronitrile
BA	Butyl Acrylate
BET	Brunauer-Emmett-Teller
CB	Carbon Black
CMC	Critical Micelle Concentration
CNF	Carbon NanoFibers
CNT	Carbon Nanotubes
CVD	Chemical Vapor Deposition
D_h	Hydrodynamic average particle diameter
DLS	Dynamic Light Scattering
DMA	Dynamic Mechanical Analysis
DMF	Dimethylformamide
DSC	Differential Scanning Calorimetry
D_{TEM}	Number average particle diameter
DVB	Di-vinyl benzene
EA	Elemental Analysis
EDOT	3,4-Ethylenedioxythiophene
FCC	Face-Centered Cubic
FLG	Few Layer Graphene
FTIR	Fourier Transform InfraRed spectroscopy
GO	Graphene Oxide
H_2SO_4	Sulfuric acid
HI	Hydrogen Iodine
KC8	Potassium-intercalated graphite
$KMnO_4$	Potassium permanganate
KPS	Potassium persulfate
LBL	Layer-by-Layer
LED	Light Emitting Diode
MLS	Multiple Light Scattering
MMA	Methyl Methacrylate
MPS	γ -Methacryloxy-Propyl trimethoxy Silane
MWCNT	Multiwall Carbon Nanotubes
$NaNO_3$	Sodium nitrate
NMG	Nanosize Multilayered Graphene
NMP	N-MethylPyrrolidone
N_{NMG}	Number of NMG particles
N_p	Number of polymer particles
P(MMA-co-BA)	Poly(Methyl methacrylate-co-Butyl acrylate)
PDI	Polydispersity index
PEDOT-PSS	Poly(3,4-ethylenedioxythiophene)/Polystyrene sulfonate
PEI	Poly(ethylenimine)
PET	Poly(ethylene terephthalate)

PMMA	Poly(methyl methacrylate)
PP	Polypropylene
PS	Polystyrene
PS <i>b</i> PEO	Polystyrene- <i>block</i> -poly(ethylene oxide)
PSSNa	Sodium poly(styrene sulfonate)
PVP	Poly(N-vinyl pyrrolidone)
rGO	Reduced Graphene Oxide
SDBS	Sodium dodecyl benzene sulfonate
SDS	Sodium dodecyl sulfate
SEM	Scanning Electron Microscopy
T _α	Relaxation temperature
TEM	Transmission Electron Microscopy
T _g	Glass transition temperature
TGA	Thermogravimetric analysis
THF	Tetrahydrofuran
VDW	Van der Waals

Résumé

L'électronique flexible s'est fortement développée depuis une dizaine d'années, entraînant ainsi la création de nombreuses applications, tel que les écrans flexibles, les puces RFID pour la sécurité ou plus récemment les vêtements dits "intelligents". Ce nouveau concept permet de transformer un vêtement ou un appareil traditionnel en un dispositif léger, sans fil et intelligent [1]. Les premiers produits commerciaux ont récemment été développés et mis sur le marché dans les secteurs tel que la santé, l'automobile, la sécurité ou le génie civil (Figure 1).

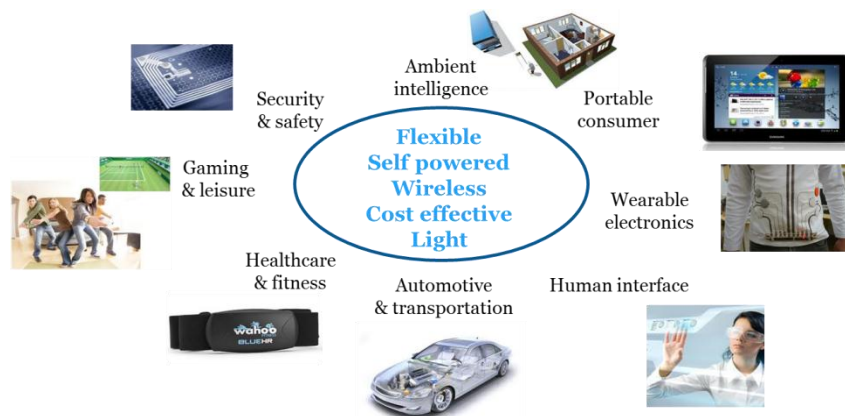


Figure 1. Secteurs et avantages de l'électronique flexible [2]

L'approche la plus simple pour le développement de ces nouveaux produits, composés d'électronique flexible, consisterait à imprimer les composants électroniques directement sur le substrat souple. Pour cela, des encres conductrices sont principalement utilisées. Actuellement, ces encres commerciales sont constituées de particules métalliques et contiennent entre 30 et 70 % massique de cette phase conductrice afin d'obtenir une conductivité électrique suffisante pour les applications visées [3][4]. La table 1 détaille les pourcentages massiques pour les principaux composants d'une encre conductrice commerciale avec des charges métalliques.

Table 1. Composants d'une encre conductrice [5]

Constituants	wt %
Phase conductrice	27-70
Matrice polymère	9-3
Solvants organiques	64-27

Cette thèse a pour objectif la production d'encres conductrices sans solvant et à bas coût (des charges conductrices peu chères et avec un taux réduit) pour une application textile. Ce projet consiste à présenter une procédure simple pour l'obtention d'encres conductrices qui devront être filmifiables à température ambiante et présenter une bonne déformabilité après séchage. Afin de satisfaire ces conditions, la stratégie est basée sur des nanocomposites architecturés

alliant les propriétés conductrices de charges carbonées (noir de carbone, nanotubes de carbone ou graphène) et la déformabilité d'une matrice polymère, un latex. Un latex est une suspension colloïdale de particules de polymères dans l'eau, avec un diamètre moyen compris entre 10 nm à 10 µm de diamètre [6]. Lors du dépôt d'un latex (filmifiable à température ambiante) sur substrat, les particules de polymère vont coalescer afin de former un film polymère continu après évaporation complète de l'eau.

Concernant les nanoparticules conductrices, et plus spécifiquement les nanotubes de carbone ou le graphène, leur intérêt scientifique s'est fortement accru depuis 10 ans. Ces charges conductrices présentent de nombreux avantages lorsqu'ils sont intégrés dans des nanocomposites à base de polymères pour des applications diverses, tel que l'électronique imprimée. Actuellement, les encres conductrices à base de particules métalliques contiennent au minimum 40% de charges. Afin de réduire le taux de charge, et par conséquent le coût global de l'encre, la voie latex sera favorisée pour formuler ces encres. Cette voie de synthèse est durable car le latex est constitué de nanosphères de polymères suspendues en phase aqueuse et ne nécessite pas l'usage de solvants organiques. De plus, la voie latex va favoriser la création d'une architecture ajustable constituée de charges conductrices. En effet, les charges conductrices seront piégées entre les nanosphères de polymères durant la filmification, favorisant ainsi la création d'un réseau percolant à bas taux de charges [7], comme indiqué sur la Figure 2.

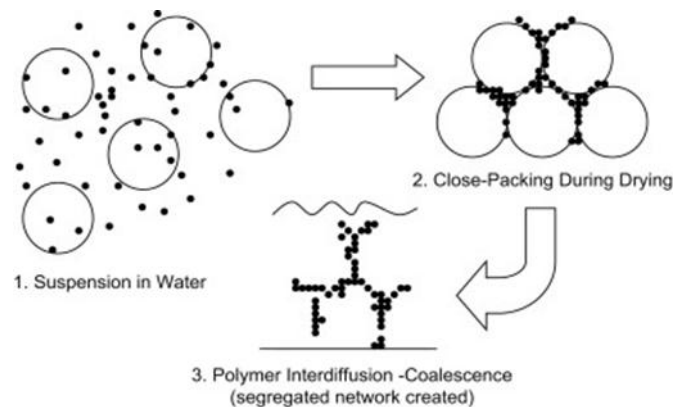


Figure 2. Orientation des charges conductrices dans un nanocomposite composé de latex.

La théorie de la percolation est utilisée pour décrire des phénomènes très différents de transition tels que la transition sol-gel ou la propagation d'un virus [8]. En science des matériaux, elle est souvent utilisée pour décrire le comportement de transition de propriétés électriques et mécaniques dans les matériaux composites [9]. La fraction volumique critique (notée seuil de percolation) correspond à la fraction de remplissage nécessaire pour obtenir la première voie de percolation dans la matrice de polymère. Dans une approche de percolation, les charges intégrées dans le composite sont décrites en utilisant deux types de groupes: les clusters finis et les clusters infinis ou percolation, comprenant un squelette et des liaisons pendantes (figure 3).

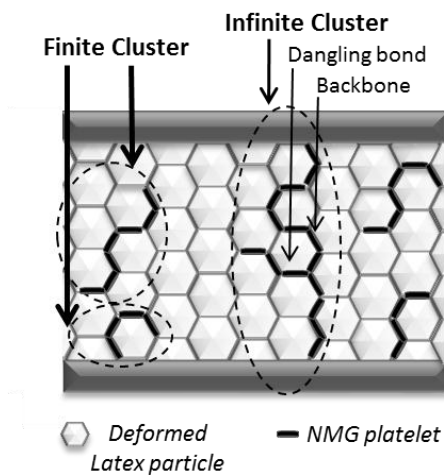


Figure 3. Phénomène de percolation dans un nanocomposite graphene/latex.

Parmi les charges carbonées, les charges en 2D (plaquettes) favoriseront les contacts entre charges en comparaison des charges 1D (nanotubes) et permettront un seuil de percolation plus bas en comparaison avec les charges en 3 dimensions (sphères). D'autre part, pour des considérations géométriques, les charges plaquettaires semblent être un choix adéquat pour la création d'un réseau percolant performant en présence de nanosphères de polymère.

Cette thèse est divisée en quatre chapitres (Figure 4), comprenant un état de l'art sur les nanocomposites graphène/polymère, suivi d'une étude sur la production de NMG et la synthèse des nanocomposites NMG/latex suivant deux voies : le mélange physique ou la polymérisation *in situ*.

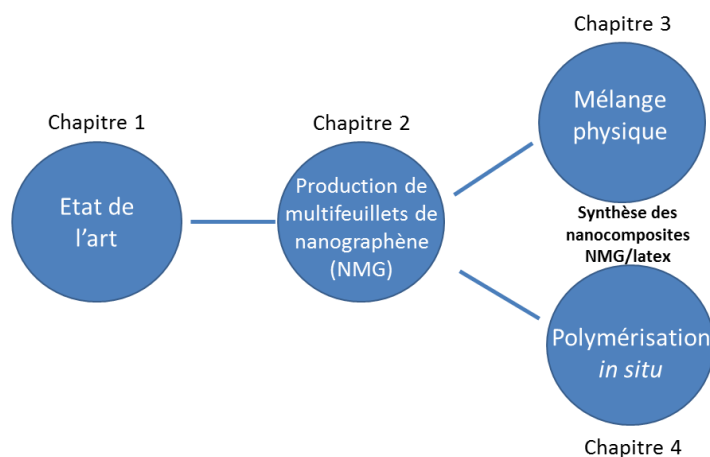


Figure 4. Schéma global décrivant l'organisation du manuscrit de thèse.

L'un des challenges consiste à produire les charges conductrices plaquettaires avec des dimensions spécifiques qui ne déstabiliseront pas le latex lors du mélange afin d'obtenir des encres conductrices. Ces encres nanocomposites seront réalisées en utilisant deux procédés distincts : le mélange physique de charges conductrices et de latex acryliques ou la polymérisation *in situ* en présence de charges conductrices, comme le montre la Figure 5.

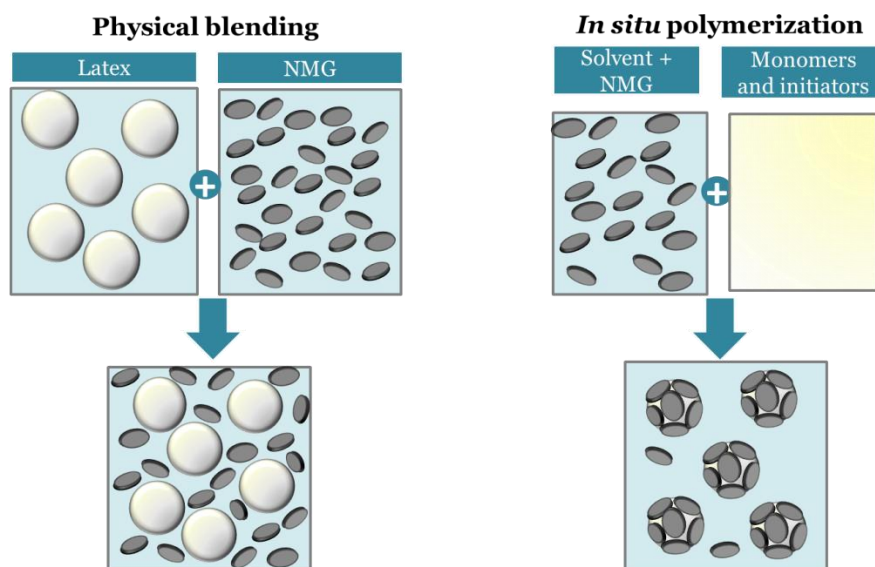


Figure 5. Deux voies utilisées pour l'obtention de nanocomposites graphene/latex.

Après une brève introduction, le Chapitre 1 propose un état de l'art basé sur une sélection d'articles de la littérature permettant un bref rappel concernant : la formulation d'encres conductrices, la synthèse des latex, la synthèse et les propriétés du graphène et enfin les nanocomposites graphène/latex. L'analyse de la littérature a permis de démontrer que des suspensions de charges carbonées étaient un choix adéquat en raison de leur faible coût. De plus, la forme et les dimensions des charges de graphène peuvent favoriser la formation d'une structure carapace autour des billes de latex pour former le nanocomposite. Cela permettra également d'obtenir d'excellentes propriétés électriques à bas taux de charge.

Dans la littérature, la méthode la plus connue pour synthétiser du graphène est basée sur une voie chimique, appelée voie Hummer [10]. Malgré sa popularité, cette méthode présente de nombreux inconvénients en raison de son procédé long et multi-étapes nécessitant l'utilisation de nombreux produits chimiques. Comme alternative à cette voie, Knieke et *al.* proposent la production de multi-feuillets de nano-graphène (noté NMG dans cette thèse) basée sur la délaminatation mécanique de graphite par broyage en voie aqueuse [11]. La Figure 6, qui compare ces deux voies de synthèse pour la production de 2g de multifeuillets de graphène, met en avant la voie mécanique en raison de son faible coût et de l'absence de solvants organiques.

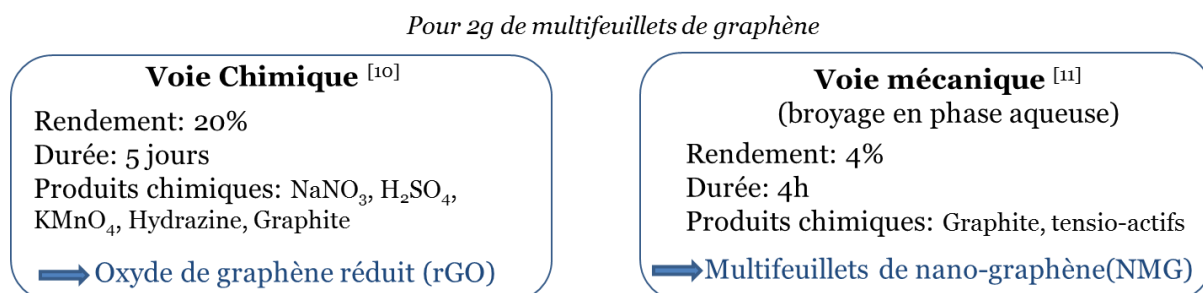


Figure 6. Deux voies de synthèses possibles pour produire 2g de multifeuillets de graphène.

Cette procédure a été préférée et les suspensions de NMG produites en phase aqueuse ont été communément utilisées dans les étapes suivantes du procédé pour la formation de matériaux nanocomposites. Le procédé de délamination nécessite l'usage d'une quantité importante de graphite. Cependant, ce matériau possède un faible coût et pourra être réutilisé pour les délaminations suivantes. La stabilité des suspensions est fournie par l'addition de molécules de tensio-actif ou de stabilisants polymériques qui possèdent une tête hydrophobe et un corps hydrophile. Ces molécules qui couvrent la surface du graphite (et du NMG) avec leurs têtes hydrophobes pointant dans l'eau favorisent les répulsions entre particules.

Le Chapitre 2 détaille la production de ces multifeuillets de nanographène (NMG), via la délamination mécanique de suspensions de graphite stabilisées par différents tensio-actifs ou stabilisants polymériques. Ce chapitre étudie l'impact de la nature du stabilisant et de sa concentration sur les dimensions finales des NMG (dimension latérale et épaisseur) mais également de leur concentration en phase aqueuse. L'objectif principal étant la production de plaquettes de graphène multicouches avec une faible dimension latérale (entre 50 à 300 nm) afin de favoriser la formation de nanocomposites latex / graphène avec une structure carapace.

La délamination mécanique de graphite dans l'eau en présence de stabilisant est combinée à l'utilisation d'ultrasons, via une sonde, afin d'optimiser les dimensions finales des NMG obtenus. Dans une étude préliminaire, la procédure expérimentale de ce broyage mécanique est décrite. Cette méthode, développée par Knieke et *al.* [11], permet d'étudier l'influence du diamètre des billes de broyage sur les dimensions finales des NMG. Des billes de broyage de 400 μm ont été préférées pour favoriser la formation de NMG de petit diamètre mais aussi de faible épaisseur, pour assurer des propriétés électriques acceptables. Par la suite, il a été démontré que quatre heures de délaminataion seront suffisantes pour obtenir des suspensions de NMG concentrées. Enfin, la combinaison de broyage et sonication induit une meilleure exfoliation des plaquettes de graphite et de faibles défauts dans la structure de carbone.

Ces paramètres ont été systématiquement utilisés dans les expériences suivantes, pour lesquelles l'influence du stabilisant sur les dimensions des NMG est étudiée. Pour cela, différents stabilisants et tensio-actifs pourront être utilisés. La figure 7 décrit la structure chimique des stabilisants étudiés dans ce chapitre. Pour augmenter la stabilité et la concentration de plaquettes NMG, le tensio-actif SDBS est utilisé à la place du SDS. Cet agent tensioactif possède un cycle aromatique, et peut ainsi créer des interactions π - π avec le graphène. Le remplacement de la SDS par SDBS induit une forte augmentation de la concentration NMG dans la suspension. La concentration des suspensions de NMG produites atteint 2 mg ml^{-1} , ce qui est deux fois plus élevé que les concentrations communes de suspensions d'oxyde de graphène obtenues par la méthode de Hummer. Ce changement de tensio-actif permet également d'obtenir des plaquettes de NMG avec une dimension latérale de 50 à 300 nm pour une épaisseur de 5 à 10 feuillets de graphène.

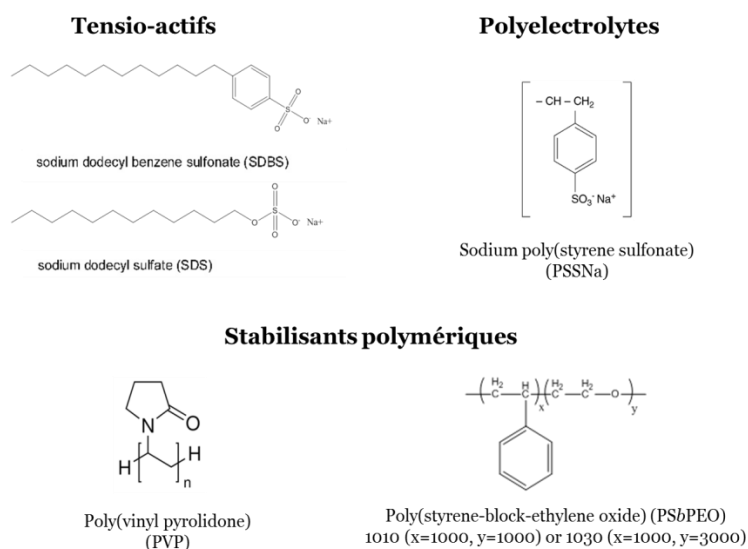


Figure 7. Structure chimique des tensio-actifs et stabilisants polymériques étudiés.

Des stabilisants polymériques, PVPk30 et PSbPEO, ou des polyélectrolytes, PSSNa, sont ensuite étudiés afin d'observer leur influence sur les dimensions et la concentration finales de NMG. Afin d'augmenter la concentration et la stabilité des plaquettes de NMG en phase aqueuse, il sera préférable d'utiliser un stabilisant pouvant créer des interactions π - π avec les plaquettes NMG. Il est démontré que les stabilisants polymériques, tel que PSbPEO ou PVPk30, sont adaptés pour la stabilisation des plaquettes NMG. Ces stabilisants permettent la production de suspensions NMG avec un rendement identique ou supérieur à celui obtenu en utilisant du SDBS ou SDS comme tensio-actif. Enfin, les plaquettes NMG obtenus posséderont des dimensions latérales et des épaisseurs inférieures.

Les suspensions de NMG obtenues en présence de différents stabilisants ont été élaborées par un procédé sans solvant, respectueux de l'environnement et à faible coût. Ces suspensions de NMG peuvent maintenant être utilisées pour synthétiser des nanocomposites conducteurs suivant deux processus: via un mélange physique de suspensions de NMG et des particules de latex (Chapitre 3) ou par polymérisation *in situ* en présence de différentes suspensions de NMG (Chapitre 4).

L'objectif est de réaliser des nanocomposites possédant une structure carapace, soit la surface de la bille de polymère sera couverte de plaquettes de graphène. Dans cet intérêt, les billes de polymère devront avoir un diamètre supérieur aux dimensions latérales des plaquettes de NMG. Pour des NMG ayant une dimension latérale d'environ 50 nm, les billes devraient avoir un diamètre entre 0.3-1 μ m. Pour produire ces latex, la polymérisation en milieu dispersé a été choisie et plus particulièrement via les procédés de polymérisation en émulsion, miniémulsion et dispersion. Les diamètres finaux de billes de latex dépendront du procédé de polymérisation mais également des conditions expérimentales.

Le chapitre 3 se focalise sur les mélanges physiques entre les suspensions de NMG et les billes de latex de deux diamètres distincts, 300 et 650 nm. Ces latex sont des copolymères poly (méthylméthacrylate-co butyl acrylate) (PMMA-co-BA) synthétisés par polymérisation en

émulsion sans tensio-actif par un procédé de batch ou semi-batch pour obtenir des diamètres de billes ayant respectivement 300 nm et 650 nm (respectivement noté D300 et D650). Ce copolymère composé de deux monomères acryliques (BA et MMA) dans les mêmes proportions 50/50 permet d'obtenir une température de transition vitreuse autour de la température ambiante. La morphologie, les propriétés thermomécaniques et électriques des deux séries de films nanocomposites, obtenus suite au mélange physique des latex acrylique (300 et 650 nm) et des suspensions de NMG/SDBS, sont successivement étudiées (Figure 8).

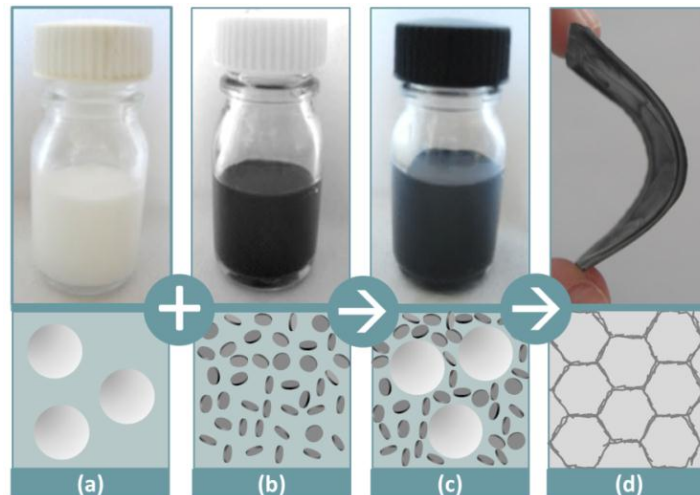


Figure 8. Les étapes de formation des matériaux nanocomposites, (a) de latex à blanc, (b) suspension de NMG, (c) mélange NMG/latex, (d) matériau souple et conducteur obtenu après évaporation de l'eau et la formation du film.

Les nanocomposites obtenus présentent une bonne stabilité en suspension et permettent la formation d'un film à température ambiante. L'influence du rapport de taille entre la charge conductrice et de la nanosphère latex est le paramètre qui conduit l'étude. Les deux séries de matériaux composites présentent des domaines cellulaires de charges conductrices (Figure 9) ainsi que de nombreux chemins percolants parcourant l'ensemble du film nanocomposites.

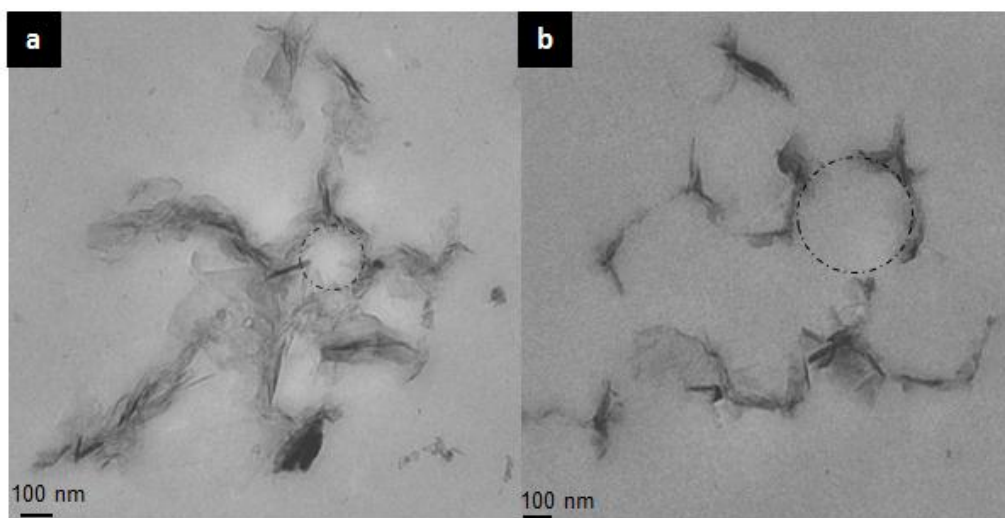


Figure 9. Images MET représentant des coupes par cryomicrotomie des films nanocomposites avec des billes de polymères de a- 650 nm et b- 300 nm pour 10%vol de NMG.

Les propriétés électriques de ces deux séries de films sont ensuite mesurées à l'aide d'un galvanomètre 4-pointes. Ces mesures expérimentales sont comparées à un modèle de percolation électrique, décrit par Stauffer [12], permettant ainsi de remonter au seuil de percolation théorique, noté ϕ_c , et à la conductivité électrique théorique intrinsèque du NMG.

La figure 10 représente les conductivités électriques théoriques (modèle) et expérimentales pour les deux séries de films en fonction du pourcentage volumique de NMG contenu dans le film nanocomposite.

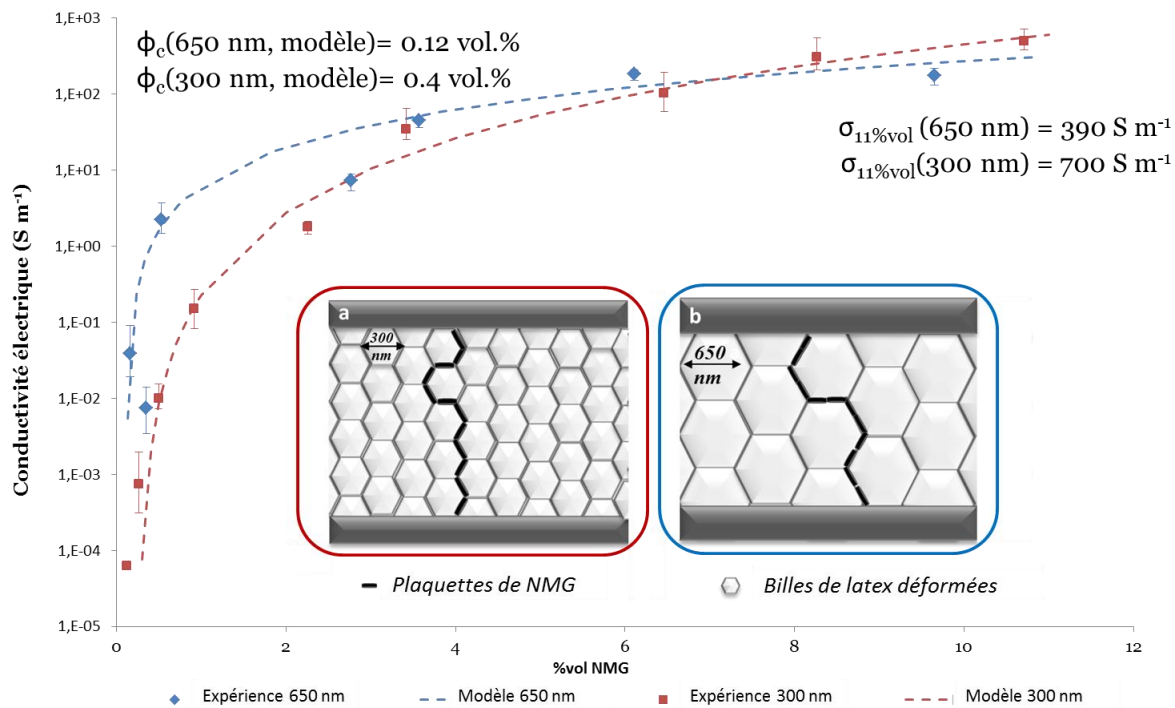


Figure 10. Comparaison des conductivités électriques en fonction du %volumique de NMG pour les deux séries de films (résultats expérimentaux et modèle)

Les seuils de percolation (ϕ_c) extraits des régressions linéaires du modèle sont 0,4 vol. % pour les échantillons de D300 et 0,12 % vol. pour les échantillons de D650. Il existe une bonne corrélation entre les courbes du modèle et les points expérimentaux. De plus, un seuil de percolation supérieur et un maximum de conductivité électrique plus élevé sont obtenus pour la série D300. Ces tendances peuvent être expliquées par les schémas de la Figure 10. Sur ces schémas, un chemin de percolation est illustré par une simple description tridimensionnelle prenant en considération le rapport de taille entre les billes de latex et les plaquettes de NMG. Pour un nombre donné de plaquettes de NMG, le nombre de chemins de percolation possibles sera plus élevé, entraînant ainsi un seuil de percolation plus élevé pour D300. Par ailleurs, le nombre total de chemins de percolation sera plus élevé pour D300 conduisant à une conductivité électrique maximale plus élevée.

Le comportement conducteur observé pour ces matériaux nanocomposites à base de graphène est compatible avec un comportement de percolation tridimensionnelle. De plus, le diamètre moyen des billes de latex a une influence significative sur le seuil de percolation et le maximum de la conductivité électrique après filmification des nanocomposites.

Afin de démontrer l'application potentielle de nos films conducteurs, un dispositif électronique constitué d'une diode électroluminescente (DEL) et d'une pile a été réalisé (Figure 11).

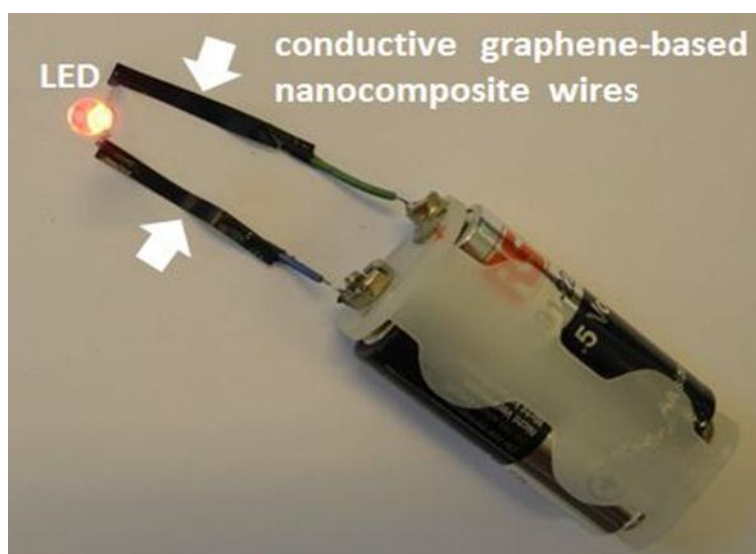


Figure 11. Dispositif comprenant une DEL reliée à une pile par des bandes de films nanocomposites en remplacement des fils de cuivre.

Dans cette configuration, les petites bandes (2 mm de large, 20 mm de longueur et de 200 μm d'épaisseur) ont été découpées dans le film nanocomposite contenant les billes de latex de 650 nm et 5,7% vol. de NMG. Ces bandes ont été utilisées pour remplacer une partie des fils de cuivre qui lient la DEL à la pile. L'efficacité de ces films pour une application électronique est ainsi démontrée.

Les deux séries de matériaux nanocomposites étudiées présentent de bonnes propriétés électriques (10^2 S m^{-1} ce qui est comparable à des encres conductrices commerciales à base de carbone) à faible teneur en charge: moins de 10 % en poids par rapport à 20 à 40 % en poids dans des encres conductrices existantes. Cette voie d'élaboration sans solvant, consistant en un simple mélange physique de plaquettes de NMG et de billes de polymères acryliques, semble être prometteuse pour la production d'encres conductrices pour l'électronique imprimée et les matériaux conducteurs fonctionnels. D'autre part, les mélanges composite à base de copolymères acryliques sont déjà couramment utilisés dans l'industrie des encres et des peintures, car ils permettent la formation de films continus et déformables, sans nécessité de chauffage ni pressage à chaud, ce qui convient pour des applications sur substrats flexibles et textiles.

Les propriétés thermo-mécaniques de ces films nanocomposites sont également étudiées, par analyse mécanique dynamique. Ces analyses démontrent que l'addition de plaquettes NMG dans la matrice de polymère peut induire une augmentation du module de nanocomposite, également appelé renforcement. D'un point de vue général, le module augmente avec la teneur en charge mais dépend également de la dispersion de charge et des interactions charge-matrice. La réponse mécanique thermique des différents échantillons a été évaluée et les modules de stockage, G' , ont été tracés en fonction de la température.

Pour les deux séries de films, une température de transition, T_{α} , est mesurée entre 0 et 30°C. Ceci est cohérent avec le fait que le processus de filmification se produit à température ambiante.

Le facteur de renforcement est défini comme le rapport entre le module du composite et le module du polymère vierge et sera mesuré au-delà de la température de transition dans le domaine caoutchoutique. La figure 12 représente les facteurs de renfort obtenus en fonction du taux de NMG à 80°C. Les résultats expérimentaux sont comparés à un modèle de percolation mécanique [13][14].

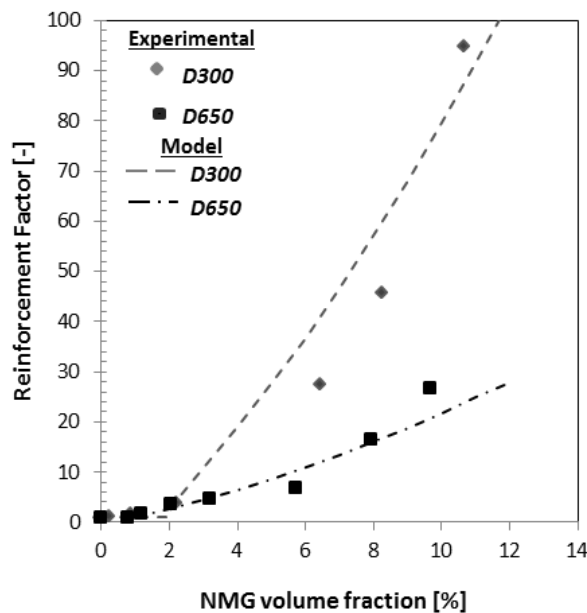


Figure 12. Facteurs de renforts expérimentaux et théoriques en fonction de la fraction volumique de NMG pour la série (◆) D300 et (■) D650.

Cette figure montre qu'un facteur de renfort supérieur est obtenu pour les films nanocomposites de la série D300. Ce comportement, comme pour le modèle électrique, peut être illustré par les schémas de la figure 10. En effet, le nombre total de chemins percolants sera plus élevé pour les échantillons D300. Ces données expérimentales sont relativement comparables aux données calculées à partir du modèle de percolation mécanique. Cependant, la sensibilité du modèle ne permet pas une détermination précise d'un seuil de percolation. Le seuil de percolation (ϕ_c) a été estimé à environ de 0,5 à 0,8% en vol. pour D300 et à 0,2 à 0,4% en vol. pour D650.

Le phénomène de percolation pour des nanocomposites conducteurs latex/NMG a été étudié d'un point de vue électrique et mécanique. L'influence du rapport de taille entre la charge conductrice et de la nanosphère de polymère a conduit l'étude. Les résultats de conductivité électrique ont pu être décrits en utilisant une approche de percolation et le renforcement mécanique obtenu avec une teneur croissante NMG était également compatible avec un comportement de percolation. Enfin, les seuils de percolation mécaniques et électriques

obtenus semblent compatibles avec le seuil de percolation géométrique pour les deux séries d'échantillons.

Suite à cette étude, afin de renforcer les interactions entre les plaquettes de NMG et les billes de polymère, le dernier chapitre détaille la synthèse de nanocomposites graphène/latex par polymérisation *in situ* en présence de suspensions de NMG. Ce travail est motivé par une simplification du processus en utilisant directement des NMG dans la polymérisation *in situ* au lieu du GO et ainsi éviter une étape de réduction (de GO en rGO) post-polymérisation. En effet, GO a été rapporté comme étant un matériau amphiphile dû à la combinaison de groupes hydrophiles tels que des acides carboxyliques en périphérie, et les régions hydrophobes graphitiques dans le plan de base. Par conséquent, GO a été démontré comme pouvant stabiliser efficacement de émulsions huile-dans-eau (H / E), noté émulsions Pickering [15]. Cependant, comme NMG n'est pas aussi stable que GO dans l'eau, l'utilisation de tensio-actif ou agent stabilisant est nécessaire. Le but est de produire des latex avec une structure carapace, ce qui signifie que la surface des particules de polymère sera recouverte par des plaquettes NMG. Géométriquement, les diamètres de latex doivent donc être supérieurs aux dimensions latérales NMG. Si les plaquettes NMG présentent une dimension latérale d'environ 50 nm, les diamètres de latex devront être autour de 0.3-1µm. Pour produire des latex, la polymérisation en milieu dispersé et en particulier les procédés de polymérisation en émulsion, miniémulsion et la dispersion sont choisis (Figure 13). En fonction des conditions expérimentales, ces procédés permettent la synthèse de particules de latex dans un large éventail de tailles. En règle générale, les polymérisations en émulsion et en miniémulsion produisent des particules polymères ayant un diamètre compris entre 50 et 500 nm, tandis que la polymérisation en dispersion permet la formation de particules ayant un diamètre compris entre 0,5 et 20 µm.

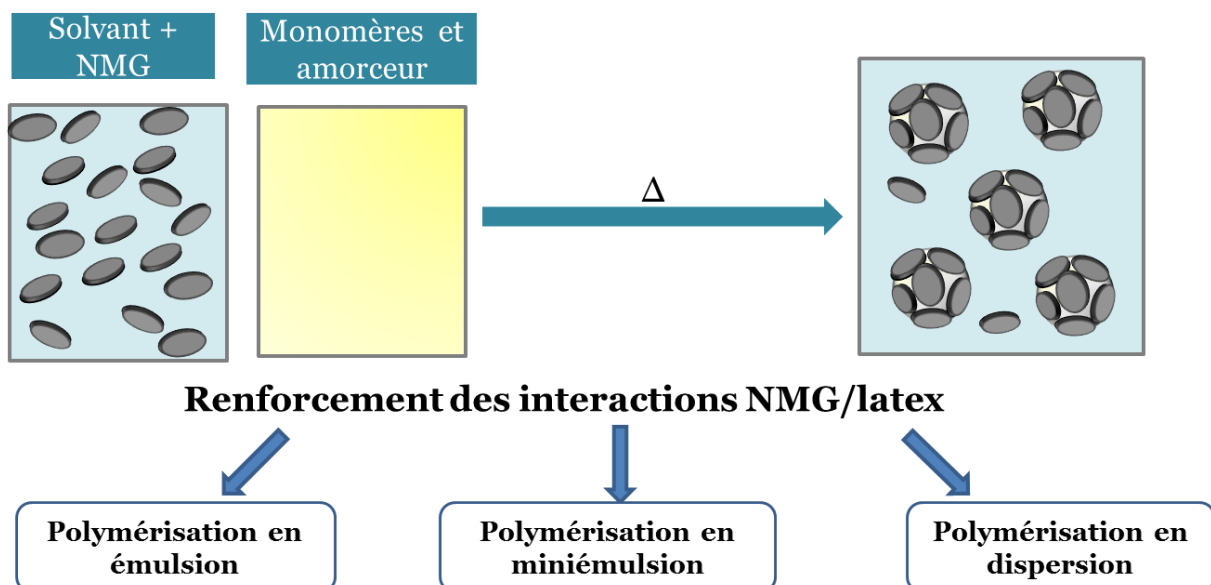


Figure 13. Schéma représentant les voies possibles de polymérisation pour l'obtention de nanocomposites par polymérisation in situ.

Un état de l'art concernant les défauts présents à la surface des feuillets de graphène mais également au sein de sa structure est d'abord présenté (Figure 14). La présence de ces défauts dépendra de la voie de synthèse utilisée pour la production de graphène et agiront comme des pièges à radicaux libres, pouvant ainsi interagir avec les amorceurs et les chaînes de polymères en croissance durant la polymérisation [16].

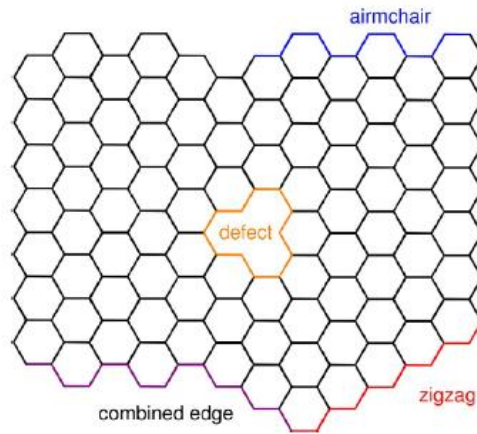


Figure 14. Schema représentant les sites réactifs sur des feuillets de graphène. [17]

Les nanocomposites sont ensuite synthétisés par polymérisation *in situ* en présence de suspensions de NMG contenant des tensio-actifs (SDBS) ou des stabilisants polymériques (PSSNa, PSbPEO ou PVP). Le choix de ces stabilisants dépend de leur efficacité pour l'obtention de concentrations en NMG élevées après délamination mécanique mais également de leur mobilité en phase aqueuse, qui sera un paramètre critique au cours de la polymérisation. Pour chaque polymérisation (émulsion, miniémulsion et dispersion) le mécanisme de polymérisation en présence de NMG est d'abord présenté. Le protocole expérimental et les résultats sont ensuite détaillés. Chaque latex nanocomposite formé est analysé afin de déterminer le diamètre des billes des polymères obtenus, le pourcentage volumique de NMG dans le nanocomposite, le taux de couverture théorique, le rendement et la cinétique de polymérisation ainsi que la stabilité des suspensions. En fonction de ces résultats, l'influence de la nature et de la concentration en stabilisant est étudiée. Les propriétés électriques de ces films nanocomposites obtenus par polymérisation *in situ* sont ensuite mesurées et comparées à celles des mélanges physiques rapportés dans le chapitre 3.

La polymérisation en émulsion en présence de suspensions de NMG stabilisées par du SDBS, du PSSNa ou du PSbPEO est d'abord réalisée. Lors de ces synthèses, le SDBS démontre une forte mobilité en phase aqueuse et induit une déstabilisation d'une partie des plaquettes de NMG durant la polymérisation. Cependant, une diminution de la concentration en SDBS, juste en dessous du CMC_{app} , permet d'obtenir une conversion quasi-totale (90%) et des particules de latex composites d'un diamètre moyen de 228 nm pour un taux de couverture théorique de 19.3%. Malheureusement les latex NMG/SDBS présentent une faible stabilité et une sédimentation est observée après 5 jours. Deux stabilisants polymériques sont ensuite étudiés : le PSSNa et le PSbPEO1030. L'augmentation de la masse molaire de l'agent stabilisant permet de réduire sa mobilité moléculaire, et augmente ainsi la stabilité de NMG pendant la polymérisation. La polymérisation *in situ* en présence de suspensions de

NMG/PSSNa conduit à la formation de latex nanocomposites stables et aucune sédimentation n'est visible après 5 jours de stabilité. Cependant, la concentration de NMG dans ces nanocomposites est faible et ne permet pas d'obtenir des films conducteurs. Un autre stabilisant polymère, le PSbPEO 1030, a donc été utilisé et les latex nanocomposites obtenus présentent une teneur élevée en NMG et aucune destabilisation n'est observée (durant la polymérisation et après 5 jours de stabilité). Les particules de polymère possèdent un diamètre moyen de 200 nm et le seul inconvénient est la conversion limitée, qui ne dépasse pas 50% malgré une augmentation de la concentration en amorceur. Il a donc été déterminé que la mobilité de stabilisant et la réactivité de l'initiateur étaient des paramètres clés pour conduire efficacement le processus de polymérisation *in situ* en émulsion.

Afin de réduire la mobilité du stabilisant en phase aqueuse et la destabilisation des plaquettes NMG pendant la polymérisation, la polymérisation en miniémulsion peut être utilisée. Des polymérisations en miniémulsion en présence de suspensions de NMG/SDBS et NMG/PSbPEO1030 sont réalisées. Les latex nanocomposites obtenus présentent respectivement un diamètre moyen de 127 nm et 250 nm (NMG/SDBS et NMG/PSbPEO1030), pour de faibles teneurs en NMG et possèdent une bonne stabilité après 5 jours. Une conversion totale n'est pas atteinte, comme pour la polymérisation en émulsion, et cela peut être dû au piégeage d'une partie des radicaux libres par les groupements oxygènes présents en surface des plaquettes de graphène [16].

Une alternative à ces deux procédés de polymérisations est la polymérisation en dispersion. Ce procédé de polymérisation en présence de PVPk30 comme stabilisant permettra de diminuer le nombre de particules de latex et par conséquent d'augmenter le diamètre des billes de polymères ainsi que le taux de couverture théorique. Après polymérisation *in situ* en dispersion en présence des suspensions de NMG/PVPk30, les latex nanocomposites obtenus présentent des diamètres beaucoup plus larges que précédemment, entre 1 et 25 μm , et par conséquent des taux de couverture théoriques supérieurs à 100%. Une forte augmentation de la taille et de la distribution de taille des billes de polymère est observable entre les polymérisations à blanc et en présence de NMG. Cela semble démontrer que la nucléation est fortement perturbée en présence de NMG. En raison de leurs larges diamètres, les latex nanocomposites obtenus sédimentent naturellement après 5 jours de stabilité.

Les propriétés électriques de ces nanocomposites synthétisés par différents procédés sont mesurées. Chaque nanocomposite est filmifié dans un moule en silicone à 40 ° C pendant une nuit. Les films sont ensuite lavés dans un bain d'eau pendant 24 h afin d'éliminer l'agent tensioactif ou stabilisant présent à la surface du film. Les mesures électriques ont été effectuées sur les deux côtés de chacun des films et la conductivité électrique σ , en S/m^{-1} , a été calculée en utilisant les équations 5 et 6 de l'annexe I. Les conductivités obtenues sont résumées dans la figure 15. Concernant les nanocomposites synthétisés par polymérisation en émulsion et en minémulsion, seuls les films contenant SDBS comme tensio-actif sont conducteurs. En effet, aucune conductivité n'est mesurable pour les nanocomposites contenant PSbPEO1030 comme stabilisant, malgré leurs taux de couverture théorique élevés. Ce stabilisant polymérique isolant peut inhiber la conductivité électrique de ces films.

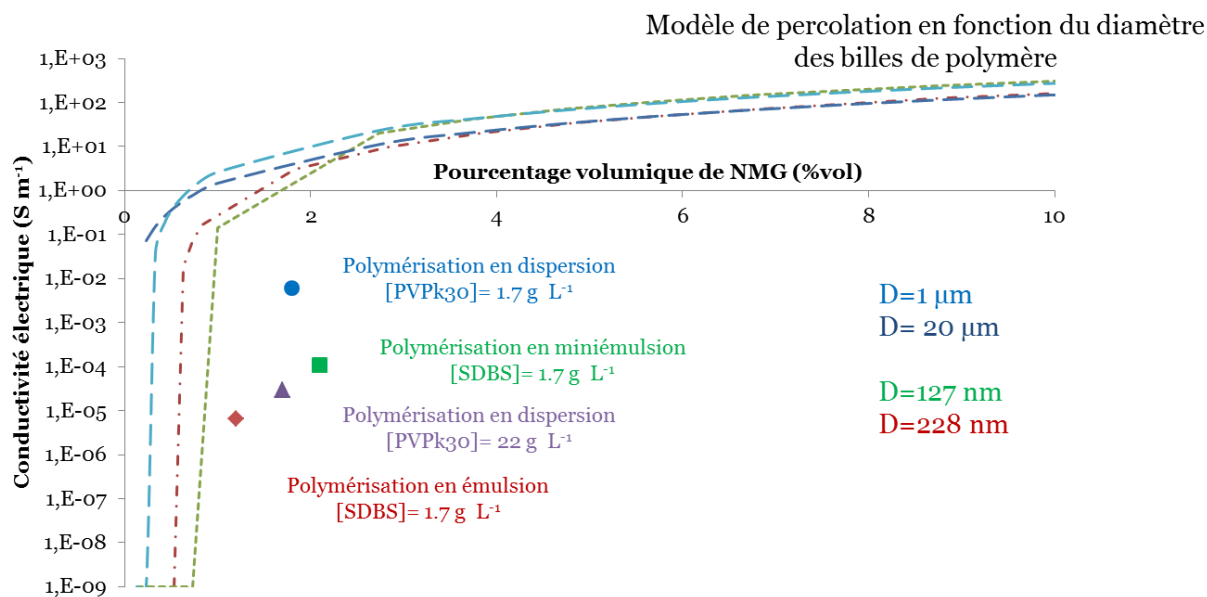


Figure 15. Conductivité électrique en fonction du pourcentage volumique de NMG pour les films nanocomposites synthétisés par polymérisation *in situ* par polymérisation en émulsion, miniémulsion ou dispersion.

Tous les nanocomposites réalisés par polymérisation en dispersion présentent une conductivité mesurable et les meilleures propriétés électriques sont obtenues pour le nanocomposite contenant les plus petites billes de polymère (D- NMG/PVPk30-9-50/50) et une teneur élevée de NMG. Enfin, ces conductivités peuvent être comparées aux conductivités issues du modèle de percolation électrique. Les résultats expérimentaux démontrent une faible corrélation avec le modèle. Cela peut être dû à des mesures qui restent proches du seuil de percolation, et d'autre part, pour ces nanocomposites l'hypothèse de monodispersité n'est pas toujours respectée.

Afin de comparer les films de nanocomposites, préparés par mélange physique ou par polymérisation *in situ* en présence de NMG, un test de solubilité dans tétrahydrofurane (THF) est réalisé (Figure 16). Après une journée, les films issus du mélange physique sont totalement dissous alors que des amas de particules sont visibles pour les films synthétisés par polymérisation *in situ*. Cela suggère l'existence d'interactions fortes entre les plaquettes de NMG et les particules de polymère.

Dans le but d'optimiser la polymérisation *insitu*, il pourrait être intéressant d'explorer le greffage de tensioactifs ou stabilisants directement sur la surface de graphène afin d'obtenir des plaquettes de graphène avec des propriétés amphiphiles.

Films immergés dans du THF durant une journée

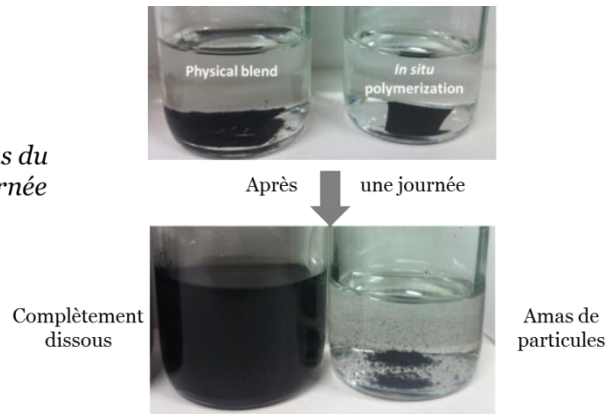


Figure 16. Test de solubilité dans le THF des films nanocomposites synthétisés par mélange physique ou par polymérisation *in situ*.

En conclusion, l'objectif global de cette thèse consistait à réaliser des nanocomposites conducteurs pour une impression sur textile via un procédé à bas coût et respectueux de l'environnement. Pour répondre à ces spécifications, des charges conductrices, les multifeuillets de nanographène (NMG), ont été produites par un procédé à bas coût et sans solvant. Pour permettre une impression sur textile, des nanocomposites conducteurs pouvant filmifier à température ambiante ont été développés et les matériaux obtenus possèdent d'excellentes propriétés électriques, leur permettant une application potentielle dans le domaine de l'électronique flexible. En effet, l'intérêt potentiel pour le domaine de l'électronique a été démontré via l'utilisation de matériaux nanocomposites à base de graphène en remplacement des fils de cuivre dans une configuration LED. D'autre part, un stylo a été rempli avec une suspension conductrice de NMG et des traits ont été tracés sur différents substrats. Les résultats de conductivités électriques obtenus pour un dépôt sur PET et sur le textile spécialisé sont semblables aux conductivités des films nanocomposites réalisés par mélange physique. Ces suspensions de nanocomposites conducteurs pourraient donc devenir une alternative moins chère que des encres conductrices à base d'argent pour l'électronique imprimée.

References

- [1] X. M. Tao, *Smart Fibres, Fabrics and Clothing: Fundamentals and Applications*, Elsevier, **2001**.
- [2] S. L. P. Tang, G. K. Stylios, *Int. J. Cloth. Sci. Technol.* **2006**, *18*, 108.
- [3] J. Felba, H. Schaefer, in *Nanopackaging* (Ed: J.E. Morris), Springer US, **2008**, pp. 239–263.
- [4] B. Abeles, P. Sheng, M. D. Coutts, Y. Arie, *Adv. Phys.* **1975**, *24*, 407.
- [5] “The Gwent Group, Leaders in paste manufacturing, sensor/ biosensor development and Instrumentation.,” can be found under http://www.gwent.org/gem_index.html#, **n.d.**
- [6] J.-C. DANIEL, C. PICHOT, *Les latex synthétiques*, Tec & Doc Lavoisier, Paris, 2006.
- [7] Y. S. Kim, J. B. Wright, J. C. Grunlan, *Polymer* **2008**, *49*, 570.
- [8] C. Moore, M. E. J. Newman, *Phys. Rev. E* **2000**, *61*, 5678.
- [9] E. Thommerel, J. C. Valmalette, J. Musso, S. Villain, J. R. Gavarrı, D. Spada, *Mater. Sci. Eng. A* **2002**, *328*, 67.
- [10] W. S. Hummers, R. E. Offeman, *J. Am. Chem. Soc.* **1958**, *80*, 1339.
- [11] C. Knieke, A. Berger, M. Voigt, R. N. K. Taylor, J. Röhl, W. Peukert, *Carbon* **2010**, *48*, 3196.
- [12] D. Stauffer, A. Aharony, *Introduction to Percolation Theory*, Taylor & Francis, 1994.
- [13] J.C. N Ouali, *Plast. Rubber Compos. Process. Appl.* *16* (1991) 55.
- [14] J. Kolařk, *Eur. Polym. J.* *34* (1998) 585.
- [15] S.U. Pickering, *J. Chem. Soc. Trans.* *91* (1907) 2001.
- [16] X. Peng, R. Ahuja, *Nano Lett.* *8* (2008) 4464.
- [17] M. Quintana, E. Vazquez, M. Prato, *Acc. Chem. Res.* *46* (2013) 138.

General introduction

Over the past ten years, flexible electronics raised a strong interest and many applications were developed, such as flexible screens, ships for security (RFID) or recently wearable electronics. This new concept enables to transform traditional textile and apparel products into lightweight, wireless and wearable intelligent devices [1]. Some commercial products were recently developed and marketed, in sectors such as health, automotive, home, security and civil engineering sectors. To build up this new device, a convenient approach is to print the electronic components onto the fabric substrate. Currently, adequate conductive inks are mostly based on metallic particles and contain 30 to 70wt.% of these conductive phase in order to reach the adequate conductivity level [2][3]. This PhD thesis is motivated by the production of low-cost (meaning low-cost fillers and low content) and solvent-free conductive inks for textile applications. The aim of this project is to present a simple processing route for producing conductive inks which form a continuous film at room temperature and show high deformability after drying.

The strategy is based on architected nanocomposites allying conductivity characteristics of carbon filler (carbon black, carbon nanotubes or graphene) and deformability of a polymer binder, a latex. A latex is a colloidal suspension in water of polymer particles (10 nm to 10 μm diameter) [4]. In adequate conditions, these particles coalesce after water evaporation to form a continuous polymer film. The interest for conductive nanoparticles, and more specifically for carbon nanotubes and graphene, has grown since the past ten years. These conductive fillers have many benefits in polymer-based nanocomposites for various applications, like printed electronics.

Currently, the metal-based conductive inks contain at minima 40% of conductive filler. The nanocomposite conductive inks can be prepared by many methods such as melt or solution route between a polymer matrix and the conductive fillers. To reduce the content of fillers, and consequently the ink cost, the latex route will be favored to formulate the inks. This synthetic route is sustainable as a latex is made of polymer nanospheres suspended in an aqueous suspension and does not require the use of organic solvent. Moreover, the latex route favors the built-up of a tunable architecture of fillers. The conductive fillers will be trapped between the foreign latex particles during the film-formation and so promote the creation of a percolating network of fillers at lower filler content [5]. Among the carbon fillers, 2D-fillers (platelets) would both favor filler contacts compared to 1D-fillers (nanotubes) and lower the percolation threshold compared to 3D-fillers (spheres). Thus, for geometrical considerations, platelet-like fillers [6] seem to be a good choice to build up an efficient network with polymer nanospheres.

In this work, the challenge relies on the production of adequate conductive fillers with specific dimensional characteristics that do not destabilize the latex during physical blending or *in situ* polymerization in order to obtain conductive inks. In literature the most popular route to synthesize graphene is based on a chemical method, so-called Hummer's method [7].

Despite its popularity, this method presents noticeable disadvantages as it relies on a long and multistep synthesis using many chemical products. As an alternative, Knieke *et al.* proposed a production of Nanosize Multilayered Graphene (NMG) based on the mechanical delamination of graphite in wet grinding media [8]. This mechanical method is cost-effective and avoids organic solvents. In this thesis, this procedure has been chosen and the NMG water suspensions are conveniently used as is in the subsequent processing steps of the nanocomposite material. The delamination process requires the use of a large amount of graphite flakes, but these are cheap and reusable raw materials. The stability of the suspensions is provided by the addition of surfactants molecules or polymeric stabilizers which bring a hydrophilic head and hydrophobic tail. These molecules will cover the surface of the graphite (and NMG) particles with the hydrophilic head pointing in the water phase favoring repulsion interactions between particles.

After the production of Nanosize Multilayered Graphene, using a low-cost and solvent-free method, nanocomposite conductive inks have been realized by two different processes: physical blending of the conductive fillers and acrylic latexes or *in situ* polymerization in the presence of graphene. The aim is to produce armored polymer particles, meaning that the surface of the polymer particle is covered with NMG platelets. Geometrically, the latex diameters need to be higher than the NMG lateral dimensions. With NMG platelets showing a lateral dimension around 50 nm, latex diameters around 0.3-1 μ m should be adequate. To produce latexes, polymerization in dispersed media is chosen and particularly polymerization processes in emulsion, miniemulsion and dispersion. With different experimental conditions, these processes allow the synthesis of latex particles in a wide range of sizes.

This thesis is divided in four chapters.

After this brief introduction, **Chapter 1** is a state-of-the-art based on selected articles of the literature which will recall a basic knowledge concerning conductive inks formulation, latex synthesis, graphene syntheses and properties and graphene-based latex nanocomposites.

Chapter 2 details the production of nanosize multilayered graphene (NMG) throughout the mechanical delamination of graphite suspensions stabilized by various surfactants and/or stabilizers. The impact of the nature of the stabilizer on the dimensions (lateral size, thickness) and concentration of the NMG formed will be investigated.

Chapter 3 focuses on physical blending's of NMG suspensions and latex particles with two different diameters, 300 and 650 nm. The morphology, electrical and thermomechanical properties of the two series of nanocomposite films are successively studied.

Chapter 4 deals with the synthesis of graphene-based nanocomposites by *in situ* polymerization in presence of NMG suspensions through various polymerizations ways (emulsion, miniemulsion or dispersion). The electrical properties of these nanocomposites are compared with the physical blending.

A conclusion will then summarize the main results of this work and will propose some opening. In the appendix, the major experimental techniques which were used in this work will be detailed.

References

- [1] L. Hu, M. Pasta, F.L. Mantia, L. Cui, S. Jeong, H.D. Deshazer, J.W. Choi, S.M. Han, Y. Cui, *Nano Lett.* **2010**, *10*, 708.
- [2] “The Gwent Group, Leaders in paste manufacturing, sensor/ biosensor development and Instrumentation.,” can be found under http://www.gwent.org/gem_index.html, **n.d.**
- [3] B. Abeles, P. Sheng, M. D. Coutts, Y. Arie, *Adv. Phys.* **1975**, *24*, 407.
- [4] P.A. Steward, J. Hearn, M.C. Wilkinson, *Adv. Colloid Interface Sci.* **2000**, *86*, 195.
- [5] E. Tkalya, M. Ghislandi, A. Alekseev, C. Koning, J. Loos, *J. Mater. Chem.* **2010**, *20*, 3035.
- [6] Z. Yang, R. Gao, N. Hu, J. Chai, Y. Cheng, L. Zhang, H. Wei, E.S.-W. Kong, Y. Zhang, *Nano-Micro Lett.* **2012**, *4*, 1.
- [7] W. S. Hummers, R. E. Offeman, *J. Am. Chem. Soc.* **1958**, *80*, 1339.
- [8] C. Knieke, A. Berger, M. Voigt, R.N.K. Taylor, J. Röhr, W. Peukert, *Carbon* **2010**, *48*, 3196.

Chapter 1: State of the art

Introduction	2
I. Context	2
1. Functional textiles	2
2. Conductive inks	4
a. Ink recipes.....	4
b. Printing techniques	6
II. Nanosize Multilayer Graphene (NMG).....	8
1. Description	8
2. Production of NMG.....	10
a. Chemical reduction of graphene oxide (GO)	10
b. Liquid phase exfoliation	12
III. Latex routes to elaborate graphene/polymer Nanocomposites	17
1. Advantages of latex routes over other elaboration routes	17
2. Percolation description of latex-based composites	21
3. Synthesis of polymer latexes.....	23
4. Nanocomposites via latex blending.....	27
a. $D_{\text{graphene}}/D_{\text{latex}} > 1$	27
b. $D_{\text{graphene}}/D_{\text{latex}} \leq 1$	30
c. Conclusions	32
5. Nanocomposites via <i>in situ</i> latex synthesis in the presence of GO or rGO particles	32
a. Emulsion polymerization.....	33
b. Miniemulsion polymerization.....	35
c. Conclusions.....	39
Conclusions	40
References	41

Introduction

This chapter provides the context and information on graphene/polymer nanocomposite materials required to understand the content of this work. First, a brief description of the flexible electronics market and development of conductive inks will be presented. Then, the existing processes for graphene synthesis and the resulting graphene properties will be described, followed by a state of the art on the incorporation of graphene in polymers and the elaboration of graphene-based nanocomposite latexes. These two last parts will focus on nanocomposites with enhanced electrical properties.

I. Context

1. Functional textiles

Textile is a familiar material used in variety of situations, such as transport, furniture, architecture, medical care, clothing... Functional textiles refer to a broad range of products that extend the functionalities of common fabrics. Numerous applications, ranging from military and security to personalized healthcare, hygiene and entertainment can be targeted ^[1]. Such smart textiles will be able to sense and react to environmental conditions or stimuli, for example, mechanical, thermal, chemical or magnetic interactions ^[2]. Functional textiles already available on the market count, for instance, refreshing or slimming functions using microencapsulation of active molecules ^[3] and also antistatic and thermo-regulating functions for bedding or sport applications by weaving of metallic threads into the fabrics (Figure 1a) ^{[4][5]}. More recently, wearable electronics or e-textiles, with incorporation of microelectronics onto the fabric, have been developed (Figure 1b) ^[6]. The patented achievement of Eleksen called 'Eleck Tex®' is a laminate of textile fabric layers (0.6 mm thick) producing flexible touch sensors (Figure 1a) ^[7]. The inbuilt sensor can detect where and how hard the fabric is pressed. Three engineering students also developed a 'data logging' compression shirt that helps baseball pitchers avoiding torn ligaments. This high-tech shirt, which is fitted with motion sensors and a web of conductive threads, tracks its wearer's pitching mechanics during a game in real time, then relays that data to a monitor (Figure 1b) ^[8].

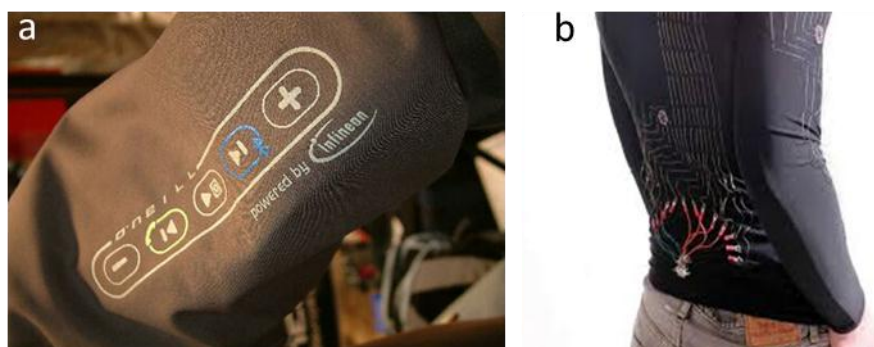


Figure 1. Examples of thermo-regulating or e-textiles applications : a) Eleck Tex® ^[7] and b) a 'data logging' compression shirt ^[8].

Hence, there are huge opportunities to add functionality and improve performances of textiles. This market, including interactive and smart textiles, is estimated at 2 billions dollars in 2015^[9] and is in development. Textronics commercializes a line of sport products (Numetrex©) which integrates sensors for heartbeat measurements. Recently, Citizen Science has produced smart textiles connected to smartphones for sports applications. The automotive industry also considers functional textiles as opportunities to reduce costs of traditional features such as heated seats or safety sensors.

The context of this PhD work focuses on smart textiles applications, with the incorporation of conductive materials on the fabric. Among possible functions considered, there are anti-static, thermo-regulating and electronic functions. Different approaches can be applied to produce electrically conductive fabrics. First, by weaving conductive yarns into the textile structure^[10]: with this technique, the softness and comfort of the final composite textile can be degraded. The conductive yarns themselves can be produced through different processes such as twisted metal wires, metal coating or metal fibers^[11]. The structure of conductive yarns, with the conductive material in red, is detailed in Figure 2.

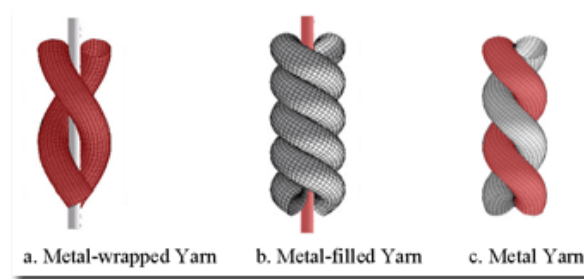


Figure 2. Weaving of metal fibers for e-textiles applications.^[12]

Low resistances of 10 to 500 Ω/m can be reached with these fibers^[13]. More recently, conductive coatings and inks have been applied onto fabrics and papers to provide flexibility to the systems and reduce stress on the substrate. The conductive coating can be deposited on a non-conductive substrate through classical printing techniques.

Another approach is to develop surface treatment adequate for application of existing conductive inks meaning inks that were developed for non-flexible substrates. In Figure 3, paper^[14] is covered with a polymer layer (PowerCoat®). This surface treatment offers excellent printability and adhesion of standard conductive inks.



Figure 3. Printing of conductive inks on flexible substrates.^[14]

This PhD work focuses on the development of a conductive ink recipe based on a polymer latex associated to graphene-based conductive particles. The state-of-the-art of conductive inks is presented hereafter.

2. Conductive inks

Conductive inks can be coarsely divided into two categories depending whether they contain a polymeric binder or not. In the first case, conductive particles are dispersed in an organic solvent using a stabilizing agent. After being deposited onto the substrate, a sintering step at high temperature ($>500^{\circ}\text{C}$) is required to form the final conductive component ^[15], which process is not adequate for flexible substrates nor textiles ^[16]. In the second case, a polymeric binder is solubilized in an organic solvent to form the medium. Then, the conductive particles are dispersed in that medium. After being deposited onto the substrate, film formation occurs at low temperature ($<120^{\circ}\text{C}$) and some flexibility of the final conductive component is given by the polymeric binder. This approach is more adequate for printing on textiles and is detailed here.

a. Ink recipes

Most of commercial conductive inks are solvent-based inks composed of fine conductive particles dispersed in an organic solvent containing a conductive or dielectric binder. A typical ink recipe is given in Table 1. The volume fraction of conductive particles is rather high and depends on their shapes and dimensions. It has to be maintained above the minimum volume fraction required for inter-particle connectivity. As more and more conductive fillers are added to the polymer matrix, a filler network begins to form that allows the composite to transition from insulator to conductor. This transition named percolation threshold corresponds to the critical volume fraction of filler needed to obtain the first percolating path throughout the polymer matrix ^[17]. The concept of percolation theory is currently used in materials science; and is often employed to describe transitional behavior of electrical and mechanical properties in composites ^[18].

Table 1. Typical ink recipe extracted from Gwent group website ^[19]

Constituents	wt %
Conductive phase	27-70
Polymeric binder	9-3
Organic solvents	64-27

Dupont, Toyo ink or Sunchemical are currently the main actors for conductive inks development. The conductive particles can be metallic (copper, silver, gold...), conductive carbon particles or conductive polymers.

Metallic particles

Metal-based conductive inks are typically composed of metallic micro and/or nano-particles (flakes or powders). Silver ^[20] or gold are most commonly chosen ^[21] for their chemical inertness in ambient atmosphere and good electrical conductivity. Metallic particles exhibit

high electrical conductivities as detailed in Table 2 ^[22] for inks containing 40-60 wt% of metallic particles. Electrical conductivities are measured after ink printing and drying.

Table 2. Electrical conductivity of printed conductive inks containing 40-60 wt% of metallic particles.

Particle	Electrical conductivity
Silver (Ag) ^[23]	$6.3 \cdot 10^7 \text{ S m}^{-1}$
Copper (Cu)	$5 \cdot 10^7 \text{ S m}^{-1}$
Gold (Au) ^[24]	$4.4 \cdot 10^7 \text{ S m}^{-1}$
Aluminum (Al)	$3.8 \cdot 10^7 \text{ S m}^{-1}$

For example, Russo and coworkers recently developed a pen-on-paper ink based on poly(acrylic acid) coated silver particles (mean diameter: $400 \pm 120 \text{ nm}$) in order to write conductive paths directly on paper ^[25]. A viscosity enhancer was added, namely hydroxyethyl cellulose, to tailor the ink rheology. These inks contain 40 to 65 wt% of silver particles and electrical conductivities reached $2 \cdot 10^6 \text{ S m}^{-1}$ after deposit on a substrate and a sintering step over 100°C .

Metallic conductive inks usually exhibit relatively high electrical conductivities, but high weight percentage of metal particles are necessary (40-60 wt%). Due to the high cost of metallic particles, other approaches have thus been developed.

Conjugated polymers

As an alternative to metallic particles, conductive polymers have been studied. These conductive polymers are characterized by their conjugated bonds that confer them electrical conductive properties. They present high conductivity ($100\text{-}1000 \text{ S m}^{-1}$) compared to classical polymers which are insulators ($10^{-7}\text{-}10^{-8} \text{ S m}^{-1}$), relatively easy process and long term-stability.

Among conductive polymers, poly(3,4-ethylenedioxythiophene)-poly(styrene sulfonate) (PEDOT-PSS), is among the most popular. It was commercialized in the 1990s ^[26]. PEDOT-PSS is a polymer blend comprising PEDOT and PSS. PEDOT is a π -conjugated polymer which is electrically conductive and optically transparent, while the addition of PSS improves the solubility. According to Nardes et al. ^[27], the microstructure of PEDOT-PSS is composed of PEDOT-rich islands surrounded by PSS thin layers. Due to their unique electric and optical properties, PEDOT-PSS thin films are widely used as conductive layers in organic electronic devices and are also suitable for fabrication of flexible electronics ^[28]. However, compared with metallic conductive inks, conductive polymers still exhibit a relatively low conductivity ^[29]. They can be combined with metallic particles such as silver to improve the overall electrical conductivity ^[30].

Carbon based particles (Carbon Nanotubes (CNT), Graphite, Graphene related)

Carbon-based particles are also attractive candidates for conductive inks due to their low cost and good electrical conductivities. Graphite and carbon black have been used as conductive fillers in acrylate polymers by Rangel et al. for pressure sensitive automatic systems applications ^[31]. Simple paper electronic applications with graphite powders have also been

developed [32]. CNTs have been used as conductive fillers for printed thin films by many researchers [33]. CNTs can be dispersed in various polymer matrices, such as PEDOT-PSS [34] or PMMA, to obtain printed thin films [35] [36].

However, carbon particles are hardly stable in water suspensions. Among the various carbon-based materials, graphene, a flat monolayer of carbon atoms tightly packed into a two-dimensional (2D) honeycomb lattice, is considered as a potential material for carbon-based inks because of its remarkable characteristics [37][38]. Graphene bi- and tri-layer was used as protective coating against oxidation on copper-based inks [39] or directly for the production graphene/water suspension inks [40]. But due to its hydrophobicity, graphene is not stable in water-based ink suspensions and graphene oxide (GO) particles were rather used instead to increase the stability of the suspensions. Indeed, the latter can be easily dispersed in water due to the presence of polar on its surface. To recover the electrical properties of graphene, a chemical or thermal reduction of GO is thus necessary. However, remaining oxygen-containing groups are responsible for a loss of electrical conductivity compared to pure graphene. Giardi et al. developed graphene/acrylic composite inks with UV reduction of the GO platelets after ink printing [41]. But the electrical conductivity obtained was still too low for flexible electronics applications. GO can also be reduced using Infrared Lamp [42], hydrazine bath [40] or an heat treatment at 500°C [43].

b. Printing techniques

The conductive ink and paste business is a large market that has generated 2 billion dollars in 2013. Classical printing techniques can be used such as inkjet printing [44], screen-printing [45], flexography [46] or offset lithography [47] (Figure 4).

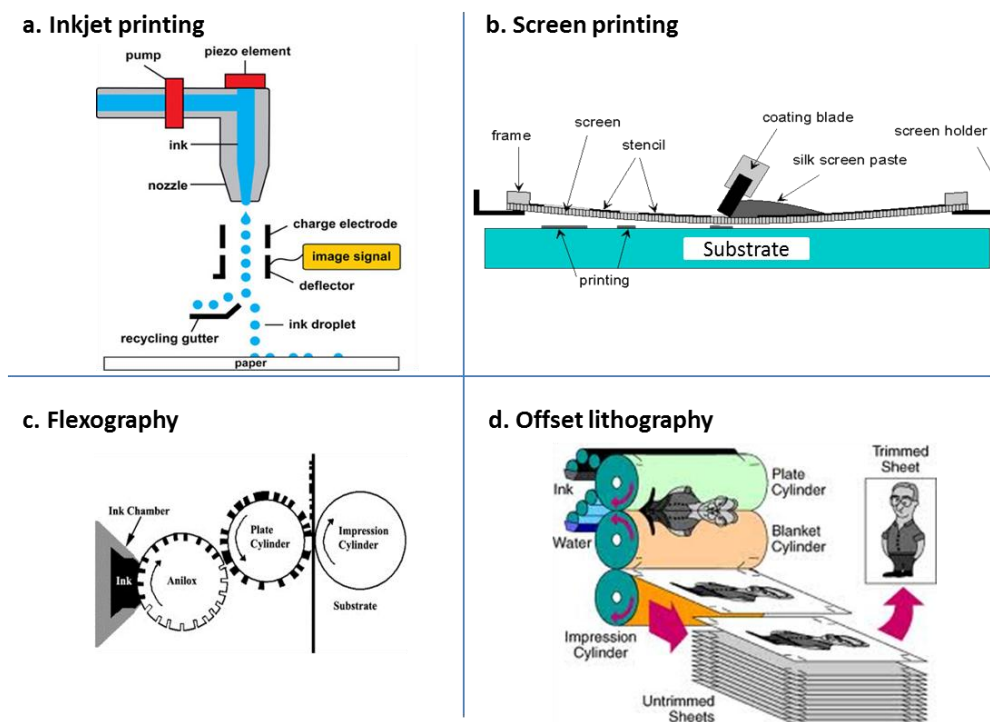


Figure 4. Main printing techniques: a) inkjet printing, b) screen printing, c) flexography and d) offset lithography.

Similarly to classical inks, each printing technique relies on specific ink characteristics such as viscosity, open-time, surface tension or solid content. Table 3 summarizes the main characteristics of the different printing processes usable for classic inks.

Table 3. Main characteristics of the different printing processes for classic inks.^[48]

Printing process		Screen printing	Flexography	Offset lithography	Inkjet printing
Applications		Printing of large area (poster, advertising)	Packaging, bags, paperboards	High quality works, packaging, polychrome	Office printers, items, textiles
Printed samples	Resolution	~ 120 dpi	Up to 200 dpi	Up to 600 dpi	Up to 600 dpi
	Film thickness	20-100 μm	6-8 μm	1-2 μm	~ 1 μm
Ink characteristics	Viscosity (Pa.s)	0.1-10	0.01-0.1	5-50	~ 0.01
	Surface tension (mN/m)	-	-	~ 35	30-40
Substrate		All substrates	Paper, paperboard, metal, polymer film, glass, etc...	Paper, paperboard, metal, polymer film, glass, etc...	All substrates
Productivity		Slow process (< 800 sheets/h)	~ 600 m/min	Sheet-fed press: ~ 10 000 sheets/h	~ up to 150 m/min or 1600 sheets/h
Remarks		Interactions between the screen and the ink can affect the homogeneity of the printed film creating irregularities in conductivity	Irregular ink films can be obtained due to the squashing of the plate on the substrate, leading to differences of thickness between the center and edge of the pattern	Presence of dampening solution can affect the ink conductivity. Waterless offset can be investigated	Risk of placement errors can induce undesirable 'satellite' drops and reach areas that should not be printed

Inkjet printing differs from other printing processes because it is a digital process that allows direct printing of various patterns on demand. This process is contactless and flexible. Ink viscosity and surface tension are crucial parameters in the formulation of an inkjet ink. The viscosity must be low enough in order to allow the exit channel of the nozzle to be refilled at high frequency. The surface tension must be adequate to favor drop formation. Typical inkjet inks have a viscosity around 10 mPa.s and a surface tension around 35 mN m⁻¹. In addition, another major concern in ink formulation is to avoid nozzle clogging when using suspensions with particles. Clogging can also occur when ink dries inside the nozzle, especially with water-based inks or with polymers which film-form at room temperature. In addition, aggregation phenomenon should be avoided: the maximum particle size must be lower than one to ten micrometers, depending on the nozzle size^[49]. Note that sedimentation without aggregation should be acceptable as far as the sediment flows back in suspension after shaking.

The aim of this PhD work is to develop a simple elaboration route for producing conductive inks that form a continuous film at room temperature and that exhibit high deformability after drying. The strategy is based on nanocomposites combining the conductivity characteristics of Multilayered Graphene and the deformability of a polymer binder and presenting a specific

meso-scale morphology that favors percolation at low content of conductive phase (<20 wt. %).

II. Nanosize Multilayer Graphene (NMG)

1. Description

The proper definition of graphene is a two-dimensional monolayer of carbon atoms closely packed in a honeycomb lattice (Figure 5a). Graphite is represented by the stacking of a large number of graphene monolayers into a three-dimensional structure (Figure 5b). A graphene monolayer has a theoretical Van Der Waals (VDW) thickness of 0.34 nm, which is the thinnest two-dimensional nanofiller reported so far ^[51]. Graphene exhibits exceptional mechanical ^[52], optical ^[53], electronic ^[54] and thermal properties ^[55].

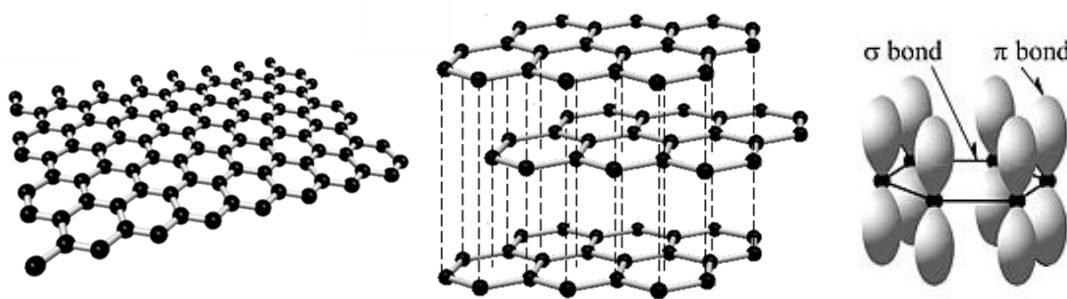


Figure 5. a) Single layer of graphene, b) graphite structure and c) distributed σ and π bonds on the graphene structure.

Within graphene, one σ -orbital and two in-plane π -orbital of carbon are associated with sp^2 hybridization ^[56]. The π bonds, available both above and below each graphene layer (Figure 5c), can overlap with those from neighboring carbon atoms. The σ -electrons are tightly bound and so they can hardly contribute in current conduction, but the π and π^* orbitals can behave like valence bands and conduction band and induce the planar conduction mechanism ^[57]. Due to these properties, graphene is known as a semi-metal. Another parameter is its extremely high aspect ratio (ratio of lateral dimensions to the thickness), 10^4 or higher, and its high intrinsic flexibility.

For clarity sake, we describe in the following the different graphene-based compounds that can be found in literature. Few Layer Graphene (FLG) designates a component made of 2 to 20 layers of graphene and exhibiting micron scale lateral sizes. Graphene and FLG can be functionalized through non-covalent approach (VDW, Electrostatic, π - π staking) ^[58] ^[59]. Few authors functionalized the end chain of their polymer with pyrene groups to favor π - π staking interactions with graphene platelets ^[60]^[61].

Common chemical derivatives of graphene are Graphene Oxide (GO) and reduced Graphene Oxide (rGO). GO designates FLG exhibiting groups containing oxygen atoms on the surface such as carboxylic, hydroxyl and epoxy groups (Figure 6).

The carboxylic and hydroxyl groups can be used for functionalization ^{[62][63] [64]}. For covalent functionalization of GO, the following modifications can be used: amination ^[65], esterification ^[66], isocyanate-grafting ^[67] or polymer grafting ^[68]. GO is an insulator and a reduction is needed to recover electrical properties. After subsequent reduction, GO is designated as rGO (and not FLG) as defects on the surface remain and electrical conductivity cannot be fully recovered.

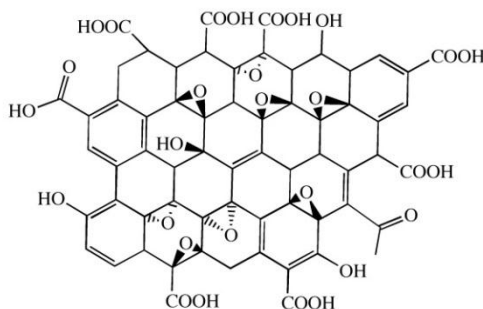


Figure 6. Structure of graphene oxide (GO).

The term rGO mostly appears in papers dealing with materials science. They might be designated abusively under the term “graphene” although the term FLG would be more appropriate. In this PhD work, the term Nanosize Multilayered Graphene (NMG) is chosen to describe FLG with a small lateral dimension (< 400 nm).

Moreover, in literature many approaches can be found to produce conductive composite through functionalization of GO with subsequent reduction. However, in this PhD work the focus is made on a direct production of conductive composites without the oxidation-reduction step.

Table 4 highlights the differences in terms of properties between graphene monolayer, that can be almost considered as a “model material” and Few Layer Graphene (FLG) that is closer to a “real material” that can be produced under industrial conditions. Values for the intrinsic conductivity of graphene monolayers are largely documented in literature and have been reported to be around 10^7 - 10^8 S m⁻¹ for in-plane conductivity. It was demonstrated that in-plane conductivity decreases with increasing number of graphene layers due to overlapping of the non-hybridized p_z orbitals perpendicular to the sheets. The addition of one layer to a monolayer was found to divide by half the conductivity while further addition leads to lower influence ^[72]. Thus the intrinsic conductivity of FLG and NMG is expected around 10^6 - 10^7 S m⁻¹. An increase of the number of graphene layers will also induce a decrease of the elastic modulus, thermal conductivity and a small increase of the opacity.

Table 4. Physical properties of graphene monolayer and few layer graphene (FLG).

Properties	Monolayer	Few layer graphene (FLG or NMG)
Elastic modulus	1 TPa ^[37]	0.5 TPa ^[69]
Thermal conductivity	$5.1 \cdot 10^3$ W mK ⁻¹ ^[55]	5 - $25 \cdot 10^1$ W mK ⁻¹ ^[70]
Electrical conductivity	10^7 S m ⁻¹ ^[71]	10^6 - 10^7 S m ⁻¹ ^[72]
Optical properties	2.3 % of opacity ^[73]	16% of opacity ^[74]

FLG and NMG are interesting compromises for conductive inks applications and their incorporation into polymers has been found to lead to substantial improvements in mechanical and electrical properties at lower contents compared to expanded graphite ^[75] ^[76].

2. Production of NMG

Graphene was discovered by A. Geim and K. Novoselov using the so-called « scotch tape » method which consists in peeling graphene sheets from a graphite pencil using an adhesive tape. They have been rewarded for this discovery with a Nobel Prize in 2004. Since then, many methods have been developed to produce graphene. These methods can be divided into two main categories : “bottom-up” approaches like Chemical Vapor Deposition (CVD) or epitaxial growth, and “top-down” approaches like adhesive tape technique or liquid phase exfoliation ^[77]. These processes are compared in Table 5.

Table 5. Synthesis ways to produce graphene flakes ^[78].

Synthesis process	Size of graphene flakes	Properties	Applications
Adhesive tape technique	5 to 100 μm	Small scale production, high cost, high quality, uneven films	Research purpose
CVD (on Ni, Cu, Co)	Thin films (< 75 μm)	Moderate scalability, high cost, high quality, high process, temperature > 1000 °C Low yield, high cost,	Touch screens, smart windows, flexible LCD & OLEDs
Epitaxial growth on SiC	Thin films (> 50 μm)	high quality, high process, temperature (1500°C) very expensive substrate	Transistors, circuits memory, semiconductors
Liquid phase exfoliation	Nanosheets in suspension (nm to few μm)	High scalability, low yield, moderate quality, low cost	Polymer fillers, transparent electrodes and sensors
Chemical reduction of graphene oxide	Nanoflakes in powder (nm to few μm)	High scalability, low cost, low purity, high defect density	Conductive inks and paints, polymer fillers, sensors

The adhesive tape technique, CVD and epitaxial growth cannot provide a large amount of free standing graphene. Due to the intended application, we will focus on liquid phase exfoliation and chemical reduction of graphene oxide in the following part.

a. Chemical reduction of graphene oxide (GO)

This approach takes advantage of the fact that, contrary to graphite, graphite oxide is easily exfoliated into GO sheets in water. Synthesis of graphite oxide has been successfully realized by Brodie in 1859 ^[79], Staudenmaier in 1900 ^[80] and Hummer in 1958 ^[81]. In this synthesis, graphite is oxidized by chemical treatment with potassium permanganate (KMnO_4) and nitric acid in concentrated sulfuric acid to form graphite oxide. Graphite oxide is then exfoliated into GO sheets by ultrasonication to form a stable GO aqueous dispersion. The final product can be purified by centrifugation and dialysis to remove aggregates and inorganic impurities such as metal ions or acids. The oxidation time and the amount of oxidants influence the size of GO sheets produced by chemical exfoliation ^[82]. GO synthesis can be realized in various

solvent, such as water [83], acetone [84], N-Methylpyrrolidone (NMP) [85] or tetrahydrofuran (THF) [86].

To recover the electrical properties of graphene, GO must be rigorously reduced after exfoliation. The chemical reduction of GO has been studied for many years and can be done using a variety of reducing agents. Hydrazine is the most common reducing agent used but its toxicity has prompted researchers to develop new reducing agents, such as sulfur compounds [87], hydroxylamine [88] or vitamin C [89] to obtain graphene suspensions in water. For reduction in organic solvent, solvothermal reduction in NMP [90] or via gamma-ray radiation have been proposed [91]. During the reducing step, a restacking of rGO can happen, which limits its effectiveness as filler for nanocomposites [92]. So, to favor rGO stabilization after reduction, surfactants or polymeric stabilizers may be used. For example, Stankovich *et al.* used sodium poly (styrene sulfonate) (PSSNa) to stabilize GO platelets during reduction with hydrazine [93]. Synthesis of reduced graphene oxide using a chemical way allows the production of concentrated graphene platelets with a lateral size between 200 nm and a few μm . Reduction of graphene oxide can also be done thermally at high temperature (1050°C) or electrochemically [94].

The reduction process influences the final properties of the graphene sheets, and particularly their capacitance [95]. Cheng *et al.* reviewed the impact of GO reduction processes on sheet resistance [96] (Figure 7) and showed that sheet resistance of pristine graphene cannot be fully recovered after reduction. Non conjugated sp^3 carbon atoms constitute most of the defects present at the surface of rGO. Some oxygen-containing groups can remain and facilitate interaction and dispersion with polymers [97], however these remaining groups also affect the final electrical properties

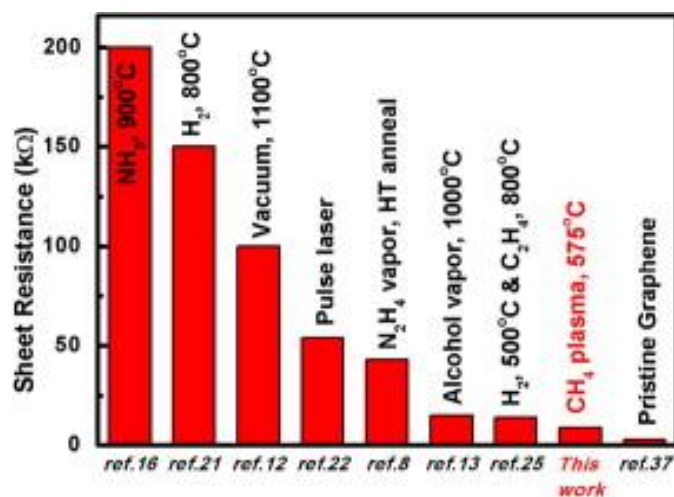


Figure 7. Impact of the GO reduction process on the sheet resistance [96].

As an alternative to reduced graphene oxide, FLG can be produced by liquid phase exfoliation. This process and its comparison with the graphene oxide reduction process are presented below.

b. Liquid phase exfoliation

Process

Strong Van Der Waals interactions bind graphene layers together so that the exfoliation of graphite in solution requires high energy input. To overcome these forces, two main approaches exist: i) sonication of graphite in solvent systems with chemical functionalization, and ii) treatment of graphite to weaken interlayer interactions. To obtain graphene sheets of few micrometers in lateral size, graphite can be sonicated in organic solvents, like N-methyl pyrrolidone (NMP) [98]. NMP is an efficient solvent because it has a surface energy close to that of graphene, which minimizes the energy cost associated with exfoliation. In this process, the cavitation bubbles generated by the ultrasonic field produce shock waves that break apart the graphite flakes, which are subsequently stabilized by the solvent. An addition of an intercalation compound, like in potassium-intercalated graphite, KC_8 [99], can also help the exfoliation of graphite and favor high concentrations of graphene in suspensions (0.7 mg mL^{-1}) [100]. The introduction of positive or negative charges between the graphite layers promotes exfoliation and stabilization of the sheets in organic or aqueous media. Sonication has been demonstrated as a decent exfoliation procedure in a liquid with a surface tension similar to that of graphite. It is known that the sonication produces different effects on exfoliated nanosheets and layered materials, for instance sonication-induced scission can break larger crystallites into smaller crystallites and vibration can chip off thin 2D nanosheets from outer surfaces of layered materials [101]. Small molecules, such as 1-pyrenecarboxylic acid, can interact with graphene via π - π stacking and easily exfoliate graphite with simple agitation [103].

To increase the concentration of graphene in solution up to 1 mg mL^{-1} , surfactant molecules can be used to help the exfoliation of pristine graphite during sonication. Pristine graphite can also be sonicated in aqueous surfactant solutions [104] to produce graphene platelets up to a few micrometers in lateral size. Guardia et al. demonstrated that non-ionic surfactants such as tween-80 allow the production of high concentrated graphene suspensions (*i.e.* up to 1 mg mL^{-1}) [105]. Lotya et al. proposed the production of graphene sheets with 6 layers using sodium dodecyl benzene sulfate (SDBS) as a surfactant [106]. Lee et al. combined SDBS with fluorinated intercalation compound to create graphene sheets in aqueous suspension [107]. This one-step process allows the creation of expanded graphene sheets with low thicknesses (*i.e.*, typically 5 layers). Moreover, the graphene obtained is sufficiently expanded to be dispersed in aqueous solutions or organic solvent.

Alternatively, ball-milling in organic solvents (Dimethylformamide (DMF)) can be used to replace sonication but low yield is obtained [102]. In order to obtain high concentrations of graphene in water suspension, Knieke et al. proposed the production of multilayered graphene via a simple mechanical process in water. This mechanical method is not popular yet, however it presents considerable advantages such as cost-effectiveness and no use of organic solvents [108]. Multilayered graphene is obtained after four hours of mechanical delamination of graphite platelets in water suspensions (Figure 8). In this process, a graphite/surfactant suspension is injected in a reactor in a close-pack circuit. The rotating reactor contains zirconia beads with a mean diameter of $800 \mu\text{m}$. The high shear energy of the ceramic beads produces the exfoliation and break of the graphite platelets.

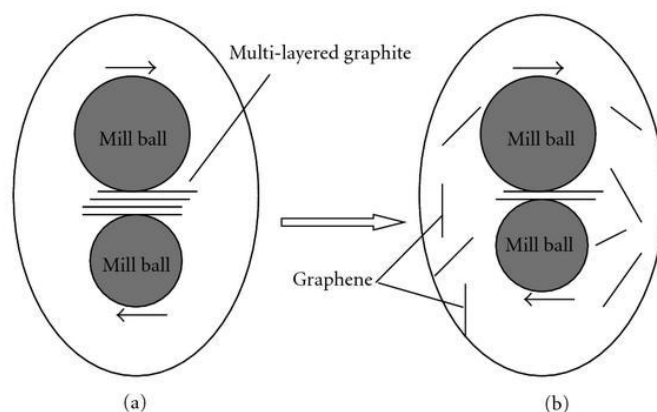


Figure 8. Scheme illustrating the creation of multilayered graphene from graphite platelets by using the wet ball-milling method ^[58]

To stabilize graphite and the resulting graphene flakes, Sodium Dodecyl Sulfate (SDS) was used as a surfactant and a concentration above the Critical Micelle Concentration (CMC) was needed. The CMC is defined as a surfactant concentration above which surfactant micelles are formed. In fact, a large surface area of graphene is created during the delamination process. This process can be a good alternative in order to produce water-based inks for inkjet printing. Indeed, the presence of surfactant allows decreasing the surface tension down to around 35 mN m, which is suitable for inkjet printing.

Table 6 summarizes the final characteristics of the multilayered graphene platelets obtained after a chemical process through Hummer oxidation, or after mechanical delamination, through wet grinding. Regarding the size characteristics, the same order of magnitude for thickness is obtained with both processes but the lateral size of the platelets can be lower using the mechanical method. The production time is shorter for the mechanical process. The yield corresponds to the final graphene mass divided by the initial graphite mass. The low yield for the mechanical method is balanced by the shorter time of production compared with the chemical method. In addition, the mechanical delamination leads to a large amount of graphite by-products that could be recycled in a subsequent mechanical delamination batch. Whereas, the chemical method uses important concentrations of dangerous products (such as sulfuric acid) and consequently only small mass of graphene can be produced at each synthesis.

Table 6. Comparison of two “top-down” processes to obtain multilayered graphene to produce 2g of graphene.

Method	Chemical products	Yield (%)	Graphene type	Lateral size (μm)	Thickness (nm)	Process duration
Chemical method	NaNO ₃ , H ₂ SO ₄ , KMnO ₄ , Hydrazine, Graphite	20%	rGO	0.1-2	1-10	5 days ^[109]
Mechanical method	Water, graphite and surfactant	4%	FLG or NMG	0.02-1	1-10	4 hours ^[108]

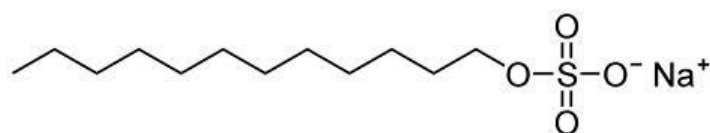
Mechanical process is a good candidate for industrial upscaling of NMG and FLG production. As it will be detailed further in chapter II, this process has been chosen in this work to produce Nanosize Multilayered Graphene.

Stabilization of NMG in suspension

Graphene platelets are difficult to suspend in water due to their high hydrophobicity. To promote their dispersion and stabilization in water, a stabilizer is usually added during the reduction of GO or during the liquid phase exfoliation of graphite. Three kinds of stabilizers are commonly reported: surfactants, polyelectrolytes and non-ionic polymeric stabilizers.

- Surfactants

Surfactants are defined as amphiphilic molecules, meaning that they contain both hydrophobic tails and hydrophilic heads. Surfactant molecules can adsorb on interfaces, and can thus stabilize hydrophobic particles suspended in water media. Sodium Dodecyl Sulfate (SDS) (Figure 9) is commonly used to stabilize carbon compounds like carbon nanotubes, graphite and graphene ^{[110], [111], [112], [113]}. One important parameter of surfactants is their CMC which is the concentration of surfactant at which micelles first appear in solution. Methods to measure CMC are all based on the fact that physical or chemical properties of the suspension abruptly change at or above the CMC (density, conductivity, surface tension, etc). Among these methods, surface tension measurements allow a rapid and reliable determination of the CMC of most surfactant molecules.

**Figure 9.** Chemical structure of Sodium Dodecyl Sulfate (SDS)

In a system consisting of only surfactant molecules in water, below the CMC, the surfactant molecules are located either in the water phase, on the walls of the container, or at the water-air interface (Figure 10). As the concentration of surfactant increases, the surface tension decreases rapidly until the CMC is reached. For surfactant concentrations above CMC,

surfactant molecules aggregate into micelles and the surface tension stays constant as there is no significant enrichment in surfactant at the water-air interface anymore. Thus on a surface tension vs. concentration curve, the start of the plateau marks the CMC (Figure 10).

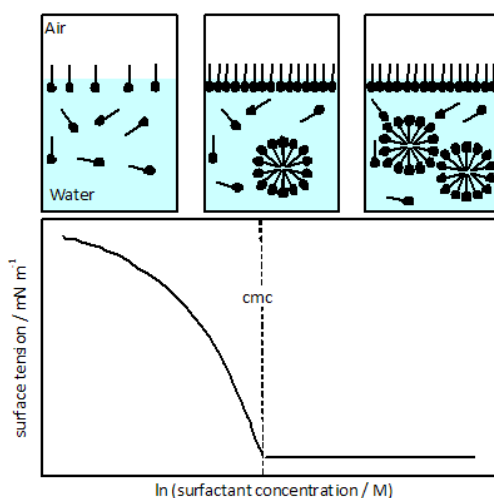


Figure 10. Scheme of the CMC measurement by interfacial tension.

Several authors have studied the adsorption behavior of surfactant molecules onto graphite surfaces. To increase the concentration of graphene in suspension, sodium dodecyl benzene sulfonate (SDBS), can be used as an alternative to SDS (Figure 11).

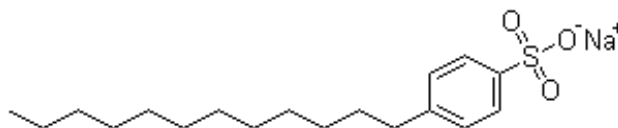


Figure 11. Chemical structure of SDBS

The planar aromatic structure of graphene can interact with surfactants with a hydrophobic tail containing planar or nearly planar polycyclic structures and/or unsaturated or aromatic rings where strong π - π interactions are possible. Compared to SDS, the hydrophobic tail of SDBS contains an aromatic ring in addition to the dodecyl chain^[114]. Several authors proved that SDBS stabilizes more than SDS (Figure 12). A concentration of up to 1.5 mg mL^{-1} of graphene was obtained with SDBS^[115] compared to 1.2 mg mL^{-1} with SDS, under similar conditions.

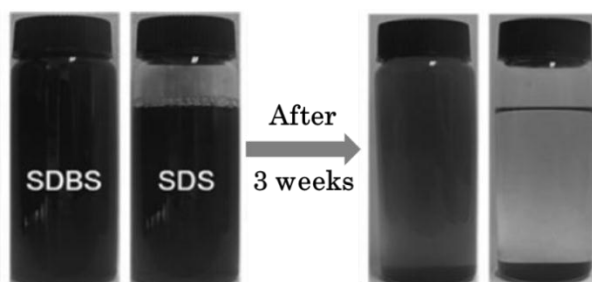


Figure 12. Stability of expanded graphite sheets (lateral size of few μm) in water with SDBS or SDS as surfactants^[116]

- Polyelectrolytes

A polyelectrolyte is a polymer with several ionizable groups along the molecule which will stabilize particles by electrostatic interactions. Sodium poly(styrene sulfonate) (PSSNa) is a polyelectrolyte, widely used for the stabilization of Multiwall Carbon Nanotubes (MWCNT) in water^[117]. PSSNa is composed of repeat units similar to the chemical structure of SDBS and is also adequate to stabilize graphene platelets in water^[114] (Figure 13).

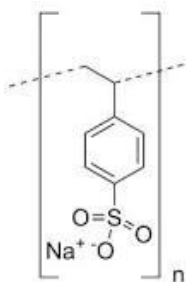


Figure 13. Chemical structure of PSSNa

The reversible association of carbon nanotubes with PSSNa in water was identified as being thermodynamically driven by the elimination of a hydrophobic interface between the tubes and the aqueous medium^[118]. A very different kinetic mechanism suggests that long-ranged entropic repulsions among polymer-decorated tubes act as a barrier that prevents the tubes from approaching^[119].

- Polymeric stabilizers

Polymeric stabilizers can be either non ionic or ionic and create physical or chemical interactions, with carbon-based fillers, thus contributing to their stabilization via electrostatic or steric mechanisms. Poly(N-vinyl pyrrolidone) (PVP) is a stabilizer containing hydrophilic pyrrolidone moieties, and a polyvinyl hydrophobic backbone (Figure 14). It can thus adsorb on hydrophobic surfaces and promote steric stabilization in aqueous solutions^[120]. PVP has been widely used to improve the stability of carbon nanotubes or rGO in water suspensions^{[118][120]}. For example, Arzac and coworkers used PVP to stabilize rGO during the reduction step.

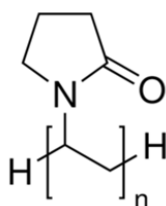


Figure 14. PVP chemical structure

Polymeric stabilizers containing PEO (Figure 15) have also been studied in literature for the stabilization of carbon compounds. One patent reports the use of polystyrene-*block*-poly(ethylene oxide) (PS*b*PEO) to stabilize graphene and other carbon-based fillers^[121]. Semaan *et al.* also demonstrated the ability of this copolymer to stabilize CNT suspensions in aqueous phase^[122].

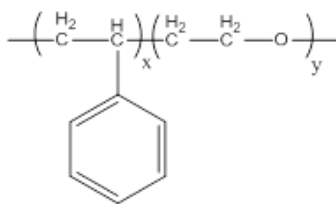


Figure 15. Chemical structure of PSbPEO

This polymeric stabilizer, PSbPEO, is known to create π - π stacking interactions with graphene platelets without an alteration of the graphene surface. The presence of an aromatic ring induces possible π - π interactions with the NMG platelets and reinforces its ability to stabilize NMG water-suspensions^{[123][124]}.

Both PVP and PSbPEO polymeric stabilizers have been used as stabilizers for the polymerization in dispersed media^{[125][126]}. In this work, stabilization of FLG in water is needed to form FLG/polymer composite via solution blending or through *in situ* polymerization. Adding surfactants or stabilizers increases the concentration of graphene in suspension and can favor further interactions between graphene platelets and polymer chains.

III. Latex routes to elaborate graphene/polymer nanocomposites

1. Advantages of latex routes over other elaboration routes

Nanocomposite materials with nanoscale fillers have emerged in the past decades as a promising novel class of materials, which takes advantage of greatly increased specific filler/polymer interfacial area, higher achievable loads and controlled interfacial interactions^[127].

Currently, multifunctional nanocomposites with improved mechanical performances are primarily fabricated by addition of pre-treated carbon nanotubes and nanofibers^[128], inorganic nanoparticles^[129], or clays to polymers^[130]. Due to its extraordinary electrical, chemical, optical and mechanical properties, graphene was found to be a promising candidate^[131] and due to the high aspect ratio, a large surface area is developed. Mechanical enhancements are sensitive to the surface area as they are also linked to polymer chain confinement effect^[132]. Due to the intercalation of polymer chains into the lamellae of layered fillers, an improvement in thermal stability can also be observed. Finally, graphene nanosheets can improve barrier properties by acting as impermeable obstacles that provide longer diffusion paths across the polymer matrix.

In addition to mechanical and barrier properties, graphene sheets can provide percolating pathways for electron transfer, making the composite electrically conductive. Similar benefits can be achieved with other conductive carbon fillers such as carbon black (CB), carbon nanofibers (CNF), and expanded graphite. However, graphene enables the insulator-to-conductor transition to occur at significantly lower loadings,^[133] comparable to electrical percolation thresholds for CNTs. Particle orientation also plays an important role: the percolation threshold becomes lower when particles are aligned in parallel.^{[134][135]}

Production of electrically-conductive polyolefins,^[133] vinyl ^{[136][59]} and acrylic ^{[137][138]} polymers, polyesters,^[139] polyamides,^[133] polyurethanes,^[140] epoxy,^[141] natural and synthetic rubbers ^[142] with graphene has been reported. These materials can be used, for example, for electromagnetic shielding, antistatic coatings and conductive paints.^[143]

Routes to produce polymer nanocomposites can be classified into four categories : i) solution or solvent blending, ii) melt processing, iii) *in situ* polymerization and iv) latex route. Each of them is developed below. The emphasis is placed on the electrical properties of the obtained nanocomposites. Note that existing Carbon-based inks containing a polymeric binder exhibits electrical conductivities around 10^1 - 10^2 S m⁻¹.

Solvent blending

Solvent blending requires three steps: the dispersion of the fillers in the solvent, the incorporation of the polymer and finally the removal of the solvent by distillation or evaporation ^{[144][145]}. An excellent compatibility of the polymer with the solvent is necessary to achieve a good dispersion. Solvent blending maximizes filler dispersion in polymer matrices by using pre-suspended graphene sheets. Different solvents (aqueous or organic) can be used to suspend graphene materials, including GO and rGO. This approach has been widely exploited due to its high dispersion efficiency, easy and fast fabrication step. Final electrical properties are measured on the nanocomposites after hot-pressing or compression of the obtained nanocomposite powder. Disadvantages of this approach are challenges in finding common solvents, toxic solvent utilization, thin-film limitations, difficulties in solvent removal, and common aggregation issues during mixing and solvent evaporation stages ^[146].

For solvent blending, many polymers have been reported in the literature as summarized in Table 7.

Table 7. Nanocomposites made by solvent blending and their electrical properties.

Polymer	Graphene diameter (D) and thickness (t)	Solvent	Percolation threshold	Maximum conductivity (S m ⁻¹)
Epoxy resin ^[147]	D=100 nm; t=1 nm	THF	0.32 vol%	10 ⁻⁵ at 2 vol%
Epoxy solution ^[148]	D= 400 nm; t= 1 nm	Acetone	0.52 vol%	100 at 9 vol%
Styrene/butadiene rubber ^[149]	D unknown; t= 3 nm	THF	5.3 vol%	10 ⁻⁵ at 17 vol%
Polystyrene ^[150]	D=1-10 μm; t= 1 nm	NMP	0.19 vol%	72.2 at 2.5 vol%
Polystyrene ^[59]	D=1 μm; t=1 nm	DMF	0.1 vol%	1 at 2.5 vol%
Polystyrene ^[151]	D=10 μm; t=1 nm	DMF	0.1 vol%	3.5 at 1.1 vol%
PMMA ^[97]	D=1-10 μm; t unknown	Methylene dichloride	0.4vol%	20 at 4.2 vol%

The percolation threshold and the maximum electrical conductivity strongly depend on the type of polymer matrix and on graphene dimensions. As shown in Table 7, high conductivities can be achieved under certain conditions. However, nanocomposites obtained by solvent blending still involve the use of toxic solvents: melt processing is an alternative to this process countering this drawback.

Melt processing

The melt process is free from toxic solvents but less effective to disperse graphene in polymer matrices at high filler content due to the viscosity increase ^[152]. But such high viscosities can also promote π - π stacking interactions between polymer and graphene, which is an obvious advantage of this process. In spite of that, very few authors have reported the use of melt processing to obtain nanocomposite materials with good electrical properties. Zhang *et al.* described the melt blending of PET and rGO. The lateral dimensions and thicknesses of rGO were 1-5 μm and 1.6 nm respectively. A percolation threshold of 0.47 vol.% was obtained and a maximum conductivity of 2.1 S m^{-1} at 3 vol.% of rGO was reached ^[153]. However as mentioned above, the drawback of this procedure is poor dispersion compared with solvent blending ^[154].

In order to increase the quality of filler dispersion, many authors used the *in situ* polymerization approach.

In situ polymerization

In situ polymerization is an efficient method to improve the dispersion of carbon-based fillers in a polymer matrix. Stronger interactions can be created between the polymer chains and the fillers if the latter are functionalized to be compatible with the matrix. Nanocomposites made through *in situ* polymerization exhibit better mechanical properties and lower percolation thresholds than those made by solvent blending or melt processing ^[155]. Table 8 summarizes the electrical properties of some polymer/graphene nanocomposites made through *in situ* polymerization. These syntheses are performed without any solvent.

Table 8. Nanocomposites made by *in situ* polymerization and their electrical properties

Polymer	Graphene diameter and thickness	Percolation threshold	Maximum conductivity (S m^{-1})
Ethylene gas ^[156]	D=100-300 nm; t unknown	3.8 vol%	10^{-2} at 10 vol%
EDOT monomer to form PEDOT:PSS ^[157]	D>10 μm ; t=1 nm	-	637 at 3 wt%
MMA ^[158] to form PMMA	D= 1-2 μm ; t unknown	0.5 vol%	10^{-4} at 2.0 vol%
MMA ^[159] to form PMMA	D=0.5-20 μm ; t=1-2.5 nm	0.31 vol%	0.1 at 5.5 vol%
Styrene ^[160] to form PS	D=15-20 μm ; t unknown	1.1 vol%	1 at 6 wt%

Many examples of *in situ* polymerization of styrene ^[161] ^[162] or MMA in the presence of graphene ^[163] have been reported in the literature. But no mention was made of the electrical conductivities of the resulting nanocomposites in these cases. As illustrated in Table 8, high

conductivities are obtained for nanocomposites combining the electrical properties of graphene and a conductive polymer such as for instance PEDOT-PSS. Furthermore, electrical conductivities of all other nanocomposites of Table 8 are low in comparison with nanocomposites obtained through solvent processing.

To conclude, both the elaboration process and the nature of the polymer have an influence on final electrical properties of graphene-based nanocomposites. Verdejo et al. ^[121] published a review which compares the percolation threshold for the different processes and showed that the lowest percolation threshold was obtained for solvent blending (Figure 16).

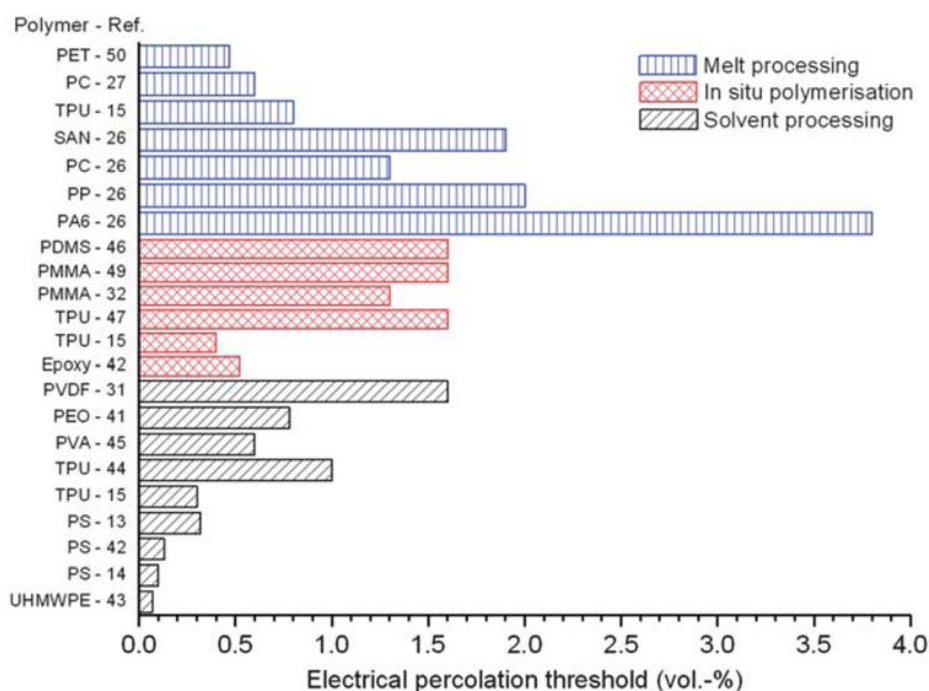


Figure 16. Influence of processing on the percolation threshold of polymer/graphene nanocomposites ^[144]

Polymer composites containing conductive nanofillers exhibit an enhancement of the electrical properties and are useful for many applications. But, high concentrations of conductive fillers are often required to achieve reasonable conductivities. Using a segregated network composed of polymer particles as a matrix (latex) can reduce the percolation threshold and increase the maximum conductivity obtained ^[164]. This processing route is detailed in the following section.

Latex route

A latex is a colloidal suspension of submicronic polymer particles stabilized in water or in polar solvents by surfactants or steric stabilizers. Kusy was the first to formalize the concept of segregated network for the hot-pressing of dry mixtures containing polymers and metal powders in order to create conductive composites ^[165]. Polymer latexes can be used to create a segregated network by forcing the conductive particles into interstitial spaces between the polymer particles during drying ^[166]. Kim et al. proposed the following scheme to illustrate

the entrapment of carbon black particles between polymer particles during the film-forming process and the resulting network architecture (Figure 17).

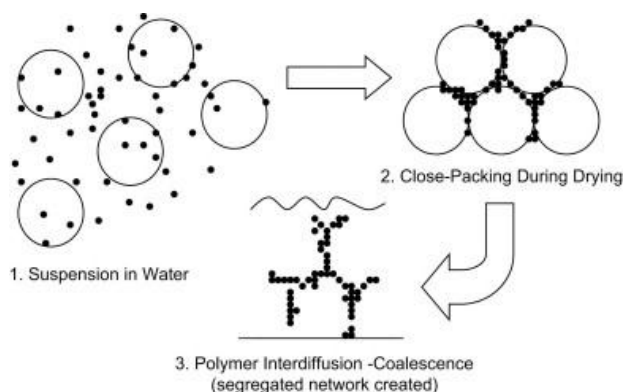


Figure 17. Scheme illustrating the production of polymer nanocomposites from an aqueous mixture of polymer particles and carbon black ^[167]

During water evaporation, the carbon black particles are entrapped between each polymer particles and this arrangement of the carbon filler induces the creation of percolating paths at low filler loadings.

For nanocomposite blends formulations, the latex route exhibits two major advantages compared to the melt or solution routes. First, this synthetic route is sustainable as a latex is made of polymer nanospheres in water suspension without using organic solvent. Second, the latex route favors the built-up of a tunable architecture of fillers. This specific architecture, in turn, favors the formation of a percolating network of fillers at lower filler contents ^[168]. As a result, the final nanocomposite microstructure counts two interpenetrated networks, one made of the polymer matrix and the other one made of percolating fillers ^[169].

2. Percolation description of latex-based composites

The percolation theory is used to describe very different transition phenomena such as sol-gel transition or virus propagation ^[170]. In materials science, it is often used to describe transitional behavior of electrical and mechanical properties in composites ^[18]. The critical volume fraction (percolation threshold) is the filler fraction needed to obtain the first percolating path throughout the polymer matrix. In a percolation approach, the fillers embedded in the composite are described using two types of clusters: the finite clusters and the infinite or percolating clusters, comprising a backbone and dangling bonds (Figure 18).

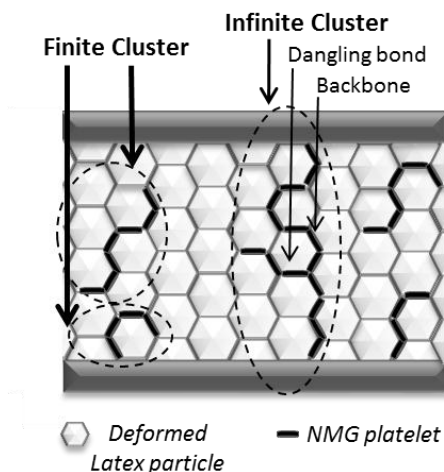


Figure 18. Percolation behavior in a latex-based graphene nanocomposite.

Graphene platelets as conductive fillers were chosen for geometrical considerations. In fact, platelet-like fillers (graphene) are a better compromise than fiber-like (carbon nanotubes) or spherical fillers (e.g. carbon black) to built-up an efficient network with polymer nanospheres. The use of platelet-like fillers favors surface contacts between fillers compared to fiber-like fillers and limits the total filler volume fraction compared to sphere-like fillers.

Ghislandi and coworkers^[171] studied the influence of various carbon-based fillers on the electrical properties of composites made from polypropylene (PP) latexes through physical blending followed by melt-compression. Figure 19 details the impact of the carbon-based fillers on the electrical properties. The shape of the filler, tubes (CNTs), platelets (Graphene) or spheres (carbon black), seems to have an impact on the percolation threshold (shown by dashed lines). Moreover, a decrease of the size dimensions of the carbon filler (between graphite and graphene) induces a sharp decrease of the percolation threshold.

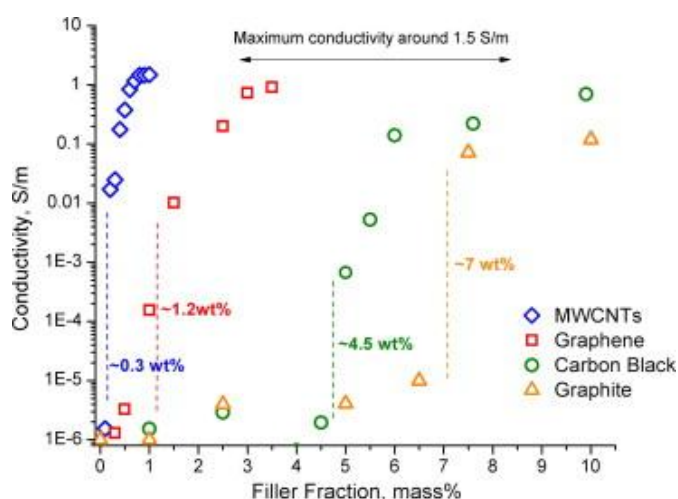


Figure 19. Impact of various carbon-based fillers on the electrical properties of PP nanocomposites^[171]

The size ratio between the polymer nanospheres and the fillers can be discussed as a compromise. On the one hand, the platelets have to be large enough to limit the number of

conductive platelets needed to cover the surface of the latex spheres and so the number of contacts. Indeed, intuitively, the contacts between fillers will have a lower conductivity than the intrinsic conductivity of the filler itself. On the other hand, the platelets have to be small enough in order not to destabilize the blend nor hinder the film formation process of the latex nanospheres.

Moriarty et al. studied the electrical properties of physical blends of P(MMA-co-BA) latex particles and carbon black ^[172] and found a correlation between the diameter of the latex beads and the percolation threshold (Figure 20). As expected, the percolation threshold decreased with an increase of the latex diameter.

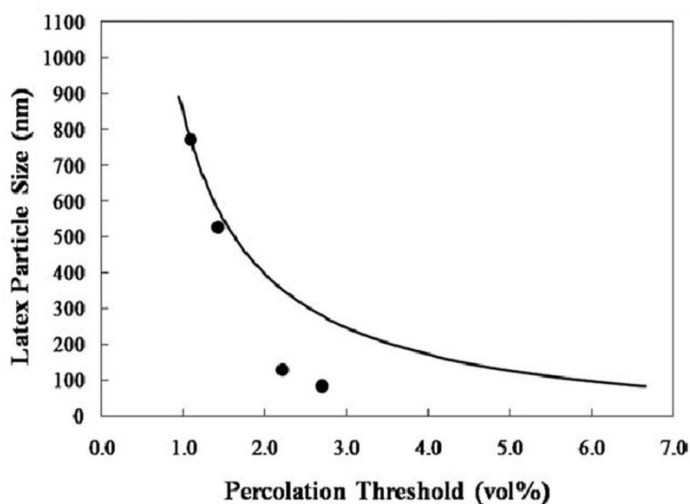


Figure 20. Percolation threshold as a function of carbon black concentration for different latex particle sizes^[166]

In this work, the nanocomposite architecture is tuned using a latex route ^[173]. Two routes are proposed to form graphene/latex nanocomposites: physical blending of blank latex particles and graphene platelets and *in-situ* polymerization in the presence of graphene.

3. Synthesis of polymer latexes

Latex particles are prepared via polymerization in dispersed media. Such polymerizations are classified into five different categories depending on the nucleation and polymerization mechanisms ^[175]:

- Emulsion polymerization
- Miniemulsion polymerization
- Dispersion polymerization
- Suspension polymerization and,
- Precipitation polymerization

The nucleation and polymerization mechanisms described in text books often correspond to ideal polymerization situations. Experimental conditions such as reactor setup, initiator, monomers, additives, etc. are finely chosen in order to promote one mechanism over another. In particular, the solubility of both the monomer and the initiator in the solvent plays an

important role on the nucleation and polymerization mechanisms and final size of the latex particles. The typical range of latex diameter obtained for each polymerization processes is detailed in Table 9. The main polymerization processes for the synthesis of graphene/latex nanocomposites are emulsion, miniemulsion and dispersion polymerizations. These three techniques will be described briefly in the following part. Emulsion and miniemulsion polymerization will induce the creation of polymer particles with a diameter between 50 and 500 nm, whereas dispersion polymerization allow the formation of particles with a diameter between 0.5 and 20 μm .

Table 9. Various synthesis ways and characteristics of the main polymerization processes used to form polymer latex particles

Polymerization process	Initiator	Monomer	Latex particle diameter
Emulsion	hydrosoluble	Hydrophobic	50 to 600 nm
Miniemulsion	hydrosoluble	Hydrophobic	50 to 500 nm
Dispersion	Soluble in the continuous phase	Soluble in the continuous phase	0.5 to 20 μm
Suspension	Oil-soluble	Hydrophobic	50 to 10,000 μm
Precipitation	hydrosoluble	hydrosoluble	Variable

In emulsion polymerization, surfactant, monomer and initiator are initially present in a heterogeneous aqueous medium where the monomers are non-water soluble. A water-soluble initiator is usually used to initiate the polymerization. In emulsion polymerization, surfactants are usually added in a concentration above the CMC, so that micelles are formed and serve as the polymerization loci. The monomer, which is partially hydrophobic, is partitioned in big reservoirs (droplets), inside the micelles and a small amount is present in the aqueous phase (left end side of Figure 21).

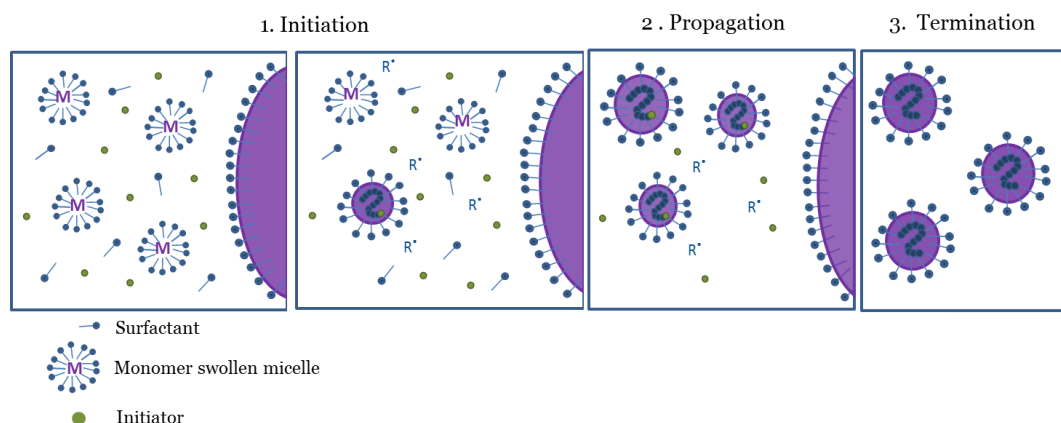


Figure 21. Schematic representation of the different stages of emulsion polymerization.

The water-soluble initiator can be decomposed thermally, photochemically or by the addition of an activator (redox) to form radicals in the aqueous phase. These radicals react with the monomer present in the water phase to form oligoradicals. These oligoradicals continue to grow by adding monomer units, until they reach a critical length for which they are no longer soluble in water, causing their migration to micelles or their precipitation depending on the nucleation mechanism. The polymerization continues inside the micelles, now called particles, swollen by monomer via diffusion of the monomer molecules from the droplets to the particle core. During polymerization, particles grow by gradual entry and consumption of monomer. Polymerization ends when the monomer is fully consumed. The size of the particles obtained ranges from 100 and 600 nm.

In miniemulsion polymerization, submicronic (50-500 nm) monomer droplets are obtained by using high-shear devices such as ultrasounds or high pressure homogenizers [176]. Miniemulsion droplets are stabilized against coalescence by using an appropriate surfactant, while monomer diffusion (*i.e.*, Ostwald ripening) can be in principle retarded using highly water-insoluble compounds (so-called hydrophobes) [177]. The nanodroplets will become the prevalent locus of nucleation [178] and each monomer droplets is converted into a polymer particle of identical chemical composition. Miniemulsion polymerization presents several advantages over emulsion polymerization: (i) there is no complex nucleation steps as in emulsion polymerization, (ii) the system exhibits only two phases throughout the polymerization reaction (the aqueous phase and the monomer/polymer particles), (iii) either an oil-soluble or a water-soluble initiator can be used and (iv) the final latex is theoretically a 1:1 copy of the initial droplets, allowing a direct control over the number of particles, although this is not always achieved in practice. Figure 22 details the miniemulsion polymerization mechanism.

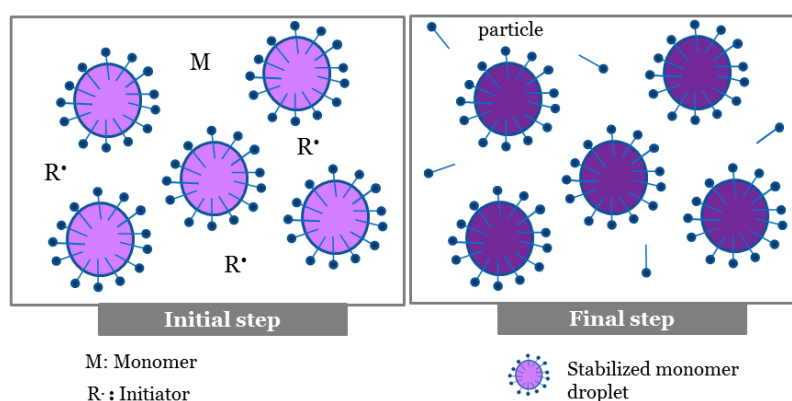


Figure 22. Initial and final state of the polymerization system in miniemulsion.

For the synthesis of bigger polymer particles, dispersion polymerization can be used. Dispersion polymerization in polar media can lead to the formation of polymer particles with a mean diameter comprised between 200 nm and 10 μm and a narrow particle size distribution [179]. In dispersion polymerization, the monomer and the initiator are both soluble in the polymerization medium; which is a poor solvent for the resulting polymer. Accordingly, the reaction mixture is homogeneous at the onset, and the polymerization is

initiated in homogeneous solution. Depending on the solvency of the medium for the resulting macroradicals and macromolecules, phase separation occurs at early or later stage. This leads to nucleation and the formation of primary particles. These primary particles may further coalesce until they have adsorbed enough stabilizers from the medium onto their surface to become sterically stabilized.

These three polymerization mechanisms will be detailed more precisely in Chapter 3 and 4. In the literature, polymer particles formed by emulsion or dispersion polymerization are mostly used for physical blending with multilayered graphene particles, whereas, *in situ* emulsion or miniemulsion polymerizations for graphene-based composites have been mostly developed with GO. As GO is partially hydrophobic, it can easily stabilize miniemulsion droplets or latex particles by adsorbing at their surface^[180]. Typically using this technique, the monomer is polymerized in the presence of GO platelets which take the place of the surfactant. Consequently, these syntheses were described as “Pickering” emulsion or “Pickering” miniemulsion polymerizations in reference to the stabilization of emulsions by inorganic particles first discovered by Ramden and Pickering in the 1900’s^[181].

Polymer latexes are essential components in a wide range of commercial products and formulation such as paints, cosmetics, inks and biotechnology. They can be used as is (*i.e.* in wet form), or in the dry form after coagulation.

Polymer latexes can also be processed into a continuous film possessing good mechanical strength through simple water evaporation. Film-forming is described by three main steps^[185] (Figure 23): water evaporation, particle compaction and polymer chain interdiffusion^[186]. First, the concentration step is characterized by evaporation of water and the latex particles concentrate to form a compact arrangement of spheres. At the end of this step, the solid content in the suspension is around 74% for monodisperse spheres. The evaporation rate is quasi constant but depends of many factors, such humidity, temperature or the surface of evaporation. In a second step, particles are compacted to form a dense network (compactness equal to 1) when residual water evaporates. This is the slowest process, deformation and evaporation, which controls this step^[187]. The last step is characterized by polymer chains interdiffusion. The polymer chains diffuse between inter-particles spaces. This step leads to a decrease of film permeability and increases the mechanical properties.

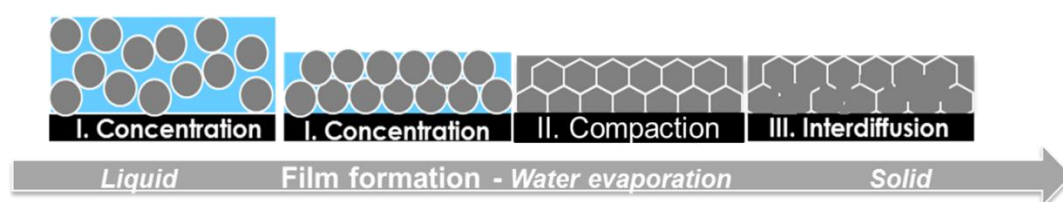


Figure 23. Different steps of the film-forming process: concentration, compaction and interdiffusion.

The use of polymer latex particles leads to a structured dispersion of the graphene platelets during the film-forming step. A short review of graphene/latex nanocomposites synthesis through physical blending or *in situ* polymerization is presented in the next part.

4. Nanocomposites via latex blending

The production of conductive nanocomposites through physical blending of a polymer latex with conductive particles such as CNTs^[188] or GO particles^[174] has been already reported by several authors.

Latex particles for physical blending can be made through different polymerization processes, in order to obtain various polymer beads diameters. In the following, we used $D_{\text{graphene}}/D_{\text{latex}}$ to define the size ratio between the FLG lateral size, D_{graphene} , and the latex beads diameter, D_{latex} . Figure 24 illustrates the influence of this parameter on the morphology of FLG/latex suspension and the microstructure of the corresponding nanocomposite after film formation. Intuitively, it can be anticipated that the final film properties will strongly depend on this microstructure and so on the relative dimensions of graphene and latex particles.

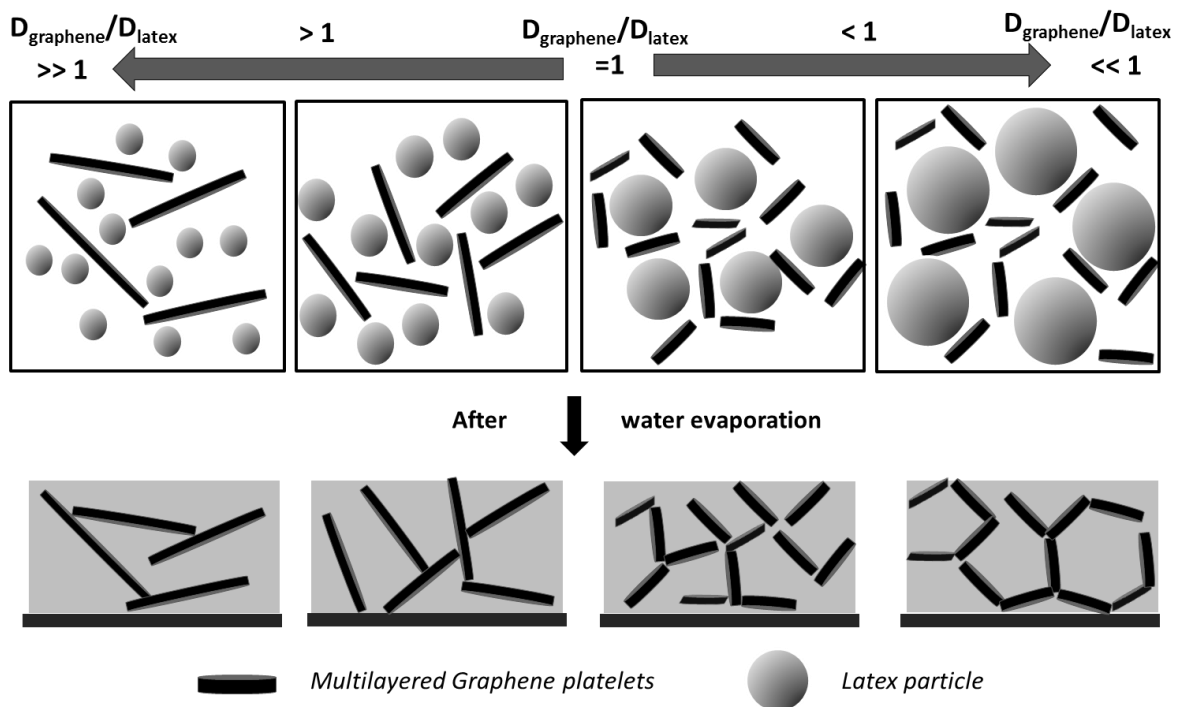


Figure 24. Evolution of the factor $D_{\text{graphene}}/D_{\text{latex}}$ depending on the NMG and latex particles sizes and the impact on the final microstructure of the film.

The $D_{\text{graphene}}/D_{\text{latex}}$ ratio should impact the final nanocomposite microstructure and thus the electrical properties. A neat cellular microstructure should be favored for $D_{\text{graphene}}/D_{\text{latex}} < 1$ and even more for $D_{\text{graphene}}/D_{\text{latex}} \ll 1$ while a $D_{\text{graphene}}/D_{\text{latex}}$ ratio higher than one should not give rise to conductive properties.

a. $D_{\text{graphene}}/D_{\text{latex}} > 1$

For $D_{\text{graphene}}/D_{\text{latex}} > 1$, the graphene platelets are larger than the latex nanospheres. This configuration does not favor the formation of a cellular microstructure. Many authors described physical blendings of large GO or rGO platelets and small latex particles. The physical blending is mainly performed in the presence of GO (with subsequent reduction into rGO after blending). Wu et al.^[174] reported the elaboration of rGO-latex composites by

coagulation of polystyrene latex particles (150-220 nm) and GO (1-2 μm in lateral size). The reduction of GO was operated after filtration (Figure 25a) by immersion of the solid into hydrogen iodide (HI) solution at 90°C for 24h. The final composite, obtained after hot pressing at 200°C exhibits high electrical conductivities, 1083 S m^{-1} . Scanning Electron Microscopy (SEM) images showed that the rGO was located around the latex beads (Figure 25b).

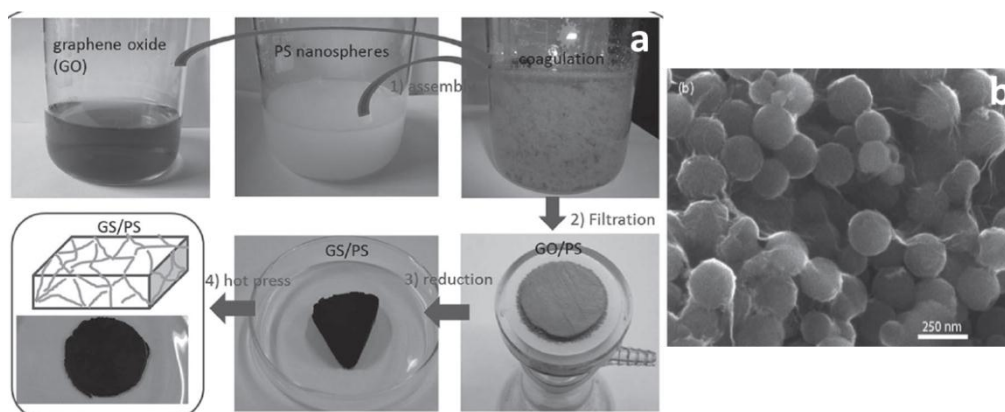


Figure 25. a- Preparation of PS/rGO nanocomposites by physical blending and b- SEM observation at 0.9 vol% of GO ^[174]

To favor the interaction between GO and the polymer particles, Pham and coworkers ^[190] prepared PMMA/rGO nanocomposites through electrostatic interaction between negatively charged GO and positively charged PMMA latex particles (using a cationic initiator during polymerization) synthesized by surfactant-free emulsion polymerization. GO is negatively charged in alkaline solution, due to the ionization of the phenolic hydroxyl and carboxylic acid groups ^[83]. Figure 26 illustrates the physical appearance of the suspension immediately after mixing and after the reduction with hydrazine.

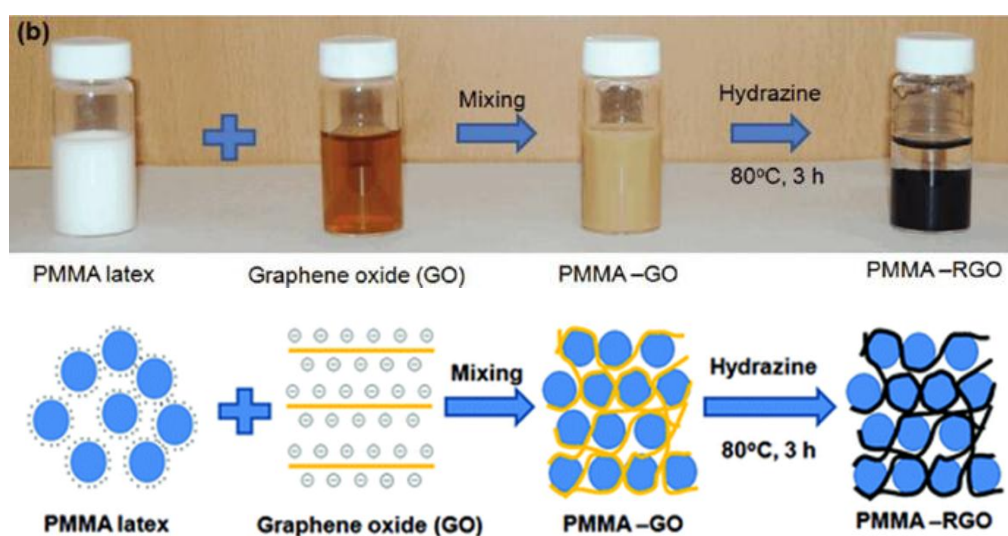


Figure 26. Schematic illustration of self-assembly of PMMA latex particles and GO, followed by hydrazine reduction of GO ^[190]

After addition of the hydrazine solution, sedimentation was observed. To measure the electrical properties, the blend was filtrated and compression molded at 210°C. SEM images showed the presence of rGO around the latex beads (Figure 27).

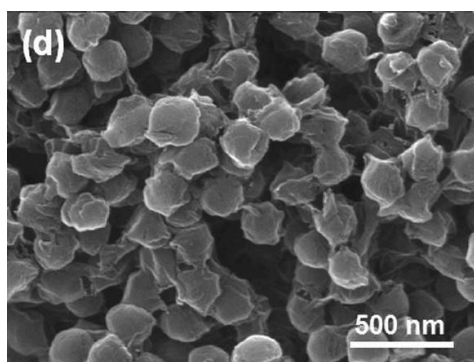


Figure 27. SEM image of PMMA-rGO nanocomposite blends obtained via electrostatic self-assembly at 4.0 wt.% rGO loading ^[190]

The nanocomposites obtained after compression molding exhibited a percolation threshold of 0.1 vol%, and a maximum electrical conductivity of 64 S m⁻¹ for 2.7 vol% of rGO.

The interactions between graphene platelets and polymer particles can also be favored by using a polymer with aromatic rings. As a consequence, π - π stacking interactions can be created between the multilayered graphene and the polymer particles. Li *et al.* described the formation of rGO/poly(styrene) nanocomposites ^[191]. The suspension obtained after GO reduction, with hydrazine monohydrate, was hot compressed resulting in a percolation threshold of 2 %wt and a maximum electrical conductivity of 2.5 S m⁻¹ for 8wt% of rGO.

These nanocomposites are not stable in suspension after GO reduction. To prevent this destabilization, Arzac *et al.* proposed a physical blending of PMMA-co-BA polymer particles and rGO platelets stabilized by a polymeric stabilizer (Poly (vinyl pyrrolidone), PVP) ^[120]. This copolymer can film-form at room temperature and the composite latex remained stable after physical blending.

The process and interactions between multilayered graphene and latex have a strong influence on the resulting nanocomposite electrical properties. Table 10 summarizes the percolation threshold and maximum conductivity for some selected examples.

As seen in Table 10, hot-pressing induces higher electrical conductivities than film-forming at room temperature. Moreover, the highest electrical conductivity is obtained for the nanocomposite that combine both electrostatic and π - π staking interactions between GO and the polymer particles and a hot-compression in the film-forming process.

Table 10. Electrical properties of graphene/latex nanocomposite obtained by physical blending

Latex		Filler		Composite		
Latex type	Polymerization process	Type of graphene used for blending step	Reduction step	$D_{\text{graphene}}/D_{\text{latex}}$	Percolation threshold and maximum conductivity ($S m^{-1}$)	Nanocomposite forming process
P(MMA-co-BA) (various ratios) ^[167]	Emulsion	Carbon black	-	5	4 vol% / 10 at 13 vol%	Film-forming at room temperature
P(MMA-co-BA) (50/50) ^[120]	Emulsion	rGO	-	3.3	Unknown/ 0.2 at 0.9 vol%	Film-forming at room temperature
PMMA ^[190]	Emulsion	GO	Hydrazine	50	0.1 vol% / 64 at 2.7 vol%	Compression molding at 210°C
PS ^[191]	Emulsion	GO	Hydrazine	10	2 wt% / 2.5 at 8 wt%	Dried and hot compressed
PS-NH₂ ^[174]	Emulsion	GO	Hydrogen Ionide (HI)	10-15	0.15 vol% / 1083 at 4.8 vol%	Hot pressing at 200°C

b. $D_{\text{graphene}}/D_{\text{latex}} \leq 1$

$D_{\text{graphene}}/D_{\text{latex}} < 1$ means that the diameter of the latex particle is larger than the lateral size of the graphene platelet. With NMG particles (of lateral size around 100 nm), polymer particle with a mean diameter larger than 1 μm must be formed. Dispersion polymerization is an attractive process for the synthesis of micron-size monodisperse polymer particles in a single batch process.

Zhao *et al.* and Long *et al.* described the physical blending of PVP-stabilized polystyrene microspheres, synthesized by dispersion polymerization in ethanol and GO suspensions. GO reduction was realized after blending using hydrazine^[192] or vitamin C solutions^[193], respectively. The electrical properties of the nanocomposites were measured after compression. In both cases, low percolation thresholds were obtained (0.08-0.09 vol% of rGO). A maximum conductivity of 20 $S m^{-1}$ was obtained for 1.2 vol%^[192] and 4 vol% of rGO respectively^[193].

To increase the electrically conductive properties of the composites and prevent graphene from aggregation, the distribution and uniformity of the graphene fillers inside the polymer was improved using a layer-by-layer (LBL) assembly approach^[194]. Polystyrene particles stabilized by PVP and SDS with a mean diameter around 2 μm were first synthesized. In parallel, a suspension of negatively charged GO and a suspension of positively charged GO (by grafting of polyethylenimine (PEI) on GO particles) were prepared. A first layer of PEI was coated on the PS microsphere to provide an uniformly and positively charged surface.

Then, negatively charged GO and positively charged GO-grafted-PEI suspensions were alternatively deposited on the PS microspheres through electrostatic interactions. The overall process and a SEM picture of the final nanocomposite particles obtained are reported on Figure 28.

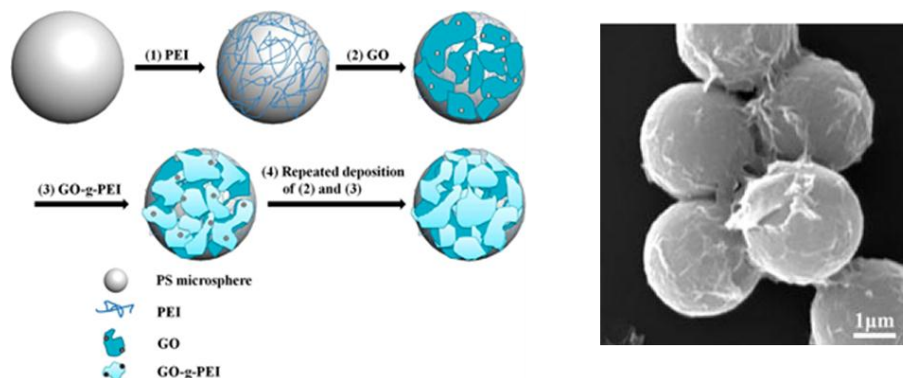


Figure 28. Schematic illustration of the deposition of oppositely charged GO onto PS microspheres via LBL assembly and SEM picture after three bilayers deposition ^[194]

The resulting nanocomposites were hot pressed and exhibited a percolation threshold near 0.9 vol% and a maximum conductivity of 0.05 S m^{-1} for 1.3 vol% of rGO: no noticeable enhancement compared to physical blending.

To improve the maximum electrical conductivity and lower the percolation threshold, Yang *et al.* proposed a strategy ^[195] to fabricate highly ordered 3D graphene-based composites. This process counts two steps: polymer microspheres are first wrapped with flexible GO particles by a thermodynamic driving heterocoagulation method and then GO is reduced using HI. These particles wrapped in graphene were then used as building blocks to construct a 3D multilayered graphene network by compression molding with additional thermal treatment. This method allowed to achieve a percolation threshold of 0.15 vol% of rGO and a maximum electrical conductivity of 500 S m^{-1} for 3.5 vol% of rGO which is higher than the values obtained in the previous strategies.

The percolation threshold and maximum conductivities obtained under $D_{\text{graphene}}/D_{\text{latex}} \leq 1$ conditions are gathered in Table 11.

Note that in most cases, compression is needed to form the final nanocomposite material prior to electrical measurements. Moreover, none of the nanocomposite suspensions were stable after the reduction of GO.

Table 11. Electrical properties of nanocomposite graphene/latex prepared by physical blending with $D_{\text{graphene}}/D_{\text{latex}} \leq 1$

Latex		Filler		Composite		
Latex type	Polymerization process	Type of graphene used for blending step	Reduction step	$D_{\text{graphene}}/D_{\text{latex}}$	Percolation threshold and maximum conductivity ($S m^{-1}$)	Nanocomposite forming process
PS ^[195]	Dispersion	GO	HI	0.45	0.15 vol%/500 for 3.5 vol%	Mold pressing at 130°C
PS (positively charged) ^[192]	Dispersion	GO	Hydrazine solution	1	0.09 vol%/25.2 for 1.2 vol%	Frozen dried and compressed
PS stabilized by PVP ^[193]	Dispersion	GO	Vitamin C	0.07-0.7	0.08 vol%/20.5 for 4 vol%	Hot pressing at 200°C
PS stabilized by PVP and SDS ^[194]	Dispersion	GO and GO-g-PEI	Hydrazine solution	0.2	0.9 vol%/0.05 for 1.3 vol%	Hot pressing at 180°C

To conclude, physical blending allows the elaboration of graphene/latex nanocomposite materials with high conductivity and low percolation threshold. The latex beads promote the dispersion of the filler in the polymer matrix. Nanocomposites with low $D_{\text{graphene}}/D_{\text{latex}}$ ratios exhibit lower percolation thresholds than nanocomposites issued from blends with high $D_{\text{graphene}}/D_{\text{latex}}$ ratios.

c. Conclusions

Nanocomposites obtained by physical blending can be divided into two categories, depending on the respective graphene and latex dimensions. In all these cases, the graphene sheets exhibits a mean lateral size around 1 μm . For polymer particles synthesized by emulsion polymerization, the polymer particles exhibit a mean diameter between 50 to 500 nm leading to $D_{\text{graphene}}/D_{\text{latex}}$ larger than 1. For polymer particles synthesized by dispersion polymerization, a mean diameter around 1 μm is obtained and consequently the $D_{\text{graphene}}/D_{\text{latex}}$ is smaller than one. $D_{\text{graphene}}/D_{\text{latex}}$ was shown to strongly influence the percolation threshold and maximum conductivity. In fact, an increase of this ratio induces a decrease of the percolation threshold and an increase of the maximum conductivity. Thus a favorable condition to produce efficient conductive composite is to use polymer particles with diameters larger than the lateral size of the conductive filler. In addition, hot-pressed nanocomposites exhibit higher conductivities than nanocomposites film-formed at room temperature.

5. Nanocomposites via *in situ* latex synthesis in the presence of GO or rGO particles

In situ polymerization in the presence of multilayered graphene is an approach which involves the polymerization of monomers in the presence of GO or graphene-based materials^[196]. This process can provide an enhancement of the graphitic filler dispersion within the polymer

matrix through the creation of both non-covalent (π - π stacking) and covalent bonding (functionalization) interactions between graphene and the polymer. The presence of fillers during the polymerization can also modify the polymerization mechanism. Many authors studied *in situ* polymerization in the presence of multilayered graphene via different polymerization processes. Emulsion and miniemulsion polymerizations are the mostly used polymerization processes found in the literature for the synthesis of these nanocomposites. Other processes, such as precipitation or suspension polymerization are more confidential. For instance, Dao *et al.* reported *in situ* suspension polymerization of methyl methacrylate (MMA) in the presence of sulfonate-functionalized graphene suspensions (obtained by reacting GO particles with potassium 2-aminoethanesulfonate) [197]. The graphene/sulfonate particles had a lateral size of 8.7 μm and the polymer particles obtained had a mean diameter between 50 and 200 μm , leading to a $D_{\text{graphene}}/D_{\text{latex}}$ ratio of 0.04-0.17. The electrical properties of the nanocomposite were measured after compression molding and a percolation threshold of 0.02 vol% was obtained. The maximum electrical conductivity was 15.7 S m^{-1} for 2.8 vol% of graphene/sulfonate. Thomassin *et al.* described the synthesis of rGO/PMMA nanocomposites via *in situ* precipitation polymerization of MMA in the presence of GO particles in a water/methanol mixture [198]. GO (with a lateral size of 100 nm) was acting as a surfactant and adsorbed on the interface between the PMMA particles and the solvent. The resulting products were thermally or chemically reduced and molded to obtain rGO/PMMA nanocomposites. The $D_{\text{graphene}}/D_{\text{latex}}$ ratio was between 0.1 and 0.5 resulting in a percolation threshold of 0.2 wt% and a maximum electrical conductivity of 10^{-2} S m^{-1} for 0.4 wt% of rGO.

The following part will detail only graphene/latex nanocomposites synthesized by *in situ* emulsion and miniemulsion polymerizations with a focus on the electrical properties of the resulting materials.

a. Emulsion polymerization

As described in section III.3, emulsion polymerization is a polymerization process which allows the formation of polymer particles with a mean diameter between 50 and 500 nm. Many authors described *in situ* emulsion polymerization in the presence of GO particles, where GO act as a sole surfactant due to its amphiphilic properties. These polymerizations are considered by the authors as “Pickering” emulsions.

Yin and coworkers reported the synthesis of GO/polystyrene nanocomposites with a final polymer particle diameter of 500 nm [199]. In this procedure, a mixture of GO suspension (0.25 mg mL^{-1}), initiator and monomer was polymerized 10 hours at 65°C. Figure 29 shows a SEM micrograph of the nanocomposite particles obtained. One platelet of GO can cover several polymer particles due to its large lateral size ($D_{\text{graphene}}/D_{\text{latex}}$ equal to 1.6-2.5).

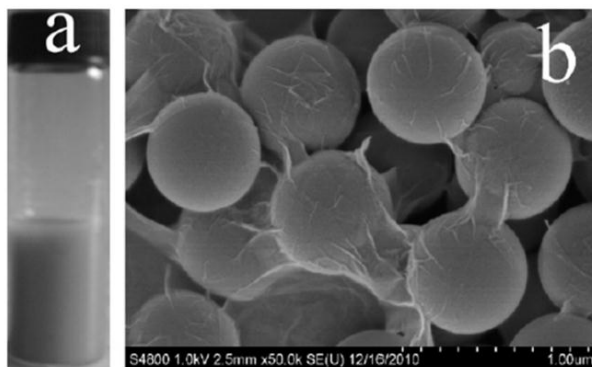


Figure 29. a- Digital photograph of a GO/PS suspension and b- SEM image of GO-coated PS nanospheres.

In reality GO is rarely used as the sole surfactant and surfactant is frequently added which leads to the formation of smaller polymer particles.

Ping *et al.* were the first to report *in situ* emulsion polymerization with GO suspension to obtain a nanocomposite with measureable electrical properties [200]. A mixture of monomer (MMA) and various amounts of GO were polymerized using potassium persulfate as an initiator and OP-10 as a nonionic surfactant. The high concentration of surfactant (30 g L^{-1}) led to the formation of small polymer particles, with a mean diameter of 100 nm. Reduction of GO platelets was performed after polymerization and the resulting nanocomposite was washed and dried at 50°C before electrical measurements. The polymer particles were smaller than the rGO platelets ($D_{\text{graphene}}/D_{\text{latex}}=10$) leading to a percolation threshold of 2 wt% and to maximum electrical conductivity of 10^{-2} S m^{-1} for 8 wt% of rGO.

Using the same polymerization process, Kuila *et al.* synthesized PMMA/rGO nanocomposites by emulsion polymerization of MMA in the presence of GO and 0.2 g L^{-1} of SDS, as a surfactant [201]. After polymerization, GO was reduced with hydrazine, dried and dissolved in chloroform for film casting by vacuum drying at 60°C . PMMA and rGO diameters are not specified in this article. An electrical conductivity of 1.5 S m^{-1} for 3 vol% of rGO was obtained. This higher conductivity, in comparison to the previous article, might be due to the nature and concentration of the surfactant which is lower. A lower surfactant concentration can lead to the formation of bigger polymer particles.

For these two syntheses, the nanocomposite suspensions were not stable after GO reduction. To avoid this destabilization, Arzac *et al.* proposed *in situ* emulsion polymerization directly in the presence of rGO particles [120]. Reduced graphene oxide was stabilized in water by PVP to increase the concentration of rGO up to 5 g L^{-1} . The authors compared the stability of the nanocomposite suspensions obtained by *in situ* polymerization with that of the nanocomposites formed by physical blending. The improved stability, found for *in situ* polymerization, was attributed to *in situ* grafting of the polymeric chains on the rGO surface. But no conductivity could be measured for these nanocomposites due to the low rGO concentration (1wt% of rGO). SEM images of the resulting materials are presented in Figure 30. One rGO sheet can cover many polymer particles and numerous percolating paths are visible on Figure 31.b despite the fact that there was no measurable electrical conductivities.

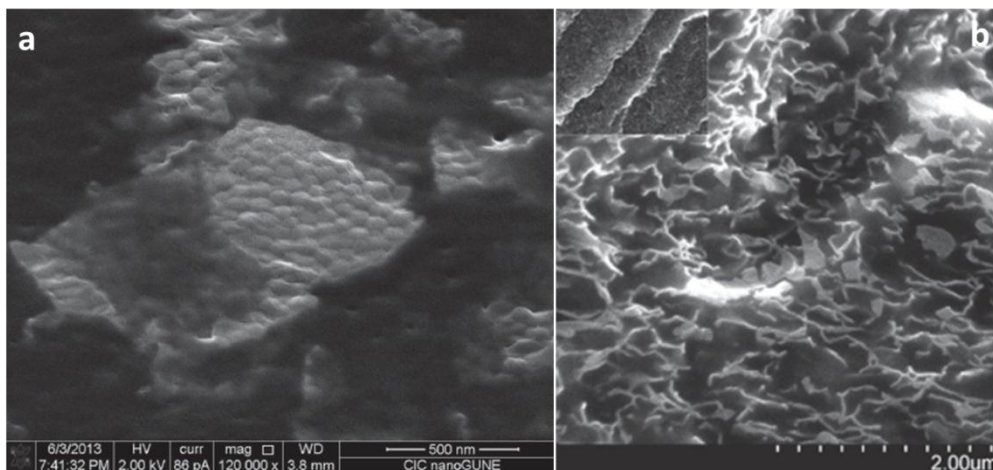


Figure 30. SEM images of P(MMA-co-BA)/rGO suspensions a-before film casting and b- after film casting (cross section) ^[120]

b. Miniemulsion polymerization

Few articles on graphene-based nanocomposite latexes through *in situ* miniemulsion polymerization are available in the literature. As said before, nanocomposite suspensions synthesized in the presence of GO are destabilized after GO reduction. To increase the stability of rGO/latex suspensions, surfactants are used during polymerization. But it induces a decrease of the final latex beads diameter which hinders the formation of the armored morphology. *In situ* miniemulsion polymerization, due to its different nucleation mechanism, will allow a better stability of the nanocomposite suspensions without adding a surfactant.

Recently, Yang *et al.* reported the synthesis of polystyrene colloidal particles using GO as stabilizer through miniemulsion polymerization ^[202]. In this Pickering polymerization procedure, the stabilized emulsion droplets act as reservoir in which the polymerization takes place. At the end of the polymerization, the composite polymer particles have a similar size than the initial droplets. Gudarzi *et al.* described a nice approach (though inadequately named “emulsion polymerization”) for efficient synthesis of PMMA/GO nanocomposites ^[203]. In this procedure, the mixture of monomer, GO suspension and initiator is emulsified using ultrasounds to help dispersion and promote GO exfoliation. Polymerization begins meanwhile and is maintained several hours. It was found that a concentration of 4wt% of GO is needed to stabilize the polymer particles. Below this concentration, GO platelets concentration is not sufficient to stabilize the polymer suspension and sedimentation occurs (Figure 31). The final armored polymer particles have a mean diameter of 300 nm.

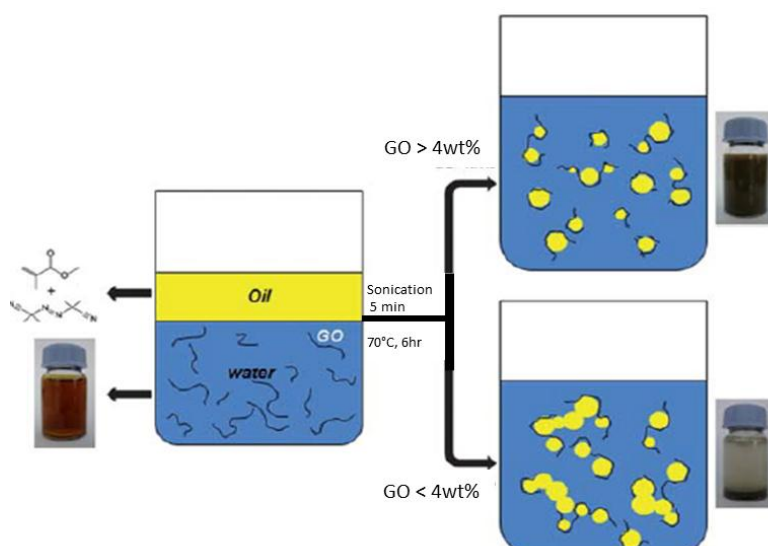


Figure 31. In situ “emulsion” polymerization in the presence of GO to form GO/PMMA nanocomposites at different concentrations of GO ^[203].

To create larger polymer particles and hence, decrease the $D_{\text{graphene}}/D_{\text{latex}}$ ratio, Che man *et al.* studied the influence of many polymerization parameters on the mean polymer particle diameter. They synthesized GO/polystyrene nanocomposites by *in situ* miniemulsion polymerization without adding surfactant ^[204]. A mixture of monomer, GO suspension, initiator (AIBN) and hexadecane (as the hydrophobe) were sonicated 10 minutes before polymerization. The final polymer particles had a mean diameter of 400 nm. Large polystyrene beads recovered by graphene sheets were obtained (Figure 32). The authors also studied the influence of the monomer polarity on the miniemulsion stability. The less polar monomers allowed the formation of more stable miniemulsion suspensions ^[205]. The amphiphilicity of GO can also be tuned by adjusting the pH or the ionic strength of the aqueous solution and led to the formation of larger polymer particles, which can reach a diameter of 3 μm depending of the polymerization conditions ^[206].

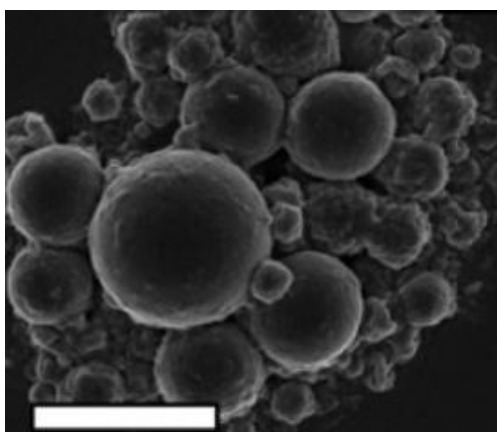


Figure 32. SEM image of PS/GO composite obtained by Che Man *et al.* ^[204] Scale bar: 2 μm .

To increase the stability of GO during the polymerization and the stability of the nanocomposites at the end of the polymerization in case of GO reduction, a surfactant can be

added (as for *in situ* emulsion polymerization). Etmimi *et al.* reported the synthesis of GO/poly (Sty-co-BA) nanocomposites by *in situ* miniemulsion^[207]. The monomer mixture, the GO suspension, the initiator (AIBN), hexadecane and a surfactant (SDBS, 2 g L⁻¹) were mixed and sonicated for 10 min. At the end of the polymerization, the final conversion was 90% and the polymer particles had a mean diameter of 150 nm. The $D_{\text{graphene}}/D_{\text{latex}}$ ratio was equal to 7.1. A maximum conductivity of 2.5 10⁻⁴ S m⁻¹ was obtained for 6wt% of rGO content.

Addition of surfactant in the polymerization reaction, despite the presence of GO to stabilize the suspension; will influence the final polymer particle diameter. Lee *et al.* synthesized graphite/PS nanocomposite by *in situ* miniemulsion polymerization in the presence of a suspension of large graphite platelets (5 μm of lateral size) stabilized by a surfactant (SDS at 2.5 g L⁻¹)^[208]. Miniemulsion polymerization was performed after sonication of mixture of styrene, initiator (AIBN), Graphite and surfactant. The $D_{\text{graphene}}/D_{\text{latex}}$ ratio was equal to 100. Small polymer particles (100 nm) dispersed on the graphite sheets were obtained (Figure 33).

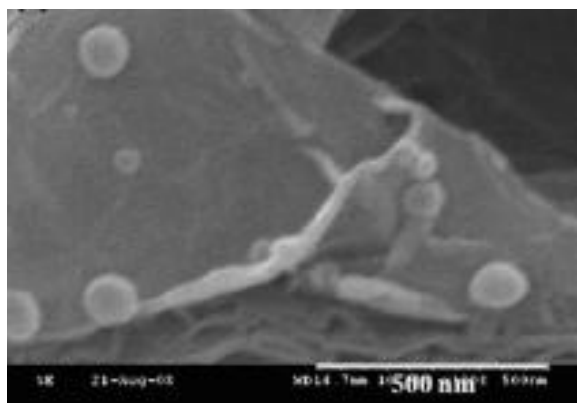


Figure 33. SEM micrograph of the PS/graphite nanocomposite produced by *in situ* miniemulsion polymerization in the presence of large graphite flakes^[208].

Despite the high concentration of graphite (10wt %), low electrical conductivity was obtained (8 10⁻³ S m⁻¹) in this case.

To increase the electrical performance of such nanocomposites, Tan *et al.* described the synthesis of conductive poly(sty-co-MMA)/rGO nanocomposites through the principle of double percolation^[209]. First, poly(sty-co-MMA)/GO nanocomposites are formed by *in situ* miniemulsion polymerization. The miniemulsion polymerization was carried out in the presence of γ -methacryloxy-propyl trimethoxysilane (MPS)-modified GO sheets using AIBN as initiator, OP-10 and SDBS as surfactants and DVB as crosslinker (Figure 34). The $D_{\text{graphene}}/D_{\text{latex}}$ ratio obtained was equal to 18. TEM micrograph of the nanocomposite is presented on Figure 35.

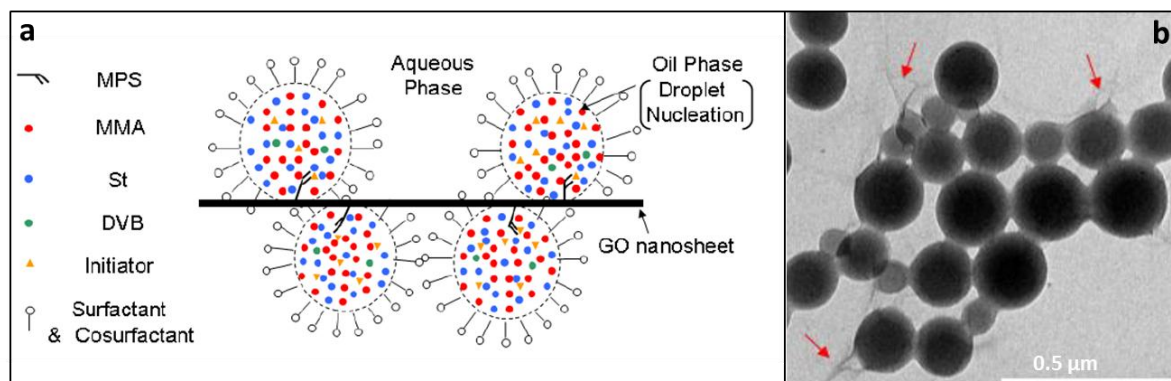


Figure 34. a- Scheme of *in situ* miniemulsion polymerization of Sty/MMA in the presence of MPS-modified GO and DVB as crosslinker and b- the TEM image of the resulting nanocomposite particles ^[209]

The nanocomposite particles were then washed, dried and redispersed in DMF to be mixed with a solution of polystyrene, poly(methyl methacrylate) and hydrazine (for GO reduction). Based on the double percolation principle, the fillers were reported to selectively distribute in one phase or concentrate at the interface of a continuous immiscible polymer blend due to the difference of affinity of the filler for each polymer. This procedure induced an interfacial distribution of the nanosheets in conductive polymer composites based on immiscible blends.

The electrical properties were measured after GO reduction and a low percolation threshold of 0.02 vol% of rGO was obtained. Furthermore, a maximum conductivity of 10^{-3} S m^{-1} was reached at 0.6 vol% of rGO.

c. Conclusion

To conclude, there are only few examples of GO or rGO/latex-based nanocomposites with enhanced electrical properties reported in the literature. Table 12 summarizes the nanocomposites synthesized by *in situ* polymerization in the presence of GO, rGO or graphite and their electrical properties.

GO is an interesting filler for *in situ* emulsion or miniemulsion polymerization due to its amphiphilic properties. But after its chemical reduction, rGO/latex nanocomposites do not remain stable in the suspension. Similarly to physical blends, lower conductivities are obtained for film-forming in comparison with compression-molding and higher conductivities are reached for $D_{\text{graphene}}/D_{\text{latex}}$ lower than 1, which favors the formation of armored nanocomposites.

Table 12. Nanocomposites made by in situ emulsion or miniemulsion polymerizations and their electrical properties.

Latex		Filler		Composite		
Latex type	Polymerization process	Type of graphene used for blending step	Reduction step	$D_{\text{graphene}}/D_{\text{latex}}$	Percolation threshold and maximum conductivity ($S m^{-1}$)	Nanocomposite forming process
PMMA ^[201]	Emulsion	GO	Hydrazine solution	-	- / 1.5 at 3 vol%	Dissolved in chloroform and film-casted
PS ^[199]	Emulsion	GO	-	1.6-2.5	-	-
P(MMA-co-BA) (50/50) ^[120]	Emulsion	rGO	-	3.3	-	Film-forming at room temperature
PMMA ^[200]	Emulsion	GO	Hydrazine solution	10	2 wt% / 10^{-2} at 8 wt%	Dried at 50°C
PMMA ^[203]	Miniemulsion	GO	-	10	-	-
PS ^[204]	Miniemulsion	GO	-	0.05-0.2	-	-
P(Sty-co-BA) (50/50) ^[207]	Miniemulsion	GO	Hydrazine solution	7.1	-	Film-forming at room temperature
PS ^[208]	Miniemulsion	Graphite	-	100	- / $8 \cdot 10^{-3}$ at 10% wt	Film-forming
P(MMA-co-Sty) ^[209]	Miniemulsion	GO	Hydrazine solution	18	0.02 vol% / 10^{-3} at 0.6 vol%	Film-forming at 50°C
PMMA ^[197]	Suspension	Sulfonate-modified graphene	-	0.04-0.17	0.02 vol% / 15.7 for 2.8 vol%	Compression molding 135°C
PMMA ^[198]	Precipitation	GO	-	0.1-0.5	0.2 wt% / $10^{-2} S m^{-1}$ over 0.4 wt%	Compression molding

Conclusions

To produce conductive nanocomposite, the latex route will be preferred among other approaches. Indeed, the presence of latex particles induces a specific filler dispersion through the concept of segregated networks and therefore lowers the percolation threshold. Two main ways of latex/graphene nanocomposites have been described in this chapter: physical blending and *in situ* polymerization in the presence of multilayered graphene.

Suspensions of carbon-based particles are an adequate choice due to their low cost compared to metallic fillers. In particular, Few Layered Graphene (FLG) as conductive filler is an interesting choice due to its shape, aspect ratio and excellent electrical properties without sintering. This filler combined with a polymer matrix can lead to the creation of conductive inks with low filler content. The production of FLG through different strategies and processes was detailed in this chapter. In particular, mechanical delamination of graphite in water seems appropriate in that a FLG suspension is obtained in output, which is adequate for further use with latex-based products. In addition, this method is quite straight forward and appears adequate for industrial scale-up. **Chapter 2** details the impact of the stabilizer on the NMG size dimensions while produced through mechanical delamination in water.

In the following, the experimental study of NMG/latex conductive nanocomposites produced through two processes is presented. First, **Chapter 3** presents the physical blending approach focusing on the impact of $D_{\text{graphene}}/D_{\text{latex}}$ parameter on the electrical and thermo-mechanical properties of the final nanocomposite. Then, in **Chapter 4**, *in situ* polymerization in the presence of NMG suspensions will be studied using three different polymerization processes: emulsion, miniemulsion and dispersion polymerizations. The electrical properties of the nanocomposites formed will be measured and compared to those of the nanocomposites obtained through physical blending.

References

- [1] X. M. Tao, *Smart Fibres, Fabrics and Clothing: Fundamentals and Applications*, Elsevier, **2001**.
- [2] S. L. P. Tang, G. K. Stylios, *Int. J. Cloth. Sci. Technol.* **2006**, *18*, 108.
- [3] M. Van Parys, in *Funct. Coat.* (Ed: S.K. Ghosh), Wiley-VCH Verlag GmbH & Co. KGaA, **2006**, pp. 221–258.
- [4] X. Zhang, in *Funct. Text. Improv. Perform. Prot. Health* (Eds: N. Pan, G. Sun), Woodhead Publishing, **2011**, pp. 27–44.
- [5] S. Mondal, in *Funct. Text. Improv. Perform. Prot. Health* (Eds: N. Pan, G. Sun), Woodhead Publishing, **2011**, pp. 163–183.
- [6] S. WAGNER, E. BONDEROVER, W. B. JORDAN, J. C. STURM, *Int. J. High Speed Electron. Syst.* **2002**, *12*, 391.
- [7] G. Cho, *Smart Clothing: Technology and Applications*, CRC Press, **2009**.
- [8] “Data logging compression shirt” can be found under http://www.northeastern.edu/news/stories/2010/02/baseball_shirt.html.
- [9] L. Buechley, M. Eisenberg, J. Catchen, A. Crockett, in *Proc. SIGCHI Conf. Hum. Factors Comput. Syst.*, ACM, New York, NY, USA, **2008**, pp. 423–432.
- [10] *Textile Fabric with Integrated Electrically Conductive Fibers and Clothing Fabricated Thereof*, **n.d.**
- [11] J. B. Lee, V. Subramanian, *IEEE Trans. Electron Devices* **2005**, *52*, 269.
- [12] “E-Textiles For Wearability: Review Of Integration Technologies,” can be found under http://www.textileworld.com/Issues/2010/April_Online_Issue/Features/E-Textiles_For_Wearability-Review_Of_Integration_Technologies, **n.d.**
- [13] S. Gimpel, U. Mohring, H. Muller, A. Neudeck, W. Scheibner, *J. Ind. Text.* **2004**, *33*, 179.
- [14] “Arjowiggin’s Powercoat® Wins Award,” can be found under <http://www.packagingeurope.com/Packaging-Europe-News/52875/Arjowiggins-Powercoat-Wins-Award.html>, **n.d.**
- [15] I. Jung, Y. H. Jo, I. Kim, H. M. Lee, *J. Electron. Mater.* **2012**, *41*, 115.
- [16] A. Chiolerio, M. Cotto, P. Pandolfi, P. Martino, V. Camarchia, M. Pirola, G. Ghione, *Microelectron. Eng.* **2012**, *97*, 8.
- [17] D. Stauffer, A. Aharony, *Introduction to Percolation Theory*, Taylor & Francis, **1994**.
- [18] E. Thommerel, J. C. Valmalette, J. Musso, S. Villain, J. R. Gavarrri, D. Spada, *Mater. Sci. Eng. A* **2002**, *328*, 67.
- [19] “The Gwent Group, Leaders in paste manufacturing, sensor/ biosensor development and Instrumentation.,” can be found under http://www.gwent.org/gem_index.html#, **n.d.**
- [20] A. Moscicki, J. Felba, P. Gwiazdzinski, M. Puchalski, in *6th Int. Conf. Polym. Adhes. Microelectron. Photonics 2007 Polytronic 2007*, **2007**, pp. 305–310.
- [21] J. Felba, H. Schaefer, in *Nanopackaging* (Ed: J.E. Morris), Springer US, **2008**, pp. 239–263.
- [22] B. Abeles, P. Sheng, M. D. Coutts, Y. Arie, *Adv. Phys.* **1975**, *24*, 407.

- [23] B.-H. Ryu, Y. Choi, H.-S. Park, J.-H. Byun, K. Kong, J.-O. Lee, H. Chang, *Colloids Surf. Physicochem. Eng. Asp.* **2005**, 270–271, 345.
- [24] S. Jang, H. Cho, S. Kang, S. Oh, D. Kim, *Appl. Phys. A* **2011**, 105, 685.
- [25] A. Russo, B. Y. Ahn, J. J. Adams, E. B. Duoss, J. T. Bernhard, J. A. Lewis, *Adv. Mater.* **2011**, 23, 3426.
- [26] Andreas Elschner, S. Kirchemeyer, Wilfried Lovenich, U. Merker, Knud Reuter, *PEDOT: Principles and Applications of an Intrinsically Conductive Polymer*, **2010**.
- [27] “On the conductivity of PEDOT:PSS thin films,” can be found under <http://www.tue.nl/en/publication/ep/p/d/ep-uid/217795/>, **n.d.**
- [28] H.-E. Yin, F.-H. Huang, W.-Y. Chiu, *J. Mater. Chem.* **2012**, 22, 14042.
- [29] J. Cho, K.-H. Shin, J. Jang, *Thin Solid Films* **2010**, 518, 5066.
- [30] Z. Xiong, C. Dong, H. Cai, C. Liu, X. Zhang, *Mater. Chem. Phys.* **2013**, 141, 416.
- [31] J. Rangel, A. del-Real, V. Castano, **2008**.
- [32] icecats, “Paper Electronics: Conductive Paints, Inks, and More,” can be found under <http://www.instructables.com/id/Paper-Electronics-Conductive-Paints-Inks-and-Mo/>, **n.d.**
- [33] A. Shimoni, S. Azoubel, S. Magdassi, *Nanoscale* **2014**, DOI 10.1039/C4NR02133A.
- [34] A. Denneulin, J. Bras, F. Carcone, C. Neuman, A. Blayo, *Carbon* **2011**, 49, 2603.
- [35] S. J. Park, S. T. Lim, M. S. Cho, H. M. Kim, J. Joo, H. J. Choi, *Curr. Appl. Phys.* **2005**, 5, 302.
- [36] M. Jakubowska, M. Sloma, A. Mlozniak, in *32nd Int. Spring Semin. Electron. Technol. 2009 ISSE 2009*, **2009**, pp. 1–5.
- [37] C. Lee, X. Wei, J. W. Kysar, J. Hone, *Science* **2008**, 321, 385.
- [38] Y. Zhang, Y.-W. Tan, H. L. Stormer, P. Kim, *Nature* **2005**, 438, 201.
- [39] N. A. Luechinger, E. K. Athanassiou, W. J. Stark, *Nanotechnology* **2008**, 19, 445201.
- [40] K.-Y. Shin, J.-Y. Hong, J. Jang, *Adv. Mater.* **2011**, 23, 2113.
- [41] R. Giardi, S. Porro, A. Chiolerio, E. Celasco, M. Sangermano, *J. Mater. Sci.* **2013**, 48, 1249.
- [42] D. Kong, L. T. Le, Y. Li, J. L. Zunino, W. Lee, *Langmuir* **2012**, 28, 13467.
- [43] F. J. Tölle, M. Fabritius, R. Mülhaupt, *Adv. Funct. Mater.* **2012**, 22, 1136.
- [44] M. Singh, H. M. Haverinen, P. Dhagat, G. E. Jabbour, *Adv. Mater.* **2010**, 22, 673.
- [45] D.-Y. Shin, Y. Lee, C. H. Kim, *Thin Solid Films* **2009**, 517, 6112.
- [46] D. Deganello, J. A. Cherry, D. T. Gethin, T. C. Claypole, *Thin Solid Films* **2010**, 518, 6113.
- [47] K. Reuter, H. Kempa, N. Brandt, M. Bartzsch, A. C. Huebler, *Prog. Org. Coat.* **2007**, 58, 312.
- [48] A. Blayo, B. Pineaux, in *Proc. 2005 Jt. Conf. Smart Objects Ambient Intell. Innov. Context-Aware Serv. Usages Technol.*, ACM, New York, NY, USA, **2005**, pp. 27–30.
- [49] S. Magdassi, *The Chemistry Of Inkjet Inks*, WORLD SCIENTIFIC, **2009**.
- [50] J. Mei, “FORMULATION AND PROCESSING OF CONDUCTIVE INKS FOR INKJET PRINTING OF ELECTRICAL COMPONENTS,” can be found under <http://d-scholarship.pitt.edu/9948/>, **2005**.
- [51] M. J. Allen, V. C. Tung, R. B. Kaner, *Chem. Rev.* **2010**, 110, 132.

- [52] K. S. Novoselov, A. K. Geim, S. V. Morozov, D. Jiang, M. I. Katsnelson, I. V. Grigorieva, S. V. Dubonos, A. A. Firsov, *Nature* **2005**, *438*, 197.
- [53] R. R. Nair, P. Blake, A. N. Grigorenko, K. S. Novoselov, T. J. Booth, T. Stauber, N. M. R. Peres, A. K. Geim, *Science* **2008**, *320*, 1308.
- [54] K. I. Bolotin, K. J. Sikes, Z. Jiang, M. Klima, G. Fudenberg, J. Hone, P. Kim, H. L. Stormer, *Solid State Commun.* **2008**, *146*, 351.
- [55] A. A. Balandin, S. Ghosh, W. Bao, I. Calizo, D. Teweldebrhan, F. Miao, C. N. Lau, *Nano Lett.* **2008**, *8*, 902.
- [56] A. H. Castro Neto, F. Guinea, N. M. R. Peres, K. S. Novoselov, A. K. Geim, *Rev. Mod. Phys.* **2009**, *81*, 109.
- [57] “Tuneable electronic properties in graphene - Nano Today,” can be found under <http://www.journals.elsevier.com/nano-today/featured-articles/tuneable-electronic-properties-in-graphene/>, **n.d.**
- [58] B. Shen, W. Zhai, C. Chen, D. Lu, J. Wang, W. Zheng, *ACS Appl. Mater. Interfaces* **2011**, *3*, 3103.
- [59] S. Stankovich, D. A. Dikin, G. H. B. Dommett, K. M. Kohlhaas, E. J. Zimney, E. A. Stach, R. D. Piner, S. T. Nguyen, R. S. Ruoff, *Nature* **2006**, *442*, 282.
- [60] Q. Duan, Y. Miura, A. Narumi, X. Shen, S.-I. Sato, T. Satoh, T. Kakuchi, *J. Polym. Sci. Part Polym. Chem.* **2006**, *44*, 1117.
- [61] J. Liu, L. Tao, W. Yang, D. Li, C. Boyer, R. Wuhrer, F. Braet, T. P. Davis, *Langmuir* **2010**, *26*, 10068.
- [62] T. Kuilla, S. Bhadra, D. Yao, N. H. Kim, S. Bose, J. H. Lee, *Prog. Polym. Sci.* **2010**, *35*, 1350.
- [63] H. J. Salavagione, M. A. Gómez, G. Martínez, *Macromolecules* **2009**, *42*, 6331.
- [64] Z. Liu, J. T. Robinson, X. Sun, H. Dai, *J. Am. Chem. Soc.* **2008**, *130*, 10876.
- [65] J.-Y. Wang, S.-Y. Yang, Y.-L. Huang, H.-W. Tien, W.-K. Chin, C.-C. M. Ma, *J. Mater. Chem.* **2011**, *21*, 13569.
- [66] T. A. Pham, N. A. Kumar, Y. T. Jeong, *Synth. Met.* **2010**, *160*, 2028.
- [67] P.-G. Ren, D.-X. Yan, T. Chen, B.-Q. Zeng, Z.-M. Li, *J. Appl. Polym. Sci.* **2011**, *121*, 3167.
- [68] G. Gonçalves, P. A. A. P. Marques, A. Barros-Timmons, I. Bdkin, M. K. Singh, N. Emami, J. Grácio, *J. Mater. Chem.* **2010**, *20*, 9927.
- [69] I. W. Frank, D. M. Tanenbaum, A. M. van der Zande, P. L. McEuen, *J. Vac. Sci. Technol. B* **2007**, *25*, 2558.
- [70] Z. Wang, R. Xie, C. T. Bui, D. Liu, X. Ni, B. Li, J. T. L. Thong, *Nano Lett.* **2011**, *11*, 113.
- [71] W. Chen, L. Yan, P. R. Bangal, *Carbon* **2010**, *48*, 1146.
- [72] H. Mousavi, J. Khodadadi, *Sci. World J.* **2014**, *2014*, e581478.
- [73] L. A. Falkovsky, *J. Phys. Conf. Ser.* **2008**, *129*, 012004.
- [74] H. J. Park, J. Meyer, S. Roth, V. Skakalova, *Carbon* **2010**, *48*, 1088.
- [75] K. Kalaitzidou, H. Fukushima, L. T. Drzal, *Compos. Sci. Technol.* **2007**, *67*, 2045.
- [76] L. M. Viculis, J. J. Mack, O. M. Mayer, H. T. Hahn, R. B. Kaner, *J. Mater. Chem.* **2005**, *15*, 974.

- [77] R. J. Young, I. A. Kinloch, L. Gong, K. S. Novoselov, *Compos. Sci. Technol.* **2012**, *72*, 1459.
- [78] S. Sivudu, Yashwant Mahajan, *NanoWerk* **2012**.
- [79] B. C. Brodie, *Philos. Trans. R. Soc. Lond.* **1859**, *149*, 249.
- [80] L. Staudenmaier, *Berichte Dtsch. Chem. Ges.* **1898**, *31*, 1481.
- [81] W. S. Hummers, R. E. Offeman, *J. Am. Chem. Soc.* **1958**, *80*, 1339.
- [82] L. Zhang, J. Liang, Y. Huang, Y. Ma, Y. Wang, Y. Chen, *Carbon* **2009**, *47*, 3365.
- [83] D. Li, M. B. Müller, S. Gilje, R. B. Kaner, G. G. Wallace, *Nat. Nanotechnol.* **2008**, *3*, 101.
- [84] Y. Si, E. T. Samulski, *Nano Lett* **2008**, *8*, 1679.
- [85] H. C. Schniepp, J.-L. Li, M. J. McAllister, H. Sai, M. Herrera-Alonso, D. H. Adamson, R. K. Prud'homme, R. Car, D. A. Saville, I. A. Aksay, *J Phys Chem B* **2006**, *110*, 8535.
- [86] M. J. McAllister, J.-L. Li, D. H. Adamson, H. C. Schniepp, A. A. Abdala, J. Liu, M. Herrera-Alonso, D. L. Milius, R. Car, R. K. Prud'homme, I. A. Aksay, *Chem Mater* **2007**, *19*, 4396.
- [87] W. Chen, L. Yan, P. R. Bangal, *J. Phys. Chem. C* **2010**, *114*, 19885.
- [88] X. Zhou, J. Zhang, H. Wu, H. Yang, J. Zhang, S. Guo, *J. Phys. Chem. C* **2011**, *115*, 11957.
- [89] M. J. Fernández-Merino, L. Guardia, J. I. Paredes, S. Villar-Rodil, P. Solís-Fernández, A. Martínez-Alonso, J. M. D. Tascón, *J. Phys. Chem. C* **2010**, *114*, 6426.
- [90] S. Dubin, S. Gilje, K. Wang, V. C. Tung, K. Cha, A. S. Hall, J. Farrar, R. Varshneya, Y. Yang, R. B. Kaner, *ACS Nano* **2010**, *4*, 3845.
- [91] Y. Zhang, H.-L. Ma, Q. Zhang, J. Peng, J. Li, M. Zhai, Z.-Z. Yu, *J. Mater. Chem.* **2012**, *22*, 13064.
- [92] H. Kim, A. A. Abdala, C. W. Macosko, *Macromolecules* **2010**, *43*, 6515.
- [93] S. Stankovich, D. A. Dikin, R. D. Piner, K. A. Kohlhaas, A. Kleinhammes, Y. Jia, Y. Wu, S. T. Nguyen, R. S. Ruoff, *Carbon* **2007**, *45*, 1558.
- [94] Y. Zhu, S. Murali, W. Cai, X. Li, J. W. Suk, J. R. Potts, R. S. Ruoff, *Adv. Mater. Deerfield Beach Fla* **2010**, *22*, 3906.
- [95] L. Buglione, E. L. K. Chng, A. Ambrosi, Z. Sofer, M. Pumera, *Electrochem. Commun.* **2012**, *14*, 5.
- [96] M. Cheng, R. Yang, L. Zhang, Z. Shi, W. Yang, D. Wang, G. Xie, D. Shi, G. Zhang, *Carbon* **2012**, *50*, 2581.
- [97] H.-B. Zhang, W.-G. Zheng, Q. Yan, Z.-G. Jiang, Z.-Z. Yu, *Carbon* **2012**, *50*, 5117.
- [98] Y. Hernandez, V. Nicolosi, M. Lotya, F. M. Blighe, Z. Sun, S. De, I. T. McGovern, B. Holland, M. Byrne, Y. K. Gun'Ko, J. J. Boland, P. Niraj, G. Duesberg, S. Krishnamurthy, R. Goodhue, J. Hutchison, V. Scardaci, A. C. Ferrari, J. N. Coleman, *Nat. Nanotechnol.* **2008**, *3*, 563.
- [99] D. E. Nixon, G. S. Parry, *J. Phys. Appl. Phys.* **1968**, *1*, 291.
- [100] A. Catheline, C. Vallés, C. Drummond, L. Ortolani, V. Morandi, M. Marcaccio, M. Iurlo, F. Paolucci, A. Pénicaud, *Chem. Commun.* **2011**, *47*, 5470.
- [101] U. Khan, H. Porwal, A. O'Neill, K. Nawaz, P. May, J. N. Coleman, *Langmuir* **2011**, *27*, 9077.

- [102] W. Zhao, F. Wu, H. Wu, G. Chen, *J. Nanomater.* **2010**, 2010, e528235.
- [103] X. An, T. Simmons, R. Shah, C. Wolfe, K. M. Lewis, M. Washington, S. K. Nayak, S. Talapatra, S. Kar, *Nano Lett.* **2010**, 10, 4295.
- [104] A. A. Green, M. C. Hersam, *Nano Lett.* **2009**, 9, 4031.
- [105] L. Guardia, M. J. Fernández-Merino, J. I. Paredes, P. Solís-Fernández, S. Villar-Rodil, A. Martínez-Alonso, J. M. D. Tascón, *Carbon* **2011**, 49, 1653.
- [106] M. Lotya, Y. Hernandez, P. J. King, R. J. Smith, V. Nicolosi, L. S. Karlsson, F. M. Blighe, S. De, Z. Wang, I. T. McGovern, G. S. Duesberg, J. N. Coleman, *J. Am. Chem. Soc.* **2009**, 131, 3611.
- [107] J. H. Lee, D. W. Shin, V. G. Makotchenko, A. S. Nazarov, V. E. Fedorov, Y. H. Kim, J.-Y. Choi, J. M. Kim, J.-B. Yoo, *Adv. Mater.* **2009**, 21, 4383.
- [108] C. Knieke, A. Berger, M. Voigt, R. N. K. Taylor, J. Röhr, W. Peukert, *Carbon* **2010**, 48, 3196.
- [109] M. Hirata, T. Gotou, S. Horiuchi, M. Fujiwara, M. Ohba, *Carbon* **2004**, 42, 2929.
- [110] N. R. Tummala, A. Striolo, *J. Phys. Chem. B* **2008**, 112, 1987.
- [111] V. K. Paruchuri, J. Nalaskowski, D. O. Shah, J. D. Miller, *Colloids Surf. Physicochem. Eng. Asp.* **2006**, 272, 157.
- [112] N. R. Tummala, B. P. Grady, A. Striolo, *Phys. Chem. Chem. Phys. PCCP* **2010**, 12, 13137.
- [113] E. J. Wanless, W. A. Ducker, *J. Phys. Chem.* **1996**, 100, 3207.
- [114] M. J. Fernández-Merino, J. I. Paredes, S. Villar-Rodil, L. Guardia, P. Solís-Fernández, D. Salinas-Torres, D. Cazorla-Amorós, E. Morallón, A. Martínez-Alonso, J. M. D. Tascón, *Carbon* **2012**, 50, 3184.
- [115] M. E. Uddin, T. Kuila, G. C. Nayak, N. H. Kim, B.-C. Ku, J. H. Lee, *J. Alloys Compd.* **2013**, 562, 134.
- [116] J. H. Lee, D. W. Shin, V. G. Makotchenko, A. S. Nazarov, V. E. Fedorov, J. H. Yoo, S. M. Yu, J.-Y. Choi, J. M. Kim, J.-B. Yoo, *Small* **2010**, 6, 58.
- [117] J. Han, H. Kim, D. Y. Kim, S. M. Jo, S.-Y. Jang, *ACS Nano* **2010**, 4, 3503.
- [118] M. J. O'Connell, P. Boul, L. M. Ericson, C. Huffman, Y. Wang, E. Haroz, C. Kuper, J. Tour, K. D. Ausman, R. E. Smalley, *Chem. Phys. Lett.* **2001**, 342, 265.
- [119] R. Shvartzman-Cohen, Y. Levi-Kalisman, E. Nativ-Roth, R. Yerushalmi-Rozen, *Langmuir* **2004**, 20, 6085.
- [120] A. Arzac, G. P. Leal, R. Fajgar, R. Tomovska, *Part. Part. Syst. Charact.* **2014**, 31, 143.
- [121] *Conductive Thin Film and Transparent Electrode Including Graphene Oxide and Carbon Nanotube, and Methods of Producing the Same*, n.d.
- [122] C. Semaan, G. Pecastaings, M. Schappacher, A. Soum, *Polym. Bull.* **2012**, 68, 465.
- [123] X. Wang, Y. Hu, L. Song, H. Yang, W. Xing, H. Lu, *J. Mater. Chem.* **2011**, 21, 4222.
- [124] X. Qi, K.-Y. Pu, H. Li, X. Zhou, S. Wu, Q.-L. Fan, B. Liu, F. Boey, W. Huang, H. Zhang, *Angew. Chem. Int. Ed.* **2010**, 49, 9426.
- [125] J.-L. Mura, G. Riess, *Polym. Adv. Technol.* **1995**, 6, 497.
- [126] G. Riess, *Colloids Surf. Physicochem. Eng. Asp.* **1999**, 153, 99.
- [127] L. S. Schadler, in *Nanocomposite Sci. Technol.* (Eds: P.M. Ajayan, L.S. Schadler, P.V. Braun), Wiley-VCH Verlag GmbH & Co. KGaA, **2003**, pp. 77–153.

- [128] Q. Cheng, B. Wang, C. Zhang, Z. Liang, *Small* **2010**, *6*, 763.
- [129] A. A. Mamedov, N. A. Kotov, *Langmuir* **2000**, *16*, 5530.
- [130] V. V. Ginzburg, O. V. Gendelman, L. I. Manevitch, *Phys. Rev. Lett.* **2001**, *86*, 5073.
- [131] J. R. Potts, D. R. Dreyer, C. W. Bielawski, R. S. Ruoff, *Polymer* **2011**, *52*, 5.
- [132] K. . Strawhecker, E. Manias, *Polymer Nanocomposites, Chapter 8: Nanocomposites Based on Water Soluble Polymers and Unmodified Smectite Clays*, Woodhead Publishing, **2006**.
- [133] P. Steurer, R. Wissert, R. Thomann, R. Mülhaupt, *Macromol. Rapid Commun.* **2009**, *30*, 316.
- [134] Munson-McGee, *Phys. Rev. B Condens. Matter* **1991**, *43*, 3331.
- [135] I. Balberg, N. Binenbaum, N. Wagner, *Phys. Rev. Lett.* **1984**, *52*, 1465.
- [136] N. Liu, F. Luo, H. Wu, Y. Liu, C. Zhang, J. Chen, *Adv. Funct. Mater.* **2008**, *18*, 1518.
- [137] J. Y. Jang, M. S. Kim, H. M. Jeong, C. M. Shin, *Compos. Sci. Technol.* **2009**, *69*, 186.
- [138] W.-P. Wang, C.-Y. Pan, *Polym. Eng. Sci.* **2004**, *44*, 2335.
- [139] H. Kim, C. W. Macosko, *Macromolecules* **2008**, *41*, 3317.
- [140] D. A. Nguyen, Y. R. Lee, A. V. Raghu, H. M. Jeong, C. M. Shin, B. K. Kim, *Polym. Int.* **2009**, *58*, 412.
- [141] J. Liang, Y. Wang, Y. Huang, Y. Ma, Z. Liu, J. Cai, C. Zhang, H. Gao, Y. Chen, *Carbon* **2009**, *47*, 922.
- [142] *Functional Graphene-Rubber Nanocomposites*, **n.d.**
- [143] *Coatings Containing Functionalized Graphene Sheets and Articles Coated Therewith*, **n.d.**
- [144] R. Verdejo, M. M. Bernal, L. J. Romasanta, M. A. Lopez-Manchado, *J. Mater. Chem.* **2011**, *21*, 3301.
- [145] D. Galpaya, *Graphene* **2012**, *01*, 30.
- [146] F. Leroux, J.-P. Besse, *Chem. Mater.* **2001**, *13*, 3507.
- [147] J. Ma, Q. Meng, I. Zaman, S. Zhu, A. Michelmoro, N. Kawashima, C. H. Wang, H.-C. Kuan, *Compos. Sci. Technol.* **2014**, *91*, 82.
- [148] A. S. Wajid, H. S. T. Ahmed, S. Das, F. Irin, A. F. Jankowski, M. J. Green, *Macromol. Mater. Eng.* **2013**, *298*, 339.
- [149] S. Araby, Q. Meng, L. Zhang, H. Kang, P. Majewski, Y. Tang, J. Ma, *Polymer* **2014**, *55*, 201.
- [150] V. H. Pham, T. V. Cuong, T. T. Dang, S. H. Hur, B.-S. Kong, E. J. Kim, E. W. Shin, J. S. Chung, *J. Mater. Chem.* **2011**, *21*, 11312.
- [151] X.-Y. Qi, D. Yan, Z. Jiang, Y.-K. Cao, Z.-Z. Yu, F. Yavari, N. Koratkar, *ACS Appl. Mater. Interfaces* **2011**, *3*, 3130.
- [152] V. Singh, D. Joung, L. Zhai, S. Das, S. I. Khondaker, S. Seal, *Prog. Mater. Sci.* **2011**, *56*, 1178.
- [153] H.-B. Zhang, W.-G. Zheng, Q. Yan, Y. Yang, J.-W. Wang, Z.-H. Lu, G.-Y. Ji, Z.-Z. Yu, *Polymer* **2010**, *51*, 1191.
- [154] H. Kim, Y. Miura, C. W. Macosko, *Chem. Mater.* **2010**, *22*, 3441.
- [155] R. Sengupta, M. Bhattacharya, S. Bandyopadhyay, A. K. Bhowmick, *Prog. Polym. Sci.* **2011**, *36*, 638.

- [156] F. de C. Fim, N. R. S. Basso, A. P. Graebin, D. S. Azambuja, G. B. Galland, *J. Appl. Polym. Sci.* **2013**, *128*, 2630.
- [157] D. Yoo, J. Kim, J. H. Kim, *Nano Res.* **2014**, *7*, 717.
- [158] S. N. Tripathi, P. Saini, D. Gupta, V. Choudhary, *J. Mater. Sci.* **2013**, *48*, 6223.
- [159] G. Chen, W. Weng, D. Wu, C. Wu, *Eur. Polym. J.* **2003**, *39*, 2329.
- [160] N. K. Srivastava, R. M. Mehra, *J. Appl. Polym. Sci.* **2008**, *109*, 3991.
- [161] M. Fang, K. Wang, H. Lu, Y. Yang, S. Nutt, *J. Mater. Chem.* **2010**, *20*, 1982.
- [162] M. Fang, K. Wang, H. Lu, Y. Yang, S. Nutt, *J. Mater. Chem.* **2009**, *19*, 7098.
- [163] S. H. Lee, D. R. Dreyer, J. An, A. Velamakanni, R. D. Piner, S. Park, Y. Zhu, S. O. Kim, C. W. Bielawski, R. S. Ruoff, *Macromol. Rapid Commun.* **2010**, *31*, 281.
- [164] Y.-S. Kim, K.-S. Liao, C. J. Jan, D. E. Bergbreiter, J. C. Grunlan, *Chem. Mater.* **2006**, *18*, 2997.
- [165] R. P. Kusy, *J. Appl. Phys.* **1977**, *48*, 5301.
- [166] J. C. Grunlan, W. W. Gerberich, L. F. Francis, *J. Appl. Polym. Sci.* **2001**, *80*, 692.
- [167] Y. S. Kim, J. B. Wright, J. C. Grunlan, *Polymer* **2008**, *49*, 570.
- [168] E. Tkalya, M. Ghislandi, A. Alekseev, C. Koning, J. Loos, *J. Mater. Chem.* **2010**, *20*, 3035.
- [169] A. Noël, J. Faucheu, M. Rieu, J.-P. Viricelle, E. Bourgeat-Lami, *Compos. Sci. Technol.* **2014**, *95*, 82.
- [170] C. Moore, M. E. J. Newman, *Phys. Rev. E* **2000**, *61*, 5678.
- [171] M. Ghislandi, E. Tkalya, B. Marinho, C. E. Koning, G. de With, *Compos. Part Appl. Sci. Manuf.* **2013**, *53*, 145.
- [172] G. P. Moriarty, J. H. Whittmore, K. A. Sun, J. W. Rawlins, J. C. Grunlan, *J. Polym. Sci. Part B Polym. Phys.* **2011**, *49*, 1547.
- [173] P. A. Steward, J. Hearn, M. C. Wilkinson, *Adv. Colloid Interface Sci.* **2000**, *86*, 195.
- [174] C. Wu, X. Huang, G. Wang, L. Lv, G. Chen, G. Li, P. Jiang, *Adv. Funct. Mater.* **2013**, *23*, 506.
- [175] J.-C. DANIEL, C. PICHOT, *Les latex synthétiques*, Tec & Doc Lavoisier, Paris, **2006**.
- [176] J. M. Asua, *Prog. Polym. Sci.* **2002**, *27*, 1283.
- [177] K. Landfester, *Macromol. Rapid Commun.* **2001**, *22*, 896.
- [178] K. Landfester, N. Bechthold, S. Förster, M. Antonietti, *Macromol. Rapid Commun.* **1999**, *20*, 81.
- [179] K. P. Lok, C. K. Ober, *Can. J. Chem.* **1985**, *63*, 209.
- [180] J. Kim, L. J. Cote, F. Kim, W. Yuan, K. R. Shull, J. Huang, *J. Am. Chem. Soc.* **2010**, *132*, 8180.
- [181] S. U. Pickering, *J. Chem. Soc. Trans.* **1907**, *91*, 2001.
- [182] P. Finkle, H. D. Draper, J. H. Hildebrand, *J. Am. Chem. Soc.* **1923**, *45*, 2780.
- [183] S. A. F. Bon, P. J. Colver, *Langmuir* **2007**, *23*, 8316.
- [184] E. Bourgeat-Lami, T. R. Guimarães, A. M. C. Pereira, G. M. Alves, J. C. Moreira, J.-L. Putaux, A. M. dos Santos, *Macromol. Rapid Commun.* **2010**, *31*, 1874.
- [185] Y. Chevalier, C. Pichot, C. Graillat, M. Joanicot, K. Wong, J. Maquet, P. Lindner, B. Cabane, *Colloid Polym. Sci.* **1992**, *270*, 806.
- [186] F. Dobler, T. Pith, Y. Holl, M. Lambla, *J. Appl. Polym. Sci.* **1992**, *44*, 1075.

- [187] P. R. Sperry, B. S. Snyder, M. L. O'dowd, P. M. Lesko, *Langmuir* **n.d.**, *10*, 2619.
- [188] J. Yu, K. Lu, E. Sourty, N. Grossiord, C. E. Koning, J. Loos, *Carbon* **2007**, *45*, 2897.
- [189] C. Wu, X. Huang, G. Wang, L. Lv, G. Chen, G. Li, P. Jiang, *Adv. Funct. Mater.* **2013**, *23*, 506.
- [190] V. H. Pham, T. T. Dang, S. H. Hur, E. J. Kim, J. S. Chung, *ACS Appl. Mater. Interfaces* **2012**, *4*, 2630.
- [191] H. Li, S. Wu, J. Wu, G. Huang, *Colloid Polym. Sci.* **2013**, *291*, 2279.
- [192] P. Zhao, Y. Luo, J. Yang, D. He, L. Kong, P. Zheng, Q. Yang, *Mater. Lett.* **2014**, *121*, 74.
- [193] G. Long, C. Tang, K. Wong, C. Man, M. Fan, W. Lau, T. Xu, B. Wang, *Green Chem.* **2013**, *15*, 821.
- [194] W. Fan, C. Zhang, W. W. Tjiu, T. Liu, *J. Mater. Res.* **2013**, *28*, 611.
- [195] L. Yang, Z. Wang, Y. Ji, J. Wang, G. Xue, *Macromolecules* **2014**, *47*, 1749.
- [196] K. Mylvaganam, L. Zhang, *J. Phys. Chem. C* **2013**, *117*, 2817.
- [197] T. D. Dao, G. Erdenedelger, H. M. Jeong, *Polymer* **2014**, *55*, 4709.
- [198] J.-M. Thomassin, M. Trifkovic, W. Alkarmo, C. Detrembleur, C. Jérôme, C. Macosko, *Macromolecules* **2014**, *47*, 2149.
- [199] G. Yin, Z. Zheng, H. Wang, Q. Du, H. Zhang, *J. Colloid Interface Sci.* **2013**, *394*, 192.
- [200] W. Wen-Ping, P. Cai-Yuan, *Polym. Eng. Sci.* **2004**, *44*, 2335.
- [201] T. Kuila, S. Bose, P. Khanra, N. H. Kim, K. Y. Rhee, J. H. Lee, *Compos. Part Appl. Sci. Manuf.* **2011**, *42*, 1856.
- [202] X. Song, Y. Yang, J. Liu, H. Zhao, *Langmuir* **2011**, *27*, 1186.
- [203] M. M. Gudarzi, F. Sharif, *Soft Matter* **2011**, *7*, 3432.
- [204] S. H. Che Man, S. C. Thickett, M. R. Whittaker, P. B. Zetterlund, *J. Polym. Sci. Part Polym. Chem.* **2013**, *51*, 47.
- [205] S. H. Che Man, N. Y. Mohd Yusof, M. R. Whittaker, S. C. Thickett, P. B. Zetterlund, *J. Polym. Sci. Part Polym. Chem.* **2013**, *51*, 5153.
- [206] S. H. Che Man, D. Ly, M. R. Whittaker, S. C. Thickett, P. B. Zetterlund, *Polymer* **2014**, *55*, 3490.
- [207] H. M. Etmimi, P. E. Mallon, *Polymer* **2013**, *54*, 6078.
- [208] J. Lee, J. Hong, S. E. Shim, D. Jung, *Macromol. Res.* **2009**, *17*, 931.
- [209] Y. Tan, L. Fang, J. Xiao, Y. Song, Q. Zheng, *Polym. Chem.* **2013**, *4*, 2939.

Chapter 2. Nanosize Multilayered Graphene (NMG): preparation and characterization

Introduction	50
I. Experimental procedures: wet-grinding of graphite suspensions.....	50
1. Description of the apparatus.....	51
2. Characterization of the graphite-NMG phase	53
3. Description of the surfactant phase	55
a. Determination of surfactant concentration in the NMG suspension	55
b. Surfactant adsorption mechanism	57
II. Influence of processing parameters.....	59
1. Influence of the size of the grinding beads	61
2. Surfactant: SDS vs. SDBS	64
3. Effect of delamination time.....	66
4. Effect of sonication and combination of sonication and wet grinding.....	67
a. Effect of the delamination process on the dimensions of the resulting NMG.....	67
b. Effect of the delamination process on the surface defects of the resulting NMG.....	68
5. Repeatability.....	69
6. Stability of the suspensions	70
III. Influence of the nature and concentration of stabilizer on NMG characteristics.....	71
1. Description of the experimental procedure	71
2. Effect of the type and concentration of stabilizers	72
a. SDBS	72
b. Sodium poly(styrene sulfonate) (PSSNa)	77
c. Poly(N-vinyl pyrrolidone) (PVP)	80
d. Polystyrene-block-polyethylene oxide (PS <i>b</i> P EO).....	82
Conclusions	85
References	86

Introduction

The interest for conductive nanoparticles, and more specifically for carbon nanotubes and graphene, has grown since the past ten years. These conductive fillers present many benefits in polymer-based nanocomposites for various applications, like printed electronics.

In this work, the challenge relies on the production of adequate conductive fillers with specific dimensional characteristics that do not destabilize the latex during physical blending or *in situ* polymerization in order to obtain conductive inks.

In the literature the most popular route to synthesize NMG is based on the so-called Hummer's method ^[1]. Despite its popularity, this method presents noticeable disadvantages as it relies on a long and multistep synthesis using many chemical products. In Hummer's method, Graphene Oxide (GO) is produced from graphite flakes and reduced into reduced graphene oxide (rGO). After this reduction step, some functional groups containing oxygen remain on the rGO surface ^[2]. These groups may affect both the interactions with the latex particles and the final electrical properties of the composite. As an alternative, Knieke *et al.* proposed a production of Nanosize Multilayered Graphene (NMG) based on the mechanical delamination of graphite flakes in wet grinding media ^[3]. This mechanical method is cost-effective and avoids organic solvents. The delamination process requires the use of a large amount of graphite flakes, but these are cheap and reusable raw materials. In our work, this procedure has been chosen and the NMG water suspensions were conveniently used as-is in the subsequent processing steps of the nanocomposite material. This process allows the creation of NMG suspensions stabilized by surfactants or steric stabilizers.

First, the experimental procedure and the main process parameters will be studied. Then, various surfactants and polymeric stabilizers will be used to exfoliate NMG and stabilize the platelets. The influence of the surfactant or polymeric stabilizer on the NMG dimensions and concentration in water will be investigated in each case.

I. Experimental procedures: wet-grinding of graphite suspensions

In this PhD work, the production of Nanosize Multilayered Graphene (NMG) through mechanical delamination has been preferred to the other techniques due to promising outputs in terms of scalability and NMG quality.

The experimental conditions used in this work derive mainly from a very detailed work performed by Knieke *et al.* ^[3] that proposes the production of multilayered graphene via wet-grinding of graphite in water stabilized by a surfactant (Sodium Dodecyl Sulfate, SDS). Surfactants are amphiphilic molecules: the hydrophilic part has some affinity with water whereas the hydrophobic part avoids water by adsorbing on the micrographite surface (and NMG formed). This phenomenon is at the origin of the stabilization of the carbon particles in water suspension. The surfactant concentration is above the critical micelle concentration (CMC) in order to have spare surfactant molecules to stabilize the additional graphitic surface created during the ball milling process.

This ball milling procedure allows a sharp decrease of the micrographite lateral size and an exfoliation of each micrographite sheet. The final dimensions of the graphene obtained strongly depend on the diameter of the grinding beads used. In their work, Knieke *et al.* used zirconia grinding beads with a mean diameter of 50 or 100 μm . The authors showed that increasing the grinding beads diameter induced a decrease of the mean lateral size of the graphene platelets but also increased the mean thickness of the delaminated sheets.

As our aim is to produce NMG with a lateral dimension between 100 nm to 300 nm and a minimum thickness, we have selected larger milling beads (400 μm or 800 μm). Basically, in our process, a mixture of micrographite and surfactant (or polymeric stabilizer) is dispersed in a water media (Figure 1). Polymeric stabilizers can create physical or chemical interactions with NMG and have therefore also been used to stabilize the micrographite particles during the delamination process. After stirring, the suspension is injected in a horizontal ball milling and grinded by zirconia yttrium beads of 400 μm or 800 μm diameter. At the end of the milling procedure, the suspension is decanted or centrifuged to remove the sediment, which contains the residual micrographite. In an industrial context, this micrographite could be reusable for another milling batch, however in this work; no graphite recycling was done for reproducibility sake. The supernatant containing the NMG and the surfactant (or stabilizer) is extracted and is used for physical blending with latex particles or *in situ* polymerization in order to form conductive nanocomposites.

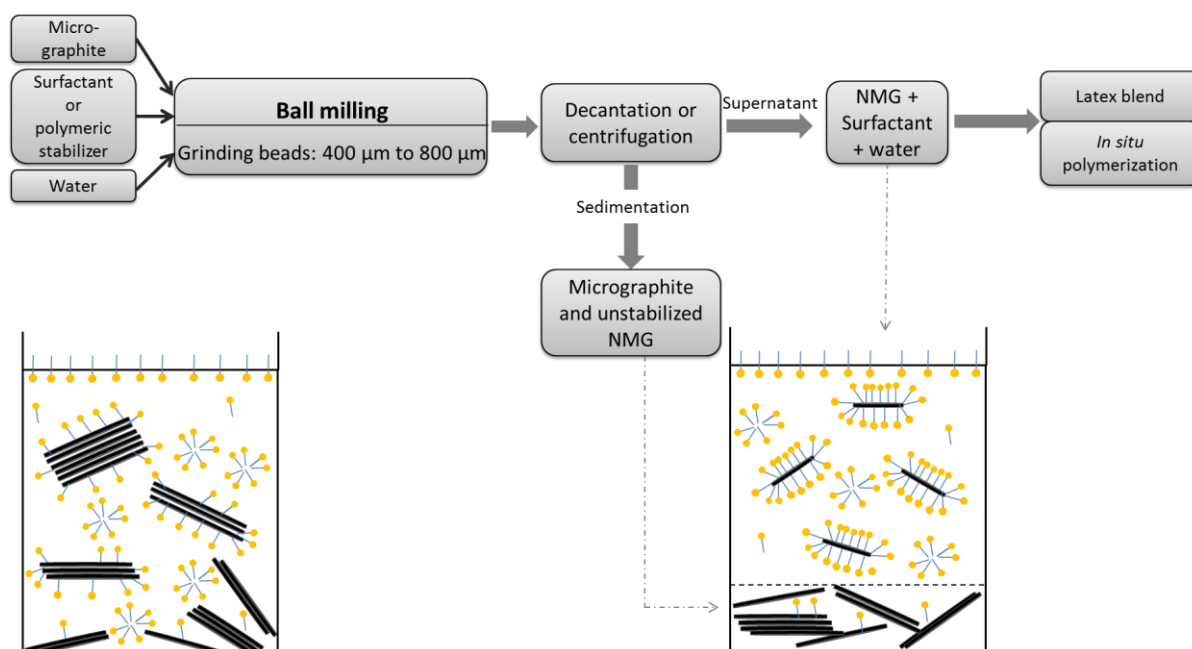


Figure 1. Scheme illustrating the wet ball-milling process and the repartition of the surfactant or stabilizer at the micrographite (and NMG formed) surface

1. Description of the apparatus

Zirconia is a hard ceramic material commonly used for grinding with a typical diameter from 50 μm to 1 mm. Approximately 200 mL of monodisperse Zirconia grinding beads (400 μm or

800 μm) are placed in the rotating reactor. The high shear energy of the ceramic beads is responsible for the exfoliation and break-up of the graphite flakes (Figure 2) [5].

Ball milling can generate two types of forces on layered materials, namely, shear force and compression force. The shear force can cleave layered materials from external surfaces, while the compression force peels off the thin nanosheets from the edges (Figure 2). During the thinning process, the ball milling energy does not cause significant damage to the in-plane structure of the nanosheets and generates only few defects and impurities [4].

In literature, sonication has also been demonstrated to be an efficient exfoliation procedure in a water media. It is known that sonication produces a number of effects on exfoliated nanosheets and layered materials (Figure 2): sonication-induced scission that can break larger crystallites into smaller crystallites and chipping off of 2D nanosheets from outer surfaces of layered materials [5]. In our experimental setup, a sonicator is added on the milling loop (Figure 3).

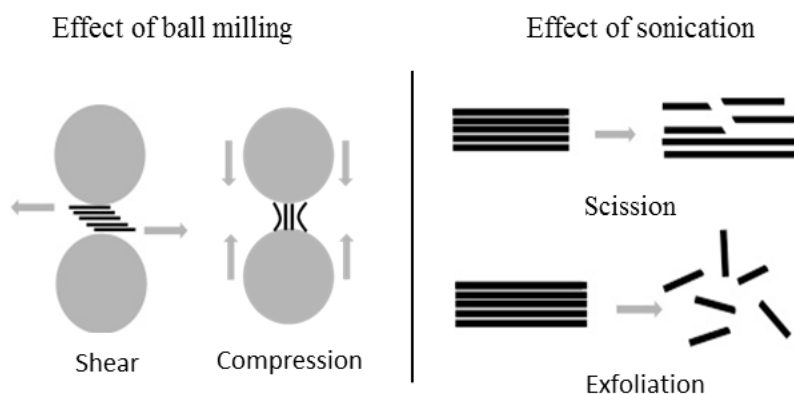


Figure 2. Effects of ball milling and sonication on graphite particles.

Experimental setup

Prior to the milling procedure, the graphite flakes (10% wt/water) and the surfactant (0.5 to 4% wt/water) were dispersed in water (400 mL) under stirring (with a roller stirrer) during 12 hours.

The grinding experiments were carried out in a horizontal laboratory stirred media mill (Minizeta, Netzsch Feinmahltechnik GmbH, Selb, Germany) at 1500 rpm, using Yttrium-stabilized zirconia oxide grinding beads (ZetaBeads Plus, 0.4 mm or 0.8 mm, Netzsch) as grinding media. A sonicator was added in the attritor loop to improve graphite flakes exfoliation and scission (Figure 3).

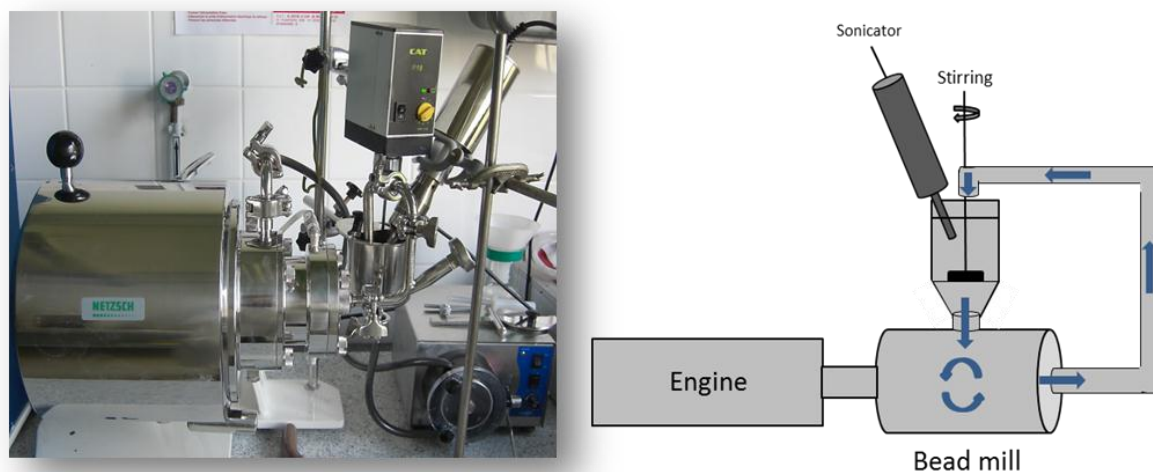


Figure 3. Picture and schematic representation of the horizontal laboratory stirred media mill used in this study.

Subsequent decantation removed the unexfoliated graphite, and finally NMG dispersions were obtained in aqueous suspensions.

2. Characterization of the graphite-NMG phase

The micrographite used for the wet grinding process exhibits a mean diameter of 7 to 10 μm . Figure 4 represents a SEM image of micrographite, which is clearly composed of multiple stacks of graphene sheets. Note that the graphene or FLG do not lie flat, but are curvy: it is known that FLG is a flexible filler. After grinding, the supernatant, containing NMG platelets and surfactant (or stabilizer), is isolated and characterized to measure the mean lateral size and thickness of the NMG produced.

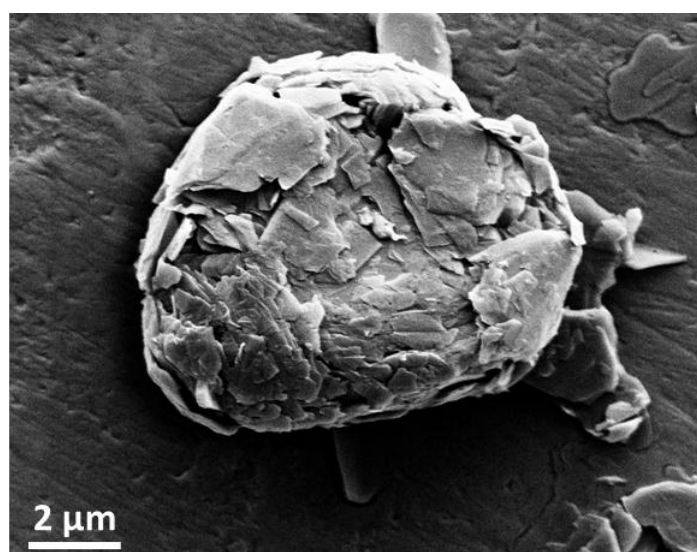


Figure 4. SEM image of micrographite before the ball milling process

Characterization of NMG size

The lateral dimensions of the NMG platelets are measured by two complementary characterization techniques, Dynamic Light Scattering (DLS) analysis and Atomic Force Microscopy (AFM) analysis. DLS analysis is performed on concentrated suspensions and provides an estimation of the mean diameter of the NMG platelets based on a model for spherical particles. The principle of this technique is described in Appendix I. For AFM analysis, the NMG suspension is spin-coated on silicon wafers and washed using deionized water prior to characterization (JPK Nanowizard 3). The washing step is performed to eliminate surfactant traces on the surface that might influence the AFM measurements. Using the AFM results, the thickness and lateral size of the NMG platelets are assessed by performing a statistical analysis on at least 150 NMG sheets from various areas of the silicon wafer. The results are gathered in an AFM histogram, containing n classes of lateral sizes (d_i), which represents the lateral size of NMG platelets vs. frequency (F_i) in percent.

Specific surface area

The NMG lateral size determined by AFM measurements is also used to calculate the specific surface area. In fact, the Brunauer–Emmett–Teller (BET) analysis cannot give access to the specific surface area of the NMG formed due to the presence of residual surfactant (or stabilizer) trapped within the platelets. When a large part of the surfactant is removed, the NMG platelets can be restacked and as a consequence the real specific surface area cannot be measured. Consequently, the surface area is calculated theoretically using the results from AFM histograms and Equation 1 to determine the total surface area $Surface_{tot}$ (NMG) that takes into account the area of both the faces and edges of NMG platelets.

$$Surface_{tot}(NMG) = \sum_{i=1}^n (F_i \times \frac{\pi d_i^2}{2} + F_i \times \pi d_i e) \quad \text{Equation 1}$$

Where e is the average thickness of the NMG platelets. The specific area is given by dividing this total surface by the total weight m_{tot} of these NMG (Equation 2, 3).

$$S_{spe} = \frac{Surface_{tot}(NMG)}{m_{tot}} \quad \text{Equation 2}$$

$$m_{tot} = Volume_{tot} \times \rho_{NMG} = \sum_{i=1}^n (F_i \times \frac{\pi d_i^2}{4}) \times e \times \rho_{NMG} \quad \text{Equation 3}$$

Where ρ_{NMG} is the density of NMG platelets ($\rho_{NMG} = 2.23 \text{ g cm}^{-3}$).

Quantification of defects and oxygen-containing groups

ThermoGravimetric Analyses (TGA) gives the mass loss vs. temperature during thermal decomposition under a controlled atmosphere. Typical TGA curves under air atmosphere obtained for GO, rGO and Graphite or Graphene are illustrated in Figure 5. For a graphite sample or graphene with a perfect carbon structure, the degradation of the carbon skeleton occurs at around 800-1000°C^[8]. This decomposition temperature decreases with the presence of structure defects in the carbon structure^[9]. Few examples of structure defects have been

added on Figure 5, with the presence of pentene cycle or zigzag configurations instead of a benzene cycle. For GO, this mass loss is visible around 500°C and a mass loss at lower temperature (170-250°C) [6] is attributed to the pyrolysis of the labile oxygen-containing groups in the forms of CO, CO₂ and steam [7].

TGA of NMG suspensions after mechanical delamination can give insights of the amount of remaining oxygen-containing groups (mass loss around 200°C) or structure defects (mass loss around 500°C) in the NMG platelets during the delamination process. This information is useful to optimize the experimental conditions in order to minimize the presence of defects or oxygen-containing groups. Indeed, the presence of defects or oxygen-containing groups can degrade NMG conductive performances.

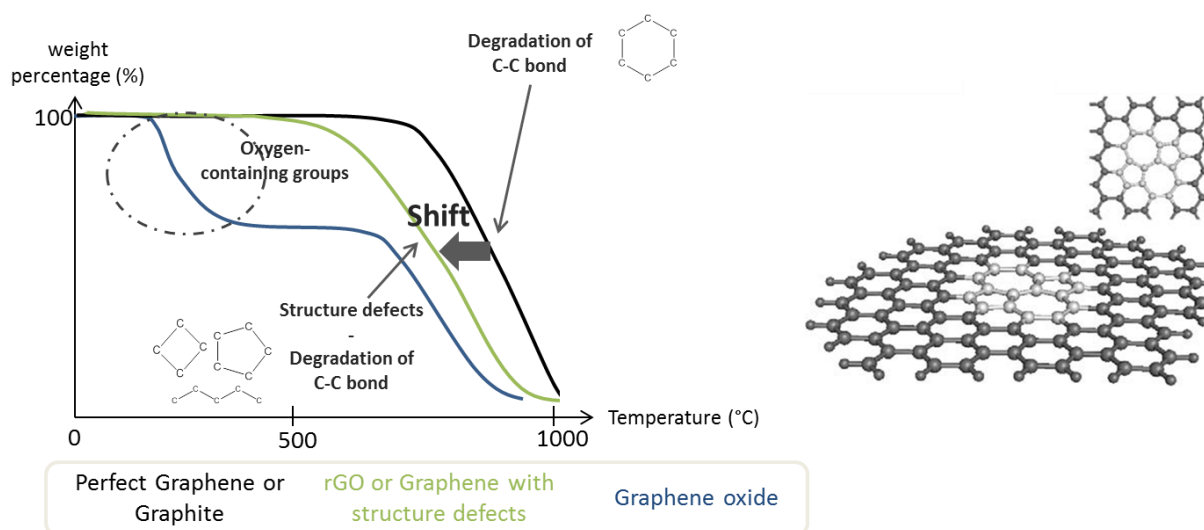


Figure 5. Schematic TGA curves for perfect graphene, graphene with structure defects and graphene oxide components, [6] and schematic representation of structure defects in the graphene structure.

Reprinted from Collins et al. [10].

3. Description of the surfactant phase

a. Determination of surfactant concentration in the NMG suspension

After mechanical delamination and decantation of the suspensions, the supernatant is collected. Few milliliters of this supernatant are dried at 100°C. The dry residue obtained contains both NMG and surfactant. Elemental analysis (EA) and TGA are used to determine the amount of surfactant present in the powder and then in the NMG/surfactant suspension. Depending on the surfactant nature, the adequate methods are chosen to evaluate the surfactant content.

Elemental analysis

Elemental analysis gives the content of each atom (carbon, hydrogen, oxygen...) in the dried suspension. For example, for Sodium Dodecyl Benzene Sulfonate (SDBS), the surfactant content %SDBS_{powder} can be calculated from the sulfur content, %S, using Equation 4. Each SDBS molecule counts one sulfur atom (Figure 6) and NMG counts no sulfur atom.

$$\%SDBS_{\text{powder}} = \frac{\%S \times M_{SDBS}}{N_{Sulfur}^{SDBS} M_{sulfur}} \quad \text{Equation 4}$$

Where N_{Sulfur}^{SDBS} represents the number of sulfur atoms per surfactant molecule ($N_{Sulfur}^{SDBS}=1$) and $M_{sulfur}= 32 \text{ g mol}^{-1}$ and $M_{SDBS}= 348.4 \text{ g mol}^{-1}$ are the molar masses of sulfur and SDBS, respectively.

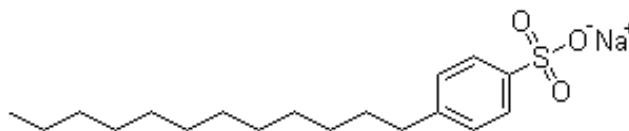


Figure 6. Chemical representation of Sodium Dodecyl Benzene Sulfonate (SDBS)

TGA

In our work, TGA was used to determine the amount of surfactant contained in the NMG suspension. Knowing that the NMG skeleton starts decomposing around 500°C , TGA curves are only usable at lower temperatures. We define $W_{\text{surfactant}}(500^{\circ}\text{C})$ as the weight loss measured on the TGA curve of pure surfactant at 500°C and $W_{\text{NMG}}(500^{\circ}\text{C})$ as the weight loss on the TGA curve of the sample containing both NMG and surfactant at 500°C (Figure 7). $W_{\text{NMG}}(500^{\circ}\text{C})$ can be attributed to the surfactant weight loss but also to the decomposition of oxygen-containing groups of NMG. This latter can be neglected as very few oxygen-containing groups are expected in NMG. $\% \text{Surfactant}_{\text{powder}}$ is obtained by dividing $W_{\text{NMG}}(500^{\circ}\text{C})$ by $W_{\text{surfactant}}(500^{\circ}\text{C})$.

As an example, for a NMG/SDBS suspension, the SDBS content in the powder, $\%SDBS_{\text{powder}}$, is determined using Equation 5. The weight loss (%) for the NMG/SDBS sample at 500°C , $W_{\text{NMG}}(500^{\circ}\text{C})$, is divided by the weight loss for the sample containing only the surfactant, $W_{\text{SDBS}}(500^{\circ}\text{C})$.

$$\%SDBS_{\text{powder}} = \frac{W_{\text{NMG}}(500^{\circ}\text{C})}{W_{\text{SDBS}}(500^{\circ}\text{C})} \times 100 \quad \text{Equation 5}$$

The surfactant content in the powder will then be used to determine the concentration of surfactant in the NMG suspension, $[\text{Surfactant}]$ in g L^{-1} , given the solids content of the NMG/surfactant suspension.

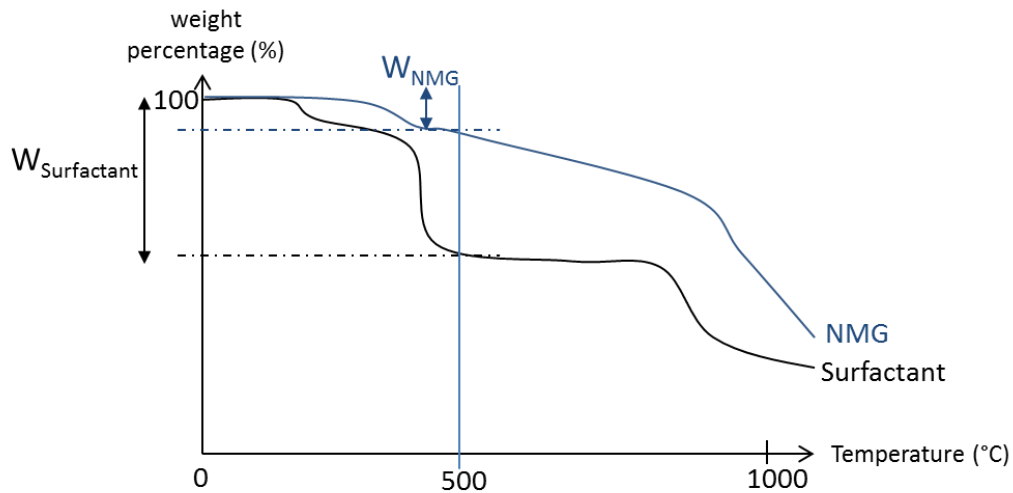


Figure 7. Schematic representation of a TGA curve for the determination of the %Surfactant_{powder}

b. Surfactant adsorption mechanism

The surfactant distribution between the aqueous phase, the air-liquid interface and the NMG platelets is measured using a Wilhelmy plate immersed in the liquid, which wets the plate upwards (Figure 8). The surface tension acts along the perimeter of the plate and the liquid pulls the plate.

The pulling force is measured and allows the determination of the surface tension, γ (in mN m^{-1}), using Equation 6.

$$P = L \cdot \gamma \cdot \cos \theta + C \quad \text{Equation 6}$$

With P the pulling force, L the perimeter of the plate, θ the contact angle between the plate and the liquid and C a constant which takes into account the plate weight and buoyancy.

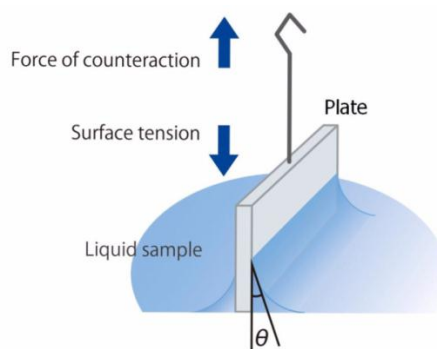


Figure 8. Scheme of the surface tension measurement.

The presence of surfactant reduces the surface tension. In a system consisting of only surfactant molecules in water, the Critical Micelle Concentration (CMC) is described by the aggregation of surfactant into micelles and corresponds to the concentration for which there is no more enrichment in surfactant at the water-air interface, *i.e.* the surface tension does not reduce further above the CMC (Figure 9). In a system composed of surfactant and NMG in water, a dynamic equilibrium exists between the free surfactant molecules in solution,

surfactant molecules located at the air-water interface and those adsorbed on the surface of the NMG. As the concentration of surfactant increases, adsorption takes place at both air-water interface and the NMG surface until both surfaces are fully covered. Micelles then form at concentrations exceeding the surfactant CMC in water. This apparent CMC (CMC_{app} , mol L⁻¹) depends on the amount of NMG and on the extent of adsorption. Similarly to the definition of CMC, on a surface tension vs. concentration curve, the start of the plateau marks the CMC_{app} . For a given NMG content, the difference between CMC and CMC_{app} is assumed to be equal to the total concentration of surfactant adsorbed on NMG surfaces at saturation^[11], meaning the maximum quantity of surfactant that can be adsorbed on the total surface of nanoplatelets. The amount of surfactant adsorbed per NMG square meter, Γ_{sat} (g m⁻²), is then given by Equation 7^{[12] [13]}.

$$\Gamma_{sat} = \frac{(CMC_{app} - CMC) \times M_{SDBS}}{S_{spec}[NMG]} \quad \text{Equation 7}$$

With $[NMG]$ the concentration of NMG platelets in g L⁻¹, M_{SDBS} (g mol⁻¹) the molar mass of SDBS and S_{spec} (g m⁻²) the NMG specific surface area.

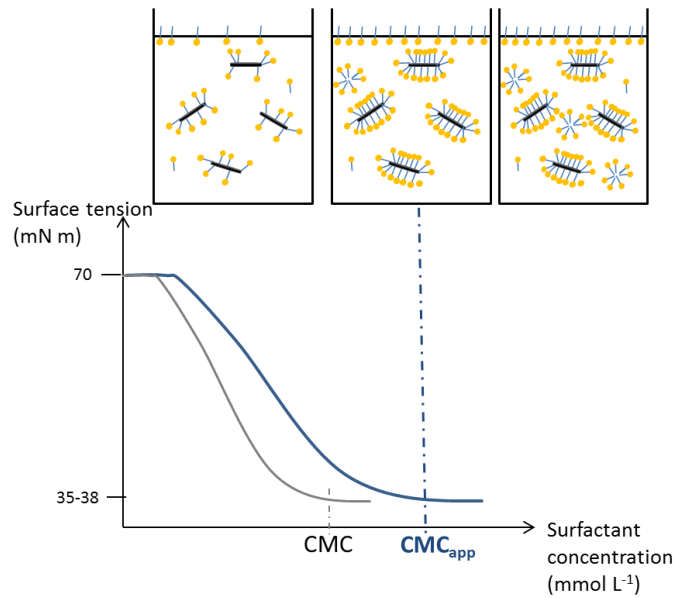


Figure 9. Scheme of the CMC_{app} measurement by surface tension measurements.

Then, the concentration of surfactant adsorbed on NMG ($[SDBS]_{NMG}$, g L⁻¹) and free surfactant ($[SDBS]_{free}$, g L⁻¹) can be calculated using Equations 8 and 9.

$$[SDBS]_{NMG} = \Gamma_{sat} \times [NMG] \times S_{spec} \quad \text{Equation 8}$$

$$[SDBS]_{water} = [SDBS]_{tot} - [SDBS]_{NMG} \quad \text{Equation 9}$$

Surfactants commonly used to stabilize Carbon Nanotubes (CNT) and graphene suspensions are Sodium Dodecyl Sulfate (SDS) and SDBS. The chemical structures of these two surfactants are presented in Figure 10 and their main characteristics are given in Table 1. The hydrophobic tail of SDBS counts an aromatic ring in addition to the dodecyl chain, which is not present in the case of SDS. Several authors have demonstrated that SDBS can better stabilize the NMG platelets than SDS in water suspensions ^[14].

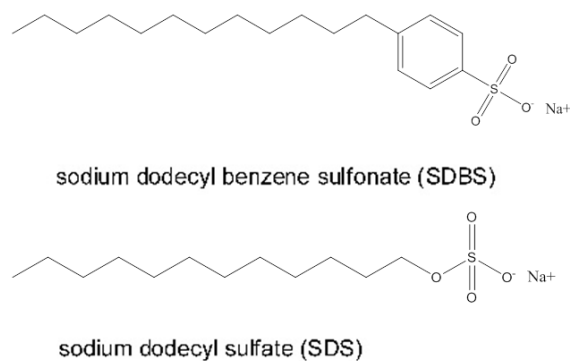


Figure 10. Chemical structures of SDS and SDBS

Table 1 describes the differences of chain length and of the mean diameter of the polar head for both surfactants. These parameters have an influence on the CMC, as reported by Yan et al. ^[15]. These authors have studied the interactions of surfactant and polymer for the surfactants C_nSO_4 , with a sulfate head, and C_nSO_3 , with a sulfonate head. They demonstrated that the surfactants C_nSO_4 are more negatively charged than C_nSO_3 and as a consequence, stronger electrostatic interactions might be formed between the polymer and the surfactant with a $-SO_4$ head. SDS molecules possess a larger head diameter than SDBS molecules, and as a consequence less surfactant molecules can be added per NMG platelets. The large diameter of the polar head of SDS combined with a small chain length induces also a higher CMC than SDBS molecules (Table 1).

Table 1. SDS and SDBS main characteristics

Surfactant	Diameter of the polar head	Chain length	CMC (mmol L ⁻¹)
SDS	9.4 Å ^[16]	17 Å ^[16]	8.3 ^[17]
SDBS	6.9 Å ^[18]	24 Å ^[18]	1.08 ^[19]

Moreover, many authors described the self-assembly structures of SDS on carbon nanotube ^[20] and graphite ^[21] surfaces (Figure 12a). These two surfactants have a similar adsorption behavior on graphitic surfaces, but the aromatic rings present on SDBS can create additional π - π interactions with the planar aromatic structure of graphene ^[22].

The conformation of SDS molecules on the graphitic surfaces has been studied by Knieke et al. The authors used SDS as a surfactant to stabilize the graphite particles, and the multilayered graphene platelets formed during the delamination process. In this article, the adsorption of SDS on graphite particles was studied and the results are shown in Figure 11.

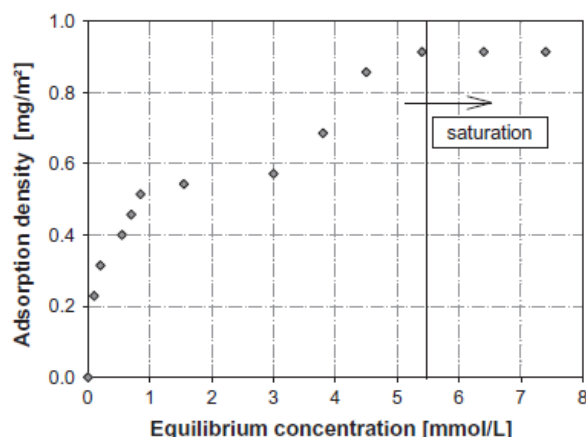


Figure 11. Adsorption isotherm of SDS on graphite particles in water according to Knieke et al.

The adsorption isotherm exhibits two plateau regions. This effect is described as a conformation change of SDS molecules on the graphitic surfaces ^[23]. At the lower plateau, the molecules lie parallel to the graphite surface resulting in a lower packing density. With increasing SDS concentration the conformation changes to hemicylinders arrangement. Self-assembly structures (hemicylinders) (Figure 12b) of adsorbed surfactants on graphite surfaces were shown to form strong alignment with the graphite symmetry axis. Similarly to the model of epitaxial adsorption on graphite, the adsorption mechanism on nanotube walls (graphene) was suggested to produce self-organization of surfactant molecules.

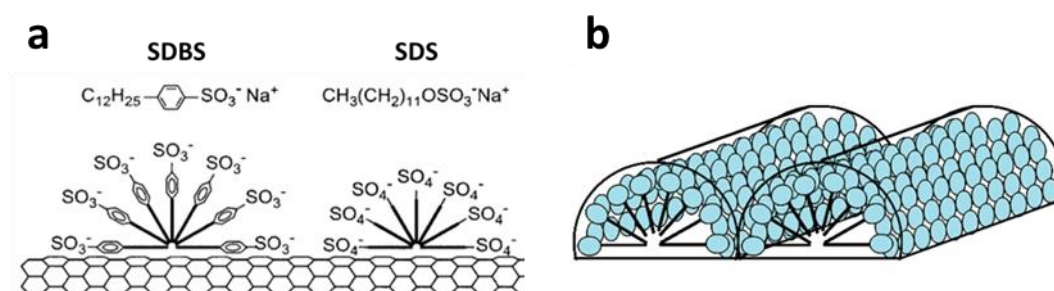


Figure 12. a) Schematic representation of how SDS and SDBS surfactants may adsorb onto nanotubes ^[24], and b) hemicylinders representation of surfactant adsorption at the graphene surface ^[25].

In this work, SDS (Sodium Dodecyl Sulfate) is used as a surfactant to stabilize graphite and a concentration above the CMC (Critical Micellar Concentration) is needed because an important surface area of graphene was created during the delamination process. This newly developed surface (NMG platelets) needs thus to be stabilized by the surfactant during the process.

The delamination process described in this part will be used to create NMG suspensions stabilized by a surfactant or a stabilizer. The characterization techniques described in Appendix I will be systematically used to determine the NMG dimensions (thickness, lateral size) and properties (defects, specific surface area); and to determine the concentration and

repartition of the surfactant in the NMG suspensions. In the following part, the main processing parameters and their influence on the NMG dimensions and properties are studied.

II. Influence of processing parameters

Table 2 summarizes the experiments performed in this preliminary part. The experimental conditions, namely the grinding beads diameter, the surfactant and graphite concentration, the delamination time and ball milling procedure, are indicated for each experiment. The parameters studied are the diameter of the grinding beads, the ball milling process (combination of wet grinding and sonication) and the delamination time for two different surfactants, SDS and SDBS. The stability and repeatability of the formed NMG suspensions are also studied.

Each sample is named according to the following convention with each segment of information separated by a slash or a dash. Segments 1 and 2 designate the type of graphene and stabilizer used, segment 3: the concentration of stabilizer in g L^{-1} and segment 4: the size of the grinding beads or the type of delamination process (WG for wet grinding, S for sonication and WG/S for wet grinding and sonication). For example, NMG/SDBS-5-400 indicates a NMG suspension elaborated by wet grinding in the presence of 5 g L^{-1} of SDBS using grinding beads of $400 \mu\text{m}$ diameters.

Table 2. Processing conditions used to produce NMG/SDS suspensions.

Sample name	Grinding beads diameter (μm)	[Surfactant] (g L^{-1})	Graphite concentration (wt%)	Delamination time (hours)	Ball milling procedure
NMG/SDS-5-400	400	5	10	4	Wet grinding
NMG/SDS-5-800	800	5	10	4	Wet grinding
NMG/SDBS-5-WG	400	5	10	4	Wet grinding
NMG/SDBS-5-WG/S	400	5	10	4	Wet grinding and sonication
NMG/SDBS-5-S	400	5	10	4	Sonication

For each experiment, the studied parameter is indicated in bold.

1. Influence of the size of the grinding beads

Knieke et al. [3] studied the effect of two grinding beads, $50 \mu\text{m}$ and $100 \mu\text{m}$ on the production of NMG/SDS suspensions. The authors showed that increasing the grinding beads diameter induced a decrease of the mean lateral size of the NMG platelets but also increased the mean thickness of the delaminated sheets.

As our aim is to produce NMG with a lateral dimension between 100 nm and 300 nm, and the minimum thickness, we have selected large milling beads. Two experiments were realized using zirconia grinding beads with a mean diameter of either 400 μm or 800 μm under otherwise the same operating conditions as Knieke *et al.*, and so without sonication. The suspensions obtained were centrifuged and the supernatant was extracted for characterizations.

Observations of the NMG morphology were first performed using SEM analysis (Figure 13). Graphite platelets have been sharply exfoliated and the NMG platelets produced using 800 μm grinding beads have a lower lateral size than the NMG platelets made through grinding with 400 μm beads. To confirm this trend, DLS and AFM were performed on both suspensions to determine the mean thickness and lateral size of the NMG platelets.

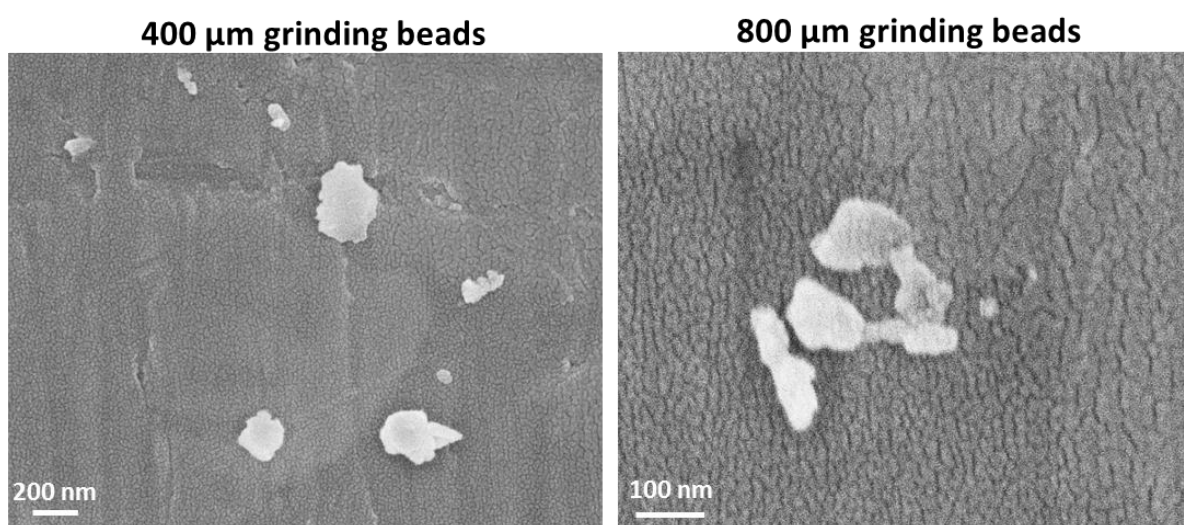


Figure 13. SEM micrographs of the NMG/SDS platelets obtained using grinding beads with diameters of 400 μm and 800 μm , respectively.

As described in section I.2., the lateral size of the NMG platelets was characterized by DLS. As an example, Figure 14 represents the histogram and frequency of NMG lateral size for the NMG/SDS-5-400 suspension. The cumulative representation will be systematically used in the following parts and allows a better visibility of the evolution of the lateral size when different NMG suspensions are compared.

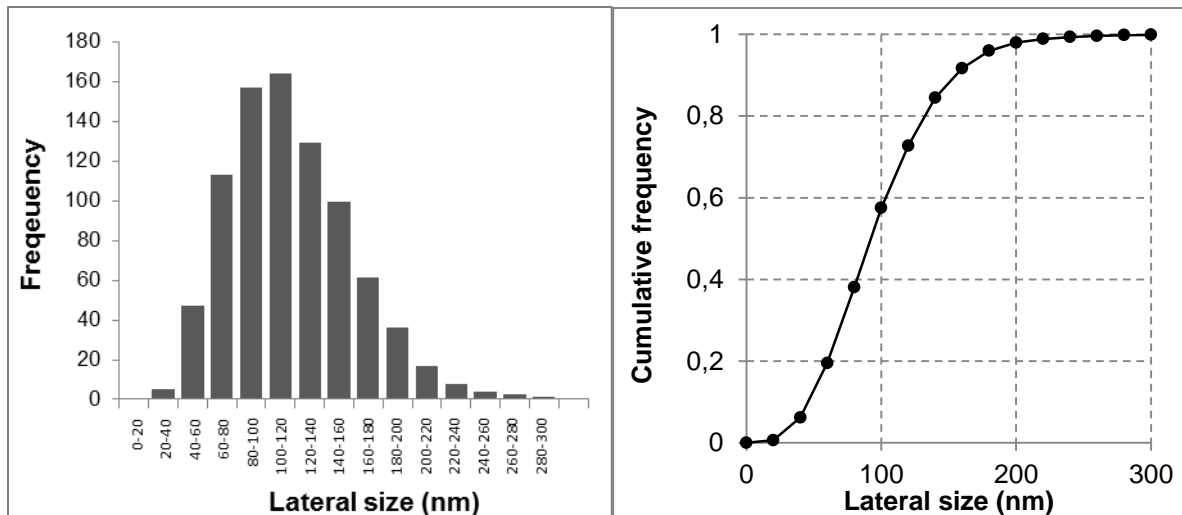


Figure 14. Example of lateral size distributions histogram and cumulative frequency determined by DLS for the NMG/SDS-5-400 suspension

The NMG thickness is calculated using Atomic force Microscopy (AFM) by performing a statistical analysis of the NMG thickness on more than 200 platelets. Figure 15 represents an example of histogram and a typical AFM micrograph for the NMG/SDS-5-400 suspension.

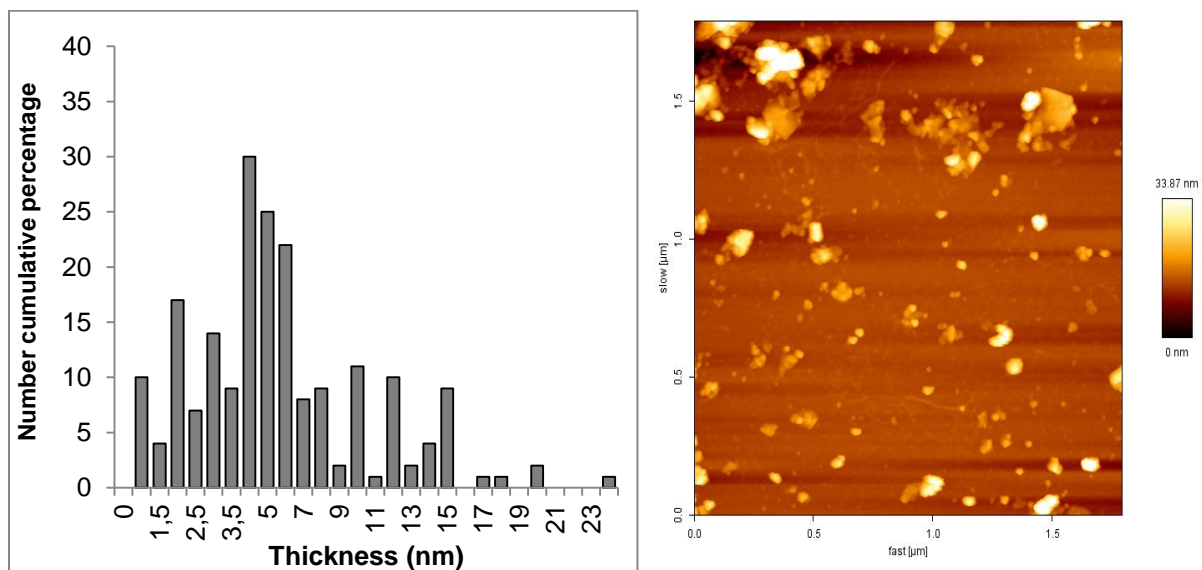


Figure 15. Example of thickness distributions histogram and AFM micrograph for the NMG/SDS-5-400 suspension. The histogram is obtained by measuring the thickness of more than 200 platelets on the AFM micrograph

The resulting lateral size and thickness measured for both suspensions are reported in Figure 16 and compared with the NMG/SDS suspensions obtained by Knieke *et al.* using grinding beads with a diameter of 50 μm or 100 μm (data taken from the article ^[31]).

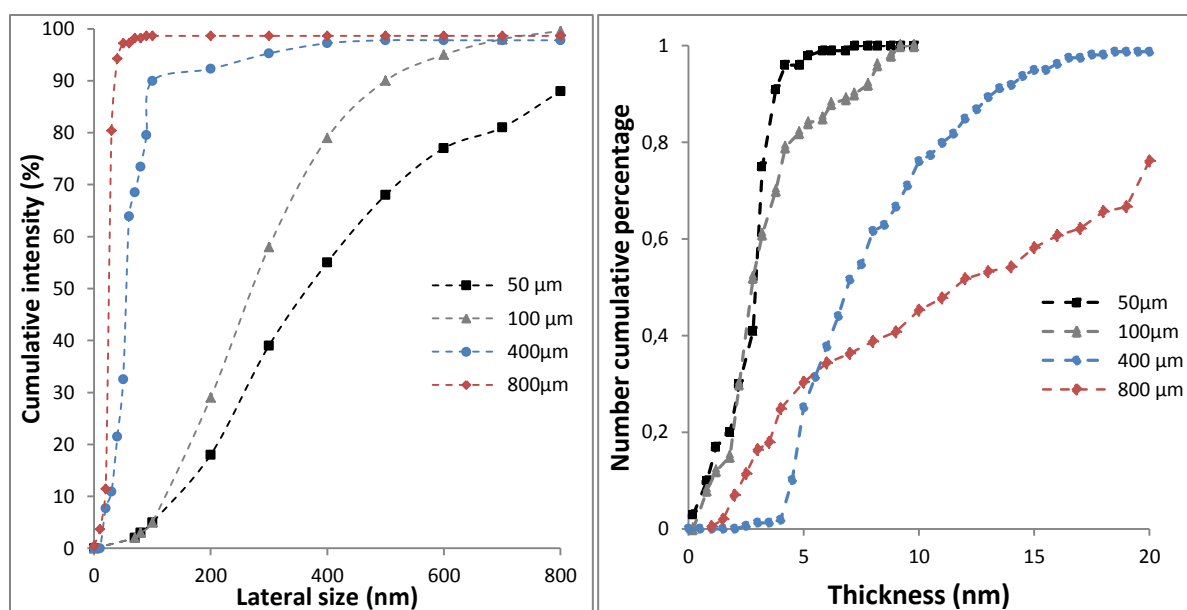


Figure 16. Cumulative lateral size and thickness distributions of delaminated sheets for the four grinding beads diameters: 50 and 100 μm [Knieke et al.], 400 and 800 μm [this work])

The trend observed by Knieke et al. is confirmed. An increase of the grinding beads diameter induces a decrease of the NMG lateral size and an increase of the NMG thickness.

Besides, to favor the formation of armored nanocomposites, NMG with a lateral size around 100 nm should be adequate in order to cover polymer beads of approximately 300 nm to 1000 nm diameter. Therefore, using grinding beads with a diameter of 400 μm should produce NMG platelets with adequate dimensions for our study. Moreover these platelets will have a lower thickness than the NMG platelets formed using the grinding beads with a diameter of 800 μm .

So, grinding beads of 400 μm will be preferred to favor the formation of NMG with small diameter but also a small thickness, and will be used in the following experiments.

2. Surfactant: SDS vs. SDBS

The effect of the surfactant was studied using 400 μm grinding beads diameter and two types of surfactants, SDS and SDBS, at a fixed concentration of 5 g L^{-1} . For these two experiments, only wet grinding was realized (no sonication). After mechanical delamination and decantation of the suspensions, DLS and AFM characterizations were performed to determine the lateral size and thickness of the NMG platelets formed. Figure 17 compares the dimensions of NMG using SDS or SDBS as a surfactant and Table 3 summarizes the results.

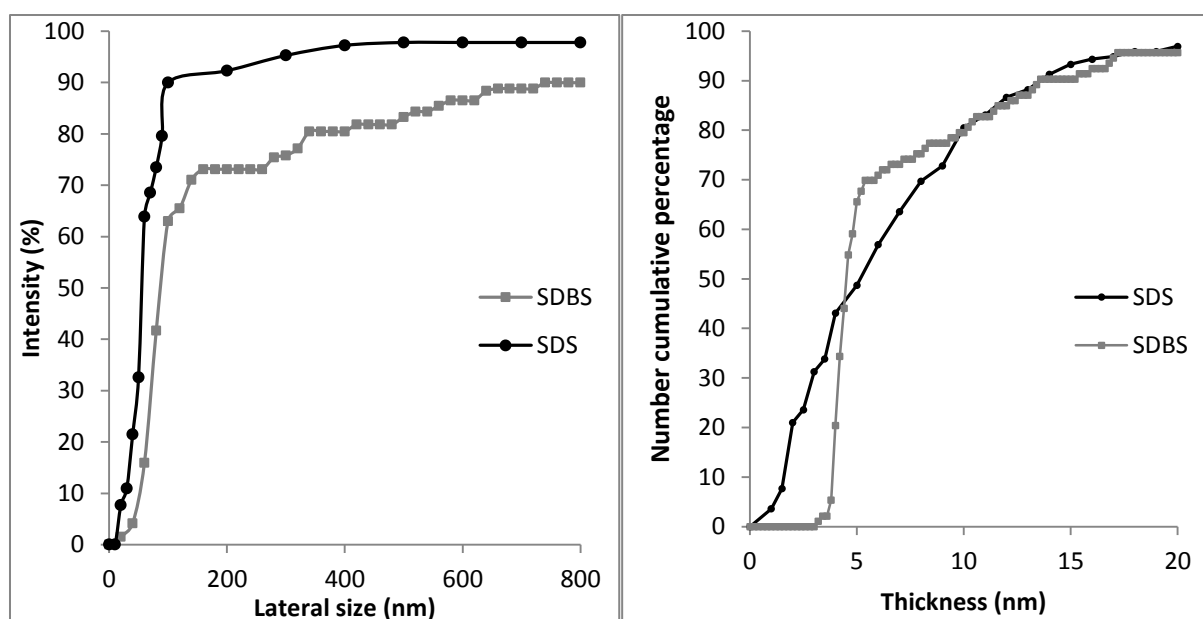


Figure 17. Cumulative lateral size and thickness distributions of delaminated sheets for NMG/SDS-5-400 and NMG/SDBS-5-400 suspensions

Using SDBS instead of SDS has no influence on the mean thickness of the formed NMG platelets. However, the lateral size increases when SDBS is used. This increase can be due to the higher molar mass of SDBS, compared to SDS. Table 3 summarizes the NMG lateral size and thickness determined from the data of Figure 17. For the lateral size, two values are noted: D50 and D90 which correspond respectively to the lateral size for 50% and 90% of the NMG sheets. Similarly, the thickness value, E50, corresponds to the thickness measured for 50% of the NMG platelets. As an example, for the NMG/SDBS-5-400 suspension, 50% of the created NMG sheets are thinner than 4.6 nm.

Table 3. Influence of the nature of the surfactant on the size characteristics of NMG/SDS-5-400 and NMG/SDBS-5-400 suspensions

Sample name	Lateral size (nm)		Thickness (nm)
	50% (D50) ^a	90% (D90) ^a	50% (E50) ^b
NMG/SDS-5-400	60	100	5
NMG/SDBS-5-400	90	860	4.6

^a Determined by DLS. ^b Determined by AFM

TGA characterizations of these two suspensions are performed to determine the amount of surfactant contained in the NMG/surfactant powder (Equation 5) and consequently the NMG and surfactant concentration in the suspension. The results are reported in Table 4. The surface area, Surface_{tot}, was also calculated using the lateral size histograms obtained by AFM measurements and the Equation 1.

Table 4. NMG and surfactant concentrations of NMG/SDS-5-400 and NMG/SDBS-5-400 suspensions

Sample name	[Surfactant] (g L ⁻¹)	[NMG] (g L ⁻¹)	Surface _{tot} (nm ²)
NMG/SDS-5-400	2.4	1.6	2 10 ⁶
NMG/SDBS-5-400	3.1	2.1	7 10 ⁶

The presence of an aromatic ring in the surfactant molecule promotes the creation of π - π interactions and increases the NMG concentration in water suspension. Furthermore, the total surface area calculated is higher using SDBS as a surfactant. Based on these results, SDBS will be used as a stabilizer for the mechanical delamination of graphite in further experiments.

3. Effect of delamination time

Knieke *et al.* have milled the graphite/SDS suspension for five hours and a NMG concentration of 1 g L⁻¹ was obtained (1% wt of graphite and [SDS] = 0.6 g L⁻¹).

To optimize the delamination time, the two suspensions previously studied (NMG/SDBS-5-400 and NMG/SDS-5-400) were produced again and few milliliters of each suspension were extracted each hour to determine the NMG concentration in function of the delamination time. The NMG concentration in the suspension can be determined by UV-visible spectroscopy [27][28]. This characterization technique was used by Lotya *et al.* at a wavelength of 660 nm to estimate the concentration of graphene in graphene/surfactant suspensions [26]. At 660 nm, no absorption of the surfactant is observed and the absorption of the benzene ring of NMG can be selectively followed to determine the NMG concentration.

Calibration curves were first established for each suspensions, and then the evolution of the NMG concentration during ball milling was determined by measuring the absorbance of the suspensions at 660 nm for various delamination times. Figure 18 represents the evolution of the NMG concentration, for the NMG/SDS-5-400 and NMG/SDBS-5-400 suspensions, as a function of the delamination time. No evolution of the NMG concentration is observed after 3 hours of delamination for both samples. Moreover, higher NMG concentrations are obtained when the suspensions are delaminated in the presence of SDBS instead of SDS. In consequence, SDBS is a better NMG stabilizer.

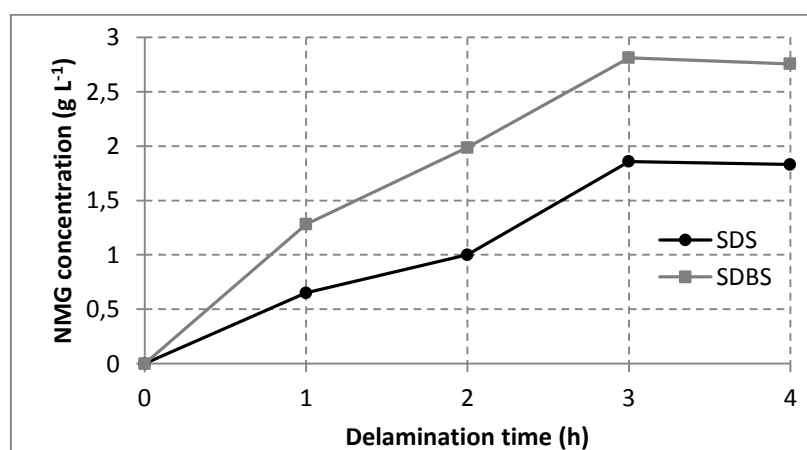


Figure 18. Evolution of NMG concentration as a function of the delamination time using SDS or SDBS as surfactants.

Four hours of delamination are sufficient to obtain concentrated NMG suspensions. The effect of the delamination process on the NMG dimensions was then investigated.

4. Effect of sonication and combination of sonication and wet grinding

As described in section I.1., wet grinding^[4] and sonication^[5] can both be used to exfoliate graphite platelets in a water media. The combination of these two processes and the influence of each process on the final dimensions of the NMG platelets were studied. The surfactant used for these experiments was SDBS instead of SDS in order to favor π - π stacking interactions with NMG platelets. The effect of the grinding process on the dimensions and on the surface defects of the resulting NMG was investigated successively.

a. Effect of the delamination process on the dimensions of the resulting NMG

The effect of the delamination process (sonication (S), wet grinding (WG) or both (WG/S)) on the dimensions of NMG platelets and NMG and surfactant concentration in the suspension is studied. The experiments were performed with 400 μm grinding beads and SDBS as a surfactant at a concentration of 5 g L⁻¹. At the end of the grinding and sonication process, the supernatant was collected and analyzed by DLS and AFM to determine the mean thickness and lateral size of the NMG platelets formed. Figure 19 represents the cumulative intensity vs. the NMG lateral size and the cumulative number vs. NMG thickness.

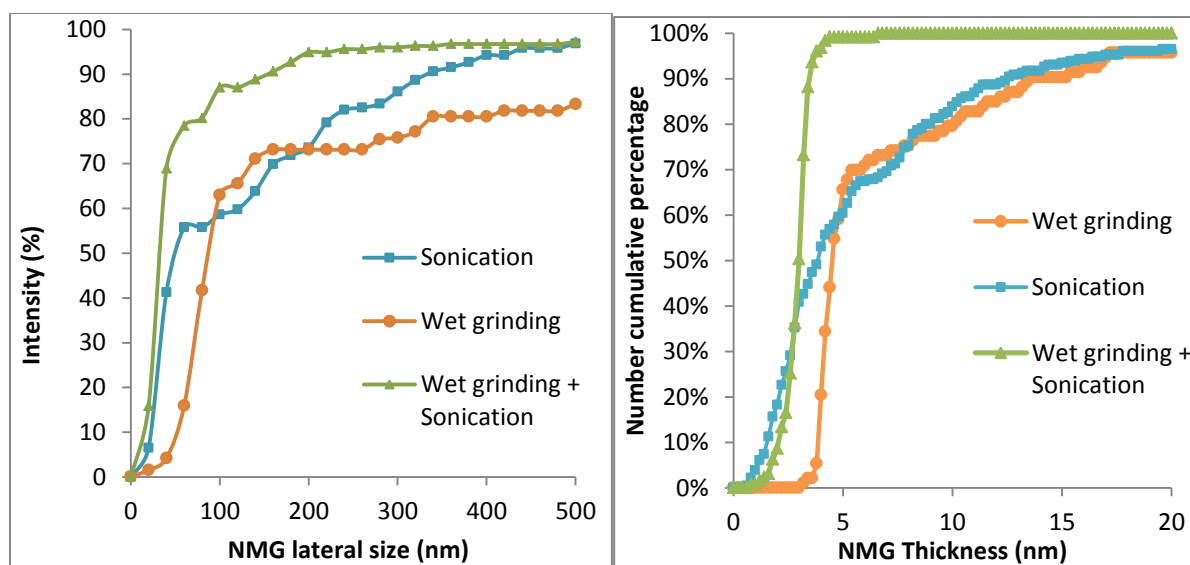


Figure 19. Cumulative lateral size and thickness distributions of NMG/SDBS-5-S, NMG/SDBS-5-WG and NMG/SDBS-5-WG/S suspensions prepared through different delamination processes.

Table 3 summarizes these two size parameters for each suspension for 50% of the sheets and 90% of the sheets. The lateral size distribution is narrower for the combination of wet grinding and sonication. The thickness of the NMG platelets is also smaller when the two processes are combined.

Table 5. Influence of the grinding and sonication processes on the characteristics of NMG/SDBS-5-S, NMG/SDBS-5-WG and NMG/SDBS-5-WG/S suspensions

Sample name	Lateral size (nm) 50% (D50) ^a	Lateral size (nm) 90% (D90) ^a	Thickness (nm) 90% (E90) ^b
NMG/SDBS-5-S	50	340	4
NMG/SDBS-5-WG	90	860	4.6
NMG/SDBS-5-WG/S	30	160	3

^a Determined by DLS. ^b Determined by AFM

In summary, the combination of wet grinding and sonication allows a decrease of both the mean lateral size and thickness of the NMG platelets.

b. Effect of the delamination process on the surface defects of the resulting NMG

We used TGA to determine the effect of each delamination process on the creation of defects in the NMG structure (Figure 20). As described in section I.2., TGA curves can be interpreted to determine the presence of oxygen-containing groups or defects. Figure 20 shows the TGA curves of the three experiments. The TGA curve of commercial GO is also added for comparison. The first weight loss corresponds to the loss of carbon oxide species, as CO and CO₂ gas [7]. This weight loss increases when the number of oxygen groups on the NMG platelets increases and is therefore less pronounced for NMG than for GO. Moreover, the proportion of oxygen-containing groups is similar for all NMG experiments indicating that their formation is independent of the delamination process.

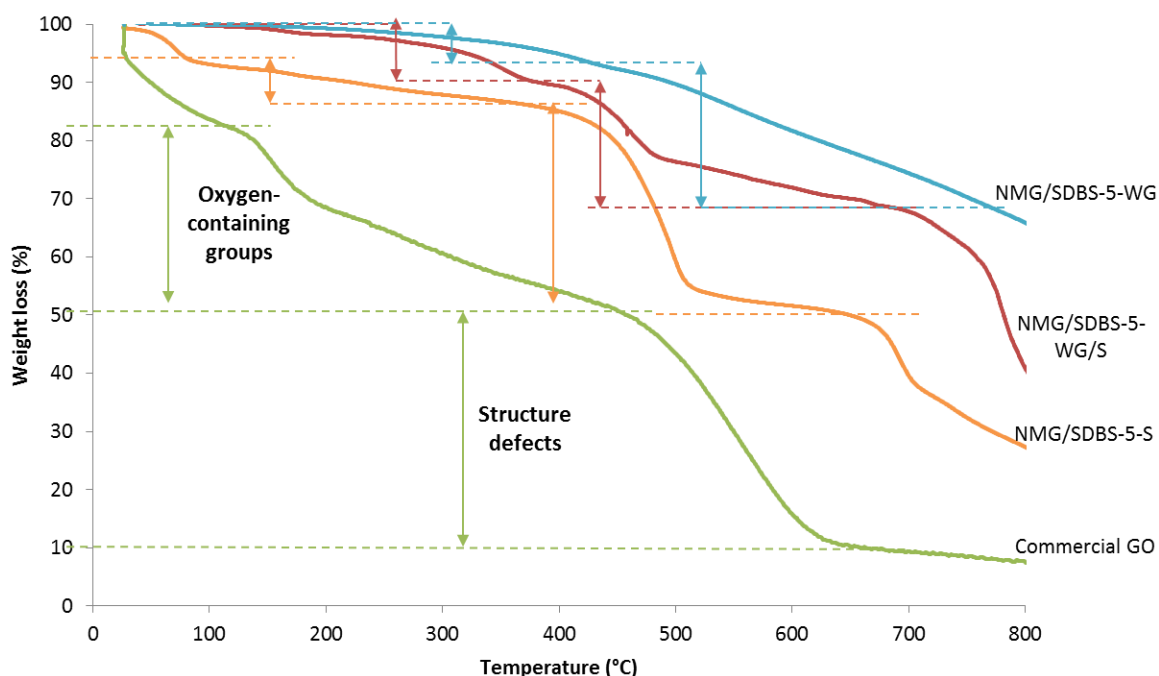


Figure 20. Influence of wet grinding and sonication on the creation of defects in the NMG structure.

The TGA curves also indicate the presence of a larger amount of structure defects in GO or NMG/SDBS-5-S than in the NMG/SDBS-5-WG/S suspension. The presence of structure

defects will induce a degradation of the electrical properties. Consequently, wet grinding or the combination of wet grinding and sonication will be favored in the following experiments as these two processes produce a minor amount of oxygen-containing groups and create less structure defects than sonication.

TGA was also used to determine the percentage of surfactant present in each suspension, as described in section I.2. The results are shown in Table 6. Knowing %SDBS_{powder} and the total amount of solid, the SDBS and NMG concentrations of each suspension were determined and reported in Table 7.

Table 6. SDBS content determined by TGA for NMG/SDBS-5-S, NMG/SDBS-5-WG and NMG/SDBS-5-WG/S samples.

Sample name	TGA		
	W _{SDBS} (%)	W _{NMG} (%)	%SDBS _{powder}
NMG/SDBS-5-S	44.2	35.3	80
NMG/SDBS-5-WG	44.2	10.1	23
NMG/SDBS-5-WG/S	44.2	26.4	59.8

The results of Table 7 shows that the combination of wet grinding and sonication allows forming highly concentrated NMG suspensions with a lower surfactant concentration, compared to the use of sonication alone.

Table 7. Influence of the grinding and sonication processes on NMG and SDBS concentrations of NMG/SDBS-5-S, NMG/SDBS-5-WG and NMG/SDBS-5-WG/S suspensions.

Sample name	[NMG/SDBS] (g L ⁻¹)	%SDBS _{powder} (wt%)	[SDBS] (g L ⁻¹)	[NMG] (g L ⁻¹)
NMG/SDBS-5-S	7.2	80	5.8	1.4
NMG/SDBS-5-WG	4.9	23	1.1	3.8
NMG/SDBS-5-WG/S	5.2	59.8	3.1	2.1

To sum up, the combination of grinding and sonication induces a better exfoliation of the graphite platelets and in consequence a smaller thickness of the NMG sheets. The lateral size and the number of defects will be also smaller with a combination of these two processes. Consequently, this process seems better adapted to minimize the loss of electrical properties of the NMG platelets.

5. Repeatability

The delamination of graphite/SDBS suspensions through the combination of wet grinding and sonication, with 400 μm grinding beads, was performed several times to test the robustness and reproducibility of the method. The concentration of SDBS was set at 5 g L⁻¹. After each

experiment, the lateral size of the NMG platelets was measured by DLS. The results are presented on Figure 21.

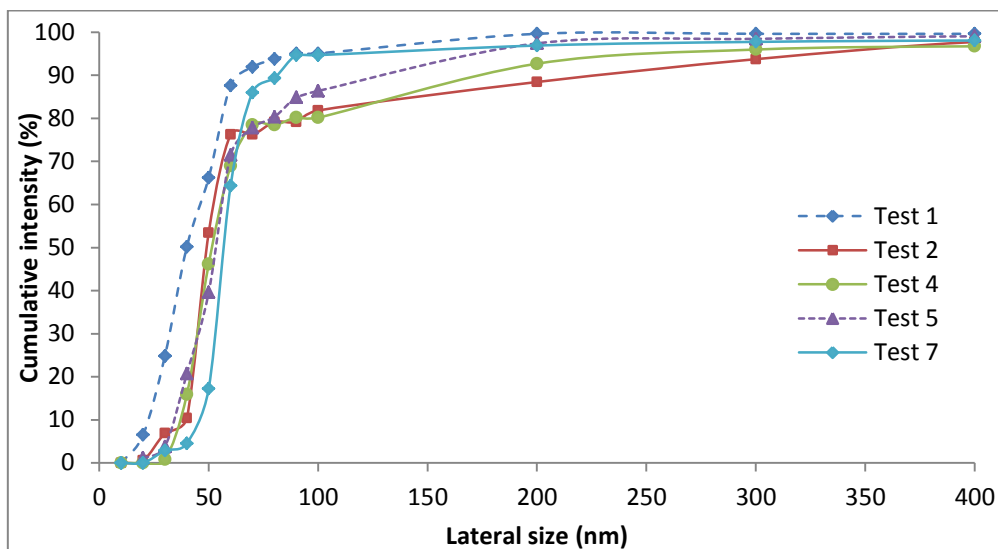


Figure 21. Cumulative lateral size distribution determined by DLS for different runs of NMG/SDBS-5-400 suspensions.

The lateral size results are replicable from one run to another. As a consequence the different runs will have the same properties and will be used indifferently in the following experiments.

6. Stability of the suspensions

The stability of the NMG/SDBS-5-400 suspension was evaluated using Turbiscan® at 25 °C every hour for 60 hours. The Turbiscan® technology is designed to monitor the stability of ink formulations and compare their stability. The detection head moves up and down along a flat-bottom cylindrical glass cell containing the suspension. The results are presented on Figure 22. No destabilization of the suspension, neither at the bottom nor at the top of the tube was visible after 60h, indicating a good stability of the NMG/SDBS-5 suspension.

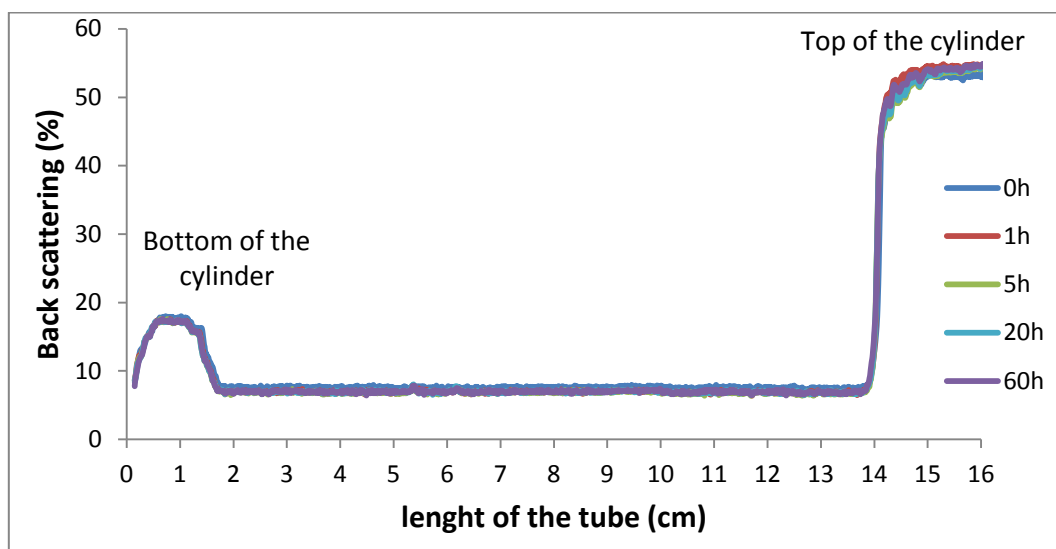


Figure 22. Turbiscan® stability analysis of the NMG/SDBS-5 suspension

Moreover, the NMG/SDBS-5 suspension was resistant to 18000 rpm centrifugation for 30 minutes.

To conclude this preliminary study, grinding beads of 400 μm will be preferred to favor the formation of NMG with small diameters but also a small thickness. Then, it was demonstrated that four hours of delamination are sufficient to obtain concentrated NMG suspensions. Furthermore, the combination of grinding and sonication induces a better exfoliation of the graphite platelets and low defects in the carbon structure. These parameters will be applied in further experiments for which the influence of the surfactant or stabilizer on NMG characteristics is investigated.

III. Influence of the nature and concentration of stabilizer on NMG characteristics

1. Description of the experimental procedure

Figure 23 shows the experimental procedure which has been selected to study the effect of the nature and concentration of stabilizer on the characteristics of the NMG platelets formed. Wet grinding was combined with a sonication process using grinding beads diameter of 400 μm . The delamination time was four hours and all the initial suspensions contained 10 wt% of micrographite.

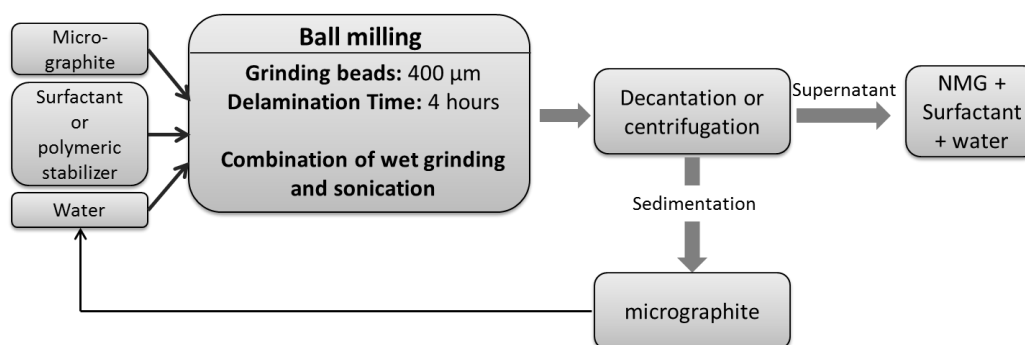


Figure 23. Scheme of the experimental procedure selected to study the effect of the nature and concentration of stabilizer on NMG characteristics.

The main parameters that were studied in the following series of experiments are the nature and concentration of stabilizer. As presented in the bibliographic chapter, a variety of surfactants or stabilizers can be used to stabilize NMG platelets in water media. Here, the two surfactants previously described have been chosen, SDS and SDBS. They will be compared to two polymeric stabilizers, sodium poly (styrene sulfonate) (PSSNa) and poly(styrene)-block-poly(ethylene oxide) (PS b PEO) which can also create π - π staking interactions with NMG surfaces. In addition, a polymeric stabilizer poly(vinylpyrrolidone) (PVPk30, molar mass 40,000 g mol⁻¹) will be used in Chapter 4 for *in situ* polymerization in the presence of NMG platelets. Therefore, this stabilizer will also be studied in this chapter.

Table 8 summarizes the experiments developed in this part with the parameters described in Figure 23.

Each sample was named according to the following convention with each segment of information separated by a slash or a dash: segment 1: type of graphene, segment 2: type of stabilizer and segment 3: concentration of stabilizer used during the delamination process (in g L^{-1}).

Table 8. . Experimental conditions to produce NMG/surfactant or NMG/stabilizer suspensions.

Experiment name	Surfactant or stabilizer	[Surfactant] (g L^{-1})
NMG/SDS-5	SDS	5
NMG/SDBS-5	SDBS	5
NMG/SDBS-2.5	SDBS	2.5
NMG/SDBS-10	SDBS	10
NMG/PSSNa-5	PSSNa	5
NMG/PSSNa-10	PSSNa	10
NMG/PVPk30-5	PVPk30	5
NMG/PVPk30-10	PVPk30	10
NMG/PS <i>b</i> PEO1010-10	PS <i>b</i> PEO 1010	10
NMG/PS <i>b</i> PEO1030-10	PS <i>b</i> PEO 1030	10

Grinding beads diameter = 400 μm . Delamination process = wet grinding + sonication

2. Effect of the type and concentration of stabilizers

a. SDBS

Influence of SDBS concentration

To observe the influence of SDBS concentration on the NMG size dimensions, we performed three experiments using a 10%wt graphite suspension and various SDBS concentrations: 2.5, 5 and 10 g L^{-1} , respectively. Note that the CMC of SDBS (i.e., 0.6 g L^{-1}) is lower than the CMC of SDS ^[12]. The delamination was realized with grinding beads of 400 μm during four hours. The NMG lateral size and thickness, for each NMG suspension, were determined by DLS and AFM. The results are presented in Figure 24 and Table 9.

Table 9. Influence of the surfactant concentration on the size characteristics of NMG/SDBS-2.5, NMG/SDBS-5 and NMG/SDBS-10 suspensions.

Sample name	Lateral size (nm) 50% (D50) ^a	Lateral size (nm) 90% (D90) ^a	Thickness (nm) 90% (E90) ^b
NMG/SDBS-2.5	290	370	9.8
NMG/SDBS-5	30	160	3.2
NMG/SDBS-10	15	100	>10

^a Determined by DLS. ^b Determined by AFM

The NMG lateral diameters decrease with increasing the SDBS concentration while the lateral size distribution becomes narrower. The NMG thickness decreases up to 5 g L⁻¹ of SDBS and then increases for higher concentrations. The thickness distribution also varies with the SDBS concentration and is larger for the low and high concentrations than for the intermediate concentration.

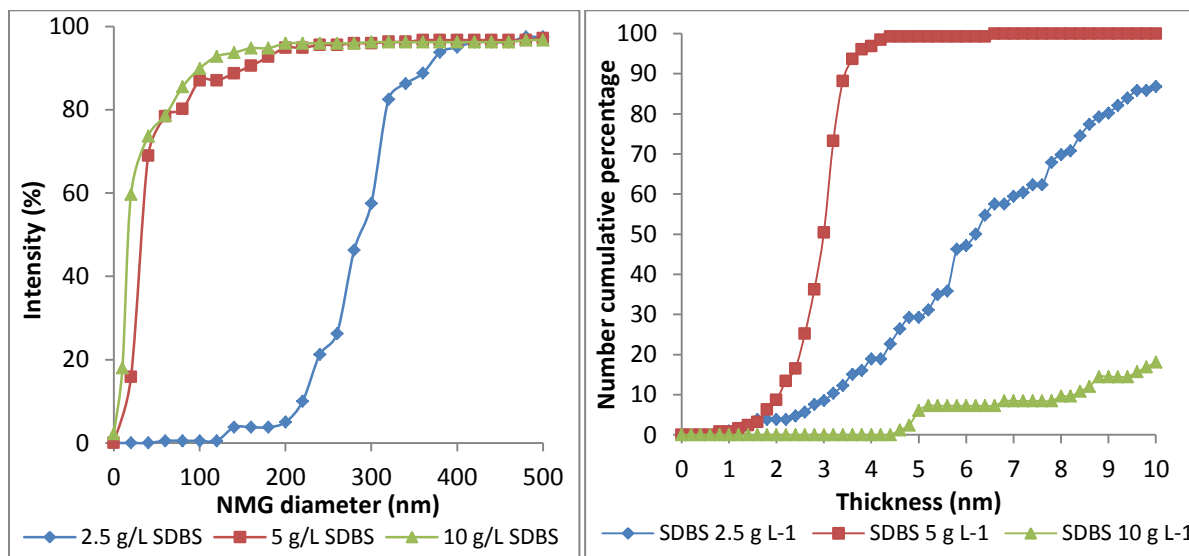


Figure 24. Cumulative lateral size and thickness distributions of NMG/SDBS-2.5, NMG/SDBS-5 and NMG/SDBS-10 suspensions

TEM and HR-TEM characterizations were also performed on the NMG/SDBS-5 suspension. On the TEM image shown on Figure 25a, two large NMG platelets (around 150 nm in lateral size) are visible (arrows). The different grey shades are consistent with different NMG thicknesses: which can be due to the NMG overlap or NMG folding.

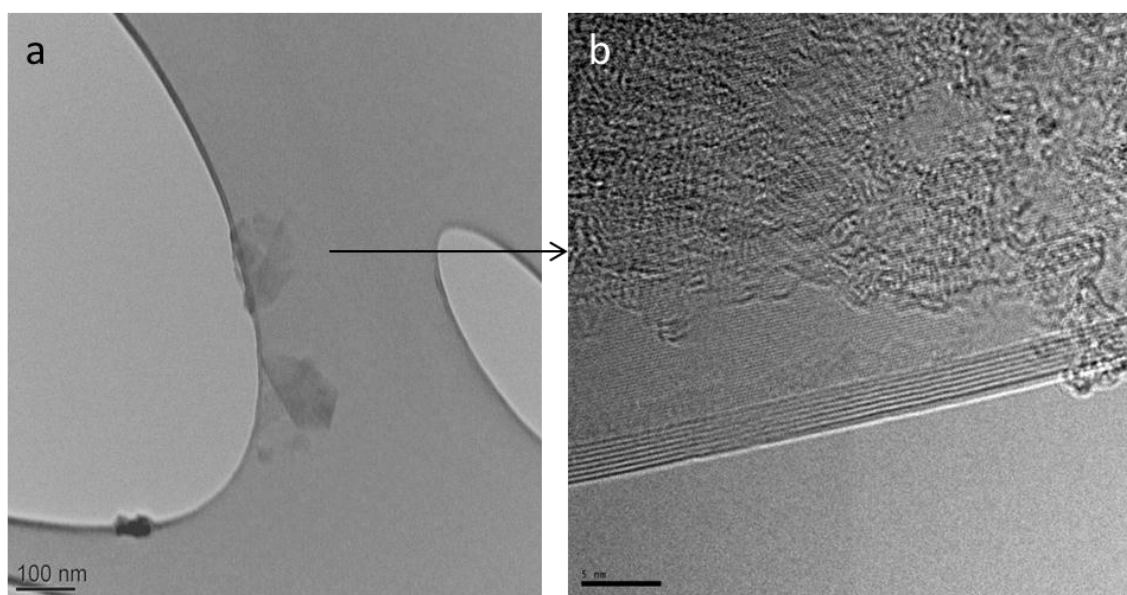


Figure 25. (a) TEM micrograph of NMG/SDBS-5 showing two NMG nanoplatelets (indicated by arrows) and (b) HR-TEM micrograph of one NMG platelet counting in average 7 graphene layers

The HR-TEM image on Figure 25b shows a NMG platelet that counts 7 graphene layers, with a distance of 0.45 nm between each sheet. The distance between two sheets for a perfect graphene is 0.34 nm. In consequence, the HR-TEM picture confirms the presence of surfactant between each graphene sheets for the NMG/SDBS-5 suspension.

The NMG and SDBS concentrations of the suspensions were determined by elemental and thermogravimetric analyses. The data are reported in Table 10 while the TGA curves of NMG/SDBS-5 and pure SDBS are shown in Figure 26.

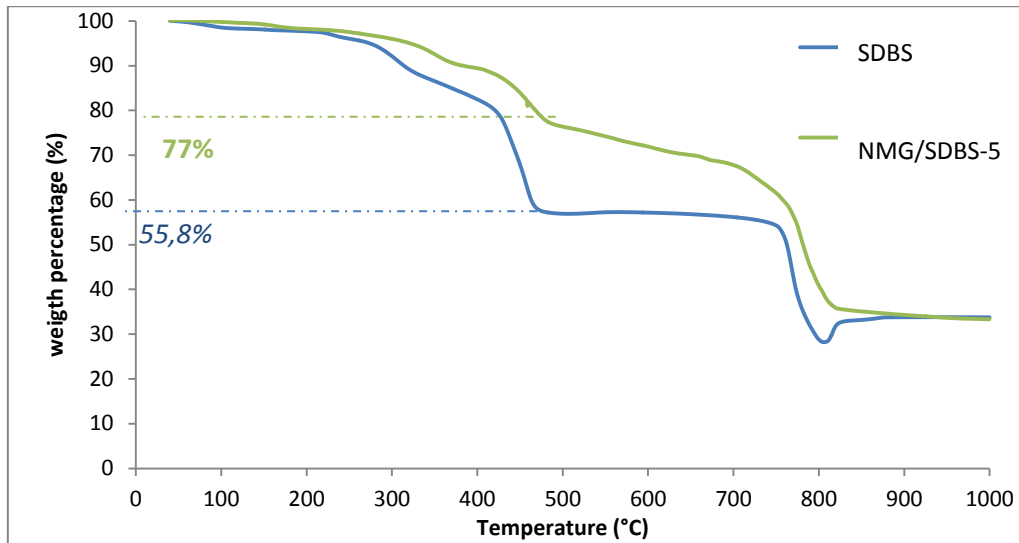


Figure 26. TGA analysis of SDBS powder and NMG/SDBS-5 powder

Table 10 shows that there is a good correlation between the two characterization techniques in the case of NMG/SDBS-5. The percentage of SDBS in the dried powder is higher for NMG/SDBS-2.5 and NMG/SDBS-10 than for NMG/SDBS-5

Table 10. %SDBS_{powder} for NMG/SDBS-2.5, NMG/SDBS-5 and NMG/SDBS-10 samples

Sample name	Elemental analysis		TGA		
	%S	%SDBS powder	W _{SDBS} (%)	W _{NMG} (%)	%SDBS _{powder}
NMG/SDBS-2.5	-	-	44.2	39.5	89.5
NMG/SDBS-5	5.49	59.8	44.2	23	52
NMG/SDBS-10	-	-	44.2	34.3	77.8

The final SDBS and NMG concentrations are indicated in Table 11 for the three initial SDBS concentrations. Increasing SDBS concentration increases the NMG concentration and yield. However, high surfactant concentrations can have a negative effect on the electrical properties of the NMG/SDBS suspensions after drying. Therefore, to minimize the effect of the surfactant on the final electrical properties of the suspension, the SDBS concentration should be limited to 5 g L⁻¹.

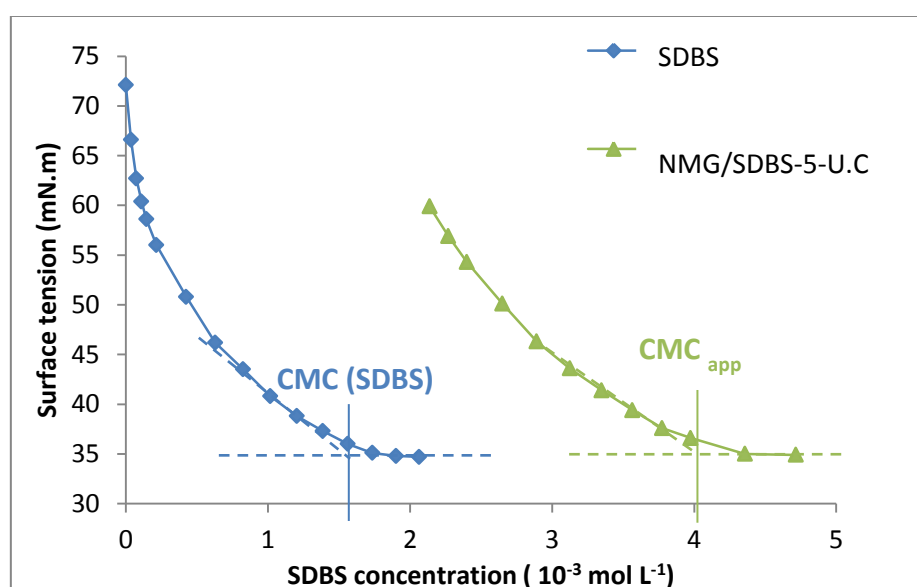
Table 11. Influence of the initial surfactant concentration on the final NMG and SDBS concentrations of NMG/SDBS-2.5, NMG/SDBS-5 and NMG/SDBS-10 suspensions.

Sample name	%SDBS _{powder}		[Surfactant] (g L ⁻¹)		[NMG] (g L ⁻¹)	
	E.A	TGA	E.A	TGA	E.A	TGA
NMG/SDBS-2.5	-	89.5	-	1.16	-	0.13
NMG/SDBS-5	59.8	52	3.1	2.7	2.1	2.4
NMG/SDBS-10	-	77.8	-	5.6	-	1.6

The surfactant plays an important role in the exfoliation of graphite platelets during the grinding process. Part of the surfactant is adsorbed on the NMG surface and part is free in solution. Surfactant partitioning is an important characteristic of the present system, as it will influence the mechanism of *in situ* emulsion polymerization as we shall see later in Chapter 4. The adsorption behavior of SDBS on NMG surfaces is thus investigated in the following paragraph.

Adsorption behavior of SDBS

Surfactant adsorption on the NMG surface was studied by surface tension measurements, as described in section I.3.b. SDBS repartition between NMG and water was determined by first measuring the CMC of SDBS in water and then the CMC_{app} in the presence of NMG. The evolution of the surface tension of SDBS in water solution at 25°C as a function of the SDBS concentration is reported in Figure 27. This enabled us determining a CMC value of $1.6 \cdot 10^{-3}$ mol L⁻¹, which is consistent with the literature [19].

**Figure 27.** Surface tension vs. SDBS concentration for SDBS and NMG/SDBS-5-U.C water suspensions.

We next determined the surface tension of the NMG/SDBS-5 suspension and found a value of 36.6 mN m^{-1} , which, according to Figure 27 is close to the surface tension of a saturated surfactant solution (i.e., at the CMC). As a consequence, we had to decrease the SDBS concentration of the NMG/SDBS-5 suspension to be able to effectively visualise the break in the curve of surface tension vs surfactant concentration corresponding to the CMC_{app} .

To do so, ultracentrifugation at 50,000 rpm rotation speed was realized on the NMG/SDBS-5 suspension. The supernatant, containing only SDBS, was removed and the bottom of the sample was redispersed in water before surface tension measurement (Figure 28). This operation was repeated until the NMG/SDBS suspension reached a surface tension of 60 mN m^{-1} .

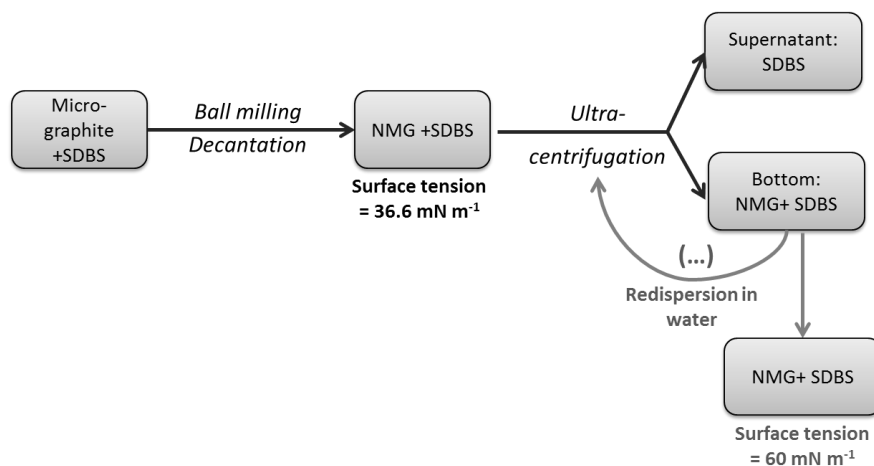


Figure 28. Scheme of the ultracentrifugation process used to decrease the surfactant concentration of the NMG/SDBS-5 suspension.

The surface tension was then measured as a function of the concentration of added SDBS and the results are plotted on Figure 27.

The CMC and CMC_{app} were used to calculate the surface concentration at saturation (Γ_{sat}), as previously described in section I.3.b. (Eq.7). Then, the concentration of surfactant adsorbed on NMG ($[\text{NMG}]_{\text{SDBS}}$) and free surfactant ($[\text{NMG}]_{\text{water}}$) can be calculated using Equation 8 and 9. The results are reported in Table 12.

Table 12. NMG concentration, specific surface area, total SDBS concentration, CMC_{app} , Γ_{sat} and SDBS partitioning of the NMG/SDBS-5-U.C suspension.

	$[\text{NMG}]$ (g L^{-1}) ^a	S_{spe} ($\text{m}^2 \text{g}^{-1}$) ^b	$[\text{SDBS}]_{\text{tot}}$ (g L^{-1}) ^a	CMC_{app} (g L^{-1}) ^c	Γ_{sat} (mol m^{-2}) ^d	$[\text{SDBS}]_{\text{NMG}}$ (g L^{-1}) ^e	$[\text{SDBS}]_{\text{free}}$ (g L^{-1}) ^f
NMG/SDBS-5-U.C	2.1	140	1.7	1.43	$1.1 \cdot 10^{-5}$	1.15	0.55

^a Determined by TGA. ^b Calculated using Eq.2 and the AFM lateral size histogram, ^c Determined by surface tension measurements. ^d Calculated using Eq.7. ^e Calculated using Eq. 8. ^f Calculated using Eq. 9.

The amount of surfactant adsorbed per NMG square meter at saturation (Γ_{sat}), allowed determining the surfactant partitioning between the aqueous phase and the NMG platelets: $[\text{SDBS}]_{\text{free}}$ and $[\text{SDBS}]_{\text{NMG}}$, respectively. The concentration of surfactant in the aqueous phase, $[\text{SDBS}]_{\text{free}}$, is below the CMC of SDBS in water. This result is consistent with the surface tension of 60 mN m^{-1} previously measured.

Thus, the NMG/SDBS-5-U.C suspension is free of surfactant micelles and will be used in Chapter 4 for *in situ* polymerization.

As shown above, the stabilizer plays an important role on the final dimensions and properties of the NMG formed. In the following, SDBS will be replaced by polymeric stabilizers such as PSSNa, PSbPEO and PVPk30. These stabilizers are known to increase the stability of graphene platelets because they can create non-covalent interactions (π - π) with the graphene sheets.

b. Sodium poly(styrene sulfonate)(PSSNa)

PSSNa is a polyelectrolyte composed of chemical repeat units similar to SDBS. It should be thus capable to stabilize graphene platelets in water solutions ^[14]. This stabilizer can indeed promote Π -stacking interactions of the benzene rings with the graphene surface, which is known to increase the adsorption of surfactants ^[24] as well as of other highly aromatic molecules ^[30] and rigid conjugated polymers ^[31]. In particular, PSSNa has been widely used for the stabilization of Multiwall Carbon Nanotubes (MWCNT) ^[29]. For instance, Han *et al.* showed that the presence of PSSNa improved the dispersion and stabilization of MWCNT in water up to 1.25 mg mL^{-1} (Figure 29).

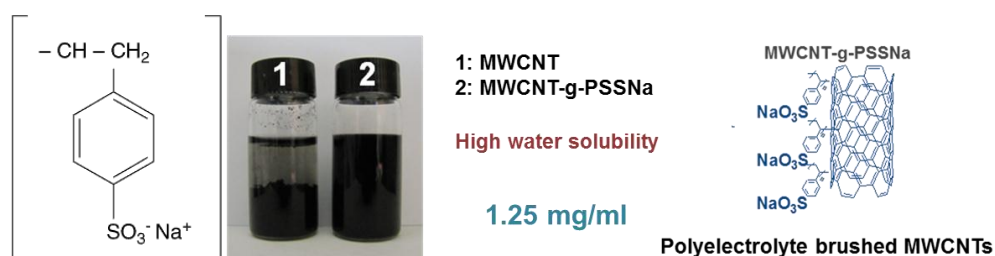


Figure 29. PSSNa structure and the grafting of PSSNa on MWCNT to improve the nanotubes stability. Reprinted from ^[29]

Stankovich *et al.* demonstrated that PSSNa can also stabilize GO platelets during the reduction process and form a complex with rGO ^[32]. Using this process, stable aqueous dispersions of polymer-coated graphitic nanoplatelets were produced for the first time. But high concentrations of PSSNa were used, 10/1 w/w PSSNa/GO.

This polyelectrolyte also proved its efficiency for large-scale synthesis of graphene from graphite by electrolytic exfoliation. PSSNa was shown to limit the defect content in the prepared graphene. According to FTIR, the edge-to-face interaction (π - π interaction) between the graphene surface and the aromatic rings of PSSNa was responsible for producing exfoliation of the graphite electrode to graphene during electrolysis ^[33]. In this article, high concentration of PSSNa was also used (i.e. up to 70 g L^{-1}).

To obtain highly stable NMG platelets in water suspensions, mechanical delamination of graphite/PSSNa suspensions was carried out with a low concentration of PSSNa (compared with the PSSNa concentrations used in the literature). Two experiments were performed at 5 and 10 g L⁻¹, respectively using the conditions described in Figure 23.

The NMG dimensions were characterized by DLS and AFM and the results are summarized in Figure 30 and Table 13.

Table 13. Effect of PSSNa concentration on size characteristics of NMG/PSSNa suspensions

Sample name	Lateral size (nm) 50% (D50) ^a	Lateral size (nm) 90% (D90) ^a	Thickness (nm) 90% (E90) ^b
NMG/PSSNa-5	200	980	5.6
NMG/PSSNa-10	80	980	6.4

^a Determined by DLS. ^b Determined by AFM

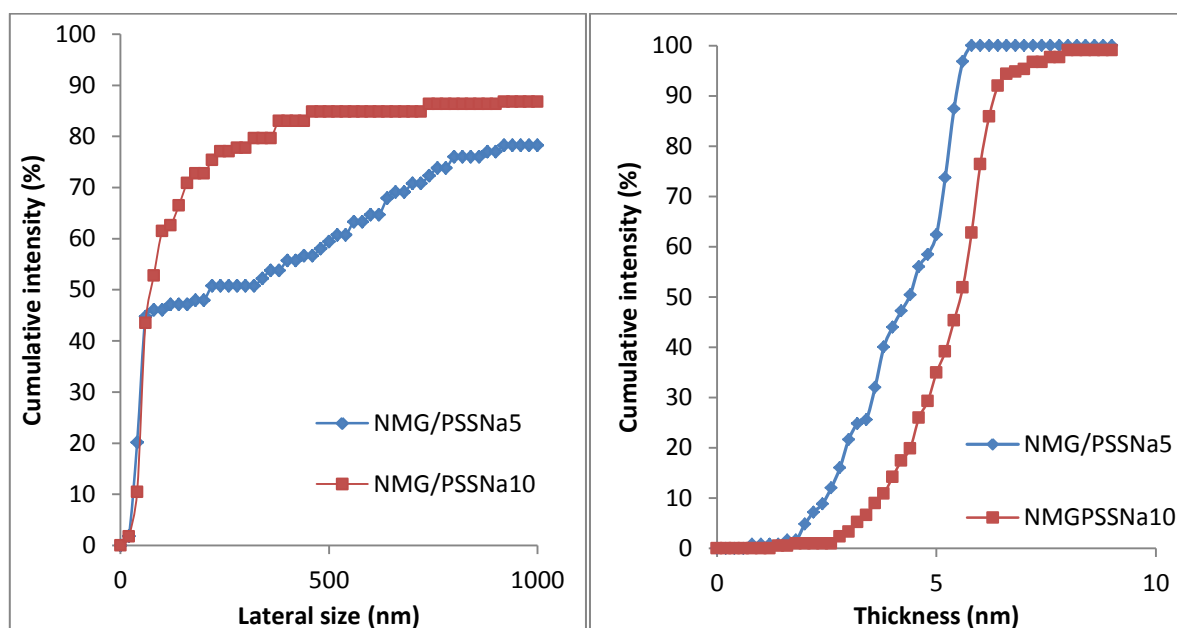


Figure 30. Cumulative lateral size and thickness distributions of NMG/PSSNa-5 and NMG/PSSNa-10 suspensions

The NMG lateral size slightly decreases when the PSSNa concentration increases but this decrease is less pronounced than for the NMG/SDBS suspensions. The NMG platelets have in both cases a large lateral size distribution. An increase of PSSNa concentration also induces an increase of the NMG thickness. The concentration of PSSNa between each NMG sheet might be higher for NMG/PSSNa-10 than for NMG/PSSNa-5, and hence the mean thickness measured by AFM increases.

The PSSNa and NMG concentrations in the suspensions after wet grinding were then calculated by elemental analysis and TGA. Table 14 summarizes the percentage of stabilizer, %PSSNa_{powder}, obtained by the two methods. Regarding elemental analysis, it should be noticed that each PSSNa molecule possesses one sulfur atom per repetition unit and that there are 294 units per polyelectrolyte molecule.

Table 14. %PSSNa_{powder} calculation for the NMG/PSSNa-5 and NMG/PSSNa-10 suspensions

Sample name	Elemental analysis		TGA		
	%S	%PSSNa _{powder}	W _{PSSNa} (%)	W _{NMG} (%)	%PSSNa _{powder}
NMG/PSSNa-5	10.72	79.7	-	-	-
NMG/PSSNa-10	13.15	98	13.3	12.4	93

TGA was performed on NMG/PSSNa-10 and pure PSSNa (Figure 31) leading to a PSSNa content of 93 wt% whose value is in agreement with the results of elemental analysis.

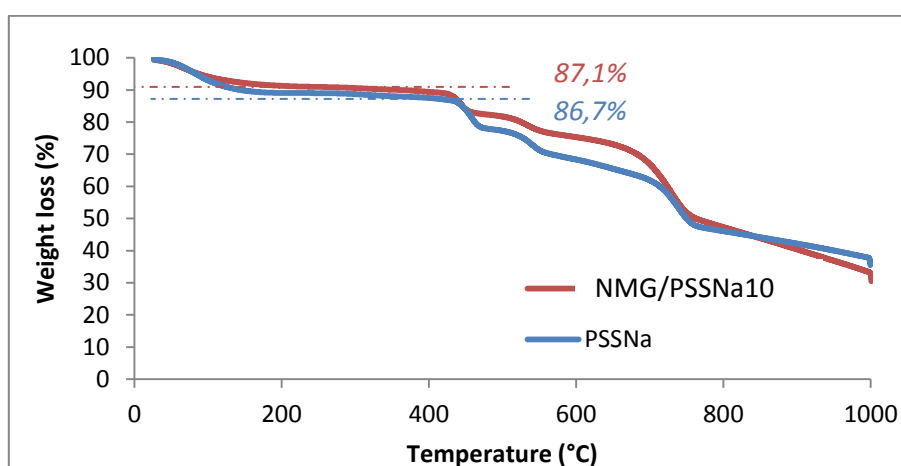


Figure 31. TGA analysis of NMG/PSSNa-10

Hence, for both suspensions, the amount of stabilizer is high, indicating that PSSNa does not well stabilize the NMG platelets. The amount of PSSNa was used to calculate the NMG and stabilizer concentrations of each suspension and the results are shown in Table 15.

Table 15. Influence of initial PSSNa concentration on the final NMG and PSSNa concentrations of NMG/PSSNa-5 and NMG/PSSNa-10 suspensions.

Sample name	%PSSNa _{powder}		[PSSNa] (g L ⁻¹)		[NMG] (g L ⁻¹)	
	E.A	TGA	E.A	TGA	E.A	TGA
NMG/PSSNa-5	79.7	-	5.6	-	1.4	-
NMG/PSSNa-10	98	93	8.9	8.4	0.2	0.6

An increase of the PSSNa concentration before grinding induces a decrease of the final NMG concentration. It therefore seems that this polyelectrolyte is a good NMG stabilizer at low concentration (5 g L^{-1}) but that increasing the polyelectrolyte concentration promotes destabilization of the NMG platelets.

In summary, this stabilizer can be used for the production of NMG suspensions but it does not stabilize the NMG platelets as well as SDBS for similar concentrations.

c. Poly(N-vinyl pyrrolidone) (PVP)

Poly(vinyl pyrrolidone) (Figure 32) has also been widely used to improve the stability of carbon nanotubes or rGO in water suspensions ^{[34][35]}. PVP is composed of an hydrophobic polyvinyl backbone, and hydrophilic pyrrolidone side groups and can thus adsorb on NMG and favor steric stabilisation ^[35]. For instance, Arzac and coworkers used PVP to stabilize rGO during the reduction step.

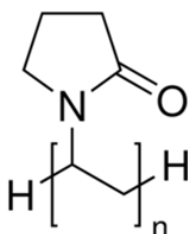


Figure 32. PVP chemical structure

Recently, Wajid *et al.* also demonstrated the ability of PVP to stabilize pristine graphene in water or ethanolic media ^[36]. Figure 33, extracted from this research article, shows that the ethanolic graphene/PVP suspensions remain stable after centrifugation.

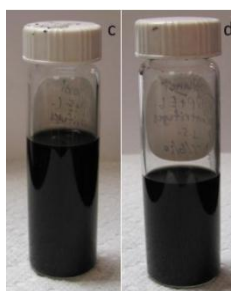


Figure 33. Graphene/PVP stability in ethanol (c) after sonication and (d) after centrifugation. Reprinted from ^[36]

PVP is also commonly used as steric stabilizer in dispersion polymerization. This process will be investigated in Chapter 4 on in situ polymerization and this is the reason why we decided to study the stabilization of NMG platelets by PVP in this chapter.

The mechanical delamination was performed using PVPk30 ($M_n=40,000 \text{ g mol}^{-1}$). Two concentrations will be investigated (5 and 10 g L^{-1}). Wet grinding was performed in the same conditions as reported in Figure 23. The DLS and AFM results are presented in Figure 34 and Table 16.

Table 16. Effect of PVPk30 concentration on size characteristics of NMG/PVPk30 suspensions.

Sample name	Lateral size (nm) (D50) ^a	Lateral size (nm) (D90) ^a	Thickness (nm) (E90) ^b
NMG/PVPk30-5	400	860	7.6
NMG/PVPk30-10	260	600	4.6

^a Determined by DLS. ^b Determined by AFM

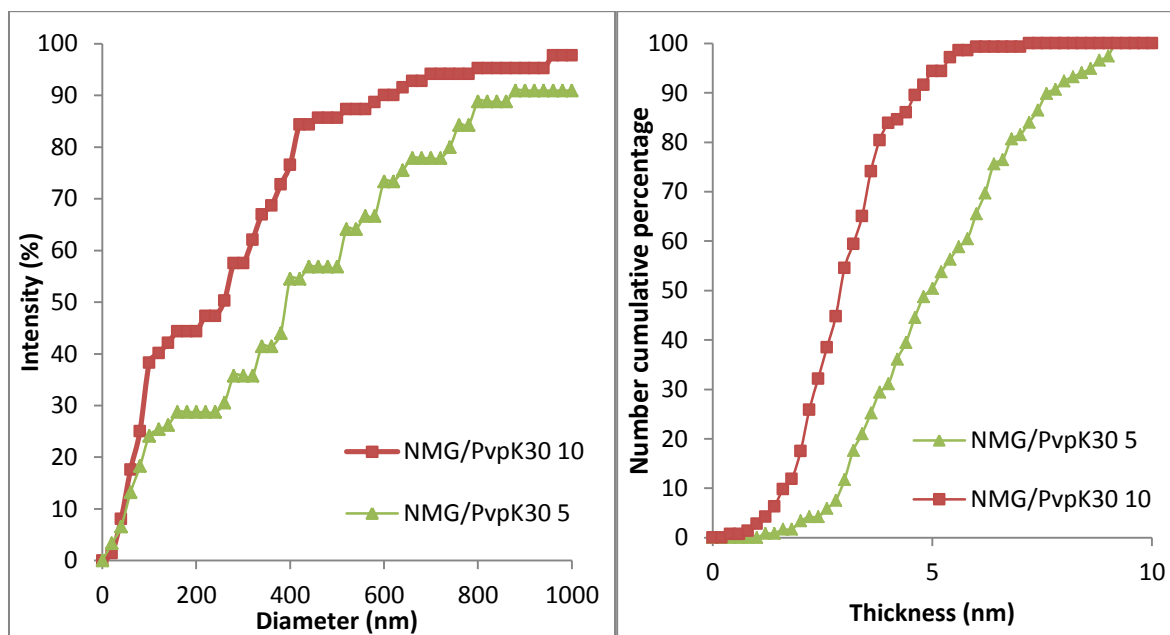


Figure 34. Cumulative lateral size and thickness distributions of NMG/PVPk30-5 and NMG/PVPk30-10 suspensions.

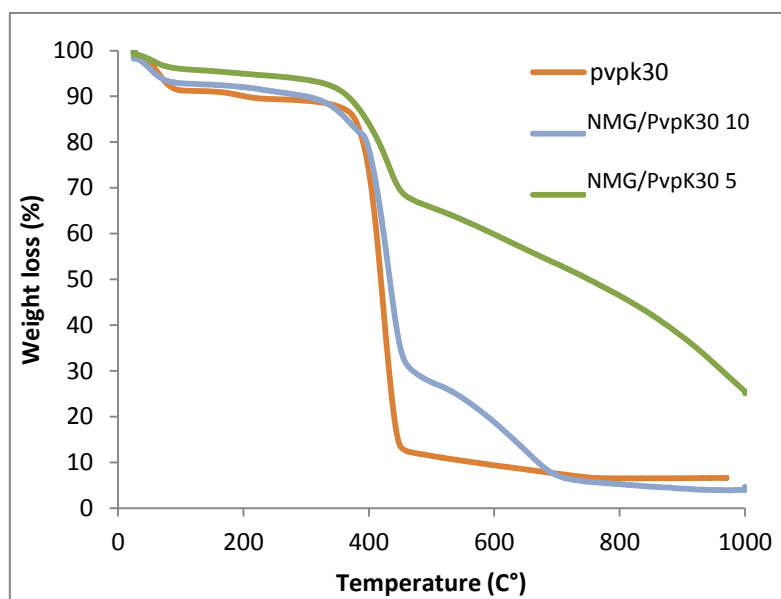
The NMG lateral sizes decrease with increasing PVPk30 concentration as for the two previous stabilizers used. The lateral size distribution is slightly narrower than for PSSNa. Moreover, the mean thickness of the NMG platelets decreases sharply with increasing the stabilizer concentration.

TGA and elemental analysis are again in good agreement and indicate that the PVP content increases with increasing the stabilizer concentration (Figure 35, Table 17).

Increasing the initial stabilizer concentration also induces a decrease of the NMG concentration in the suspension (Table 18). This is similar to the results previously reported for PSSNa except that the NMG concentration is higher.

Table 17. %PVPk30_{powder} calculation for the suspensions NMG/PVPk30-5 and NMG/PVPk30-10

Sample name	Elemental analysis		TGA		
	%N	%PVPk30 powder	W _{PVPk30} (%)	W _{NMG} (%)	%PVPk30 powder
NMG/PVPk30-5	6.1	48.4	82.8	27.3	33
NMG/PVPk30-10	9.82	77.9	82.8	67.2	81

**Figure 35.** TGA analysis of NMG/PVPk30-5, NMG/PVPk30-10 and pure PVP**Table 18.** Effect of the initial PVPk30 concentration on the final NMG and PVPk30 concentrations of the NMG/PVPk30-5 and NMG/PVPk30-10 suspensions.

Sample name	[PVPk30] (g L ⁻¹)		[NMG] (g L ⁻¹)	
	E.A	TGA	E.A	TGA
NMG/PVPk30-5	2.2	1.7	2.3	2.8
NMG/PVPk30-10	4.5	4.6	1.3	1.2

d. Polystyrene-*block*-polyethylene oxide (PS*b*PfEO)

PS*b*PfEO copolymers have been widely studied in the literature as stabilizers for polymerizations in dispersed media ^{[37][38]}. Due to their chemical structure (Figure 36), these copolymers are amphiphilic and can stabilize polymer latex particles.

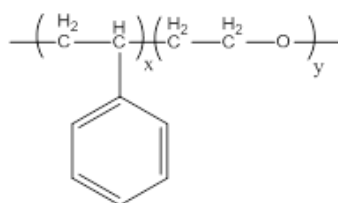


Figure 36. Chemical structure of PSbPEO 1010 ($x=1000$ and $y=1000$) and 1030 ($x=1000$ and $y=3000$)

In addition, the presence of an aromatic ring induces possible (π - π) interactions with the NMG platelets and reinforces its ability to stabilize NMG water-suspensions.

Two PSbPEO with a different molar mass have been used, PSbPEO1010 ($M_n= 148\ 000\ \text{g mol}^{-1}$) and PSbPEO1030 ($M_n= 236\ 000\ \text{g mol}^{-1}$), to study the influence of the stabilizer molar mass on the size dimensions of NMG platelets and stability of the suspensions. The experiments were performed in the same conditions as described in Figure 23 for two concentrations of stabilizer: 5 and 10 g L^{-1} .

In the case of the low concentration (NMG/PSbPEO1030-5), no NMG platelets were obtained in the supernatant. Therefore this concentration was not studied further. The mean lateral size and thickness for the NMG/PSbPEO1010-10 and NMG/PSbPEO1030-10 suspensions are summarized in Figure 37 and Table 19.

Table 19. Effect of PSbPEO composition on the size characteristics of NMG/PSbPEO1010-10 and NMG/PSbPEO1030-10 suspensions

Sample name	Lateral size (nm) (D50) ^a	Lateral size (nm) (D90) ^a	Thickness (nm) (E90) ^b
NMG/PSbPEO1010-10	200	220	2.8
NMG/PSbPEO1030-10	140	640	3

^a Determined by DLS. ^b Determined by AFM

Decreasing the PEO chain length induces a decrease of the NMG lateral size and a narrowing of the lateral size distribution. Moreover, similar values of thickness are obtained for both suspensions. These thickness values are lower than for all the NMG suspensions previously described, meaning that the PSbPEO1010 and PSbPEO1030 are better exfoliants than the other stabilizers.

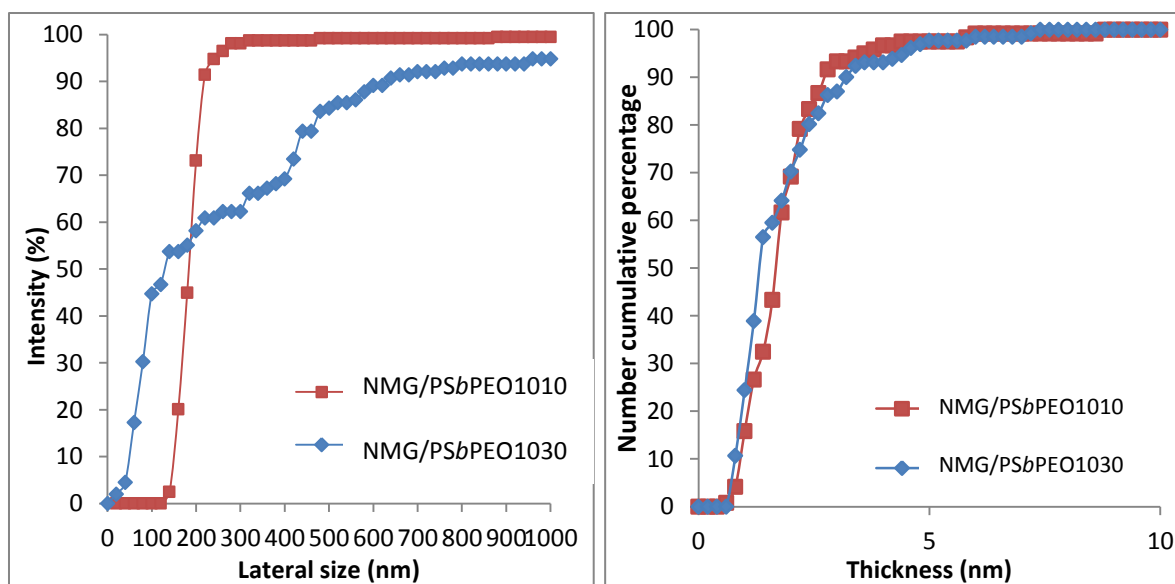


Figure 37. Cumulative lateral size and thickness distributions of NMG/PSbPEO1010 and NMG/PSbPEO1030 suspensions

As PSbPEO does not contain any heteroatom, elemental analysis could not be used in this case to calculate the amount of stabilizer. The later was thus determined by TGA (Figure 38). The results are gathered in Table 20.

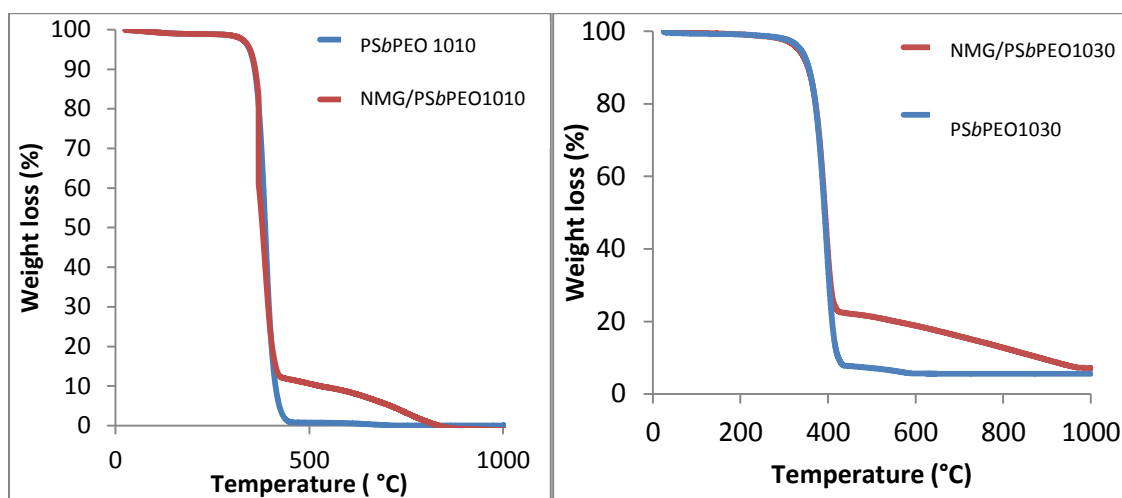


Figure 38. TGA analysis for NMG/PSbPEO1010 and NMG/PSbPEO1030

Table 20. %PSbPEO_{powder} calculation for NMG/PSbPEO1010-10 and NMG/PSbPEO1030-10 suspensions.

Sample name	TGA		
	W _{PSbPEO} (%)	W _{NMG} (%)	%PSbPEO _{powder}
NMG/PSbPEO1010-10	99.2	86.8	87.5
NMG/PSbPEO1030-10	91.3	75.4	82.5

Table 20 shows that both samples contain a high amount of stabilizer. The NMG and stabilizer concentrations in solution are then calculated and summarized in Table 21.

Table 21. Influence of PEO chain length on the NMG and PSbPEO concentrations of NMG/PSbPEO1010 and NMG/PSbPEO1030 suspensions.

Sample name	[PSbPEO] (g L ⁻¹)		[NMG] (g L ⁻¹)	
	E.A	TGA	E.A	TGA
NMG/PSbPEO1010-10	-	3.8	-	0.5
NMG/PSbPEO1030-10	-	6.9	-	1.3

It is seen that the NMG concentration in water increases with increasing the number of EO units in the stabilizer. Increasing PEO chain length increases the hydrophilicity of the block copolymer, which promotes stabilization of the NMG platelets in water. Table 21 indeed shows that PSbPEO1010 is not as efficient as PSbPEO1030 under the same conditions. In order to increase NMG concentration with PSbPEO1010, one might need to increase its initial concentration.

In conclusion, PSbPEO1030 is a good stabilizer of the NMG platelets and the final sheets possess a smaller thickness than when SDBS was used as surfactant.

Conclusions

Waterborne suspensions of Nanosize Multilayered Graphene (NMG) have been elaborated through a low cost and environmental friendly process. To stabilize the formed NMG platelets, a surfactant or a polymeric stabilizer was used. The main goal was the production of multilayered graphene platelets with a small lateral size (*i.e.* typically between 50 to 300 nm) with the aim to produce further armored latex/graphene nanocomposites.

In a preliminary study, the experimental procedure of ball milling of micrographite in a wet media was described. This method, developed by Knieke *et al.* ^[3], produces NMG platelets with a small lateral size using grinding beads and sonication. The main parameters of this process were studied and grinding beads of 400 μm have been preferred to favor to formation of NMG with small diameter but also a small thickness, to ensure acceptable electrical properties. Then, it was demonstrated that four hours of delamination are sufficient to obtain concentrated NMG suspensions. Finally, the combination of grinding and sonication induces a better exfoliation of the graphite platelets and low defects in the carbon structure. These parameters have been used in further experiments for which the influence of the surfactant or stabilizer on NMG characteristics was investigated.

To increase the stability and concentration of NMG platelets, SDBS was used instead of SDS. This surfactant possesses an aromatic ring, and can thus create π - π interactions with graphene. The replacement of SDS by SDBS induced a sharp increase of the NMG concentration in the suspension. The concentration of the produced NMG suspensions was 2 mg mL^{-1} which is two time higher than common concentrations of graphene oxide suspensions obtained through Hummer's method.

Then, polymeric stabilizers have been studied: PSSNa, PS*b*PfEO and PVPk30. The influence of their structure and concentration on the NMG characteristics and yield was investigated. It turns out that, to increase the NMG concentration and stability in the suspension, the stabilizer used must preferentially have some aromatic rings to create π - π stacking interactions with the NMG platelets.

To conclude, polymeric stabilizers, like PS*b*PfEO or PVPk30, can be effectively used to stabilize NMG platelets. These stabilizers allow producing NMG suspensions with the same or higher yield than SDBS or SDS. Furthermore, the NMG platelets obtained possess small lateral sizes and thicknesses.

These NMG suspensions can now be used for the production of conductive nanocomposite latexes through two processes: a physical blending of NMG/SDBS suspensions and latex particles (in Chapter 3) and *in situ* polymerization with various NMG suspensions, developed in Chapter 4.

References

- [1] W. S. Hummers, R. E. Offeman, *J. Am. Chem. Soc.* **1958**, *80*, 1339.
- [2] X. Gao, J. Jang, S. Nagase, *J. Phys. Chem. C* **2010**, *114*, 832.
- [3] C. Knieke, A. Berger, M. Voigt, R. N. K. Taylor, J. Röhl, W. Peukert, *Carbon* **2010**, *48*, 3196.
- [4] W. Zhao, F. Wu, H. Wu, G. Chen, *J. Nanomater.* **2010**, *2010*, 1.
- [5] U. Khan, H. Porwal, A. O'Neill, K. Nawaz, P. May, J. N. Coleman, *Langmuir* **2011**, *27*, 9077.
- [6] Y. Zhang, H.-L. Ma, Q. Zhang, J. Peng, J. Li, M. Zhai, Z.-Z. Yu, *J. Mater. Chem.* **2012**, *22*, 13064.
- [7] Y. Zhu, S. Murali, M. D. Stoller, A. Velamakanni, R. D. Piner, R. S. Ruoff, *Carbon* **2010**, *48*, 2118.
- [8] F.-P. Du, J.-J. Wang, C.-Y. Tang, C.-P. Tsui, X.-P. Zhou, X.-L. Xie, Y.-G. Liao, *Nanotechnology* **2012**, *23*, 475704.
- [9] A. Misra, P. K. Tyagi, M. K. Singh, D. S. Misra, *Diam. Relat. Mater.* **2006**, *15*, 385.
- [10] P. G. Collins, *Oxf. Handb. Nanosci. Technol. Front. Adv.* **2010**.
- [11] L. Vaisman, H. D. Wagner, G. Marom, *Adv. Colloid Interface Sci.* **2006**, *128–130*, 37.
- [12] H. Vale, T. Mckenna, **n.d.**
- [13] N. Grossiord, P. van der Schoot, J. Meuldijk, C. E. Koning, *Langmuir* **2007**, *23*, 3646.
- [14] M. J. Fernández-Merino, J. I. Paredes, S. Villar-Rodil, L. Guardia, P. Solís-Fernández, D. Salinas-Torres, D. Cazorla-Amorós, E. Morallón, A. Martínez-Alonso, J. M. D. Tascón, *Carbon* **2012**, *50*, 3184.
- [15] P. Yan, J.-X. Xiao, *Colloids Surf. Physicochem. Eng. Asp.* **2004**, *244*, 39.
- [16] “CONGRÈS FRANÇAIS DE MÉCANIQUE. Contribution au phénomène de mouillabilité en présence d’un tensioactif anionique (SDS) et non ionique C11E5,” can be found under <http://documents.irevues.inist.fr/handle/2042/36745>, **n.d.**
- [17] A. Cifuentes, J. L. Bernal, J. C. Diez-Masa, *Anal. Chem.* **1997**, *69*, 4271.
- [18] O. Matarredona, H. Rhoads, Z. Li, J. H. Harwell, L. Balzano, D. E. Resasco, *J. Phys. Chem. B* **2003**, *107*, 13357.
- [19] S. Utsumi, M. Kanamaru, H. Honda, H. Kanoh, H. Tanaka, T. Ohkubo, H. Sakai, M. Abe, K. Kaneko, *J. Colloid Interface Sci.* **2007**, *308*, 276.
- [20] K. Yurekli, C. A. Mitchell, R. Krishnamoorti, *J. Am. Chem. Soc.* **2004**, *126*, 9902.
- [21] H. N. Patrick, G. G. Warr, *Colloids Surf. Physicochem. Eng. Asp.* **2000**, *162*, 149.
- [22] E. J. Wanless, W. A. Ducker, *J. Phys. Chem.* **1996**, *100*, 3207.
- [23] A. C. Zettlemoyer, *J. Colloid Interface Sci.* **1968**, *28*, 343.
- [24] M. F. Islam, E. Rojas, D. M. Bergey, A. T. Johnson, A. G. Yodh, *Nano Lett.* **2003**, *3*, 269.
- [25] N. R. Tummala, A. Striolo, *J. Phys. Chem. B* **2008**, *112*, 1987.
- [26] M. Lotya, Y. Hernandez, P. J. King, R. J. Smith, V. Nicolosi, L. S. Karlsson, F. M. Blighe, S. De, Z. Wang, I. T. McGovern, G. S. Duesberg, J. N. Coleman, *J. Am. Chem. Soc.* **2009**, *131*, 3611.

- [27] S. Wang, M. Yi, S. Liang, Z. Shen, X. Zhang, S. Ma, *ArXiv14062113 Cond-Mat* **2014**.
- [28] S. Das, A. S. Wajid, J. L. Shelburne, Y.-C. Liao, M. J. Green, *ACS Appl. Mater. Interfaces* **2011**, 3, 1844.
- [29] J. Han, H. Kim, D. Y. Kim, S. M. Jo, S.-Y. Jang, *ACS Nano* **2010**, 4, 3503.
- [30] R. J. Chen, S. Bangsaruntip, K. A. Drouvalakis, N. W. S. Kam, M. Shim, Y. Li, W. Kim, P. J. Utz, H. Dai, *Proc. Natl. Acad. Sci.* **2003**, 100, 4984.
- [31] J. Chen, H. Liu, W. A. Weimer, M. D. Halls, D. H. Waldeck, G. C. Walker, *J. Am. Chem. Soc.* **2002**, 124, 9034.
- [32] S. Stankovich, D. A. Dikin, R. D. Piner, K. A. Kohlhaas, A. Kleinhammes, Y. Jia, Y. Wu, S. T. Nguyen, R. S. Ruoff, *Carbon* **2007**, 45, 1558.
- [33] G. Wang, B. Wang, J. Park, Y. Wang, B. Sun, J. Yao, *Carbon* **2009**, 47, 3242.
- [34] M. J. O'Connell, P. Boul, L. M. Ericson, C. Huffman, Y. Wang, E. Haroz, C. Kuper, J. Tour, K. D. Ausman, R. E. Smalley, *Chem. Phys. Lett.* **2001**, 342, 265.
- [35] A. Arzac, G. P. Leal, R. Fajgar, R. Tomovska, *Part. Part. Syst. Charact.* **2014**, 31, 143.
- [36] A. S. Wajid, S. Das, F. Irin, H. S. T. Ahmed, J. L. Shelburne, D. Parviz, R. J. Fullerton, A. F. Jankowski, R. C. Hedden, M. J. Green, *Carbon* **2012**, 50, 526.
- [37] J.-L. Mura, G. Riess, *Polym. Adv. Technol.* **1995**, 6, 497.
- [38] G. Riess, *Colloids Surf. Physicochem. Eng. Asp.* **1999**, 153, 99.

Chapter 3: Film-forming conductive inks obtained by physical blending

Introduction	90
I. State of the art on percolation theory	91
1. General considerations	91
2. Geometrical percolation	92
3. Percolation approach for electrical properties	93
4. Percolation approach for mechanical properties	94
II. Experimental part: physical blends preparation	95
1. NMG suspensions	95
2. Synthesis of surfactant-free latexes	96
a. State of the art on free-radical emulsion polymerization	96
b. Latex synthesis	100
3. Preparation of the physical blending	101
III. Morphological characterization of the NMG/latex nanocomposites	102
IV. Electrical conductivity of the nanocomposites	104
1. Effect of the NMG delamination process	104
2. Effect of the latex beads diameter	105
V. Thermo-mechanical properties of the nanocomposites	109
1. Comparison of T_{α} and T_g	110
2. Thermo-mechanical measurements	111
Conclusions	114
References	115

This chapter is a combination of two published articles:

- A. Noël, J. Faucheu, M. Rieu, J.-P. Viricelle, E. Bourgeat-Lami, *Tunable architecture for flexible and highly conductive graphene-polymer composites*, *Compos. Sci. Technol.* 95 (2014) 82–88.

- A. Noël, J. Faucheu, J.-M. Chenal, J.-P. Viricelle, E. Bourgeat-Lami, *Electrical and mechanical percolation in graphene-latex nanocomposites*, *Polymer.* 55 (2014) 5140–5145.

Introduction

In the past decades, flexible and textile substrates raised a strong interest in printed electronics applications. Wearable electronics would transform traditional textile and apparel products into lightweight, wireless and wearable intelligent devices [1]. Currently, conductive inks, in particular ink-jet inks, are mostly based on dispersions of metallic particles in an aqueous or organic medium [2]. To reach the adequate particle sintering, an annealing step at high temperature is required, around 500-1000 °C [3]. Moreover, the resulting sintered material can undergo only very small deformations. For those two reasons, flexible and textile substrates cannot be used with these inks.

The aim of this chapter is to present a simple processing route for producing conductive inks that form a continuous film at room temperature and that exhibit high deformability after drying. The strategy is based on architected nanocomposites allying conductivity characteristics of Nanosize Multilayered Graphene (NMG) and deformability of a polymer binder. The nanocomposite architecture is tuned using a latex route [4]. The production of conductive nanocomposites by blending a polymer latex with graphene-based particles has been already presented by several authors [5][6][7]. However in all of these works, Graphene Oxide (GO) and reduced Graphene Oxide (rGO) were used, increasing the number of processing steps and chemical products needed. Moreover, in most of these works, the composite blends were not stable: the composite solids ended up flocculating and a subsequent hot-pressing step was needed to produce a continuous composite material with acceptable mechanical and electrical properties. Alternatively, for nanocomposite blends formulation, the latex route exhibits two major advantages as compared to the melt route or solution route. First, this synthetic route is sustainable as a latex is made of polymer nanospheres suspended in an aqueous suspension and does not require the use of organic solvent. Second, the latex route favors the built-up of a tunable architecture of fillers (Figure 1). Figure 1 represents the architecture obtained after blending of latex particles and Nanosize Multilayered Graphene (NMG) and subsequent film-formation. The NMG platelets are trapped between the foreign latex particles. This specific architecture, in turn, favors the formation of a percolating network of fillers at lower filler content [8]. As a result, the final nanocomposite microstructure counts two interpenetrated networks, one made of the polymer matrix and the other one made of percolating fillers [9],[10].

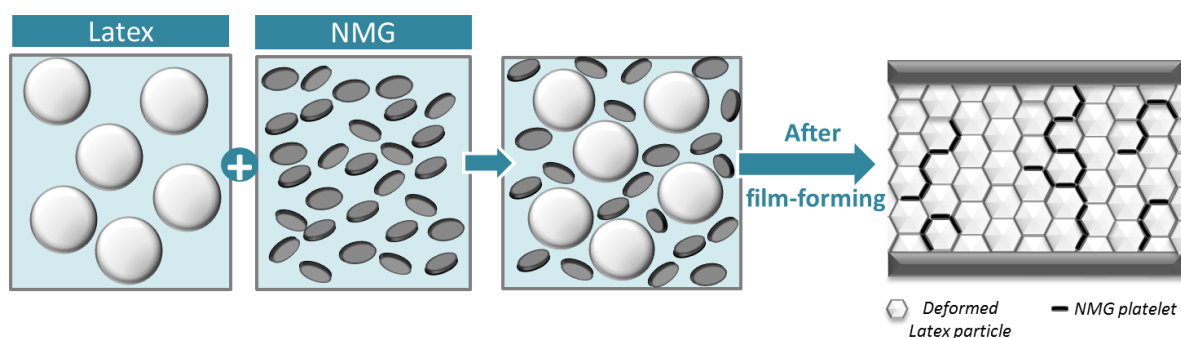


Figure 1. Scheme of the specific architecture obtained after film-forming of a nanocomposite blend containing latex particles and Nanosize Multilayered Graphene (NMG) platelets.

The use of 2D-fillers (platelets) would both favor filler contacts compared to 1D-fillers (nanotubes) and lower the percolation threshold compared to 3D-fillers (spheres). Thus, for geometrical considerations, platelet-like fillers [11] seem to be a good choice to build up an efficient network with polymer nanospheres.

The chosen size ratio between the polymer nanospheres and the fillers is a compromise. On the one hand, the platelets have to be large enough to limit the number of conductive platelets needed to cover the surface of the latex spheres and so the number of contacts. Indeed, intuitively, the contacts between fillers will have a lower conductivity than the intrinsic conductivity of the filler itself. On the other hand, the platelets have to be small enough in order not to destabilize the blend or hinder the film formation process of the latex nanospheres.

Hereafter, a state of the art on percolation theory for geometrical, electrical and mechanical percolation is presented. Then, the fabrication process and characterization of home-made conductive graphene-based nanoplatelets (NMG) and latex particles used are detailed. Thereafter, the morphological characterization and the highly conductive behavior of NMG-based nanocomposites obtained through latex blends are discussed in terms of filler architecture through a percolation approach. Finally, the influence of the NMG content on the global mechanical reinforcement is studied through the characterization of the thermomechanical properties of these nanocomposites.

I. State of the art on percolation theory

Physical blends between multilayered graphene and polymer particles have been studied by many authors. Latex particles for physical blending can be made through different polymerization processes, depending on the targeted beads diameter. Small latex beads diameters can be obtained through emulsion polymerization while larger beads diameters are usually obtained using dispersion polymerization. One of the advantages of physical blend with polymer particles and graphene filler is the creation of a segregated network by forcing the conductive particles into interstitial spaces between the polymer particles during the drying of the nanocomposite [12]. This segregated network is defined as a percolating network. In this part, the phenomenon of percolation will be explained for geometrical, electrical and mechanical properties.

1. General considerations

The percolation theory is used to describe very different transition phenomena such as sol-gel transition or virus propagation [13]. In materials science, it is often used to describe transitional behavior of electrical and mechanical properties in composites [14]. The percolation threshold is the filler critical volume fraction needed to obtain the first percolating path throughout the polymer matrix. In a percolation approach, the fillers embedded in the composite are described using two types of clusters: the finite clusters and the infinite or percolating clusters, comprising a backbone and dangling bonds (Figure 2). The finite clusters do not participate to the percolation.

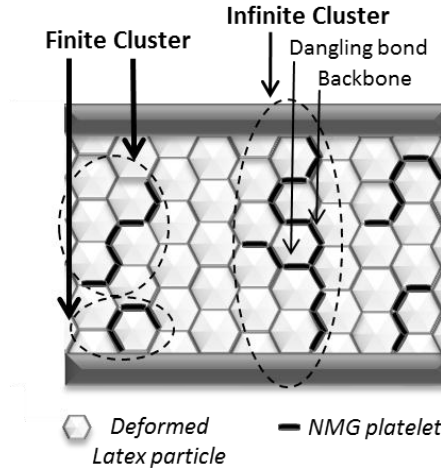


Figure 2. Percolation behavior in a latex-based graphene nanocomposite.

2. Geometrical percolation

The percolation theory is the formation of long-range connectivity in random systems to create a three-dimensional network. This network is composed of neighbor “sites” connected by “bonds”. In an infinite square network, both percolation can be defined, the “site” percolation and the “bond” percolation. The “site” percolation threshold corresponds to the smallest concentration of sites at which an infinite cluster of sites emerges. The “bond” percolation threshold is a similar concept.

Around the percolation threshold, the conductivity and mechanical properties are closely related to the weight P of the infinite cluster defined as [15]:

$$P(\phi) = A(\phi - \phi_c)^\beta \quad \text{Equation 1}$$

Where ϕ is the volume fraction of fillers relative to the total volume, ϕ_c is the critical volume fraction at the percolation threshold, A is a dimensionless constant and β is a critical exponent that only depends on the dimensionality of the material (for 3D-systems, $\beta = 0.4$).

The geometrical percolation behavior in a monodisperse latex system can be compared to a bond percolation threshold in a three-dimensional Face Centered Cubic (FCC) arrangement. This bond percolation threshold in terms of probability is $p_c = 0.119$ [18]. The percolation threshold in volume fraction, ϕ_c^{geom} , is obtained by multiplying p_c by the filling factor which can be described as the filler content corresponding to a theoretical graphene half-monolayer covering each latex bead (Figure 3). In these conditions, once in close packing configuration, a perfect NMG-cellular structure is obtained with a wall thickness equal to a full NMG-monolayer (Figure 3). The percolation threshold in volume fraction is then given by:

$$\phi_c^{\text{geometrical}} (\text{vol.}\%) = p_c \times \frac{V_{\text{NMG half-monolayer}}}{V_{\text{latex}}} \times 100 = 0.119 \times \frac{3 \cdot t_{\text{NMG}}}{D_{\text{latex}}} \times 100 \quad \text{Equation 2}$$

With $V_{\text{NMG half-monolayer}} = 4\pi R_{\text{latex}}^2 (t_{\text{NMG}}/2)$ and $V_{\text{latex}} = 4/3\pi R_{\text{latex}}^3$, D_{latex} (equal to $2R_{\text{latex}}$) is the latex diameter and t_{NMG} is the average thickness of the NMG platelets (measured experimentally, $t_{\text{NMG}}=3.2$ nm). Figure 3 describes the filling factor used to describe ϕ_c^{geom} .

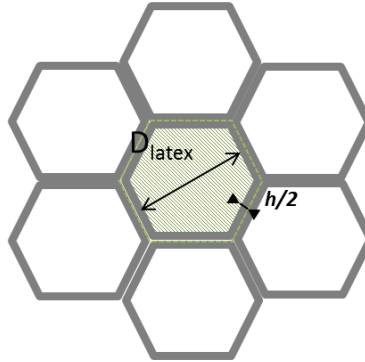


Figure 3. Scheme describing the filling factor used to describe the geometrical percolation threshold.

3. Percolation approach for electrical properties

In a conductive nanocomposite, the conductive fillers can be divided in two parts, the isolated clusters and the infinite cluster. The infinite cluster carries the electrical current, whereas the isolated clusters do not contribute to transport of electrons. The infinite cluster can be divided into two different structures: the “backbone” demonstrating the real path that carries the current and the “dangling ends”, which can be removed from the infinite cluster when a voltage is applied to the system because they do not carry any current [16].

Because of the close relationship between the conductivity, σ , and the weight, P , of the infinite network, it was demonstrated that in percolating systems, σ follows a similar power law [17]:

$$\sigma = \sigma_0 \left(\frac{\phi - \phi_c}{1 - \phi_c} \right)^t \quad \text{Equation 3}$$

where σ_0 is the macroscopic conductivity of the fillers. Except for rare symmetric situations, all the backbone bonds will carry some current when a voltage is set between the upper and lower edges of the cluster. At the percolation threshold most of the weight of the infinite cluster belongs to dangling bonds, not to the backbone. As described by Xie et al. for nanocomposites with Carbon Nanotubes (CNT) dispersed in a cement matrix, the backbone density represents only 15% at the percolation threshold [18].

Thus most of the weight contained in P makes no contribution to the conductivity σ , and therefore, the critical exponent t differs from the critical exponent β [17]. The values of conductivity critical exponent were considered to be universal such as $t=1.6-2.0$ in three dimensions lattices based on the renormalization group theory [19]. As described by Xie et al., the value of the critical exponent t strongly depend on the mass proportion of backbone and dangling ends density in the system [18]. The backbone or dangling ends density is defined as the portion of the total backbone or dangling ends that belong to the percolation

infinite clusters, respectively. When the backbone density goes to infinite, i.e., no dangling ends in the system, the t value goes to zero.

As expected, the critical exponent t is higher than β as β takes into account the non-conductive dangling bonds of the infinite clusters.

4. Percolation approach for mechanical properties

The percolation approach for mechanical properties is more complex. Indeed, while the question of conductivity has a binary response, either the cluster conducts, either it does not, in the case of mechanical properties, both finite and infinite (backbone and dangling bonds) clusters can influence the final mechanical response, to various extents. The infinite cluster will have the most reinforcing effect, the finite cluster the lowest one, and the effect of the dangling bonds will lie in between. A phenomenological model associating springs in series and parallel (Figure 4) has been proposed to describe the effect of filler percolation on the mechanical response of composites [20][21].

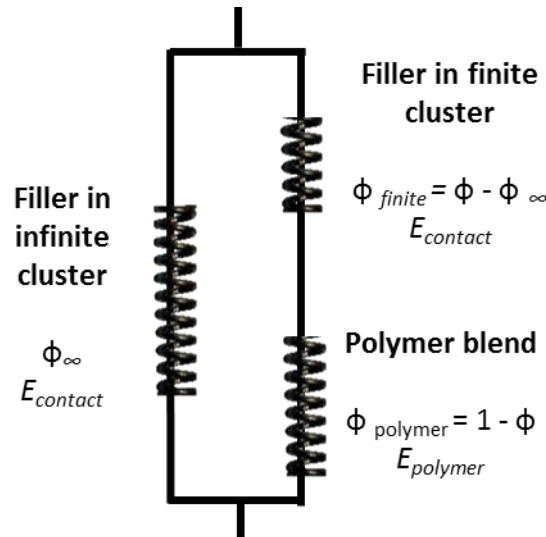


Figure 4. Series/parallel model extended with a percolation concept.

In that model, the reinforcement due to fillers in finite clusters has been considered as low (associated in series with the polymer matrix) while fillers in infinite clusters are associated in parallel. In this description, for $\phi < \phi_c$, the infinite cluster is not yet formed, thus its volume fraction ϕ_{∞} is zero. For $\phi \geq \phi_c$, ϕ_{∞} is established using the power law:

$$\phi_{\infty} = \left(\frac{\phi - \phi_c}{1 - \phi_c} \right)^b \quad \text{Equation 4}$$

The value of the critical exponent b lies between 0.4 and 1.6. If $b=0.4$, the reinforcing effect of the dangling bonds is considered as similar to the one of the backbone and if $b=1.6$, the dangling bonds are considered as non-reinforcing, similarly to the conductivity behavior. The

stronger the interaction between fillers and polymer matrix, the lower the value of critical exponent b will be. In nanocomposites where interfacial surface is developed, a low value for b is expected. In literature, Bauhofer *et al.* used $b=0.7$ for composite materials composed of single walled nanotubes dispersed in a poly(methyl methacrylate) matrix [22] while Nawaz used $b=0.8$ for graphene oxide/elastomer composites [23]. At least, Faucheu *et al.* used $b=0.4$ for clay-polymer nanocomposites [24]. b is an adjustable parameter, in this work it has been fitted to 0.6 considering our experimental data.

Based on this series-parallel phenomenological model, the elastic modulus, $E_{\text{composite}}$, of the composite is then given by [20]:

$$E_{\text{composite}} = \frac{(1 - 2\phi_{\infty} + \phi_{\infty}\phi)E_{\text{filler-filler}}E_{\text{polymer}} + \phi_{\infty}(1 - \phi)E_{\text{filler-filler}}^2}{E_{\text{polymer}}(\phi - \phi_{\infty}) + E_{\text{filler-filler}}(1 - \phi)} \quad \text{Equation 5}$$

where $E_{\text{filler-filler}}$ and E_{polymer} are respectively the elastic moduli of the reinforcing and the soft components (i.e. the NMG platelets and the polymer matrix). $E_{\text{filler-filler}}$ represents the stiffness of the filler-filler clusters and so takes into account both the intrinsic stiffness of the filler and the stiffness of the filler-filler contacts. In literature, the filler-filler stiffness for cellulose nanofibrils was set at 1.9 GPa [25], and for polymer blends this value was set at 2.0 GPa [20] and 1.8 GPa, [21] depending on the nanocomposite composition. As a consequence, in this paper, $E_{\text{filler-filler}}$ for NMG was set arbitrarily at 1.8 GPa.

In the following, these different percolation approaches will be used to compare the electrical and mechanical properties of nanocomposite films obtained through physical blending of NMG platelets and polymer particles. The challenge relies on the production of adequate conductive fillers with specific dimensional characteristics that do not destabilize the latex during blending. First, the NMG suspensions and latexes particles used for the physical blend will be described. Then, physical blending of polymer particles with two different diameters and NMG particles will be physically blended and film-formed at room temperature. Finally, their electrical and mechanical properties will be studied.

II. Experimental part: physical blends preparation

1. NMG suspensions

As described in Chapter 2, the conductive particles, NMG, were obtained using a bead milling procedure in wet media combined with sonication. A stable NMG suspension stabilized by a surfactant was isolated through decantation. It was used as-is or after increasing the NMG-content by water evaporation. For the preparation of the nanocomposites, we used the suspension NMG/SDBS-5 described in Chapter 2. The influence of the mechanical delamination and sonication during the NMG production process was been studied. The goal was to evaluate the impact of the NMG formation process on the final electrical properties of

the nanocomposites formed. The main characteristics of the NMG/SDBS-5 suspensions used in this chapter are reminded in Table 1.

Their dimensions were measured by AFM for the thickness and DLS for the lateral size. The proportion of surfactant in each suspension was measured by TGA. In addition to adequate NMG size characteristics for latex blending, these NMG water suspensions exhibited good self-stability (no sedimentation nor flocculation after 2 weeks).

Table 1. Characterization of the NMG-SDBS5 suspensions after sonication, wet grinding or the combination of the two processes.

NMG/surfactant suspension name	[Surfactant] (g L ⁻¹) ^a	[NMG] (g L ⁻¹) ^a	Lateral size (nm)		Thickness (nm) 90% (E90) ^c
			50% (D50) ^b	90% (D90) ^b	
NMG/SDBS5_S	5.8	1.4	50	340	4
NMG/SDBS5_WG	3.1	1.8	90	860	4.6
NMG/SDBS5_WG/S	3.1	2.1	30	160	3

S=sonication, WG=wet-grinding and WG/S= wet grinding and sonication

^a measured by TGA, ^b measured by DLS and ^c measured by AFM.

The delamination process has an influence on the mean lateral size and thickness of the NMG platelets formed, but it will also have an influence on the electrical properties.

Influence of these three suspensions on the final electrical properties will be studied first for a physical blending of the NMG suspensions with polymer particles with a mean diameter of 650 nm. Then the influence of the polymer particle diameter on the final electrical and mechanical properties will be studied for a physical blending of NMG/SDBS5-WG/S and polymer particles with two different diameters (300 nm and 650 nm).

First, the preparation of the latex particles will different diameter without surfactant is described in the following part. Owing the presence of surfactant in the NMG suspensions and to favor the formation of large polymer particles, the latexes will be synthetized without surfactant in this work.

2. Synthesis of surfactant-free latexes

a. State of the art on free-radical emulsion polymerization

Free radical polymerization is a well-established polymerization technique for the synthesis of polymeric materials. This polymerization method is the most versatile type of chain growth due to its compatibility with most monomers. Moreover this technique is tolerant to impurities and adaptable for large-scale production. Free radical polymerization can be done in bulk, solution, or in dispersed media. Basically, this polymerization process involves four concomitant steps: initiation, propagation, chain transfer and termination (Figure 5).

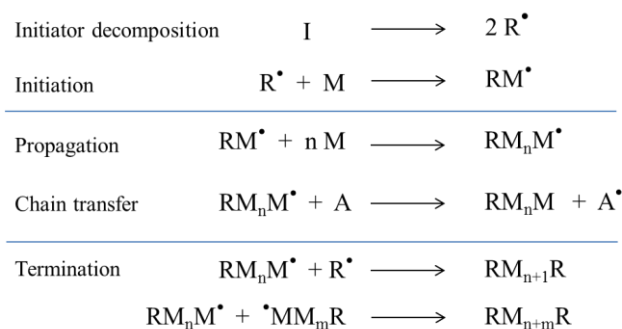


Figure 5. Reaction steps in radical free polymerization.

Initiation is the first step of the polymerization process. During initiation, an active center is created from which a polymer chain is generated. Initiation involves two steps. In a first step, one or two radicals (R^{\bullet}) are created from the initiating molecules. In a second step, radicals are transferred from the initiator molecules to the monomer units (M) present. Propagation reactions follow after the initiation step and the increase in polymer chain length occurs during this process. Chain transfer results in the annihilation of one radical, but also the creation of another radical. Several chain transfers to the solvent, to the monomer, to the initiator or to the polymer can occur. The main effect of chain transfer is a decrease of the polymer chain length. Finally the growth of the polymer chains is stopped by termination.

Radical polymerizations in bulk or solvent media are associated with several issues such as viscosity, high cost, dissipation or environmental problems. In dispersed media, where the continuous phase is usually water, polymerization is much more convenient and has long been widely used for the preparation of colloidal latex particles [26].

Radical polymerization in dispersed systems can be conducted by various methods e.g. suspension, dispersion, precipitation, emulsion, miniemulsion or dispersion polymerizations [27]. These methods are similar in terms of components (monomer(s), initiator and emulsifier and/or stabilizer). However, they can be distinguished based on (i) initial state of the polymerization mixture, (ii) nucleation loci and kinetics of polymerization, and (iii) the size of the final polymer particles.

In this chapter, we will only describe the emulsion polymerization process. Miniemulsion and dispersion polymerizations will be discussed in Chapter 4.

Emulsion polymerization is a free-radical polymerization process in heterogeneous dispersed media. This process is among the most widely used polymerization method in industry for the synthesis of large quantities of latex for paints, coatings and adhesives [28].

In emulsion polymerization, the surfactant, the monomer and the initiator are initially present in a heterogeneous aqueous medium where the monomers are non-water soluble. A water-soluble initiator is usually used to initiate the polymerization. In emulsion polymerization, surfactants are usually added in a concentration above the Critical Micelle Concentration (CMC), so that micelles (aggregates of surfactant molecules) are formed and serve as the polymerization loci. The monomer, which is partially hydrophobic, is partitioned in big

reservoirs (droplets), inside the micelles and a small amount is present in the aqueous phase (Figure 6).

The water-soluble initiator can be decomposed thermally, photochemically or by the addition of an activator (redox) to form radicals in the aqueous phase. These radicals react with the monomer present in the water phase to form oligoradicals. These oligoradicals continue to grow by adding monomer units, until they reach a critical length for which they are no longer soluble in water, causing their migration to micelles or their precipitation depending on the nucleation mechanism. The polymerization continues inside the micelles, now called particles, swollen by monomer via diffusion of the monomer molecules from the droplets to the particle core. Along the polymerization, particles grow by gradual entry and consumption of monomer. Polymerization ends when all monomer is consumed. The size of the particles obtained ranges from 100 to 600 nm.

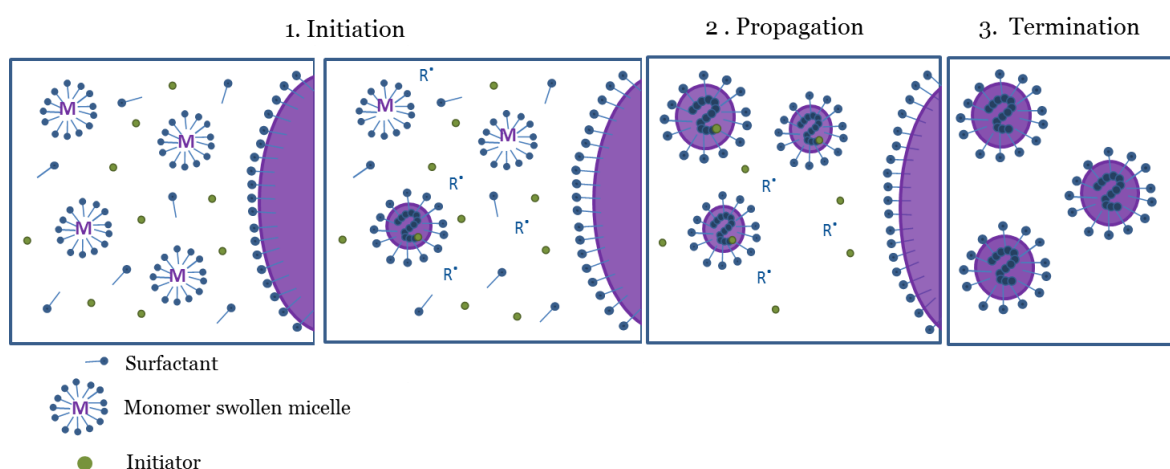


Figure 6. Schematic representation of the different stages of emulsion polymerization.

During the polymerization, two processes occur simultaneously: (i) initiation, propagation and termination of the polymer chains via free radical polymerization, and (ii) nucleation, formation and growth of latex particles. Smith and Ewart [29] proposed an arbitrary division of the later process in three phases, giving Phase I as the nucleation process; Phase II as the growth of particles; and phase III as the end of polymerization (Figure 7).

i- *Phase I* is characterized by the formation of radicals and oligoradicals in the aqueous phase and their migration to the micelles core to nucleate the first particles. During this initial phase, the polymerization rate increases owing to the formation of new particles. This phase goes from 0 to 15% of conversion [30].

ii- *Phase II* starts after nucleation when the number of particles is constant. It consists in the growth of the nucleated particles by consumption of the monomer present inside the monomer swollen particles. The polymerization rate is constant during this phase due to the constant monomer concentration inside each particle and the constant number of particles.

iii- *Phase III* comprises the consumption of the residual monomer inside latex particles, after all droplets are consumed. During this phase the polymerization rate decreases due to the gradual decrease of monomer concentration. The transition from phase II to phase III occurs generally at a monomer conversion between 80 to 90 %.

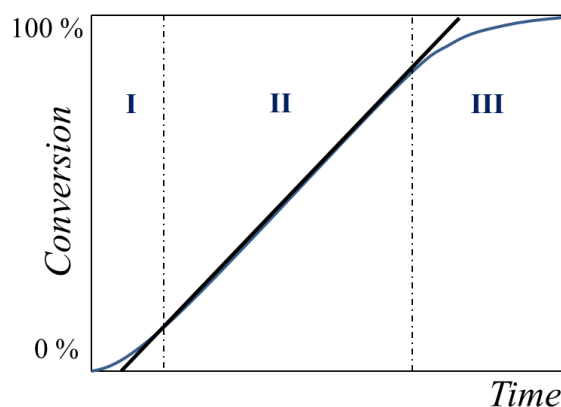


Figure 7. Typical kinetic profile of emulsion polymerization.

Different types of nucleation mechanisms can be distinguished depending on the surfactant concentration and the nature of the monomer. All mechanisms take place simultaneously during polymerization:

- (i) Micellar nucleation, occurs when the surfactant concentration is above its CMC and micelles are present. First oligoradicals start to grow until they reach a critical length for which they are no longer soluble in water, causing the migration to the micelles [31].
- (ii) Homogeneous nucleation occurs by the collision of two precipitated oligoradicals, which have also reached a certain length for which they lose solubility in water. This type of nucleation occurs mainly when a large concentration of monomer is found in water or in the absence of micelles [32].
- (iii) Coagulative nucleation can be considered as an extension of homogeneous nucleation. The very small nuclei formed by one of the precedent mechanisms agglomerate to form new larger particles, due to their poor colloidal stability or difficulty on swelling with monomer [33].

To favor the synthesis of larger polymer particles, surfactant-free emulsion polymerization can be realized. This heterogeneous process takes place without micelles [34] [35].

Emulsion polymerization can be performed under three different processes, namely (i) batch, (ii) semi-batch or semi-continuous and (iii) continuous.

- (i) In close reactors or batch systems, all the reagents are added in the same time before starting polymerization, and time is the only variable.
- (ii) Semi-batch or semi-continuous processes are carried out by initially loading the reactor with part of the reagents, to enable the control over temperature and nucleation and to fix the number of particles in the medium. The other part of the reagents is added in a second step to continue the process. This technique is widely used industrially, since it allows the control over polymer composition or the control over particles morphology.
- (iii) Continuous systems are constituted of various reactors connected in series where the reagents are continuously fed and the product is also continuously recovered at the end of the

cascade line. This process is used for large scale productions, but it is difficult to control the granulometry and the morphology of the particles.

Batch and semi-batch processes will be used in this work to create latex particles with various diameters through soap-free emulsion polymerization.

b. Latex synthesis

To obtain film-forming nanocomposites, the polymer matrix was chosen in order to have a polymer glass transition temperature around the room temperature. To do so, a copolymer of butyl acrylate and methyl methacrylate in equal proportions (50/50, wt/wt) was chosen. Moreover, to obtain polymer particles with a large diameter, the copolymerization was performed in the absence of surfactant. The mean polymer particle diameter can be increased by changing the process from a batch to a semi-batch process.

Submicronic latex particles were obtained by surfactant-free polymerization. To do so, the monomers (MMA, 12.5 g and BA, 12.5 g) were poured in the reactor and degassed under nitrogen. Water (95 g) was added for further degassing and the reactor was pre-heated at 70°C. After injection of the initiator (KPS, 0.25 g) dissolved in water (5.0 g), the polymerization was carried out during 5 hours at 70 °C. A final monomer conversion of 99 % was reached. The average hydrodynamic particle diameter determined by DLS was 300 nm (Figure 8) (0.03 Polydispersity Index). Polydispersity index represents the distribution of polymer particles in a sample. This latex will be named D300 in this chapter.

Larger latex particles were obtained through a semi-batch process. The mixture of both monomers was added in the reactor during the polymerization at 12.5 mL/hour rate. The average particle size determined by DLS was 650 nm (0.15 Polydispersity Index) (Figure 8). This latex will be named hereafter D650.

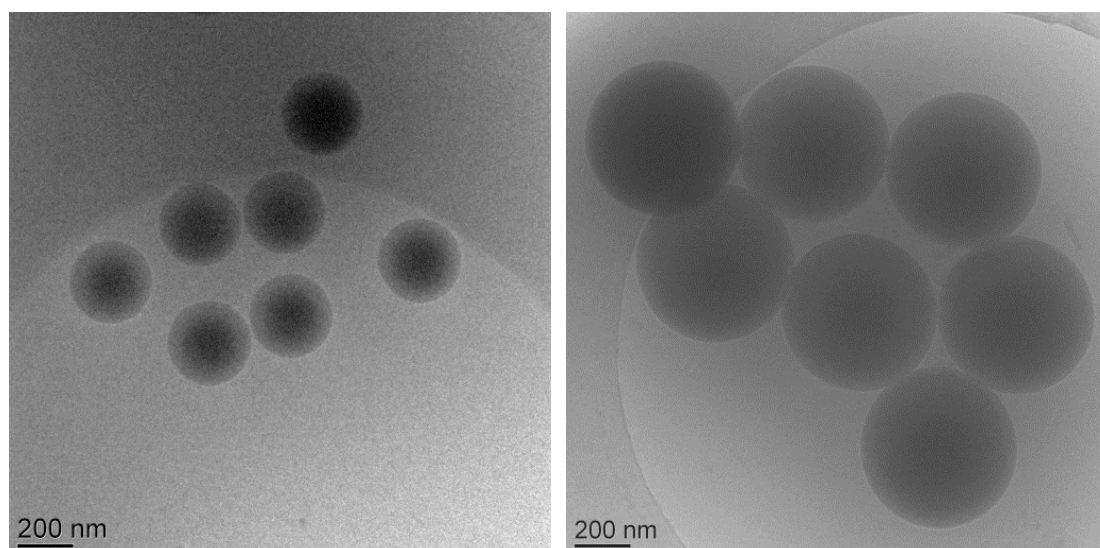


Figure 8. Cryo-TEM picture of the polymer particles with a mean diameter of 300 nm and 650 nm obtained by surfactant-free emulsion polymerization in batch and semi-batch process respectively.

These two latexes will be used for physical blending with the NMG/SDBS suspensions described.

3. Preparation of the physical blending

The physical blends were obtained by slowly introducing the NMG platelets into the latex suspension drop-by-drop to promote the NMG adsorption onto the latex nanospheres. In a typical experiment, the latex (1.0 g) was poured in a beaker and placed in an ultrasonic bath. The adequate amount of NMG suspension was placed in a syringe. The NMG-content and the volume of suspension depended on NMG-content of the final composite that was aimed. The NMG suspensions of different solids contents were slowly added to the P(MMA-co-BA) latex in an ultrasonic bath and left standing for 10 min (Figure 9).

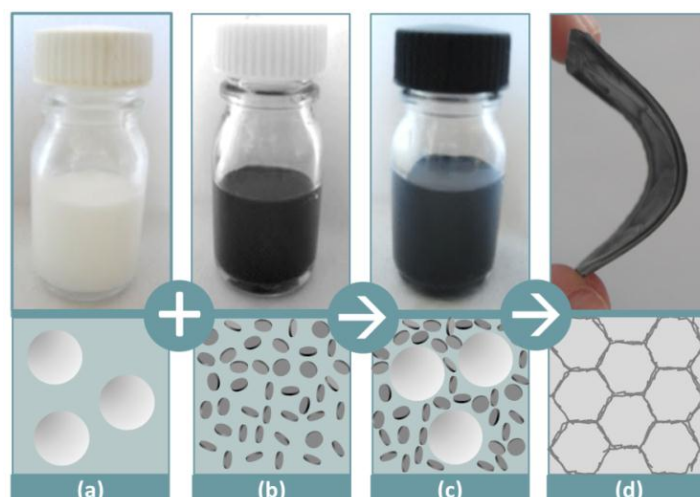


Figure 9. Processing steps of the nanocomposite materials, (a) blank latex, (b) NMG suspension, (c) NMG-latex blend, (d) flexible and conductive material obtained after water evaporation and film formation.

The blends exhibited a homogeneous dark grey color and no sedimentation, phase separation nor flocculation was observed. They were poured into silicone molds and left to film-form overnight at 40 °C. Despite the presence of nanoplatelets in the water phase, flexible free-standing films (around 200 μm thick) were easily extracted from the silicon molds after film formation.

In the following, the samples will be referenced according to the mean polymer particle diameter (D300 or D650), the volume percentage of NMG in the nanocomposite film (from 0 to 12.1 vol%) and the delamination process used to obtain the NMG platelets (WG/S, WG or S) (Table 6).

Note that after the film forming process, surfactant molecules may exude at the air-film and mold-film interfaces which might influence the conductivity measurements [36]. Thus, all the composite films were washed several times in deionized water prior to further characterization.

Table 6. NMG volume content for each NMG/latex suspensions

Sample reference	NMG content (vol.%)						
D300-0	0.0	D650-WG/S-0	0.0	D650-WG-0	0.0	D650-S-0	0.0
D300-0.3	0.3	D650-WG/S-0.8	0.8	D650-WG-0.3	0.3	D650-S-0.1	0.1
D300-1	1.0	D650-WG/S-1.2	1.2	D650-WG-1.1	1.1	D650-S-0.2	0.2
D300-2.3	2.3	D650-WG/S-2	2.0	D650-WG-1.9	1.9	D650-S-0.4	0.4
D300-6.5	6.5	D650-WG/S-3.2	3.2	D650-WG-4.6	4.6	D650-S-0.8	0.8
D300-8.3	8.3	D650-WG/S-5.7	5.7	D650-WG-7.7	7.7	D650-S-2.4	2.4
D300-10.7	10.7	D650-WG/S-7.9	7.9	D650-WG-10.1	10.1	D650-S-4.0	4.0
-	-	D650-WG/S-9.6	9.6	D650-WG-12.1	12.1	D650-S-5.5	5.5
				-		D650-S-6.8	6.8

Influence of these three suspensions on the final electrical properties will be studied. Then the influence of the polymer particle diameter on the final electrical and mechanical properties will be studied for a physical blending of NMG/SDBS5-WG/S and polymer particles with two different diameters (300 nm and 650 nm). First, thin cross sections of the nanocomposites films D300 and D650 were performed for morphological characterization in order to observe the repartition of the NMG platelets in the nanocomposite films.

III. Morphological characterization of the NMG/latex nanocomposites

Thin foil TEM-specimens were prepared to assess the nanostructure of the final composite films. These thin foil specimens (< 100 nm) of the nanocomposite materials were prepared using a diamond knife on a cryo-ultramicrotome and observed using Transmission Electron Microscopy (TEM Philips CM120) at the CT μ (Centre Technologique des Microstructures, Lyon 1 University). First, the influence of the NMG concentration on the film microstructure is observed on Figure 10 for the samples D650-WGS-1.2 and D650-WG/S-7.9.

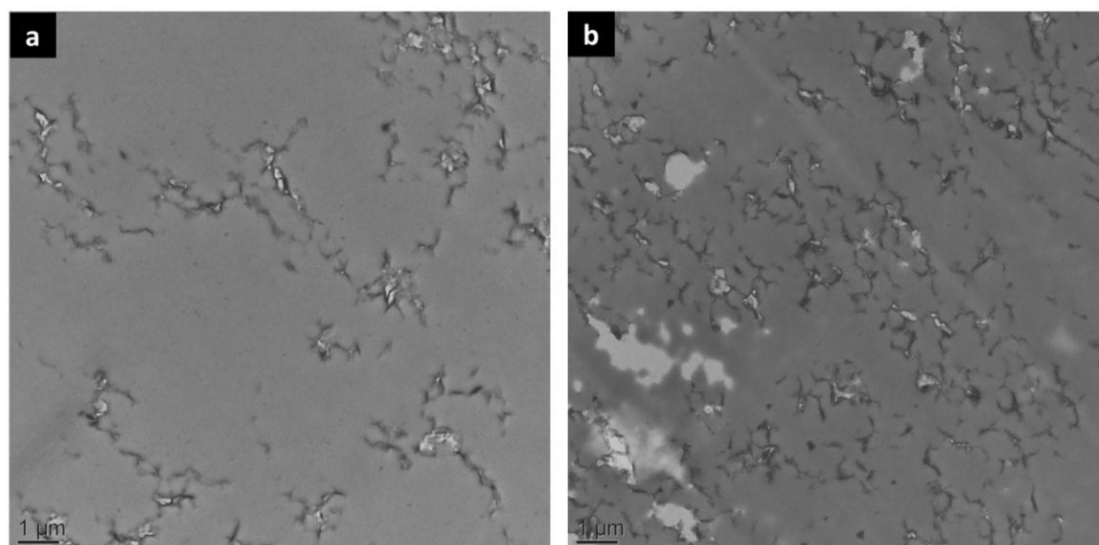


Figure 10. TEM micrograph of a thin foil extracted from (a) D650-WG/S-1.2 and (b) D650-WG/S-7.9.

On the TEM micrographs, light grey domains are holes in the thin cross section. The polymer matrix appears in medium grey as a homogeneous background. Due to their very small thickness, the NMG platelets are visible when they are edge on, then they appear as dark sticks or dark aggregates. Compact arrangement of latex particles surrounded with NMG platelets is visible as domains distributed as a cellular structure. These TEM observations are consistent with a geometrical description of the composite as a close-packed cubic arrangement of deformed spheres.

At lower magnification, NMG paths are visible throughout the nanocomposite material. The TEM micrograph shows a 2D-cross-section of the 3D-NMG network that is developed throughout the whole material. These cross-sections give insights of the network density. As expected, with an increase of NMG content from 1.2 % vol to 7.9% vol, the network density is clearly higher: an increasing number of paths are visible and an overall cellular architecture appears (Figure 10).

The morphology of the composites was then assessed through TEM observation on thin-foils cut from the most concentrated films for both sample series to observe the influence of the polymer beads diameter (Figure 11). The morphology of the D300-10.7 sample (Figure 11b)

seems less organized than the one of the D650-WG/S-9.6 sample (Figure 11a). That might be due to the fact that the size ratio between the NMG platelet and the latex nanosphere is less favorable for a neat deformed close-packing in the case of D300 series compared to D650 series.

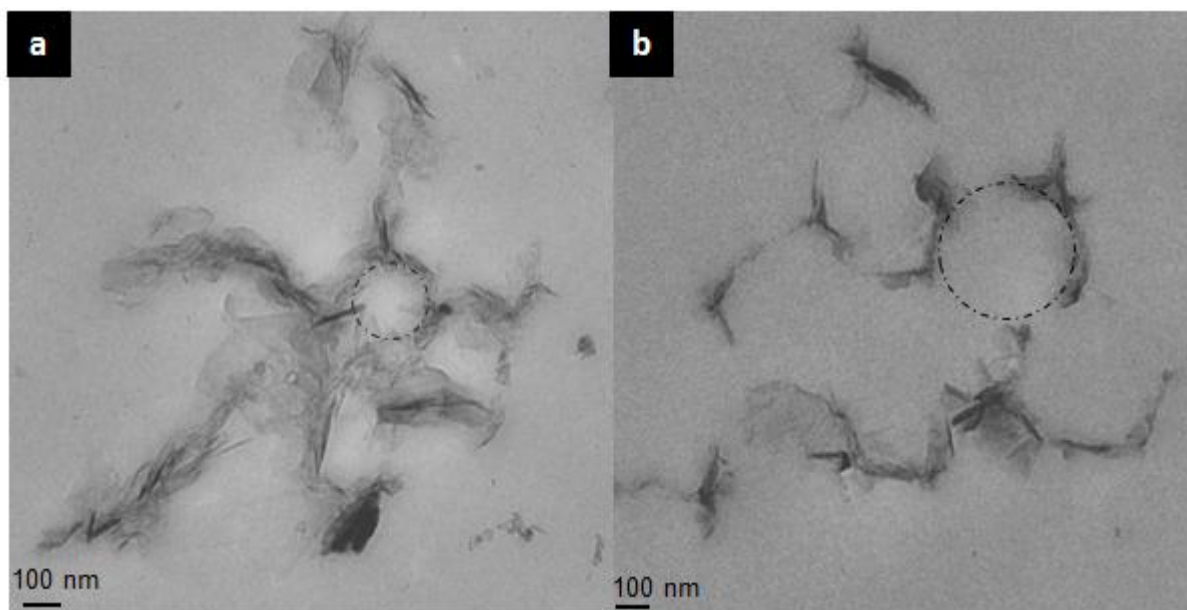


Figure 11. TEM pictures of cryo-ultramicrotome cross sections of nanocomposite films made with polymeric beads of a- 650 nm and b- 300 nm for 10 vol % of NMG volume fraction.

Thanks to the latex blending route, using fillers with adequate sizes, flexible NMG/polymer composite materials with an architected microstructure were elaborated. The influence of latex beads diameter on electrical and mechanical properties are explored hereafter.

IV. Electrical conductivity of the nanocomposites

The electrical conductivity was measured directly using a four-probe setup equipped with a conductimeter (Keithley 2400) [22]. Measurements can be done on free-standing films or on film deposited on a substrate. In our case, ten measurements on free-standing films were performed on each side of each composite film. The mean value was considered and standard deviation is reported on the graphs. Conductivity results are normalized regarding samples shape and thickness using form factors (Appendix I).

1. Effect of the NMG delamination process

As recalled in Table 1, processing conditions influence the concentrations of NMG and surfactant in the final suspension as well as the dimensional characteristics of the NMG. Based on the characteristics of the NMG suspension, it was shown that the combination of mechanical delamination and sonication is the most interesting choice (Chap 2.II.4). Nanocomposite films D650-WG/S, D650-WG and D650-S were produced and electrical measurements were performed. Figure 12 presents the experimental results for the three series (dark diamonds for D650-WG/S, grey squares for D650-WG and dark grey circles for D650-S).

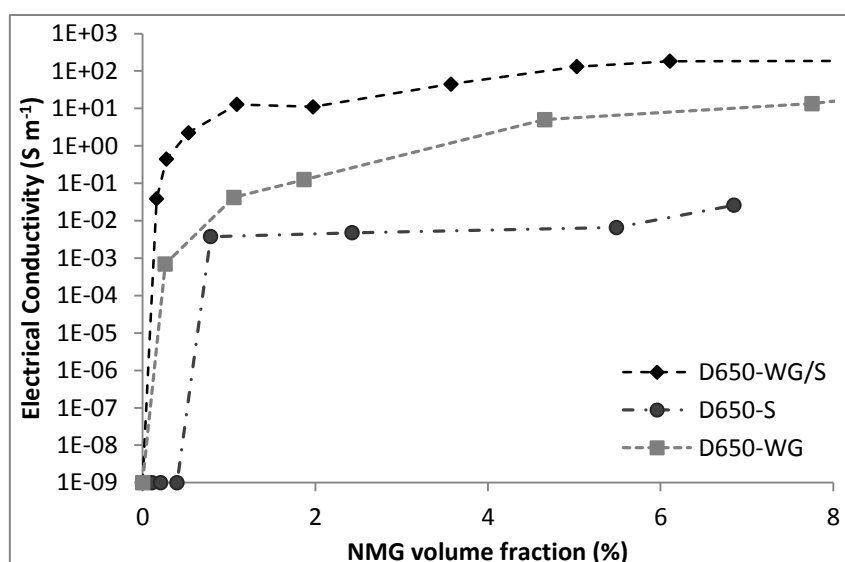


Figure 12. Measured electrical conductivity of the nanocomposite specimens.

Note that the conductivity of the blank sample ($vol\%(NMG) = 0$) was not measured but set to a value for common dielectric materials (10^{-9} S m^{-1}) [37]. The experimental values exhibit first a steep increase in electrical conductivity from 10^{-4} to 1 S m^{-1} , at low NMG volume fraction followed by a softer increase for NMG volume fraction above 2-3 vol.%.

The steep increase of the conductivity corresponds to the percolation threshold. Figure 12 shows that the percolation threshold is influenced by the process used to produce the NMG platelets. The lowest percolation threshold is for the combination of mechanical delamination and sonication. Furthermore, the maximum conductivity is also higher for the NMG platelets made through this process. These results confirm that the combination of mechanical delamination and sonication is also the most interesting choice considering the final electrical properties of the nanocomposite.

2. Effect of the latex beads diameter

Figure 13 presents the experimental measurements of electrical conductivity for both sample series (grey diamonds for D300 and dark squares for D650). The experimental values exhibit first a steep increase in electrical conductivity from 10^{-4} to 1 S m^{-1} , at low NMG volume fraction followed by a softer increase for NMG volume fraction above 2-3 vol.%. A quasi-plateau is reached around 10-11 vol.% of NMG with a maximum electrical conductivity of 700 S m^{-1} for D300-11 and 217 S m^{-1} for D650-10. To the best of our knowledge, these conductivity values are among the highest values available in literature for graphene-latex composites [38].

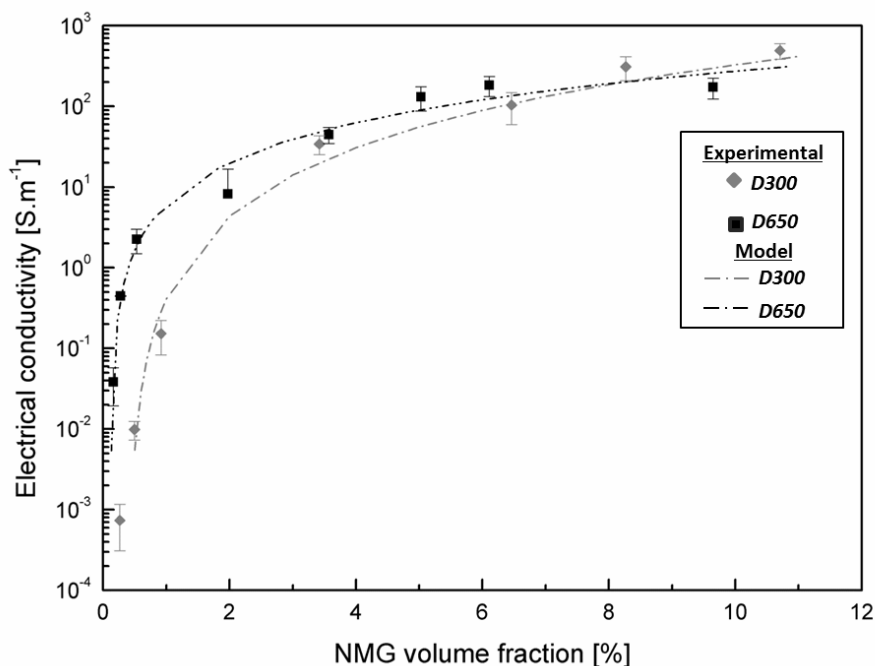


Figure 13. Electrical conductivity in function of the NMG volume fraction for D300 (grey diamond) and D650 (black Square).

To highlight the influence of the NMG 3D-network on conductivity, the behavior of graphene-based nanocomposites is usually described through a probabilistic approach called percolation theory described in the first part of this chapter [17].

Based on Equation 3, the conductivity of the nanocomposite material, σ , can be plotted in function of the filler volume percentage, ϕ [39] [40]. In literature, the statistical percolation threshold is said to depend on the lattice dimensionality (3 dimensions in our case) and lattice geometry (more likely close to faced-centered cubic in these latex-based materials) [41]. The critical exponent t is a universal exponent that is said to mainly depend on the dimensionality of the lattice. To use the conductivity model (eq.3), the percolation threshold is adjusted in order to obtain a linear regression consistent with the experimental data (Figure 14) and with acceptable values for both parameters σ_0 and t .

In the conductivity model, σ_0 describes the conductivity of NMG clusters in the nanocomposite. This conductivity is strongly related to both the intrinsic characteristics of the filler and the quality of interactions between fillers. Values for the intrinsic conductivity of graphene monolayers are largely documented in literature around 10^7 - 10^8 S m⁻¹ for in-plane graphene monolayer conductivity [42]. It was demonstrated that in-plane conductivity decreases with increasing the number of graphene layers due to overlapping of the non-hybridized p_z orbitals perpendicular to the sheets. The addition of one layer to a monolayer was found to divide by half the conductivity while further addition leads to lower influence [43], thus the conductivity of few-layer graphene is expected around 10^6 - 10^7 S m⁻¹. However, these extremely high values do not take into account the filler-filler contacts.

Marinho et al. conducted an experimental study on conductivity of powder compacts made of graphite and graphene powders [44]. They measured $2.12 \cdot 10^3 \text{ S m}^{-1}$ for the graphite compacts and $2.62 \cdot 10^2 \text{ S m}^{-1}$ for the graphene compacts. The higher conductivity exhibited by the graphite compacts might be due to larger particle-particle contacts that overcome the lower intrinsic conductivity of graphite compared to graphene. In this work, a compact made of the homemade NMG-powder was produced with measured conductivity of 5.10^4 S m^{-1} .

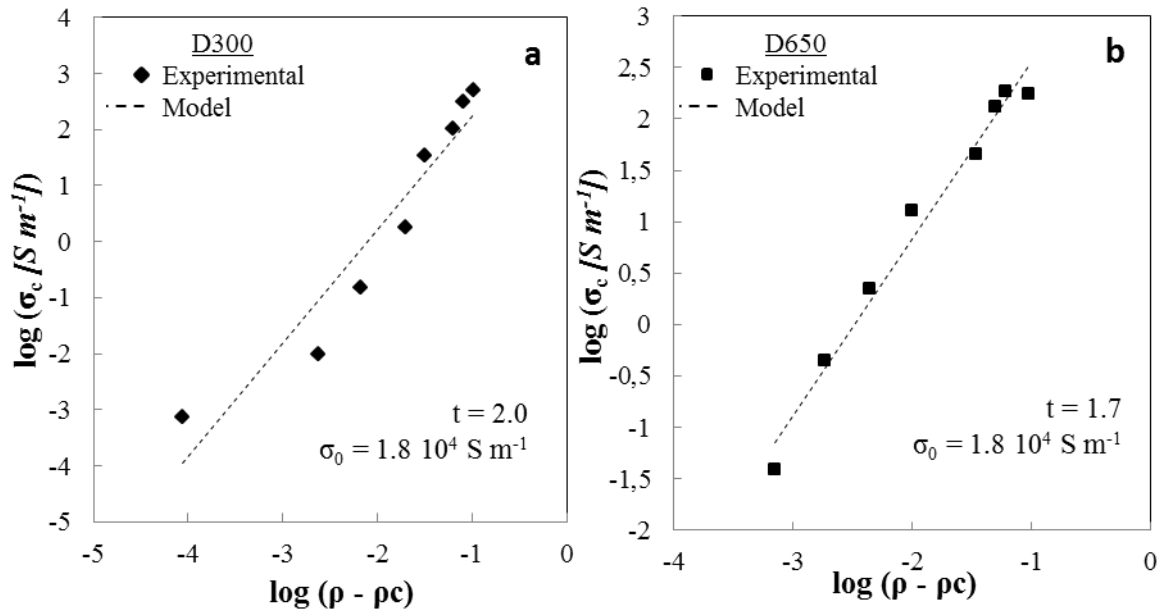


Figure 14. Log-Log plot illustrating the percolation model for a- D300 and b- D650.

For both series, σ_0 carries the acceptable value of $1.8 \cdot 10^4 \text{ S m}^{-1}$. This value is consistent with the conductivity of NMG-powder discussed here-before. The critical exponent t remains in the 1.6-2.0 acceptable range [45], [46]. Under these conditions, linear regression (Figure 14) of good quality is obtained from the model equation. The percolation thresholds (ϕ_c^{elec}) extracted from these linear regressions are 0.4 vol.% for D300 samples and 0.12 vol.% for D650 samples.

A fair consistency is found between the model curves and the experimental measurements on Figure 13. Moreover a higher percolation threshold and a higher electrical conductivity maximum are found for D300 series. These results can be qualitatively discussed considering the description of percolation behavior described in Figure 15. In this Figure, a percolation path in the compact arrangement of latex beads is illustrated in a two dimensional simple description taking into account the size ratio between latex beads and NMG-platelets. For a given number of NMG-platelets, on the one hand, the number of possible percolating paths is higher for D300 leading to a higher percolation threshold. On the other hand, the total number of percolating paths is higher for D300 leading to a higher maximum electrical conductivity.

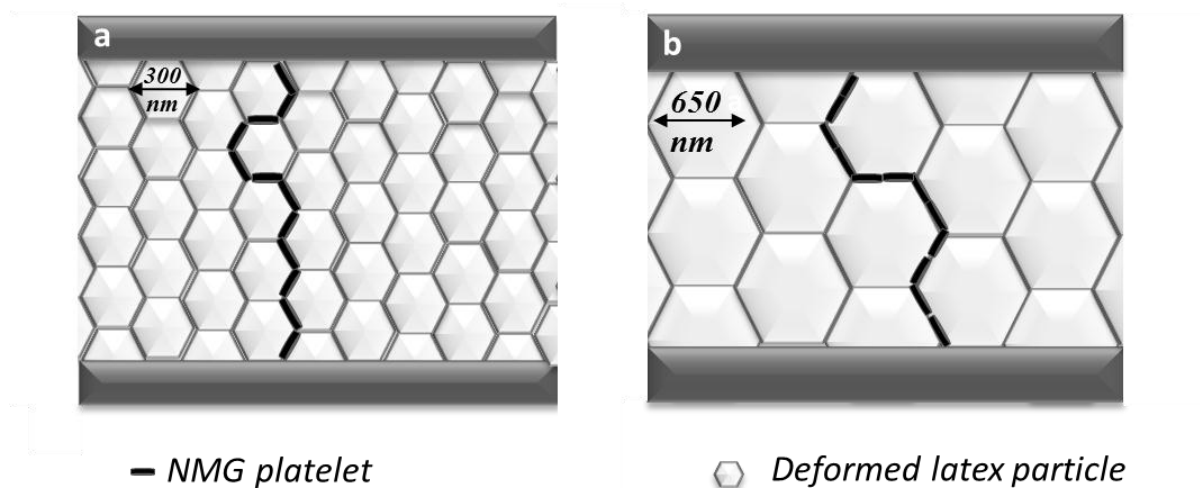


Figure 15. Scheme of a percolating path throughout the polymer matrix made of a- D300 and b- D650.

In summary, the conductivity behavior observed for these graphene-based nanocomposite materials is consistent with a three-dimensional percolation behavior. The mean diameter of the latex beads has a significant influence on the percolation threshold and the maximum of electrical conductivity after film-forming of the nanocomposites.

In order to demonstrate the potential application of our conductive films, a basic electronic setup based on a light emitting diode (LED) was mounted (Figure 16).

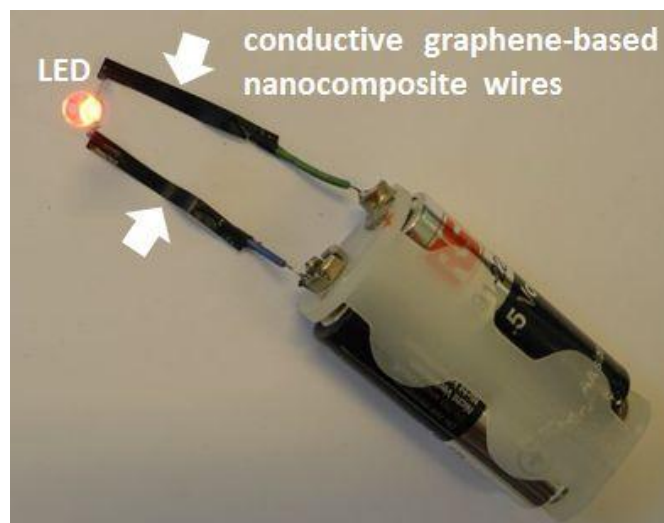


Figure 16. LED setup with conductive graphene-based nanocomposite wires (sample 8) in replacement of classical copper wires.

In this setup, small strips (2 mm-wide, 20 mm-length and 200 μm -thick) were cut out of D650-5.7 (5.7 NMG volume %). These strips were used to replace part of the copper wires that bond the LED to the batteries. An unexpected advantage of the nanocomposite material was obtained in that in a classical LED setup a current-limiting resistor is added to protect the LED. In our proposition, a built-in resistor was obtained and the resistance value could be tuned by changing the NMG content and the dimensional characteristics of the material strip.

Similarly, a pen was filled with the nanocomposite conductive latex D653-WG/S-3.2, and deposits were made on different substrates such as paper, PET film and coated fabric (specific for ink printing). Five layers were successively deposited and the substrate was dried between each deposit. A final thickness of 30 μm was obtained. The electrical properties were then measured and the results are summarized in Figure 17.

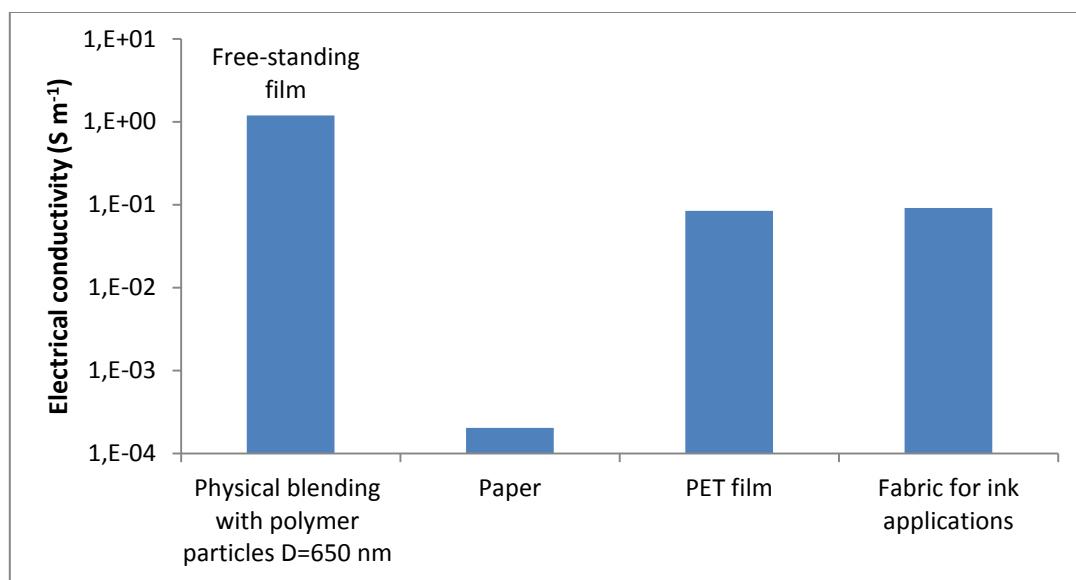


Figure 17. Electrical conductivities for the D650-WG/S-3.2 free-standing films and after deposition on various substrates: paper, PET film and fabric.

These results are compared with the electrical conductivity of free-standing film obtained as reported above in section II.3. Similar electrical conductivities are obtained for a deposit on PET film and fabric. But low electrical conductivities are obtained for a deposit on paper. Part of the composite latex can be absorbed by the paper fibers. These results are promising in that this composite latex could be further formulated into a conductive ink: a thickener could be added to adjust the viscosity in order to deposit the right amount of ink in a single layer. For instance, polyacrylic Acid is commonly used as thickener for latexes.

V. Thermo-mechanical properties of the nanocomposites

The thermo-mechanical response of the materials was evaluated through Dynamic Mechanical Analysis (DMA). A sinusoidal stress ($\gamma^* = \gamma_0 \exp(i\omega t)$) is applied and the strain ($\varepsilon^* = \varepsilon_0 \exp(i\omega t + \delta)$) in the material is measured, giving the complex modulus ($G^* = \gamma^* / \varepsilon^* = G' + iG''$). The material undergoes a small deformation and remains in its elastic domain. A temperature scan is performed, leading to variations in the complex modulus linked to the variations in the internal molecular motions. This approach can be used to locate the temperature (T_α) of the main mechanical relaxation of the material, defined as the temperature of the maximum of G'' . The material is said to be in the glass state or energy elastic state at temperatures lower than T_α and in the rubber or entropy elastic state at temperatures higher than T_α . T_α is often assimilated to T_g .

The DMA measurements were performed in torsion mode at a fixed frequency (1 Hz) from 200 K to 380 K with a heating rate of 1 K min⁻¹ on custom-made equipment. The storage modulus (G') and the loss modulus (G'') were measured as a function of temperature. Sample dimensions were about 10x3.5x0.2 mm³. To minimize uncertainties due to errors in dimensional measurements of the samples, all curves were adjusted in the glassy domain using a three-phase autocohherent model [47].

1. Comparison of T_α and T_g

Prior to investigating the nanocomposites, the DMA response of the blank samples obtained through both polymerizations has been compared (0% vol). The evolution of the loss modulus vs. temperature plotted in Figure 20 clearly shows a relaxation temperature (T_α) of 14°C for the sample D650 and a large relaxation temperature between -10°C and 21°C for the sample D300 at 0% vol of NMG.

These values can be compared with the glass transition temperatures (T_g) measured by Differential Scanning Calorimetry (DSC) (Figure 18). DSC is an analytical technique in which the difference in the amount of heat (ΔH) required to increase the temperature of a sample and reference is measured as a function of temperature. The resulting DSC curve exhibits a step. The glass transition temperature T_g corresponds to the temperature of the inflexion point. DSC measurements were carried out by heating 20 mg of sample from -40 to 140 °C at a heating rate of 20°C/min. This temperature scan was repeated twice. The second set of scanning data was used to measure the T_g . DSC experiments were performed on a Mettler Toledo DSC.

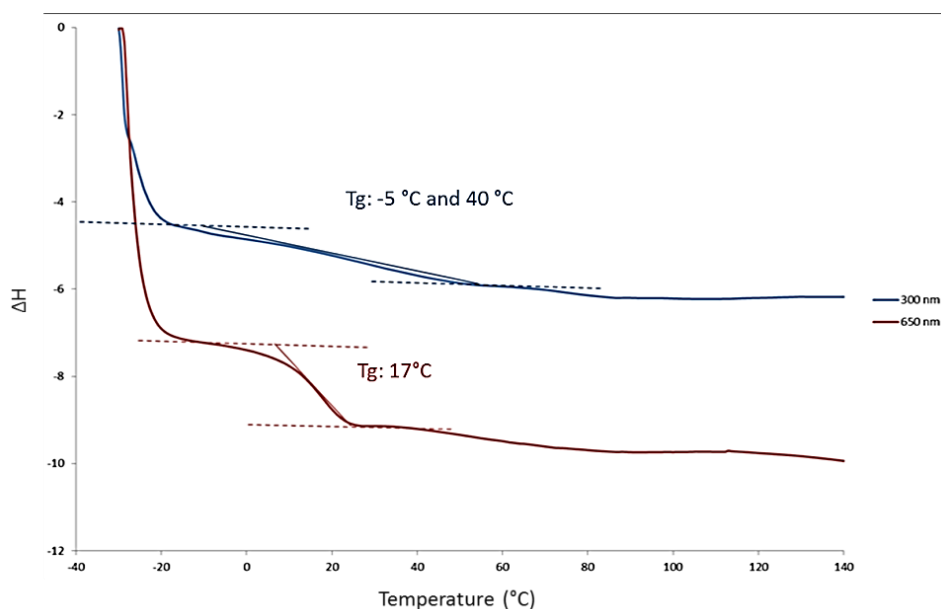


Figure 18. DSC analysis (exo up) of the polymer particles with a mean diameter of 300 nm and 650 nm.

The glass transition temperatures measured by DMA and DSC are summarized in Table 8. Both copolymers have a glass transition temperature around room temperature. This is

consistent with a film-formation at room temperature. The semi-batch process (D650) induces a well-defined T_g in comparison with the batch process (D300).

Table 8. T_α and T_g measurements for both samples D300 and D650

Samples	T_α (DMA measurements)	T_g (DSC measurements)
D300	-10°C to 21°C	-5°C to 40°C
D650	14°C	17°C

In nanocomposite studies, authors reported a shift of T_g toward higher temperatures with increasing filler content compared to its polymer matrix due to the decrease of polymer chain mobility in the close vicinity of the filler [48]. The loss modulus G'' versus temperature for different loads of NMG in the nanocomposites (D650 and D300 series) is also studied (Figure 19). In both samples, the relaxation temperature does not depend on the concentration of NMG added. So, no decrease of polymer chain mobility is observed in these nanocomposites.

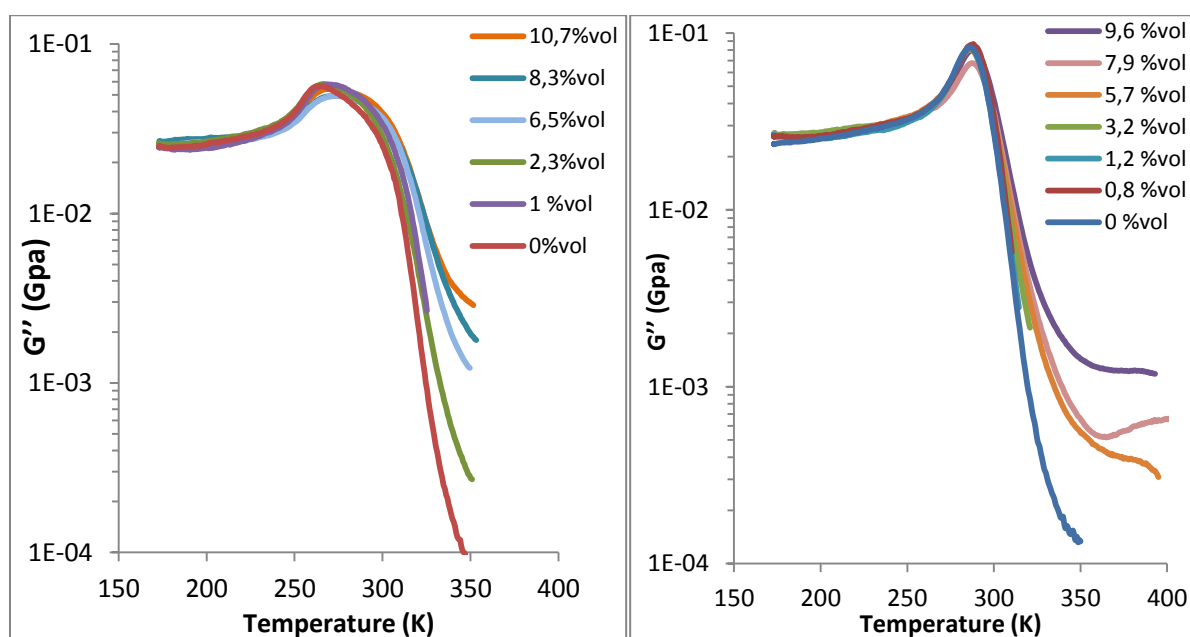


Figure 19. Loss modulus vs. temperature for a- D300 and b- D650 samples.

2. Thermo-mechanical measurements

The addition of NMG platelets in the polymer matrix can induce an increase of the nanocomposite modulus, also called reinforcement. From a general point of view, the modulus increases with the filler content and the aspect ratio but also depends on the dispersion and on filler-filler or filler-matrix interactions. The thermo mechanical response of the different samples was evaluated and the storage moduli, G' , are plotted versus temperature in Figure 20. For two experiments, the samples passed the main mechanical relaxation but broke before reaching 80°C. Consequently the curves were graphically extrapolated (dash

plots) to allow a comparison between all experiments. For all samples, the main mechanical relaxation T_α occurs around 0-30 °C, which is consistent with film-forming process occurring at room temperature.

To address the reinforcement induced by the NMG-clusters, the storage modulus has to be considered in temperature range 50-80°C, where the polymeric matrix is under rubbery state (low modulus). For both sample series, the rubbery plateau is clearly shifted toward high modulus values with increasing NMG volume fraction.

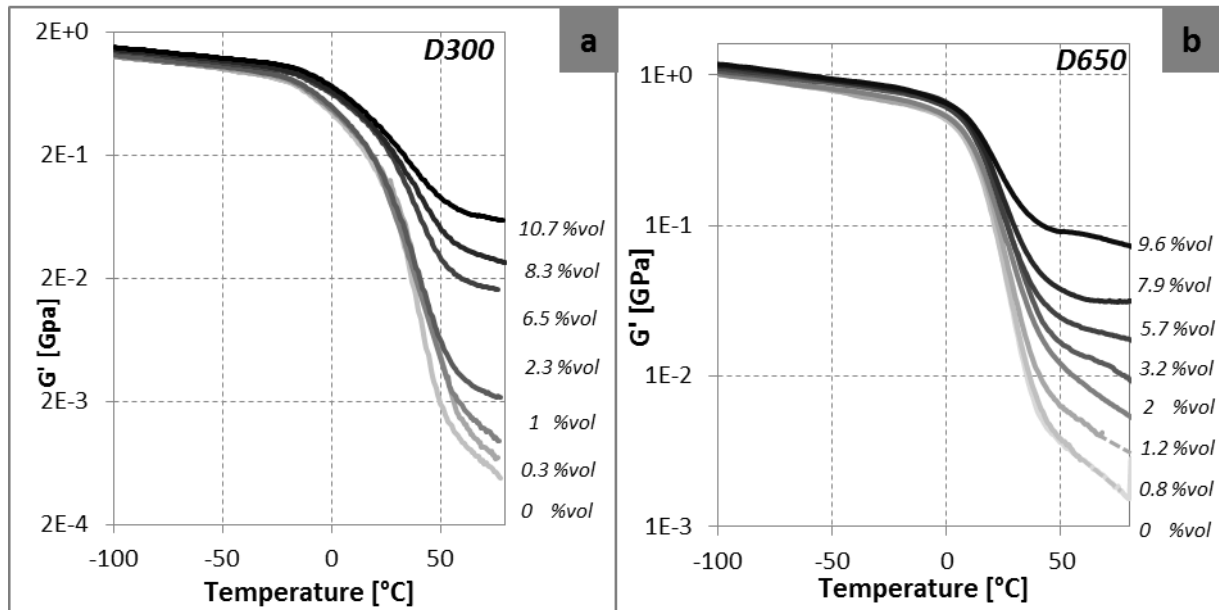


Figure 20. DMA results for a- D300 samples and b- D650 samples.

The reinforcement factor is defined as the ratio between the modulus of the composite and the modulus of the blank polymer. Figure 21 shows the reinforcement factors calculated at 80°C. A higher reinforcement factor is clearly obtained for the D300 series. Similarly to the electrical behavior, the difference between mechanical reinforcement in D300 and D650 series can be illustrated using Figure 21. In fact, the total number of percolating paths is higher for D300 samples. These experimental data are compared to data calculated from the mechanical percolation model using the experimental moduli of blank polymers (1.8 GPa) as input parameters (Equation 5).

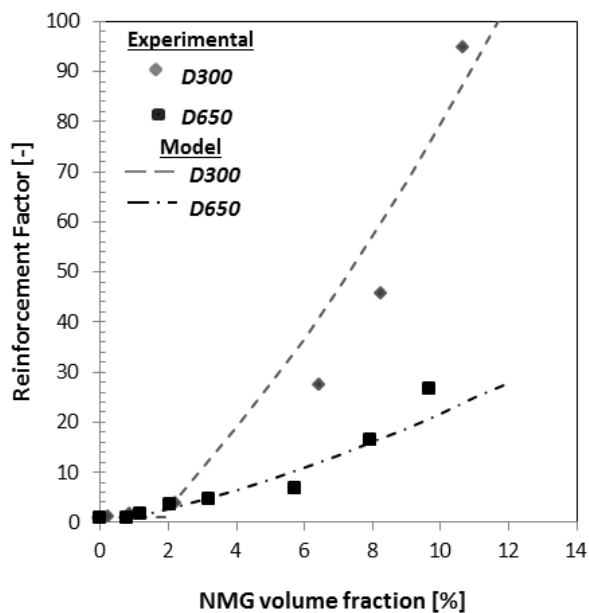


Figure 21. Experimental and model reinforcement factor as a function of NMG volume fraction (◆) D300 and (■) D650 series.

The model fairly correlates the experimental data (Figure 21). However, the sensitivity of the model does not allow a precise determination of a percolation threshold. The percolation threshold (ϕ_c^{mecha}) was estimated around 0.5-0.8 vol.% for D300 and at 0.2-0.4 vol.% for D650.

Conclusions

The percolation behavior of conductive composites obtained through latex route has been studied in terms of conductivity and mechanical reinforcement. The influence of the size ratio between the conductive filler and the latex nanosphere drove the study.

The final composite materials exhibit micrometer-scale domain size with filler paths running throughout the material. The conductivity behavior is successfully described using a percolation approach that confirms the presence of a three dimensional filler network efficiently spread across the material. Mechanical reinforcement with increasing NMG content is also consistent with a percolation behavior. The experimental percolation thresholds determined using both electrical and mechanical results are comparable to geometrical percolation thresholds (Table 9) calculated theoretically using equation 2.

Table 9. Geometrical, mechanical and electrical percolation threshold for the 300 nm and 650 nm latex beads diameter.

Sample series reference	ϕ_c^{geom} (%vol)	ϕ_c^{elec} (%vol)	ϕ_c^{mecha} (%vol)
D300	0.38	0.4	0.5-0.8
D650	0.17	0.12	0.2-0.4

Highly conductive graphene-based composite materials have been produced through a latex route (solvent-free procedure). The composite-latex blend is based on acrylate copolymers that are already mature in the ink and paint industry: they can form continuous and deformable films without neither high temperature curing nor additional hot-pressing, which is adequate for flexible and textile substrates. The composite latex blends exhibited good shelf-stability.

The nanocomposite materials exhibit good electrical properties (10^2 S m^{-1} comparable to commercial carbon-based conductive inks) with low filler content: less than 10 wt.% compared to 20-40 wt.% in existing conductive inks. This elaboration route based on blends of NMG platelets and polymer latex particles provides a promising candidate for conductive inks for printed electronics and functional conductive materials. These conductive nanocomposite suspensions could become a cheaper alternative to silver-based conductive inks for printed electronics and could open more versatile electronic applications due to the deformability of the polymer matrix, for instance, on textile substrates. The potential interest for electronics has been demonstrated by the use of the nanocomposite material in replacement of copper wires in a LED setup.

References

- [1] L. Hu, M. Pasta, F.L. Mantia, L. Cui, S. Jeong, H.D. Deshazer, J.W. Choi, S.M. Han, Y. Cui, *Nano Lett.* 10 (2010) 708.
- [2] M.A.H. Khondoker, S.C. Mun, J. Kim, *Appl. Phys. A* 112 (2013) 411.
- [3] R. Cauchois, M. Saadaoui, A. Yakoub, K. Inal, B. Dubois-Bonvalot, J.-C. Fidalgo, *J. Mater. Sci.* 47 (2012) 7110.
- [4] P.A. Steward, J. Hearn, M.C. Wilkinson, *Adv. Colloid Interface Sci.* 86 (2000) 195.
- [5] C. Wu, X. Huang, G. Wang, L. Lv, G. Chen, G. Li, P. Jiang, *Adv. Funct. Mater.* 23 (2013) 506.
- [6] X. Li, G. Zhang, X. Bai, X. Sun, X. Wang, E. Wang, H. Dai, *Nat. Nanotechnol.* 3 (2008) 538.
- [7] A. Arzac, G.P. Leal, R. Fajgar, R. Tomovska, *Part. Part. Syst. Charact.* 31 (2014) 143.
- [8] E. Tkalya, M. Ghislandi, A. Alekseev, C. Koning, J. Loos, *J. Mater. Chem.* 20 (2010) 3035.
- [9] J.C. Grunlan, A.R. Mehrabi, M.V. Bannon, J.L. Bahr, *Adv. Mater.* 16 (2004) 150.
- [10] N. Grossiord, J. Loos, C.E. Koning, *J. Mater. Chem.* 15 (2005) 2349.
- [11] Z. Yang, R. Gao, N. Hu, J. Chai, Y. Cheng, L. Zhang, H. Wei, E.S.-W. Kong, Y. Zhang, *Nano-Micro Lett.* 4 (2012) 1.
- [12] J.C. Grunlan, W.W. Gerberich, L.F. Francis, *J. Appl. Polym. Sci.* 80 (2001) 692.
- [13] C. Moore, M.E.J. Newman, *Phys. Rev. E* 61 (2000) 5678.
- [14] E. Thommerel, J.C. Valmalette, J. Musso, S. Villain, J.R. Gavarrri, D. Spada, *Mater. Sci. Eng. A* 328 (2002) 67.
- [15] R. Zallen, in: *Phys. Amorph. Solids*, Wiley-VCH Verlag GmbH & Co. KGaA, 1983, pp. 135–204.
- [16] A. Hunt, R. Ewing, *Percolation Theory for Flow in Porous Media*, Springer Science & Business Media, 2009.
- [17] D. Stauffer, A. Aharony, *Introduction to Percolation Theory*, Taylor & Francis, 1994.
- [18] N. Xie, X. Shi, D. Feng, B. Kuang, H. Li, *Compos. Part B Eng.* 43 (2012) 3270.
- [19] I. Balberg, N. Binenbaum, *Phys. Rev. B* 28 (1983) 3799.
- [20] J.C. N Ouali, *Plast. Rubber Compos. Process. Appl.* 16 (1991) 55.
- [21] J. Kolařk, *Eur. Polym. J.* 34 (1998) 585.
- [22] W. Bauhofer, J.Z. Kovacs, *Compos. Sci. Technol.* 69 (2009) 1486.
- [23] K. Nawaz, U. Khan, N. Ul-Haq, P. May, A. O'Neill, J.N. Coleman, *Carbon* 50 (2012) 4489.
- [24] J. Faucheu, C. Gauthier, L. Chazeau, J.-Y. Cavallé, V. Mellon, E.B. Lami, *Polymer* 51 (2010) 6.
- [25] F. Dalmas, J.-Y. Cavallé, C. Gauthier, L. Chazeau, R. Dendievel, *Compos. Sci. Technol.* 67 (2007) 829.
- [26] P.A. Steward, J. Hearn, M.C. Wilkinson, *Adv. Colloid Interface Sci.* 86 (2000) 195.
- [27] J.-C. DANIEL, C. PICHOT, *Les latex synthétiques*, Tec & Doc Lavoisier, Paris, 2006.
- [28] M.F. Cunningham, R. Hutchinson, in: *K.J.C.W. of N. Sciences*, T.P. Davis (Eds.), *Handb. Radic. Polym.*, John Wiley & Sons, Inc., 2002, pp. 333–359.

- [29] W.V. Smith, R.H. Ewart, *J. Chem. Phys.* 16 (1948) 592.
- [30] R.G. Gilbert, *Emulsion Polymerization: A Mechanistic Approach*, Academic Press, 1995.
- [31] W.D. Harkins, *J. Am. Chem. Soc.* 69 (1947) 1428.
- [32] W.J. Priest, *J. Phys. Chem.* 56 (1952) 1077.
- [33] D.H. Napper, R.G. Gilbert, *Makromol. Chem. Macromol. Symp.* 10-11 (1987) 503.
- [34] T. Matsumoto, Akihiro Ochi, *Kobunshi Kagaku* 22 (1965) 481.
- [35] R.M. Fitch, *Br. Polym. J.* 5 (1973) 467.
- [36] E. Kientz, Y. Holl, *Colloids Surf. Physicochem. Eng. Asp.* 78 (1993) 255.
- [37] J.P. Mária Omastová, *Polymer* 39 (1998) 6559.
- [38] V.H. Pham, T.T. Dang, S.H. Hur, E.J. Kim, J.S. Chung, *ACS Appl Mater Interfaces* (2012).
- [39] S. Kirkpatrick, *Rev. Mod. Phys.* 45 (1973) 574.
- [40] D.S. McLachlan, C. Chiteme, C. Park, K.E. Wise, S.E. Lowther, P.T. Lillehei, E.J. Siochi, J.S. Harrison, *J. Polym. Sci. Part B Polym. Phys.* 43 (2005) 3273.
- [41] P.R. Sperry, B.S. Snyder, M.L. O'Dowd, P.M. Lesko, *Langmuir* 10 (1994) 2619.
- [42] W. Chen, L. Yan, P.R. Bangal, *Carbon* 48 (2010) 1146.
- [43] H. Mousavi, J. Khodadadi, *Sci. World J.* 2014 (2014) e581478.
- [44] B. Marinho, M. Ghislandi, E. Tkalya, C.E. Koning, G. de With, *Powder Technol.* 221 (2012) 351.
- [45] A.L. Efros, B.I. Shklovskii, *Phys. Status Solidi B* 76 (1976) 475.
- [46] J.P. Clerc, G. Giraud, J.M. Laugier, J.M. Luck, *Adv. Phys.* 39 (1990) 191.
- [47] E.H. Kerner, *Proc. Phys. Soc. Sect. B* 69 (1956) 808.
- [48] T. Ramanathan, A.A. Abdala, S. Stankovich, D.A. Dikin, M. Herrera-Alonso, R.D. Piner, D.H. Adamson, H.C. Schniepp, X. Chen, R.S. Ruoff, S.T. Nguyen, I.A. Aksay, R.K. Prud'Homme, L.C. Brinson, *Nat. Nanotechnol.* 3 (2008) 327.

Chapter 4: *In situ* polymerization with Nanosize Multilayered Graphene (NMG)

Introduction	118
I. <i>In situ</i> polymerization in the presence of graphene.....	119
1. <i>In situ</i> polymerization with graphene	119
2. Reactivity of graphene platelets	119
3. Characterization techniques	121
II. Emulsion polymerization in the presence of NMG suspensions.....	126
1. Emulsion polymerization mechanisms and impact of NMG	126
a. Nucleation mechanisms	126
b. Impact of the presence of NMG platelets in the system.....	126
2. Experimental procedure for <i>in situ</i> emulsion polymerization with NMG suspensions.....	128
3. <i>In situ</i> emulsion polymerization with NMG/SDBS suspensions	131
a. Influence of initiator concentration	131
b. Influence of the surfactant concentration	133
4. <i>In situ</i> emulsion polymerization with NMG/PSSNa suspensions.....	139
5. <i>In situ</i> emulsion polymerization with NMG/PS <i>b</i> PEO 1030 suspensions	144
6. Conclusions	149
III. Miniemulsion polymerization in the presence of NMG.....	149
1. Generalities on miniemulsion polymerization	149
2. Experimental part	151
3. <i>In situ</i> miniemulsion polymerization with NMG/SDBS suspensions.....	152
4. <i>In situ</i> miniemulsion with NMG/PS <i>b</i> PEO 1030 suspensions	157
5. Conclusions	161
IV. Dispersion polymerization in the presence of NMG.....	162
1. Generalities on dispersion polymerization	162
2. Preliminary study	164
a. Experimental procedure.....	164
b. Influence of solvent composition	164

c.	Influence of temperature.....	165
d.	Influence of the stabilizer concentration	166
e.	Influence of the type of stabilizer	167
3.	NMG suspensions stabilized by PVPk30.....	168
a.	Experimental procedure.....	168
b.	Influence of NMG concentration.....	168
c.	Influence of stabilizer concentration	171
d.	Influence of the comonomer composition	175
4.	Conclusions	177
V.	Electrical properties of the nanocomposites synthesized by <i>in situ</i> polymerization ...	178
	Conclusions	181
	References	181

Introduction

This chapter presents the synthesis of NMG-armored nanocomposite latexes prepared by polymerization in the presence of NMG, so called *in situ* polymerization. As illustrated in chapter 1, GO (followed by a reduction step) is largely preferred to NMG in literature for syntheses of nanocomposites through *in situ* polymerization. GO has been reported to be an amphiphilic material due to the combination of hydrophilic groups such as carboxylic acids at the sheet periphery, and hydrophobic graphitic regions in the basal plane. Consequently, GO has been shown to stabilize oil-in-water (o/w) emulsions, resulting in Pickering emulsions [1].

This work is motivated by a simplification of the process by using directly NMG in *in situ* polymerization, and so without any post-polymerization reduction step. However, as NMG is not as stable as GO in water, the use of surfactant or stabilizer is needed. The aim is to produce armored polymer particles, meaning that the surface of the polymer particle is covered with NMG platelets. Geometrically, the latex diameters need to be higher than the NMG lateral dimensions. With NMG platelets exhibiting a lateral dimension around 50 nm, latex diameters around 0.3-1 μm should be adequate.

To produce latexes, polymerization in dispersed media is chosen and particularly polymerization processes in emulsion, miniemulsion and dispersion. With different experimental conditions, these processes allow the synthesis of latex particles in a wide range of sizes. Typically, emulsion and miniemulsion polymerizations produce polymer particles with a diameter between 50 and 500 nm, while dispersion polymerization allows the formation of particles with a diameter between 0.5 and 20 μm .

The following chapter is divided in three sections. First the mechanism of *in situ* polymerizations in the presence of graphene will be presented. Second, experimental *in situ* emulsion and miniemulsion polymerizations in the presence of NMG stabilized in water with different stabilizers will be developed. In particular, the impact of the choice of stabilizer nature and concentration will be studied. Then, in order to increase the polymer particle diameter, *in situ* dispersion polymerization will be investigated using NMG suspensions with poly(vinyl pyrrolidone) (PVP). In a third section, the electrical properties of these nanocomposite films obtained through *in situ* polymerization will be measured and compared with those of the physical blends reported in chapter 3.

I. *In situ* polymerization in the presence of graphene

As discussed in the last chapter, free-radical polymerization is a well-established polymerization technique for the synthesis of numerous polymer materials due to its compatibility with most monomers. In chapter 1, examples of *in situ* polymerization of graphene-based composite extracted from literature have been presented. In the following, the polymerization mechanisms of *in situ* polymerization in the presence of graphene platelets will be detailed.

1. *In situ* polymerization with graphene

Here, the Nanosize Multilayered Graphene (NMG) suspensions stabilized with a surfactant or a stabilizer will be used instead of GO particles. The main advantage will be to avoid the reduction process of GO which currently induces a destabilization of the final nanocomposite suspensions formed. Yet, the main challenge of this chapter will be to synthesize large polymer particles in the presence of surfactant or stabilizer, meaning a polymer particle diameter superior to the NMG lateral size. Moreover, an armored nanocomposite, with latex particles surrounded by NMG platelets, with only non-covalent bonding is also a challenge. To perform these requests, three main polymerization processes will be successively developed: *in situ* emulsion, miniemulsion and dispersion polymerization in the presence of NMG suspensions. [2] The reactivity of graphene platelets is first investigated.

2. Reactivity of graphene platelets

Current methods for graphene production lead to graphene layers with so-called defects. Defects are structural imperfections and chemical impurities randomly distributed on the face or edges of the graphene sheet [3]. These defects reduce the intrinsic electrical properties but can also provide additional reactive sites for further graphene functionalization. In addition, the graphene edges are considered to be more reactive than the inner surface faces [4]. Finally, a graphene sheet exhibits reactive sites on its edges and defects (Figure 1). It is also expected that zigzag edges will display higher reactivity compared to armchair ones. However, it is technically challenging to control the edge structure, so, in practice, graphene contains a combination of both types of edge configurations (combined edge), which makes it difficult to control the functionalization process [5]. Numerical simulations [6] indicates that

hydroxyl, carboxyl, or other groups can easily be attached to vacancy-type defects. The same is true for graphene edges that are normally saturated with hydrogen [7].

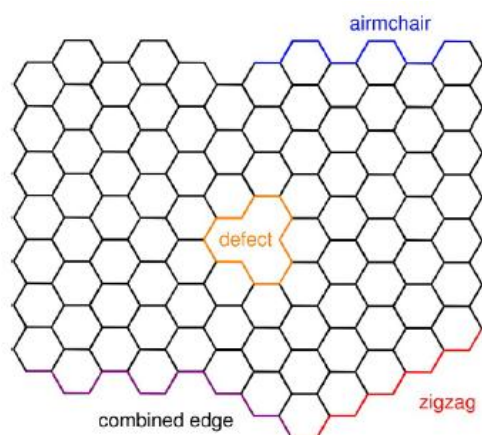


Figure 1. Scheme representing the reactive sites on graphene sheets. [4]

In brief, the functionalization of graphene sheets might result from unpaired electrons enhancing the reactivity there and leading to a chain reaction from the initial point of attack [8]. Due to the presence of unpaired electrons available on the graphene, the carbon compounds are currently used as trapping agent [9][10]. In fact, radical polymerizations of vinyl monomers are remarkably retarded in the presence of nano-carbons, such as carbon black, carbon nanotubes, and fullerene, because initiator radicals and growing polymer radicals are readily trapped by these nano-carbons [11][12].

GO had also been used for trapping of polymer radicals [13] for functionalization with styrene, for example, as described by Beckert et al. [14]. The presence of radicals can also interact with the polymer initiators during *in situ* polymerization in the presence of nano-carbon compounds. It was reported that during the polymerization initiated by conventional radical initiators in presence of carbon black, a part of the polymer formed is grafted onto the carbon surface. But the percentage of polymer-grafting on the carbon surface is less than 10%. Most of trapped radicals are initiators fragments instead of polymer chains [11].

The retardation or inhibition of the polymerization, due to the presence of nano-carbon compounds, strongly depends of the nature of the monomers [15]. An inhibition was first observed in the polymerization of styrene with carbon black. In fact, the growing polymer chains are more reactive toward carbon black surface than initiator fragments and the growth of polymer is stopped prematurely during this induction period. Whereas, in the case of methyl methacrylate or vinyl acetate polymerization with carbon black, a marked retardation of the polymerization is visible due to the predominant reaction of initiator fragments with the carbon black surface.

The possible interactions of the graphene surfaces with the initiators and monomers can create a modification of the polymerization rate. Furthermore, the presence of radicals on the graphene surface can lead to the creation of covalent bonds between the graphene platelets and the growing polymer without upstream functionalization of graphene platelets.

3. Characterization techniques

The characterization techniques used in this chapter to analyze the properties, the NMG platelets and nanocomposite latexes formed are succinctly presented in this section.

Latex characterization

To evaluate the latex size distribution and mean diameter, two complementary methods, Dynamic Light Scattering (DLS) and Transmission Electron Microscopy (TEM), have been used. The hydrodynamic average particle diameter (D_h , nm) and the dispersity of the samples (indicated by the *poly value* - the higher this value, the broader the size distribution) were determined by DLS in a Nano Zetasizer Malvern Instrument. The DLS technique is mainly adapted to spherical objects [16]. Since our samples contained non-spherical particles, the results obtained were only considered as indicatives of particles size.

Particle morphology was determined by TEM. For TEM analysis, the diluted latex samples were dropped on a carbon/formvar-coated copper grid and dried under air. Observations were made either at room temperature or under cryogenic conditions (cryo-TEM). Based on TEM micrographs, statistics over 50 particles give a mean diameter D_{TEM} to be compared with D_h .

The number of polymer particles can be calculated using the D_h and Equation 1.

$$N_{latex} = \frac{m_{latex} \times 6}{\rho_{latex} \times \pi \times D_h^3} \quad \text{Equation 1}$$

with m_{latex} the weight of polymer (taking into account the polymer conversion) and ρ_{latex} (1.18 g cm⁻³) the polymer density.

The polymerization kinetics is the conversion degree versus time. It is experimentally calculated by gravimetric analysis. At different time during the polymerization, a known mass of suspension is extracted from the reactor and left evaporated in an oven. The ratio of the solid content over the initial mass gives the conversion degree.

Stability of the nanocomposite suspensions

The stability of the nanocomposite suspension was assessed using a Turbiscan® Static Multiple Light Scattering (MLS). The Turbiscan® technology is designed to monitor the stability of ink formulations and compare their stability. The detection head moves up and down along a flat-bottom cylindrical glass cell containing the suspension. The detection head comprises a near infrared pulsed light source ($\lambda = 880$ nm) and two detectors. The transmission detector (facing the light source) receives the light that goes through the sample, while the backscattering detector placed at 45° from the light source direction receives the light scattered backward by the sample (Figure 2). The transmission detector is used for non-opaque samples, whereas the backscattering detector is used for opaque samples.

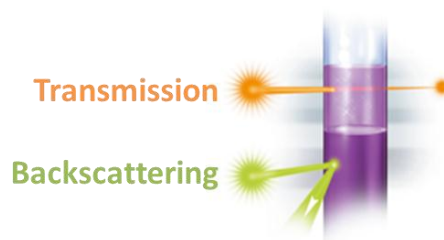


Figure 2. Scheme illustrating transmission and backscattering during Turbiscan® analysis.

To analyze our suspensions, only the backscattering detector was used due to their opacity. The backscattering intensity depends on particle size, concentration and absorbance. Changes in particle size such as flocculation or coalescence can be detected as well as local changes in volume fraction such as migration phenomena (creaming, sedimentation).

Concerning changes in particle size, for particles smaller than the incident light (< 500 nm), an increase of particle size is showed by an increase in backscattering. Conversely, for particles bigger than the incident light (>500 nm), an increase in size leads to a decrease in backscattering [17]. Figure 3 shows the backscattering intensity versus the total height of the sample.

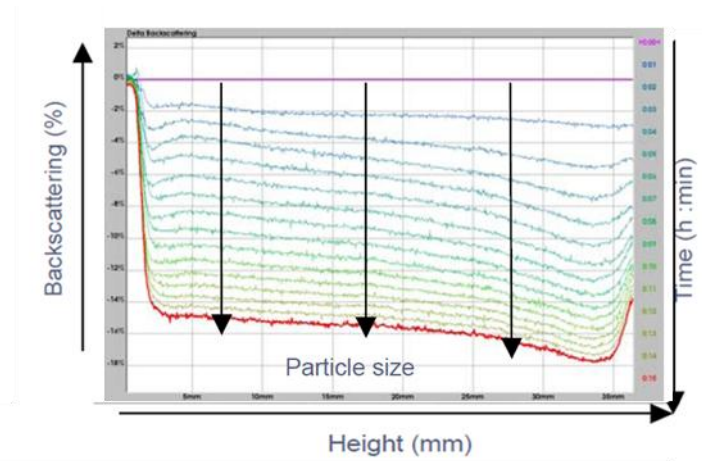


Figure 3. Example of profiles for a flocculation phenomenon for particles diameter of $1 \mu\text{m}$ [18]

Turbiscan profiles showing backscattering intensity versus height are also used to characterize the stability of a suspension. Particle migration in the suspension (sedimentation or creaming) leads to local changes of the particles concentration. These phenomena are detected in Turbiscan profiles by localized changes of the backscattering intensity. The variation of the backscattering intensity will be named $\Delta R(\%)$ in the following Turbiscan graphic, and represents the variation of the backscattering in comparison with the spectrum at $t=0$.

Figure 4 shows examples of curves obtained for a stable (a) and unstable (b and c) suspensions. The backscattering value is obtained by subtracting the initial backscattering profile to each other profile, in order to enhance variations. For a stable suspension, all the profiles overlap whereas for unstable suspensions, variations are visible (Figure 4). In Figure 4b, at the top of the cylinder, the backscattering intensity increases due to the increase of

particle concentration consecutive to a creaming phenomenon. At the bottom of the cylinder, the backscattering intensity decreases due to a decrease of the particles concentration, meaning a clarification phenomenon is occurring.

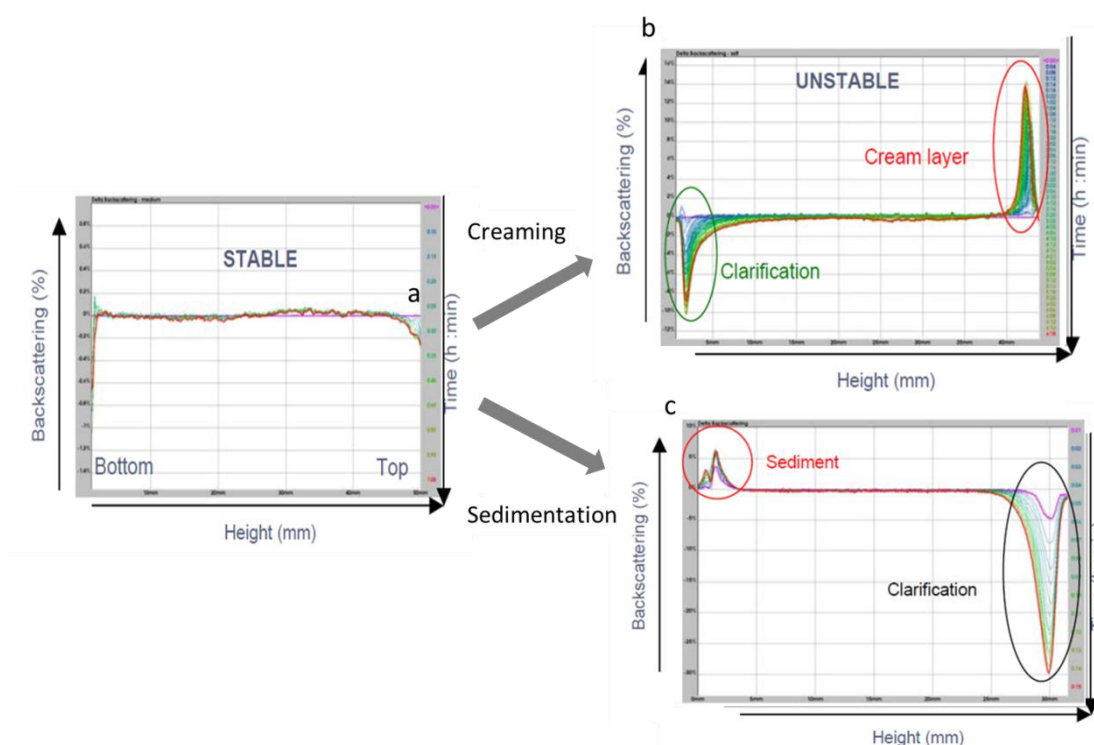


Figure 4. Superposition of scans with time for a- stable sample and unstable samples, b- creaming and c-sedimentation phenomena [18]

In Figure 4c, another example of unstable suspension is presented. The backscattering intensity decreases at the top of the cylinder due to a decrease of the particles concentration, hence a clarification is occurring. At the bottom of the cylinder, the backscattering intensity increases due to the increase of particle concentration consecutive to a sedimentation phenomenon.

In the case of a mixture of two different particles, as for latex particles and graphene platelets, the behavior of the suspension might be more complex to analyze through Turbiscan®. To draw a parallel, the behavior of a suspension containing green pigments and white pigments is presented in Figure 5. A clarification phenomenon is visible at the top of the cylinder and sedimentation phenomenon is visible at the bottom of the cylinder. In addition to these two negative peaks, positive peaks in the upper part of the cylinder are also visible. These specific curves are analyzed as follow. The green pigments are the one falling faster and lead to a sediment that absorbs light as the emitting source is in the near infra-red leading to a negative backscattering signal at the bottom of the cylinder. Once the green pigments have fallen, the white pigments remain in suspension. Therefore, the positive peaks are attributed to the white pigments that are slowly falling to the bottom exhibiting positive peaks as they are known to be highly diffusive species. A similar behavior might be observed for our composite latex particles with latex acting as diffusive species and NMG platelets acting as light absorbers.

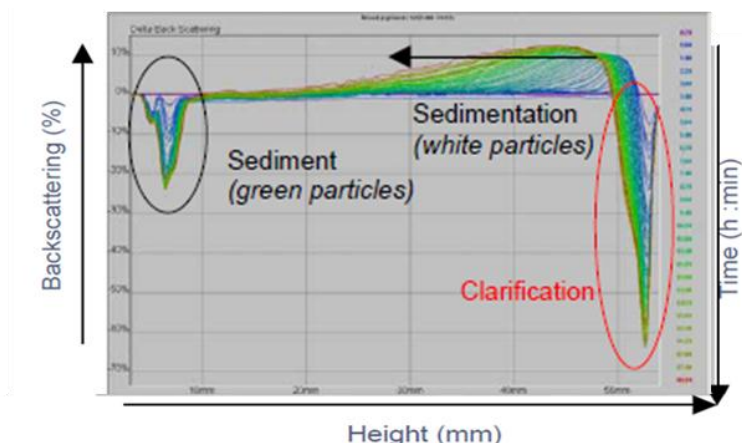


Figure 5. Backscattering profiles for a mixture of pigments [18].

The diffusion and adsorption phenomenon, as it has been seen in the previous examples, strongly modify the backscattering intensity. As for example, colored or black particles will adsorb part of the backscattering intensity and in consequence the backscattering signal might decrease.

NMG concentration in the nanocomposite suspension and theoretical surface coverage

In order to compare the nanocomposite films made through physical blending and *in situ* polymerization, the weight percentage of NMG in the composite latexes was calculated using Equation 2.

$$NMG_{th} (wt\%) = \frac{m_{NMG}^{Initial}}{m_{NMG}^{Initial} + m_{Stabilizer}^{initial} + m_{monomers}^{initial}} \times \frac{conversion}{100} \times 100 \quad \text{Equation 2}$$

This equation takes into account the initial mass of NMG introduced in the reactor, $m_{NMG}^{initial}$, the mass of stabilizer and monomers introduced, respectively $m_{stabilizer}^{initial}$ and $m_{monomers}^{initial}$, and the final conversion (namely conversion in the Equation 2) calculated by gravimetric analysis at the end of the polymerization.

The percentage of surface coverage of the latex particles by NMG platelets can be determined using Equation 3 assuming a 2D square lateral packing of the NMG platelets, meaning that the platelets lie flat on the surface (Figure 6) and packing can easily be changed to different arrangements, such as hexagonal or random [19].

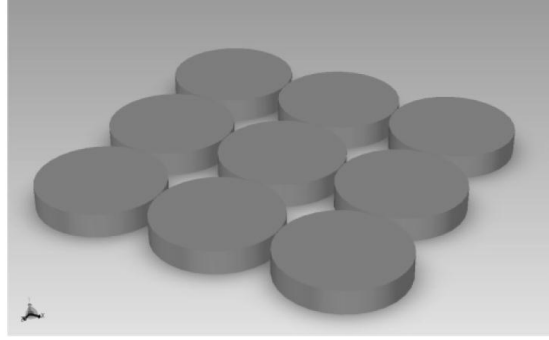


Figure 6. Schematic representation of the 2D square lateral packing of NMG platelets on a flat surface [19].

$$\tau_{coverage}(\%) = \frac{N_{NMG} \times S_{NMG}}{N_{latex} \times S_{latex}} \times 100 \quad \text{Equation 3}$$

Where N_{NMG} is the number of NMG platelets,

$$N_{NMG} = \frac{4 \times m_{NMG}^{initial}}{\rho_{NMG} \times \pi \times d_{NMG}^2 \times t_{NMG}} \quad \text{Equation 4}$$

N_{latex} is the number of polymer particles, S_{NMG} is the area occupied by one NMG ($S_{NMG} = d_{NMG}^2$) and S_{latex} is the surface area of one polymer particle (Eq. 5).

$$S_{latex} = \pi \times D_h^2 \quad \text{Equation 5}$$

Where m_{NMG} is the weight of NMG, ρ_{NMG} (2.23 g cm^{-3}), d_{NMG} is the mean lateral size of the NMG platelet and t_{NMG} is the mean thickness of the platelets. It turns:

$$\tau_{coverage}(\%) = \frac{4}{6\pi} \times \frac{\rho_{latex}}{\rho_{NMG}} \times \frac{m_{NMG} d_{latex}}{m_{latex} t_{NMG}} \times 100 \quad \text{Equation 6}$$

The surface coverage is not real because it means a homogeneous coverage on monodisperse latex particle, which is hardly obtained under experimental conditions. However, this parameter is useful to evaluate the ability of the latex to be conductive after film formation and compare the different latexes obtained through *in situ* polymerization. In chapter 3, the geometrical percolation threshold for 3D nanocomposites is said to need a surface coverage of 19%. In the following parts, the number of NMG and polymer particles, N_{NMG} and N_{latex} and the surface coverage, $\tau_{coverage}$, will be calculated for each synthesis.

II. Emulsion polymerization in the presence of NMG suspensions

In situ emulsion polymerization in the presence of NMG suspensions will be conducted with three types of NMG suspensions (previously characterized in chapter 2): NMG/SDBS, NMG/PSSNa and NMG/PS*b*PfEO. The objective is the synthesis of NMG/latex nanocomposites which remain stable at the end of the polymerization process. The NMG concentration in these suspensions needs to be above the percolation threshold, previously defined in chapter 3 around 0.2 vol% of NMG for 300 nm latex beads diameter. Moreover, as it was previously defined, the mean latex particle diameter needs to be 300 nm at the minimum in order to create armored nanocomposites. The impact of the surfactant or stabilizer on the latex dimensions will be studied in this part for the *in situ* emulsion polymerization in the presence of NMG.

1. Emulsion polymerization mechanisms and impact of NMG

Basics of emulsion polymerization have been described in chapter 3. Here, specific nucleation and polymerization mechanisms in the presence of NMG platelets are presented.

a. Nucleation mechanisms

Three nucleation mechanisms can be used to describe particles formation and strongly depend of experimental conditions and monomer solubility.

First, heterogeneous or micellar nucleation implies the presence of surfactant micelles and so a concentration of surfactant above the CMC. In this mechanism, proposed by Harkins et al. [20], oligoradicals grow until they reach a critical length z_{crit} for which they become enough hydrophobic to enter in the monomer swollen micelles. Polymerization then continues in the micelles.

The second nucleation mechanism is the homogeneous or coagulative nucleation, which has been particularly studied by Roe et al. [21]. In this case, oligoradicals grow in the continuous phase until they raise a critical length $j_{crit} > z_{crit}$. At this length they become insoluble and precipitate to form primary particles. These primary particles can either grow by reacting with monomers or coagulate with another primary particle to form bigger particles and decrease their surface energy.

The third nucleation mechanism is the monomer droplets nucleation, described by capture of radicals by the monomers droplets. This mechanism is favored when the size of the monomer droplets is significantly reduced, and so favorable in miniemulsion or microemulsion polymerization. This mechanism was highlighted first by Ugelstad et al. in miniemulsion polymerization of styrene with SDS and cetylic alcohol [22].

b. Impact of the presence of NMG platelets in the system

The introduction of NMG platelets in the polymerization system will modify the nucleation mechanisms of emulsion polymerization. Two cases can be distinguished: below the CMC_{app} and above the CMC_{app} in water.

If the surfactant concentration is above the CMC_{app} at the beginning of polymerization, micellar nucleation both in free micelles and adsorbed micelles are in competition (Figure 2a).

Monomers are mainly in droplets; however some are solubilized in water and also swollen in surfactant micelles. When the NMG concentration is in small quantities (which is always the case for our systems) the nucleation will preferentially start in the free micelles. As the polymer particles grow, the polymer-water interface increases. If the surfactant exhibits a high mobility in the water phase, for example due to its low molar mass, the surfactant will quit the NMG surface and adsorb on the growing polymer particle leading to a destabilization of NMG platelets (Figure 7a). Experimentally, NMG powder will be expelled on the glass wall of the reactor during the polymerization process.

For the second case (Figure 7b), below the CMC_{app} , no surfactant micelles are present in water. During the nucleation step, oligoradicals are formed in water, precipitated and looked for stabilization by a direct adsorption on the NMG platelets or by adsorbing the complex NMG/surfactant. This process thus combines coagulative nucleation with heterocoagulation throughout the polymerization reaction. In this case, the formation of NMG-armed composite latexes will be favored (Figure 7b).

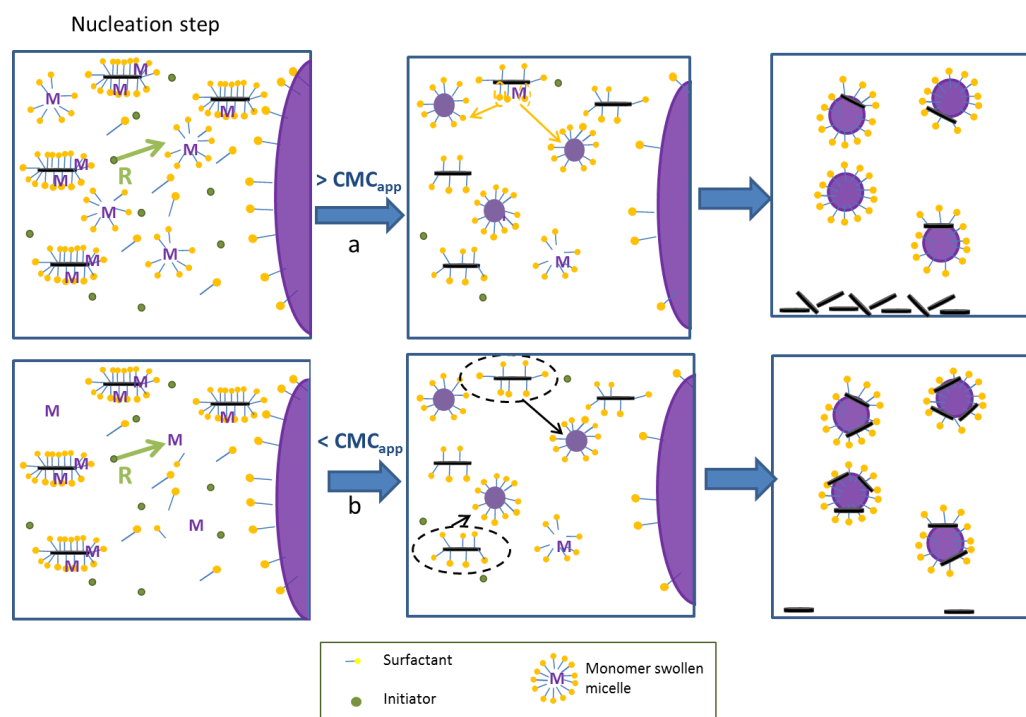


Figure 7. Scheme illustrating the possible mechanisms occurring during *in situ* emulsion polymerization in the presence of NMG platelets a- above CMC_{app} and b- below CMC_{app} .

The following part will describe the experimental procedure used to synthesize nanocomposite latexes through *in situ* emulsion polymerization in the presence of NMG as well as the characterization techniques.

2. Experimental procedure for *in situ* emulsion polymerization with NMG suspensions

As already mentioned, three different types of NMG suspensions will be used, which correspond to different stabilizers: SDBS, PSSNa and PS*b*P EO 1030, respectively.

In a typical *in situ* emulsion polymerization run, 20 g of NMG suspensions (at different concentrations) and 2 g of a mixture of styrene and butyl acrylate monomers (50/50%wt) are introduced in a 50 mL polymerization reactor and degased under nitrogen during 30 minutes. In parallel, the initiator (1 wt%/monomers or 2 wt%/monomers) (potassium persulfate, KPS) is dissolved in water and degased under nitrogen. This mixture is then introduced in the polymerization reactor and the polymerization starts when the temperature reaches 70°C. The agitation is performed by an anchor blade. This 50 mL polymerization reactor was specifically made for this project (Figure 8).



Figure 8. Picture of the 50 mL polymerization reactor

For the polymerizations without NMG, also named blank experiments, the 20 g of NMG suspensions are replaced by 20 g of deionized water and a certain amount of surfactant (the concentration is fixed to be the same than for the syntheses with NMG/surfactant suspensions). The following tables detail the experimental conditions for each NMG/stabilizer suspensions used. First, Table 1 describes the experimental conditions for *in situ* emulsion polymerizations with NMG/SDBS suspensions. As an alternative to SDBS as a surfactant, two other polymeric stabilizers are used for these polymerizations, PSSNa and PS*b*P EO 1030. Table 2 summarizes the experimental conditions for *in situ* emulsion polymerizations using these stabilizers.

Each polymerization sample was named according to the following convention with each segment of information separated by a slash or a dash. Segment 1: type of polymerization process (E for emulsion, mE for miniemulsion and D for dispersion), segment 2: percentage of initiator (1%/monomers or 2%/monomers), segment 3: type of polymerization (B for blank experiment or NMG for *in situ* polymerization), segment 4: type of surfactant or stabilizer and segment 5: actual stabilizer concentration in the suspension (in g L⁻¹) as determined by TGA (see chapter 2). This nomenclature will be identical for all the polymerizations presented in this chapter.

Table 1. Experimental conditions for all in situ emulsion polymerizations performed in the presence of SDBS or NMG/SDBS.

Experiment name	NMG suspension	[NMG] (g L ⁻¹)	[SDBS] (g L ⁻¹)	Monomers Sty/BA (g/g)	Initiator (%/M)
E-1%-B/SDBS-2	-	-	2	1/1	1
E-2%-B/SDBS-2	-	-	2	1/1	2
E-1%-NMG/SDBS-2.7	NMG/SDBS-5	2.4	2.7	1/1	1
E-2%-NMG/SDBS-2.7	NMG/SDBS-5	2.4	2.7	1/1	2
E-2%-NMG/SDBS-1.2	NMG/SDBS-2.5	0.2	1.2	1/1	2
E-2%-NMG/SDBS-0.3	NMG/SDBS-5-dial	0.8	0.3	1/1	2
E-2%-NMG/SDBS-1.7	NMG/SDBS-5-U.C	2.1	1.7	1/1	2

Table 2. Experimental conditions for all in situ emulsion polymerizations performed in the presence of PSSNa, PSbPEO 1030, NMG/PSSNa, or NMG/PSbPEO 1030.

Experiment name	NMG suspension	[NMG] (g L ⁻¹)	[Stabilizer] (g L ⁻¹)	Monomers Sty/BA (g/g)	Initiator (%/M)
E-2%-B/PSSNa-8	-	-	8	1/1	2
E-2%-NMG/PSSNa-5.6	NMG/PSSNa-5	1.4	5.6	1/1	2
E-2%-NMG/PSSNa-8.4	NMG/PSSNa-10	0.6	8.4	1/1	2
E-2%-NMG/PSSNa-27	NMG/PSSNa-10-conc	1.2	27	1/1	2
E-2%-B/PSbPEO-7.6	-	-	7.6	1/1	2
E-2%-NMG/PSbPEO-6.9	NMG/PSbPEO 1030-10	1.3	6.9	1/1	2
E-1%-NMG/PSbPEO-6.9	NMG/PSbPEO 1030-10	1.3	6.9	1/1	1

At the end of the polymerizations, the nanocomposite suspensions formed are characterized to measure the final concentration of NMG platelets, the stability of the suspensions and the polymer particles diameter. The following part details these characterization techniques.

3. *In situ* emulsion polymerization with NMG/SDBS suspensions

As presented in Table 1, the syntheses will be performed first with NMG/SDBS-2.5 and NMG/SDBS-5 suspensions. The main characteristics of these suspensions are summarized in Table 3.

Table 3. Main characteristics of NMG/SDBS-2.5 and NMG/SDBS-5 suspensions

Sample name	[SDBS] (g L ⁻¹)	[NMG] (g L ⁻¹)	Surface tension (mN m ⁻¹)	Lateral size (nm) 90% (D90)	Thickness (nm) 90% (E90)
NMG/SDBS-2.5	1.2	0.2	49.2	370	9.8
NMG/SDBS-5	2.7	2.4	36.6	160	3.2

The NMG concentrations are different in both suspensions, which might impact the nucleation mechanism during the *in situ* polymerization. In addition, the surfactant concentrations in these two suspensions are different. According to the surface tension measurements, the surfactant concentration is below CMC_{app} for NMG/SDBS-2.5 and above for NMG/SDBS-5 meaning that NMG/SDBS-2.5 counts no surfactant micelles whereas surfactant micelles are present in NMG/SDBS-5. This difference leads to a difference in terms of nucleation mechanisms during the *in situ* emulsion polymerizations. The influence of the concentration of initiator on characteristics of the nanocomposites formed is studied first.

a. Influence of initiator concentration

Four polymerizations are performed. Two *in situ* polymerizations with the NMG/SDBS-5 suspension (with styrene and butyl acrylate as monomers and KPS as initiator) and two polymerizations without NMG (with styrene and butyl acrylate as monomers and KPS as initiator) with 2 g L⁻¹ of SDBS were synthesized. The experimental conditions are a polymerization temperature of 70°C and an agitation of 200 rpm during 7 hours. To compare these polymerizations, the mean polymer particle diameter, the particle size distribution and the polymerization kinetics are measured using the techniques developed above.

The polymerization kinetics is presented in Figure 9. For blank polymerizations, 100% conversion is obtained. Moreover the polymerization rate increased with the initiator concentration. For *in situ* polymerizations, a full conversion is not obtained with 1% initiator but with 2% initiator and the polymerization rate decreases compared to blank experiments (at the same KPS concentration).

NMG platelets count defects and unsaturated electrons in their structure. These radicals can react with the initiator and with the monomers [23]. In fact, Casado *et al.* showed that carbon black, which contained chemisorbed oxygen-containing species, is known as inhibitors of radicals during polymerization. The consequence of this interaction will be a decrease of the

polymerization rate and final conversion, as observed in Figure 9. Final conversions are detailed in Table 4.

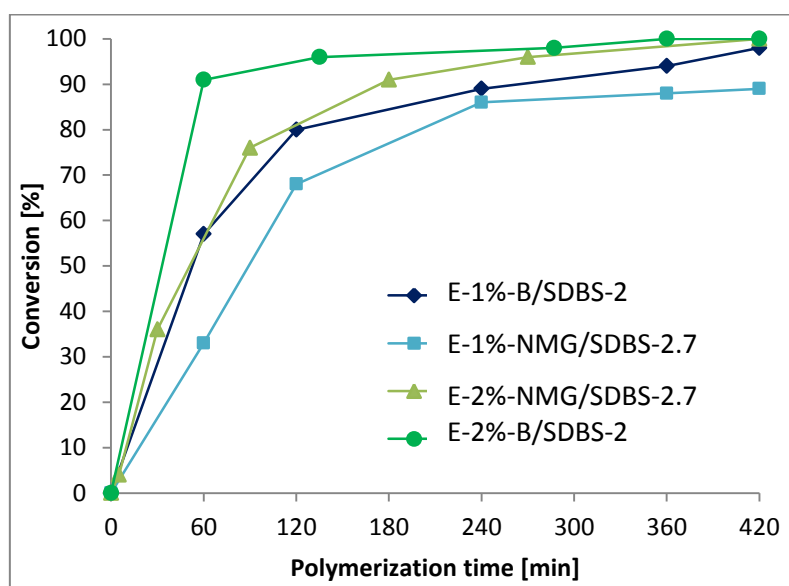


Figure 9. Polymerization kinetics for two concentrations of initiator with and without NMG.

The polymer particle diameters, measured by DLS and TEM are detailed in Table 4. For all the samples, the polymer particles have a final diameter between 50 and 85 nm. A small decrease of the polymer particle diameter is observed when the concentration of initiator increases for both blank and *in situ* polymerizations. The introduction of NMG platelets in the polymerization induces an increase of the mean polymer particle diameter.

Moreover, for the experiments with 1%KPS, a sharp increase of the poly value is observed between the blank and *in situ* polymerizations. This increase of the polymer particles size distribution may be related to the different nucleation mechanism in the presence of graphene platelets and to a poor stability of the resulting particles for the low initiator concentration. As described in section I.2., part of the radicals can be trapped by the NMG platelets and in consequence less radicals and charged initiator fragments are available for the polymerization reaction and latex stabilization, respectively.

Table 4. Polymer particle diameters and conversion for blank emulsion polymerization and *in situ* emulsion polymerization in the presence of NMG/SDBS-5 suspensions for two KPS concentrations.

Experiment name	DLS		TEM	Final conversion (%)
	D _h (nm)	Poly	D _{TEM} (nm)	
E-1%-B/SDBS-2	63	0.04	-	100
E-2%-B/SDBS-2	54	0.03	-	100
E-1%-NMG/SDBS-2.7	84	0.36	-	89
E-2%-NMG/SDBS-2.7	70	0.05	72	100

For further *in situ* polymerizations, 2%/M of KPS (corresponding to 0.04 g of KPS in our polymerization conditions) will be used in order to obtain a total conversion.

b. Influence of surfactant concentration

The influence of the surfactant concentration on the final polymer particle diameter and conversion is studied with the NMG/SDBS-2.5 and NMG/SDBS-5 suspensions. As presented in Table 3, the concentration of surfactant in the NMG/SDBS-2.5 suspension is below the CMC_{app} . This parameter might have an impact on the polymerization mechanism. The *in situ* emulsion polymerizations were performed in the polymerization conditions described in section II.2.a.

For both polymerizations, part of NMG was expelled on the glass wall of the reactor. This proportion of NMG is lost but taken into account in the calculations of NMG wt%. This destabilization of the NMG platelets might be due to the high mobility of SDBS in the aqueous phase. During the nucleation phase, the growth of the polymer particles induces an increase of the surface tension at the polymer/water interface. As a consequence, more surfactant is needed to stabilize the growing polymer particles: Surfactants desorb from the NMG platelet to adsorb on the growing polymer particles, leading to destabilized NMG platelets that are expelled on the glass wall of the reactor (Figure 10).

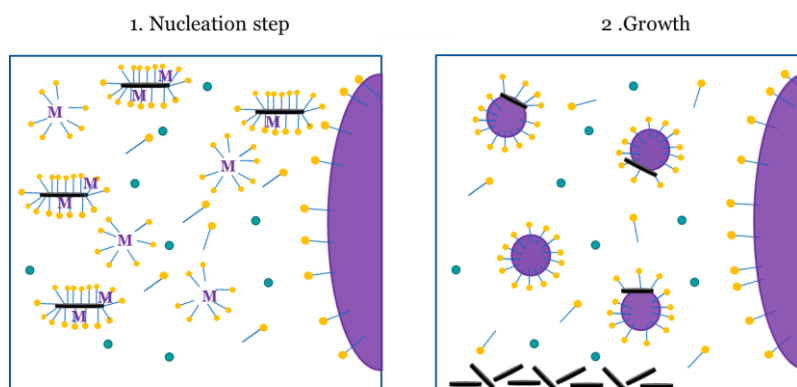


Figure 10. Hypothetic nucleation in the presence of NMG platelets for *in situ* emulsion polymerization.

The morphology of the final latexes is presented on the cryo-TEM micrographs of Figure 11. TEM contrast between polymer and NMG is low. NMG are visible if they are thick enough or if they are edge up. Few NMG platelets are visible on the polymer particles, indicated with arrows. The NMG platelets seem to be concentrated on the biggest polymer particles.

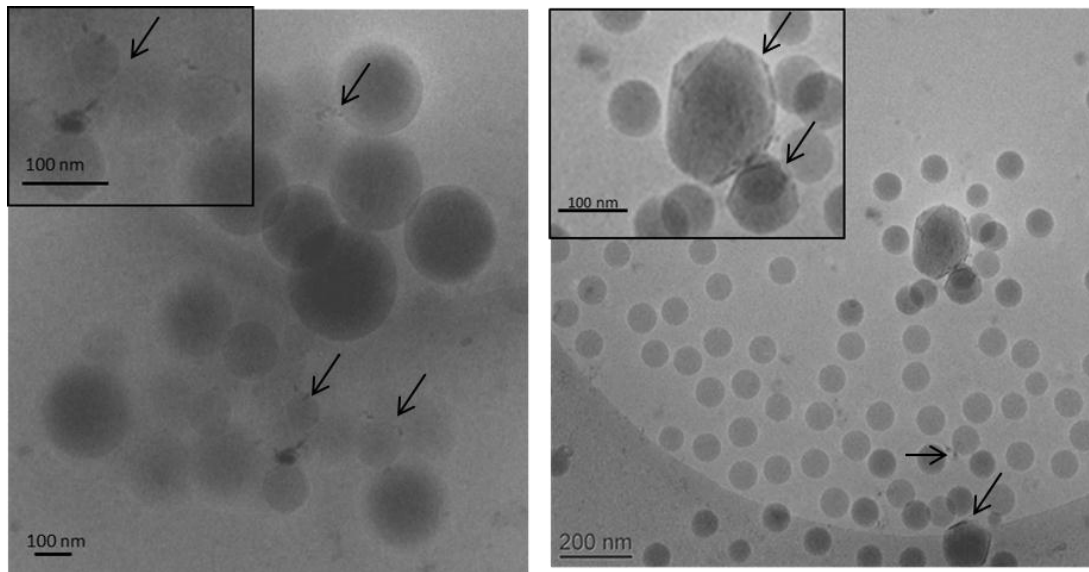


Figure 11. Cryo-TEM pictures for a) E-2%-NMG/SDBS-1.2 and b) E-2%-NMG/SDBS-2.7 after polymerization

The particle diameter, size distribution and final conversion are gathered in Table 5 along with the NMG content in the nanocomposite suspension. The number of NMG and polymer particles, N_{NMG} and N_{latex} , has also been calculated and a theoretical surface coverage, τ_{coverage} , has been evaluated. A sharp difference of particle size is noticed. This variation is due to the decrease of the SDBS and NMG concentration for the composite latex E-2%-NMG/SDBS-1.2. In fact, the decrease of the surfactant implies that less surfactant molecules can stabilize the growing particles and the interfacial tension between the water phase and the particles will be higher. Consequently, the latex particles can have a larger diameter. With a surfactant concentration below CMC_{app} , the latex size is much larger compared to the latex size obtained with a surfactant concentration above CMC_{app} . The same phenomenon will happen for the NMG platelets, a high concentration of NMG platelets will induce the formation of polymer particles with a lower diameter. Moreover, the mean latex diameters obtained by TEM and DLS are consistent. The conversion is not total for the E-2%-NMG/SDBS-1.2 nanocomposite latex despite an amount of initiator of 2%/M.

Table 5. Polymer particle diameters and conversion for in situ emulsion polymerization in the presence of NMG/SDBS-2.5 and NMG/SDBS-5 suspensions.

Experiment name	NMG (g L ⁻¹)	DLS		TEM	Conversion (%)	N_{NMG}	N_{latex}	τ_{coverage}
		D_h (nm)	Poly	D_{TEM} (nm)				
E-2%-NMG/SDBS-1.2	0.3	260	0.05	220	65	$6.8 \cdot 10^{12}$	$1.2 \cdot 10^{14}$	2.2
E-2%-NMG/SDBS-2.7	2.4	70	0.05	72	100	$1.6 \cdot 10^{15}$	$9.4 \cdot 10^{15}$	6.3

For both syntheses, the number of NMG platelets is lower than the number of polymer particles, which is consistent with the few NMG platelets observed on the cryo-TEM micrographs (Figure 11). With the increase of NMG concentration, the evaluated theoretical surface coverage naturally increases despite the decrease of particle size.

To study more specifically the impact of surfactant concentration on the polymer particle diameter, the surfactant concentration in the NMG/SDBS-5 suspension has been decreased while maintaining a reasonably high NMG concentration. Two processes are used: dialysis or ultracentrifugation. For dialysis, 50 g of NMG/SDBS-5 are introduced inside a dialysis membrane. Two liters of water are placed outside the membrane; surfactant molecules can go through the membrane pushed by osmotic pressure. Water is changed every day until equal surface tension is reached inside the membrane (NMG suspension) and outside the membrane. After a month of dialysis, the surfactant concentration is 0.3 g L^{-1} , which corresponds to a surface tension of 64.1 mN m (Table 6). This process induces a sharp decrease of the surfactant concentration. As an alternative, ultracentrifugation is performed at 50,000 rpm rotation speed on the NMG/SDBS-5 suspension. The supernatant, containing only SDBS, is removed and the bottom of the sample is dispersed in water. A final SDBS concentration of 1.7 g L^{-1} is reached, which corresponds to a surface tension of 41.3 mN m (Table 6).

Table 6. Main characteristics of NMG/SDBS-5-dial and NMG/SDBS-5-U.C suspensions

Sample name	[SDBS] (g L^{-1})	[NMG] (g L^{-1})	Surface tension (mN m^{-1})
NMG/SDBS-5-dial	0.3	0.8	64.1
NMG/SDBS-5-UC	1.7	2.2	41.3

Two *in situ* emulsion polymerizations are realized with the suspensions NMG/SDBS-5-dial and NMG/SDBS-5-U.C respectively in the conditions described in the section II.2.a. These syntheses will be named E-2%-NMG/SDBS-0.3 and E-2%-NMG/SDBS-1.7, respectively. During the *in situ* polymerization containing a low surfactant concentration (E-2%-NMG/SDBS-0.3), destabilization of all the NMG platelets appeared 30 minutes after the beginning of the polymerization. This polymerization was stopped and not further characterized.

The polymerization kinetics of the polymerization E-2%-NMG/SDBS-1.7 and E-2%-NMG/SDBS-2.7 are compared in Figure 12. These two polymerizations were performed with a similar concentration of NMG but a different concentration of SDBS. A small decrease of the surfactant concentration leads to a sharp decrease of the polymerization rate. A full conversion is not reached for E-2%-NMG/SDBS-1.7. As expected, by reducing the surfactant concentration below the CMC_{app} , NMG platelets are not fully covered with surfactant leading to more residual functional groups or defects available to react with the initiator leading to the trapping of a part of the radicals.

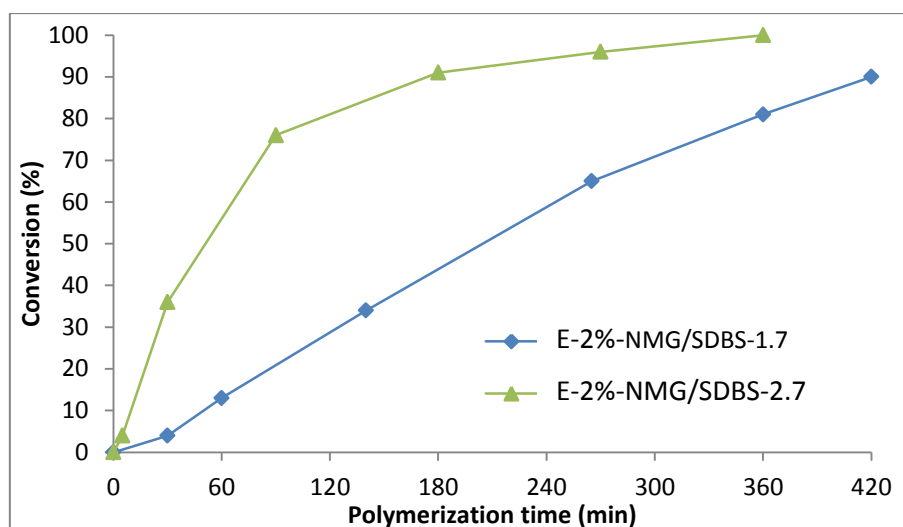


Figure 12. Polymerization kinetics for the nanocomposites E-2%-NMG/SDBS-1.7 and E-2%-NMG/SDBS-2.7.

The cryo-TEM micrograph of latex E-2%-NMG/SDBS-1.7 is presented in Figure 13. Few NMG platelets are visible around the largest latex particles (pointed by the black arrows) and a wide latex size distribution is observed.

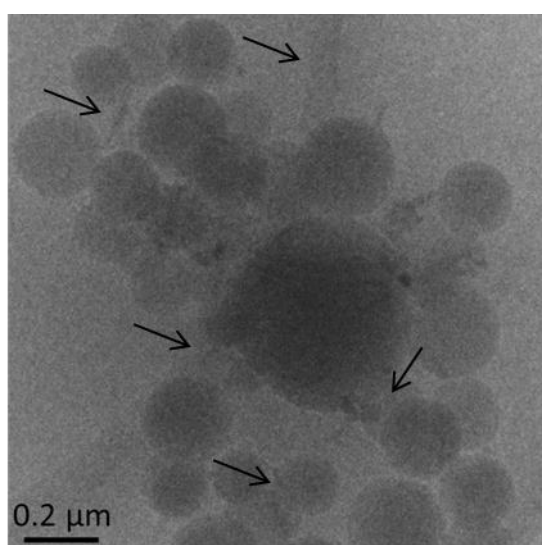


Figure 13. Cryo-TEM picture of E-2%-NMG/SDBS-1.7 nanocomposite latex.

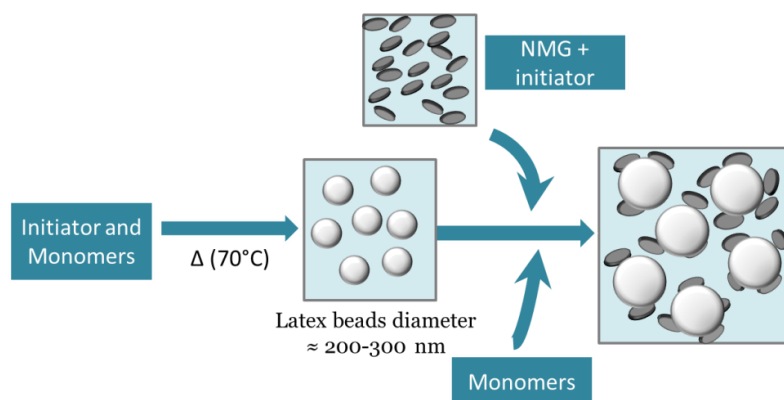
The mean polymer particle diameter is measured by DLS and TEM. The NMG weight percentage and surface coverage are calculated. The results are collected in Table 7 and can be compared to the characteristics of samples E-2%-NMG/SDBS-1.2 and E-2%-NMG/SDBS-2.7 presented in Table 5.

Table 7. Polymer particle diameter, monomer conversion, particle number and theoretical surface coverage for the E-2%-NMG/SDBS-1.7 nanocomposite latex.

Experiment reference	NMG (g L ⁻¹)	DLS		TEM	Conversion (%)	N _{NMG}	N _{latex}	$\tau_{coverage}$
		D _h (nm)	Poly	D _{TEM} (nm)				
E-2%-NMG/SDBS-1.7	2.2	216	0.04	228	90	1.4 10 ¹⁵	2.9 10 ¹⁴	19.3

The decrease of SDBS concentration just below the CMC_{app}, induces a sharp increase of the mean polymer particle diameter without an increase of the particle size distribution. With a weight percentage of NMG similar to E-2%-NMG/SDBS-2.7, a higher theoretical surface coverage is reached: almost two particles of NMG are available for one polymer particle. Note that this surface coverage takes into account all the NMG introduced into the reactor, but a part of NMG is expulsed on the reactor wall for most of these polymerizations.

In order to obtain larger polymer particles and so increase the surface coverage, a semi-batch process is proposed (Figure 14). The aim of this synthesis is to avoid the nucleation step which induced a destabilization of part of the NMG platelets. First, a surfactant-free polymerization is performed at 70°C until the latex particles reach a diameter of 200 to 300 nm. Then, a solution of monomers on one side and a suspension of NMG containing initiator in another side will be added continuously into the reactor with a rate of 12.5 mL per hour. The suspension NMG/SDBS-5-U.C will be used in order to have a surfactant concentration below the CMC_{app}.

**Figure 14.** Scheme of the semi-batch process to favor interactions between NMG platelets and forming latex particles.

Unfortunately, NMG platelets are destabilized just after their introduction in the polymerization reactor and no NMG platelets are visible in the nanocomposite suspension at the end the polymerization.

Stability of the nanocomposite latexes

The global stability of the nanocomposite latexes formed in this part with 2%/M of KPS are studied. First, pictures of the samples were taken at the end of the polymerization and after 5 days (Figure 15). The color of the latex depends on the size of the polymer beads. For large particles, the latex will be white, whereas for small particles (< 100 nm approximately) the latex will be more transparent or bluish. Consequently, the color of the nanocomposite latex will depend both of the size of the polymer particles and the concentration of NMG platelets.

The E-2%-NMG/SDBS-2.7 nanocomposite latex is darker than the other samples due to its high concentration of NMG platelets but the polymer particles formed are really small. When, the polymer particles are bigger, the suspension appears more with a grey opaque color. After five days, a small dark deposit is visible in the bottom of the samples for all the *in situ* polymerizations. But, the supernatant still have a grey color, meaning that part of the NMG platelets remains in suspension.

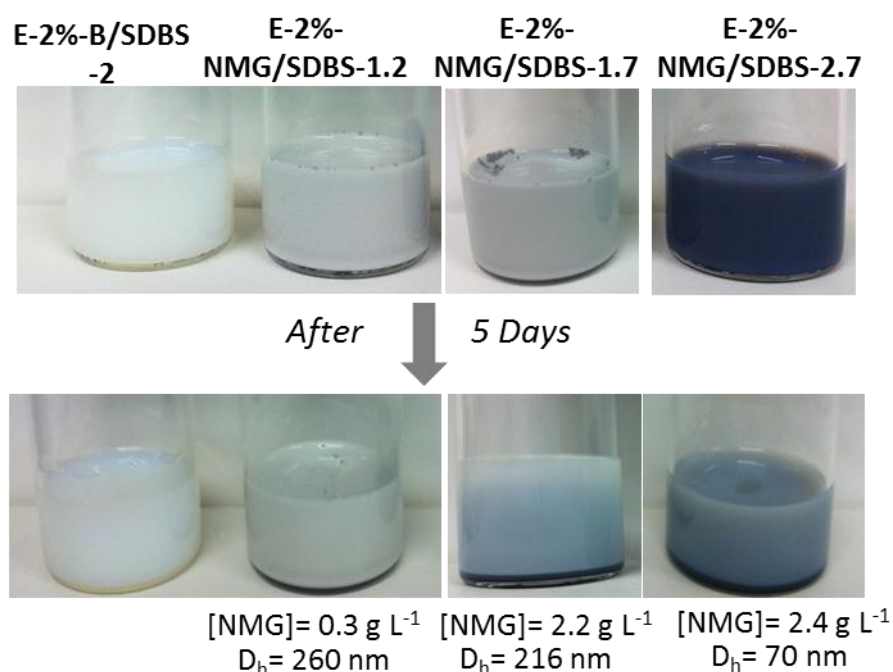


Figure 15. Pictures showing the stability of the blank latex E-2%-B/SDBS-2, and nanocomposite latexes E-2%-NMG/SDBS-1.2, E-2%-NMG/SDBS-1.7 and E-2%-NMG/SDBS-2.7, with time.

The stability of the latexes E-2%-B/SDBS-2, E-2%-NMG/SDBS-2.7 and E-2%-NMG/SDBS-1.7 were analyzed via Turbiscan® (Figure 16). For all three graphs, the backscattering intensity increases with time at the top of the cylinder. And at the bottom of the cylinder, the backscattering intensity decreases with time. The sedimentation of part of the polymer particles covered by NMG and the free NMG induces an increase of the adsorption intensity in the bottom of the cylinder. Similarly, less NMG is present in the top of the cylinder and consequently it induces an increase of the backscattering. In the middle of the cylinder, the backscattering signal could be caused by a gradient in the sedimentation rates: the latex exhibits a wide size distribution, and so the sedimentation phenomenon occurs with a wide

range of rates. In addition, the sediment seems higher for the nanocomposite latex E-2%-NMG/SDBS-1.7 which is the nanocomposite containing a lower concentration of surfactant.

These stability analyses demonstrate that part of the suspension can sediment for the suspensions less charged in surfactant. But a simple shaking of the suspension induces a redispersion of the particles with no variation of the particle size (measured by DLS).

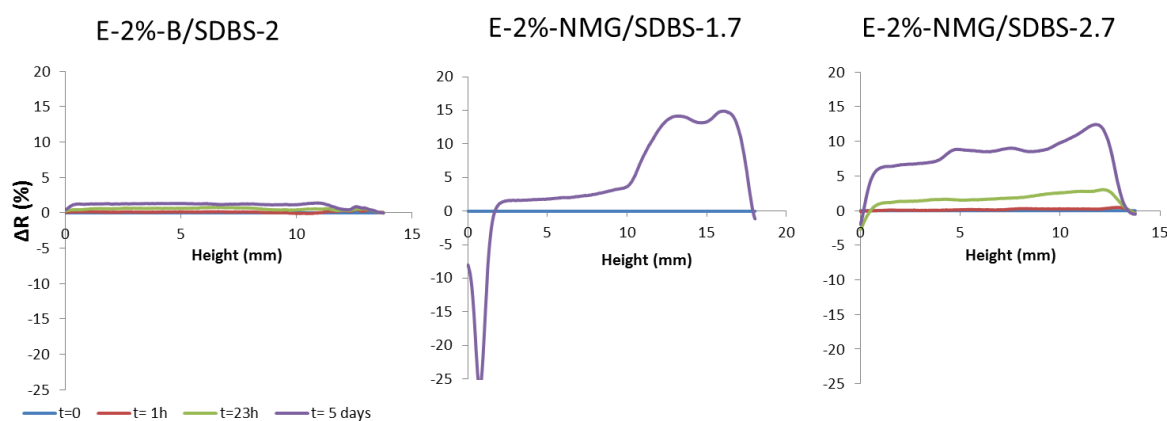


Figure 16. Turbiscan® stability analysis of the nanocomposite latexes E-2%-B/SDBS-2, E-2%-NMG/SDBS-1.7 and E-2%-NMG/SDBS-2.7

To conclude, *in situ* polymerizations with NMG/SDBS suspensions allow the formation of nanocomposite particles with a maximum diameter of 260 nm by decreasing the surfactant concentration just below the CMC_{app} . The surfactant, SDBS, presents a high mobility in the aqueous phase and induces a destabilization of part of the NMG platelets during polymerization. In order to counteract the destabilization of NMG platelets due to surfactant mobility in water, two polymeric stabilizers (NMG/PSSNa and NMG/PS*b*PEO1030) exhibiting a lower molecular mobility in the aqueous phase due to their high molar mass, have been selected and investigated in the following section.

4. *In situ* emulsion polymerization with NMG/PSSNa suspensions

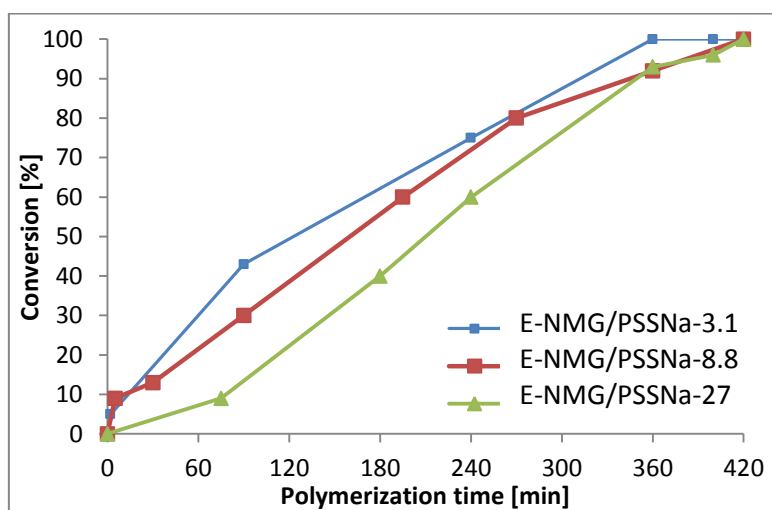
The PSSNa used is a polyelectrolyte with a molar mass of $70,000 \text{ g mol}^{-1}$. It is known to create π - π staking interactions with NMG platelets [24]. Due to the high molar mass of this stabilizer, its mobility in solution is lower than SDBS mobility, and should induce a lower destabilization of NMG platelets. As seen in chapter 2, the use of PSSNa as stabilizer during mechanical delamination of graphite powder is not as efficient as the use of SDBS, the suspensions are less concentrated in NMG. *In situ* emulsion polymerizations were realized with two NMG suspensions (prepared in Chapter 2): NMG/PSSNa-5 and NMG/PSSNa-10. Another suspension, named NMG/PSSNa-conc, was also prepared by partial water evaporation from the NMG/PSSNa-10 suspension in order to increase the NMG concentration in the suspension. PSSNa and NMG concentrations and NMG dimensions are summarized in Table 8.

Table 8. Main characteristics of NMG/PSSNa-5, NMG/PSSNa-10 and NMG/PSSNa-conc suspensions

Sample name	[PSSNa] (g L ⁻¹)	[NMG] (g L ⁻¹)	Lateral size (nm)	Lateral size (nm)	Thickness (nm)
			50% (D50)	90% (D90)	90% (E90)
NMG/PSSNa-5	3.1	0.8	200	980	5.6
NMG/PSSNa-10	8.8	0.3	80	980	6.4
NMG/PSSNa-conc	27	1.2	80	980	6.4

As a reference, a blank polymerization with PSSNa was performed using the same PSSNa concentration than the NMG/PSSNa-10 suspension (i.e., 8 g L⁻¹). Blank and *in situ* emulsion polymerizations were performed using the polymerization conditions described in section II.2.a. The resulting nanocomposites: E-2%-B/PSSNa-8, E-2%-NMG/PSSNa-3.1, E-2%-NMG/PSSNa-8.8 and E-2%-NMG/PSSNa-27 were characterized and compared. The polymerization kinetics for the nanocomposite latex containing NMG platelets are presented on Figure 17.

As expected, the use of a polyelectrolyte induced less destabilization of NMG particles and none are visible on the glass walls of the reactor during the polymerization. A final conversion of 100% was reached for the three syntheses. Moreover, the stabilizer and NMG concentrations seem to have no significant impact on the polymerization rate and final conversion.

**Figure 17.** Polymerization kinetics for nanocomposites with the three NMG/PSSNa concentrations.

Cryo-TEM was performed on the samples E-2%-B/PSSNa-8 and E-2%-NMG/PSSNa-3.1 (Figure 18a and b) and TEM observations were realized on the samples E-2%-NMG/PSSNa-8 and E-2%-NMG/PSSNa-27 (Figure 18c and d). TEM micrographs show that the polymer film forms however information on morphology is still adequate (Figure 18). Due to their small thickness and their flexibility, part of the NMG platelets might be invisible on the pictures. Only one platelet is visible for E-NMG/PSSNa-3.1 on the cryo-TEM picture.

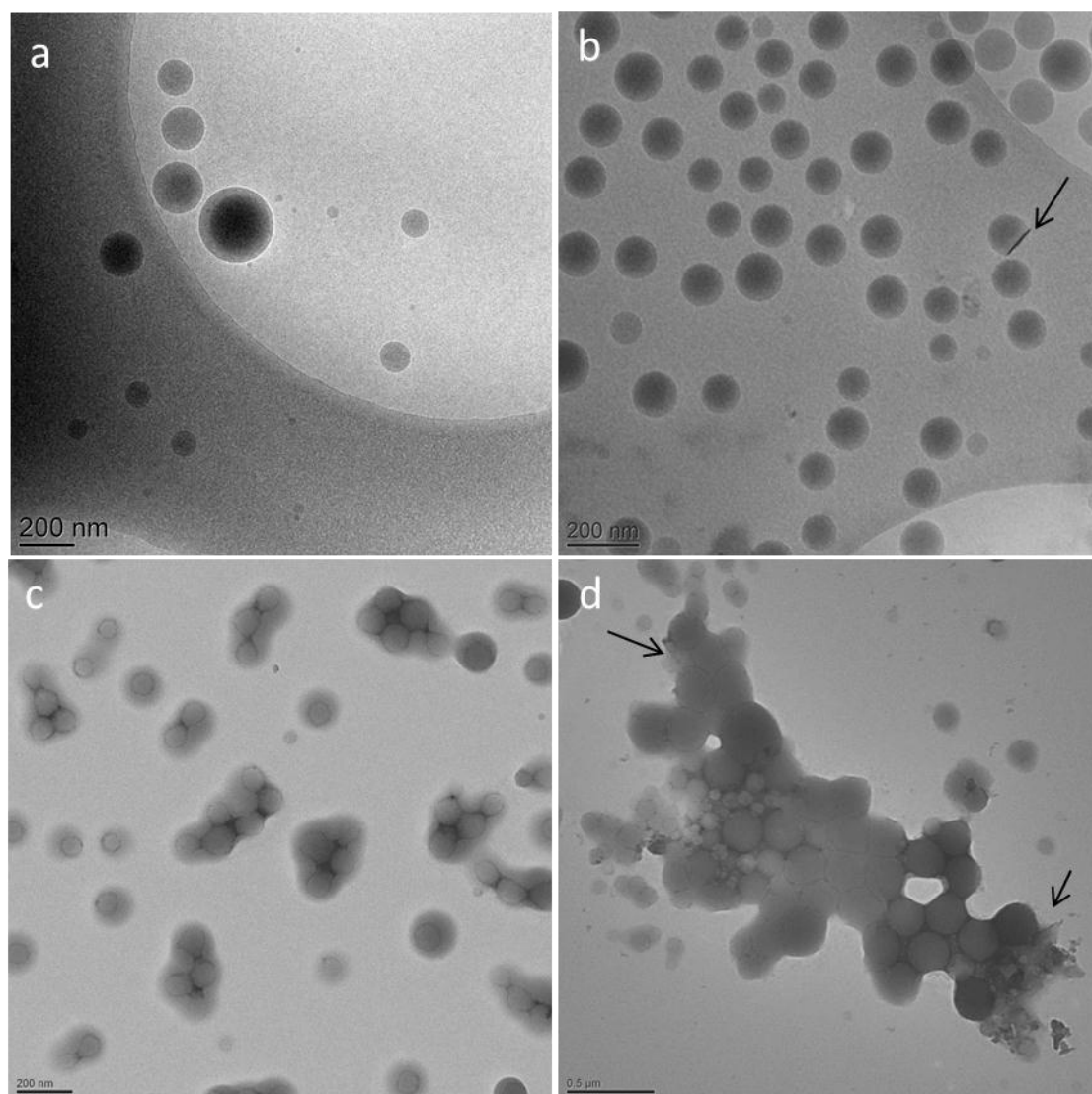


Figure 18. Cryo-TEM pictures of a) the blank experiment E-2%-B/PSSNa-8 and b) the nanocomposite latex E-2%-NMG/PSSNa-3.1 and c, d) TEM pictures of the nanocomposites E-2%-NMG/PSSNa-8 and E-2%-NMG/PSSNa-27, respectively.

The polymer particle diameter was also measured by DLS and the NMG weight percentage and surface coverage of latex particles by NMG platelets was calculated for each nanocomposite latex. These values are summarized in Table 9. The number of NMG platelets is lower than the number of latex particles, which can explain that no (or very few) NMG platelets are seen on the TEM pictures. Despite an increase of the NMG concentration, the surface coverage remains very low.

For the blank polymerization, the particles obtained presented a diameter of 340 nm, which is higher than the previous polymerizations with SDBS. Full conversion is not reached, meaning that the polymerization time can be increased in order to reach a total conversion. Addition of NMG platelets induces a decrease of the latex diameter compared to the blank polymerization. An increase of the PSSNa and NMG concentration induces a small decrease of the latex diameter. This behavior can be due to a lower surface tension at the water/polymer interface when the concentrations of PSSNa and NMG increase.

Table 9. Polymer particle diameter, monomer conversion, particle number and theoretical surface coverage for blank and in situ emulsion polymerizations performed using PSSNa as stabilizer.

Experiment name	NMG (g L ⁻¹)	DLS		TEM	Conversion (%)	N _{NMG}	N _{latex}	$\tau_{coverage}$
		D _h (nm)	Poly	D _{TEM} (nm)				
E-2%- B /PSSNa-8	0	340	0.04	-	75	0	-	-
E-2%-NMG /PSSNa-3.1	0.8	184	0.02	162	100	5.1 10 ¹³	5.2 10 ¹⁴	3.7
E-2%-NMG /PSSNa-8	0.2	170	0.03	130	100	9.6 10 ¹³	6.6 10 ¹⁴	1
E-2%-NMG /PSSNa-27	1.2	147	0.04	185	95	3.8 10 ¹⁴	9.7 10 ¹⁴	3.8

As before for SDBS, the stability of the nanocomposite latexes formed in this part was studied first by visual inspection and then using Turbiscan®. After five days, only a very small dark deposit was visible in the bottom of the samples containing NMG platelets (Figure 19). But, the latexes seemed more stable than when SBDS was used as surfactant, because no discoloration of the supernatant was visible.

The Turbiscan® results are shown in Figure 20. For the blank curve (E-2%-B/PSSNa-8), a sedimentation phenomenon is visible. This sedimentation can be due to the size of the polymer particles, which will naturally form a sediment. Concerning the nanocomposite latex samples, the variation of ΔR (%) is very small and does not exceed -5% for the nanocomposite latexes E-2%-NMG/PSSNa-3.1 and E-2%-NMG/PSSNa-8 in the bottom of the cylinders. Only the nanocomposite with the highest percentage of NMG (E-2%-NMG/PSSNa-27) presents a sediment in the bottom of the cylinder.

To conclude, the nanocomposite latexes synthesized in the presence of NMG/PSSNa present a low weight percentage of NMG and the diameter of the polymer particles formed does not exceed 180 nm. But these nanocomposites present an excellent stability after five days at room temperature and during the polymerization, no destabilization of the NMG platelets is observed due to the low mobility of the polyelectrolyte in the aqueous phase compared with SDBS.

In order to increase the weight percentage of NMG in the suspensions and increase the polymer particles size, a copolymer (PS*b*PEO 1030, $M_n = 236\,000\text{ mol}^{-1}$) is used for *in situ* emulsion polymerization. This copolymer has a high molar mass and consequently a lower molecular mobility in the aqueous phase.

5. *In situ* emulsion polymerization with NMG/PS*b*PEO 1030 suspensions

Using PS*b*PEO copolymer as a stabilizer for polymerization in dispersed media has been widely studied in the literature [25][26]. Berger *et al.* used PS*b*PEO as an emulsifier in emulsion polymerization with styrene and methyl methacrylate [27] and obtained particles diameter from 50 to 300 nm, depending on the polymerization temperature. In literature the CMC of PS*b*PEO 1030 is reported to be 5.6 g L^{-1} [28]. At this concentration, the copolymer begins to form micelles. This CMC will increase in the presence of NMG platelets.

Nucleation mechanism in the presence of a copolymer is different than in the presence of a surfactant. Mura *et al.* [29] showed that particle size increases with conversion by diffusion of the monomer into the growing latex particles but also by partial flocculation. This partial flocculation is attributed to the low migration rate at the interface. This migration rate should allow a better suspension of the NMG platelets during polymerization. Moreover, macromolecular stabilizers diffuse slower than their molecular homologues and form denser adsorbed layer at interfaces [30]. Furthermore, the adsorption of amphiphilic macromolecules at interfaces, contrary to that of molecular surfactants is kinetically irreversible. This property may strongly modify the stability of monomer emulsions regarding ageing or dilution. This strong and dense adsorption may also limit the possibilities of mass transfer between the inner parts of droplets and the continuous phase, which could alter the kinetics of some polymerization reactions.

Here, two NMG suspensions containing PS*b*PEO or PS*b*PEO 1030 were available. The main characteristics of these two suspensions are summarized in Table 10. However, due to the low concentration of NMG in the NMG/PS*b*PEO 1010 suspension, this suspension could not be used for *in situ* polymerization. In the following, PS*b*PEO will be used in most of the time to designate the PS*b*PEO 1030 block copolymer.

Table 10. Main characteristics of NMG/PSbPEO1010 and NMG/PSbPEO1030 suspensions

Sample name	[Copolymer] (g L ⁻¹)	[NMG] (g L ⁻¹)	Lateral size (nm)		Thickness (nm) 90% (E90)
			50% (D50)	90% (D90)	
NMG/PSbPEO 1010-10	3.8	0.5	200	220	2.8
NMG/PSbPEO 1030-10	6.9	1.3	140	640	3

As a reference, a blank polymerization with PSbPEO 1030 was performed using the same stabilizer concentration than the NMG/PSbPEO 1030-10 suspension (i.e., 7 g L⁻¹). *In situ* emulsion polymerization experiments were carried out using the polymerization conditions described in section II.2.a. Two initiator (KPS) concentrations were used: 1%/M and 2%/M. The resulting nanocomposites: E-2%-B/PSbPEO-7.6, E-2%-NMG/PSbPEO-6.9 and E-1%-NMG/PSbPEO-6.9 were characterized and compared. No sedimentation of NMG platelets was observed on the glass walls of the reactors during the polymerization. The polymerization kinetics is plotted in Figure 21.

For blank polymerizations, full conversion is rapidly reached whereas the conversion hardly reaches 50% for *in situ* polymerizations in the presence of NMG. Addition of NMG induces a sharp decrease of the maximum conversion that levels off at about 50%. At first sight, the decrease of the conversion can be due to the trapping of part of the radicals by NMG platelets. However, no modification of the polymerization rate or maximum conversion with increasing the initiator concentration was observed, meaning that the decrease of conversion might not be linked to NMG radicals trapping. In consequence, we have no rational explanation for this phenomenon that would deserve deeper investigations. But we might notice that the initial polymerization rate is not affected by the introduction of NMG in the polymerization.

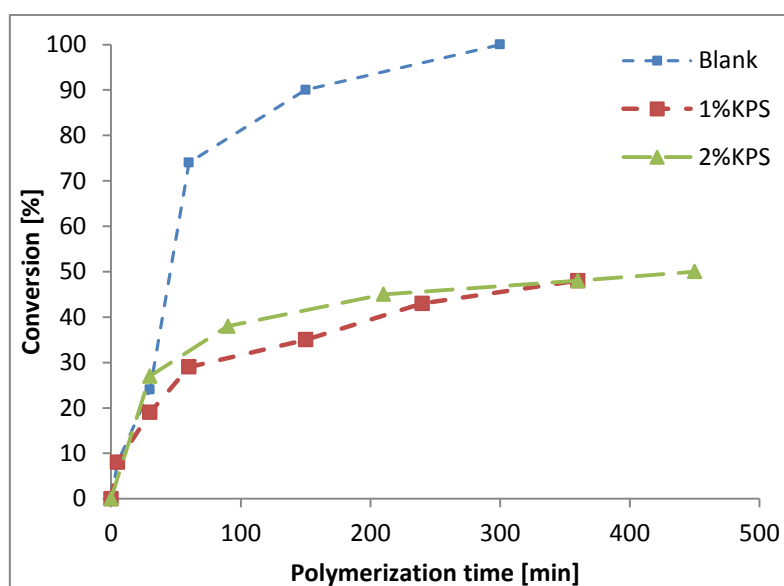


Figure 21. Polymerization kinetics of the blank latex E-2%-B/PSbPEO-7.6 and nanocomposite latexes E-2%-NMG/PSbPEO-6.9 and E-1%-NMG/PSbPEO-6.9.

TEM and cryo-TEM micrographs of the blank polymerization E-2%-B/PS*b*PEO-7.6 and of the nanocomposite latex E-2%-NMG/PS*b*PEO-6.9 are presented in Figure 22. TEM contrast between polymer and NMG is low but in Figure 23b, few NMG platelets are visible on each polymer bead.

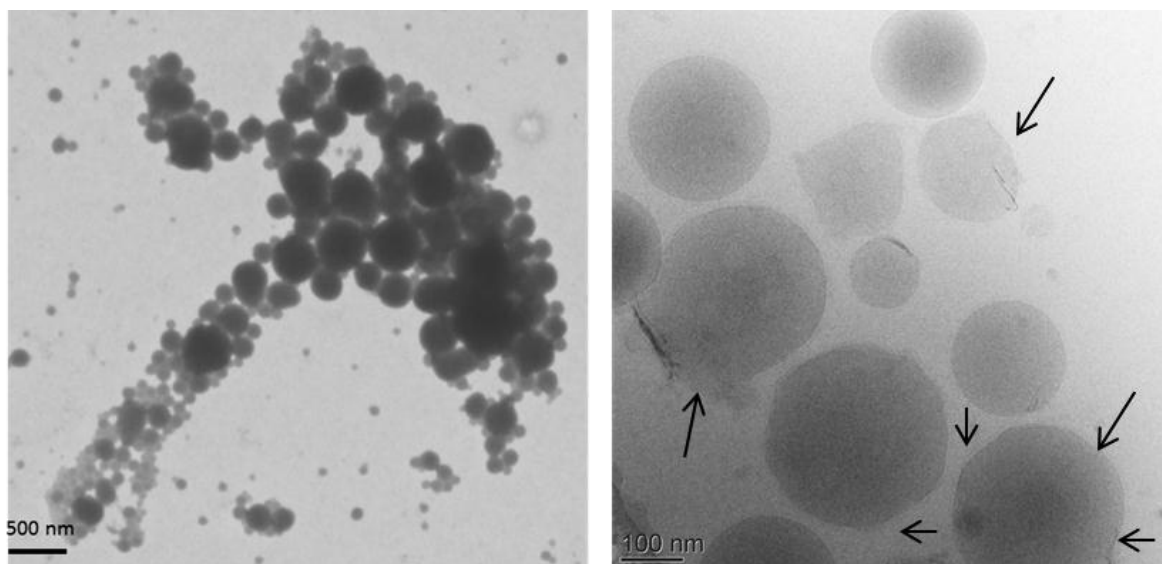


Figure 22. Left: TEM picture of the blank latex E-2%-B/PS*b*PEO-7.6 and right: cryo-TEM picture of the nanocomposite latex E-2%-NMG/PS*b*PEO-6.9.

The mean particle diameter, particles distribution and polymerization conversion are gathered in Table 11. The number of polymer particles and NMG platelets are also determined in order to calculate the theoretical surface coverage. TEM and DLS give a good correlation for latex diameters. The blank experiment and the two *in situ* polymerizations show a similar mean latex diameter, however a large particle size distribution is observed for all three syntheses. This large particle size distribution can be explained by the presence of a second latex population. As described by Hergeth *et al.*, non-ionic surfactants and copolymers, such as PS*b*PEO, are shared between the water phase and the droplets. Part of the copolymer will be initially solubilized in the droplets and in consequence no useable for the stabilization. When the monomer droplets are consumed, the copolymer is released and new polymer particles are then formed [31]. This phenomenon can be visible as light grey spots into the polymer beads on the cryo-TEM pictures (Figure 22-right). These spots correspond to the trapping of water molecules by embedded PEO chains resulting in the formation of nanosized water-pool domains inside the particles [32].

Table 11. Polymer particle diameter, monomer conversion, particle number and theoretical surface coverage for blank and in situ emulsion polymerizations performed using PSbPEO as stabilizer

Experiment name	NMG (g L ⁻¹)	DLS		TEM	Conversion (%)	N _{NMG}	N _{latex}	$\tau_{coverage}$
		D _h (nm)	Poly	D _{TEM} (nm)				
E-2%-B/PSbPEO-7.6	0	214	0.3	240	100	0	-	-
E-2%-NMG/PSbPEO-6.9	1.3	200	0.5	224	50	5.4 10 ¹⁴	2.0 10 ¹⁴	41.8
E-1%-NMG/PSbPEO-6.9	1.3	203	0.45	-	50	5.4 10 ¹⁴	1.9 10 ¹⁴	42.3

Polymer particles obtained via emulsion polymerization in the presence of NMG/PSbPEO 1030 are slightly larger than polymer particles obtained with the stabilizer PSSNa and exhibits higher NMG weight percentages. The number of NMG platelets is higher than the calculated number of latex particles, which is consistent with the cryo-TEM micrographs (Figure 22-right). As a consequence, the surface coverage calculated is quite high and conductive properties are likely expected after film-forming process.

Stability of the blank latex E-2%-B/PSbPEO-7.6 and of the nanocomposite latex E-2%-NMG/PSbPEO-6.9 was studied over five days. Figure 23 shows pictures of the suspensions right after polymerization and five days later. The suspension with NMG is black and seems darker than previous composite latexes made with SDBS surfactant or PSSNa (see Figures 15 and 19). Compared to the polymerization with SDBS, similar weight percentage of NMG was introduced in the reactor at the beginning of the polymerization: it is likely that the final composite still counts a high NMG content. After five days, no visible destabilization was observed while sedimentation was visible for the SDBS series: this high stability might be due to the lower mobility of PSbPEO 1030 compared to SDBS. Moreover, the dark coloration of the nanocomposite latex E-2%-NMG/PSbPEO-6.9 might also be due to the diameter of the polymer particles (200 nm), which is higher than that of the nanocomposite latex E-2%-NMG/SDBS-2.7 (70 nm), for example.

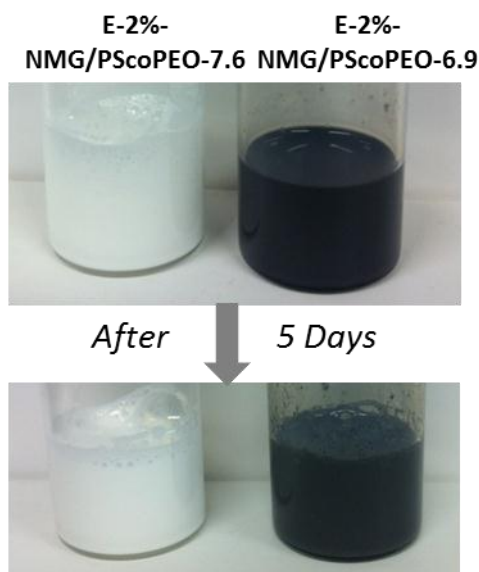


Figure 23. Pictures showing the stability of the blank latex E-2%-B/PSbPEO-7.6 and nanocomposite latex E-2%-NMG/PSbPEO-6.9 with time.

Turbiscan® analyses of the E-2%-NMG/PSbPEO-6.9 suspension are presented in Figure 24. Similarly to the nanocomposite latexes E-2%-NMG/PSSNa-3.1 and E-2%-NMG/PSSNa-8, the backscattering signal ΔR (%), does not vary significantly within the 5 days of analyses. These variations are small compared to results obtained for the nanocomposite latexes containing NMG/SDBS suspensions. These analyses confirm that there is neither destabilization nor sedimentation for the E-2%-NMG/PSbPEO-6.9 sample.

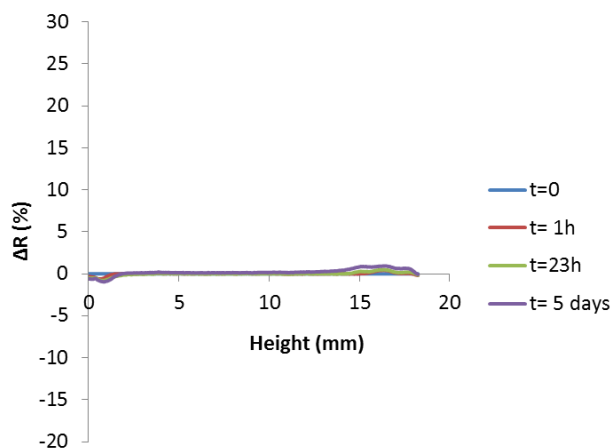


Figure 24. Turbiscan® stability analysis of the nanocomposite latex E-2%-NMG/PSbPEO-6.9.

The choice of PSbPEO as stabilizer during *in situ* polymerization allowed the formation of polymer particles with a mean diameter of 200 nm. Cryo-TEM images showed that the latex particles count one to several NMG platelets on their surface. A theoretical surface coverage around 42% was reached meaning that conductive properties are expected. The nanocomposite latex E-2%-NMG/PSbPEO-6.9 exhibits high stability and no destabilization

was observed during five days. Unfortunately, total conversion was not reached despite an increase of the initiator (KPS) concentration.

6. Conclusions

Three different types of stabilizers: a surfactant (SDBS), a polyelectrolyte (PSSNa) and a block copolymer (PS*b*PtEO) have been used for *in situ* emulsion polymerization. Their choice was balanced between their ability to produce high content and stable NMG suspensions during the NMG mechanical delamination and their mobility in the water phase, which is a critical characteristic during polymerization. SDBS presents a high mobility in the aqueous phase and induces a destabilization of part of the NMG platelets during the polymerization process. By decreasing the SDBS content just below the CMC_{app} , almost full conversion (90%) was reached and composite latex particles of 228 nm mean diameter with high theoretical surface coverage ($\tau_{coverage}=19.3$) were produced. Unfortunately NMG/SDBS latexes exhibited low stability and sedimentation was observed within five days. Latexes obtained from NMG/PSSNa present a low NMG weight percentage (note that NMG/PSSNa suspensions initially exhibit low NMG content after delamination step). In addition the diameter of the latex particles hardly reached 180 nm, which is small and does not favor the creation of armored structures (NMG diameter is about 50 nm). On the other hand, these composite latexes showed no destabilization of NMG platelets during polymerization, probably due to the low mobility of PSSNa in the aqueous phase compared to SDBS. In addition, these latexes showed excellent stability within five days at room temperature. At last, a polymeric stabilizer, PS*b*PtEO1030, was used. The final composite latexes showed high NMG content and no destabilization neither during polymerization nor within five days. Based on the theoretical surface coverage calculated, two latexes should exhibit conductive properties after film-forming, E-2%-NMG/SDBS-1.7 and E-2%-NMG/PS*b*PtEO-6.9. As a perspective, it has been shown that mobility of stabilizer and reactivity of initiator are key parameters to efficiently conduct the *in situ* emulsion polymerization process.

To overcome the problem of surfactant mobility in the aqueous phase and prevent destabilization of the NMG platelets during the polymerization, miniemulsion polymerization can be adequate. In this polymerization mechanism, polymerization within the monomer droplets is favored and with condition that the “NMG/surfactant” complex is effectively adsorbed on the surface of the monomer droplets, there will be less transport phenomena (surfactant, NMG or the two) involved in this process, which should warrant a better colloidal stability during the nucleation step. To favor such mechanism, several experimental conditions have to be fulfilled.

III. Miniemulsion polymerization in the presence of NMG

1. Generalities on miniemulsion polymerization

The idea of miniemulsion polymerization is to initiate the polymerization in each of the small stabilized droplets meaning that there is ideally neither micelles nor need for monomer transport through the aqueous phase. Miniemulsion polymerization has gained significant

importance with extensive studies in research disciplines such as medical, pharmaceutical and chemical fields due to the unique characteristics of this method in comparison to the other dispersed systems [33]. This recent synthesis route was first reported by Ugelstad *et al.* in 1973. It was demonstrated that the polymerization could be initiated in the monomer droplets when the droplets reach a sufficiently small size [22]. Miniemulsion polymerization induces the formation of particles who are about the same size as in emulsion polymerization, (i.e., between 50 and 500 nm in diameter), but which are obtained with a different mechanism.

Miniemulsion droplets are formed at high shear with high-energy shear devices, as for example ultrasound, ultraturax probe or high-pressure homogenizer. To create stable emulsions of very small droplets, which are called miniemulsions, the droplets must be stabilized against molecular diffusion degradation (i.e., Ostwald ripening) and against coalescence by collisions. Coalescence can be prevented using ionic or non-ionic surfactants. In miniemulsion, the fusion-fission rate equilibrium during sonication, and therefore the size of the droplets directly after primary equilibration, depends on the amount of surfactant. For instance, Reimers *et al.* showed that the final particle size decreases with an increase of the surfactant concentration [34]. Ostwald ripening refers to the monomer migration from small droplets to bigger ones resulting in an increase of the mean droplet size. This phenomenon can be limited by adding a highly hydrophobic agent or osmotic pressure agent with a weak solubility in water [35]. For miniemulsion to achieve an equilibrium state, the osmotic pressure inside the droplet needs to be higher than the Laplace pressure (pressure difference between two fluids separated by a common interface) [36]. The presence of a hydrophobe (also called co-stabilizer) hinders the diffusion of monomer from a droplet to another, therefore the polymerization is confined in each droplet and finally one droplet leads to one latex particle. A hydrophobe is usually a long alkene chain compound. Hexadecane [37] and cetyl alcohol [38] are typical examples of hydrophobes that are used in miniemulsion. The addition of hydrophobe in miniemulsion is vital to curb the collapse of monomer droplets by Ostwald Ripening [39].

After the formation of the miniemulsion droplets, the vast majority of the droplets are nucleated, so that the ratio between the initial number of droplets and the final number of particles is close to one [40]. Ideally, droplet nucleation is the unique mechanism of particle formation in miniemulsion [41]. This critical difference means that miniemulsion will behave differently from a kinetic point of view. In addition, we can imagine that the properties obtainable with this type of system will be different, for instance the incorporation of hydrophobic components or the encapsulation of inorganic solids in the final polymer might be more efficient in miniemulsion processes [42].

Figure 25 details the envisioned miniemulsion polymerization mechanism in the presence of NMG platelets. The whole “NMG/surfactant” complex is expected to migrate to the surface of the monomer droplets created during the sonication step to form NMG-armored droplets that will be converted further into NMG-armored latexes.

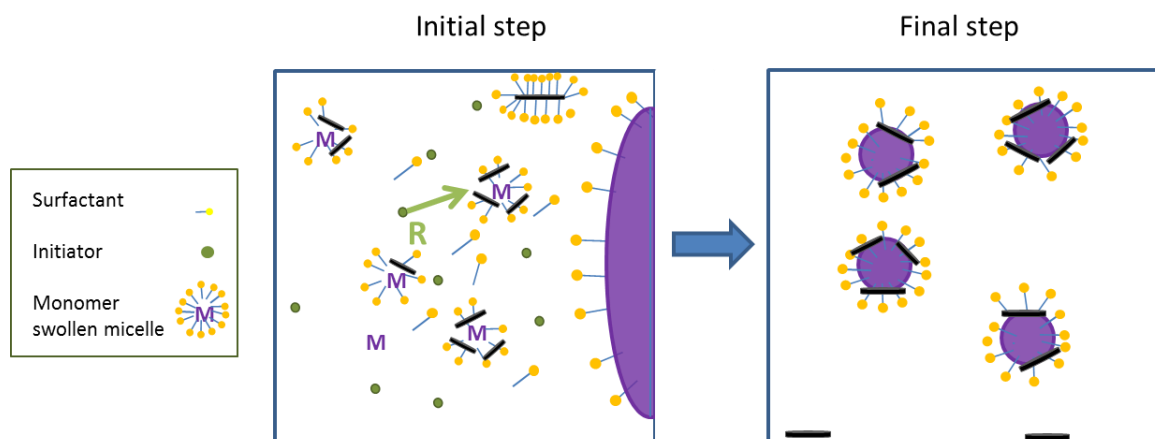


Figure 25. Envisioned miniemulsion polymerization mechanism in the presence of NMG platelets.

Recently, this polymerization process was developed in the presence of GO particles to produce polymeric nanocomposite materials [43] [44]. In most of these works, GO sheets are used as the sole surfactant [45] due to its capacity to stabilize the monomer droplets. But the resulting nanocomposite latexes did not remain stable after GO reduction. As a consequence, it turns out that there is no report in the literature describing the synthesis of stable graphene (or rGO)-based nanocomposite latexes with good electrical properties through miniemulsion polymerization.

In the following, *in situ* miniemulsion polymerizations in the presence of NMG/SDBS and NMG/PS*b*PEO suspensions are presented. The impact of the surfactant or stabilizer nature and concentration on the final dimensions of the polymer particles is discussed.

2. Experimental part

In a typical *in situ* miniemulsion polymerization procedure, 20g of the NMG suspension is mixed with 2 g of a mixture of styrene and butyl acrylate monomers (50/50% wt) and 0.04g of a hydrophobe (Hexadecane). This mixture is sonicated with an ultrasonic probe at 60% of amplitude until the diameter of the droplets remains stable. After each minute of sonication, the droplet diameter is measured by DLS and this operation is repeated until there is no variation of the droplet diameter. The mixture is then degased under nitrogen during 30 minutes. In parallel, the initiator (KPS, 1 wt%/monomers or 2 wt%/monomers) is dissolved in water and degased under nitrogen. These two mixtures are then introduced in the 50 mL polymerization reactor and the polymerization starts when the temperature reaches 70°C. The agitation is performed by an anchor blade. At the end of the polymerizations, the latexes are characterized as described in the part II.2.b.

For the polymerizations without NMG, also named blank experiments, the 20 g of NMG suspensions are replaced by 20 g of deionized water and a certain amount of surfactant (the concentration is fixed to be the same than for the syntheses with NMG/surfactant suspensions). Table 12 details the experimental conditions for each NMG/stabilizer suspensions used for *in situ* miniemulsion polymerization. Each polymerization sample was named according to the convention defined in section II.2. Only 2%/M of KPS was used in this part, hence, the percentage of initiator does not appear in the name of the experiment.

The NMG suspensions used for *in situ* miniemulsion polymerizations are also detailed in Table 12. Note that the NMG/PSSNa-5 and NMG/PSSNa-10 suspensions were not used in this part due to their low NMG content.

Table 12. Experimental conditions for *in situ* miniemulsion polymerizations with NMG/SDBS or NMG/PSbPEO suspensions.

Experiment name	NMG suspension	[NMG] (g L ⁻¹)	[Stabilizer] (g L ⁻¹)	Initiator (%/M)
mE-B/SDBS-2	-	0	2	2
mE-NMG/SDBS-0.3	NMG/SDBS-5-dial	0.8	0.3	2
mE-NMG/SDBS-1.7	NMG/SDBS-5-U.C	3.9	1.7	2
mE-NMG/SDBS-2.7	NMG/SDBS-5	2.4	2.7	2
mE-B/PSbPEO-7	-	0	7	2
mE-NMG/PSbPEO-7	NMG/PSbPEO 1030	2.2	7	2

3. *In situ* miniemulsion polymerization with NMG/SDBS suspensions

In situ miniemulsion polymerizations with NMG/SDBS suspensions were carried out using the experimental conditions described in section III.2. In miniemulsion polymerization, the complex formed by the NMG platelets and adsorbed surfactant molecules is expected to adsorb at the monomer/water interface during the ultrasonication step. As a consequence, a lower destabilization of NMG platelets during the polymerization should be achieved.

For the sake of comparison, a blank experiment was carried out using roughly the same surfactant concentration as for the *in situ* miniemulsion polymerization experiment mE-NMG/SDBS-1.7 (i.e., 2 g L⁻¹). The other samples contain various NMG and SDBS concentrations (see Table 12). As before, the latexes were characterized by DLS and TEM and their kinetics followed by gravimetric analysis. Interestingly enough, all miniemulsions were stable and there was no destabilization of the NMG platelets observed in the course of the polymerization, in agreement with the above-depicted mechanism.

The polymerization kinetics of mE-B/SDBS-2, mE-NMG/SBDS-2.7, mE-NMG/SDBS5-0.3 and mE-NMG/SDBS-1.7 are presented in Figure 26 and can be qualitatively discussed as follow. For the blank polymerization, a total conversion is promptly obtained. For mE-NMG/SBDS-1.7, that has the same SDBS content, the addition of NMG platelets induces a decrease of the total conversion. This decrease can be due to the trapping of part of the radicals by the NMG platelets, as described for *in situ* emulsion polymerization. In addition, previous analyses of *in situ* emulsion polymerization results (see section II.3.b) demonstrated that a decrease in surfactant concentration induces the NMG platelets to be less covered with surfactant and as a consequence, surface oxygen-groups and/or structure defects are more accessible to trap free radicals. This is consistent with the polymerization mE-NMG/SDBS-1.7. This sample shows lower SDBS content and higher NMG content than the mE-NMG/SDBS-2.7 sample. Both the polymerization rate and final conversion are reduced in this

case. Finally, the polymerization kinetics of mE-NMG/SDBS-0.3 lies in between the two others. This behavior is the results of two antagonist effects. Indeed, on the one hand, the NMG/SDBS-5 dialysis suspension counts a low SDBS content compared to the two other suspensions. This would lower the surfactant coverage on NMG and so increase the number of sites per NMG for radical trapping. On the other hand, the NMG/SDBS-5-dialysis suspension also counts a low NMG content that would reduce the total concentration of sites for radical trapping compared to NMG/SDBS-5.

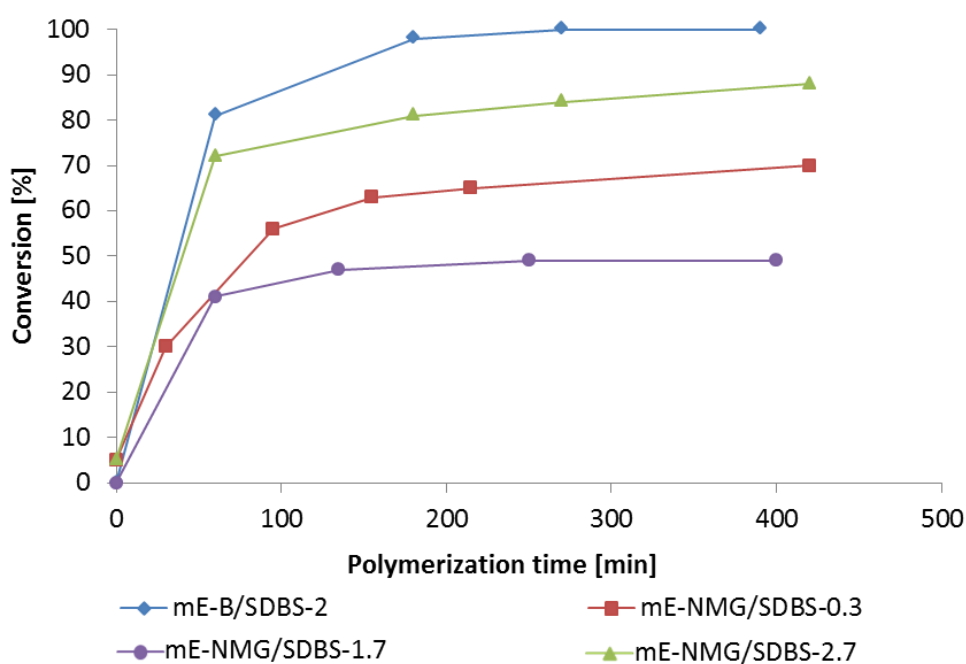


Figure 26. Polymerization kinetics for the blank latex mE-B/SDBS-2, and for the nanocomposite latexes mE-NMG/SDBS-0.3, mE-NMG/SDBS-1.7 and mE-NMG/SDBS-2.7.

Figure 27 and 28 show cryo-TEM pictures of the nanocomposite latexes. Only few NMG platelets are visible around the bigger latex particles on Figure 27, which corresponds to samples containing low NMG contents. Due to the flexibility of NMG, the platelets seem wrapped around the latex beads.

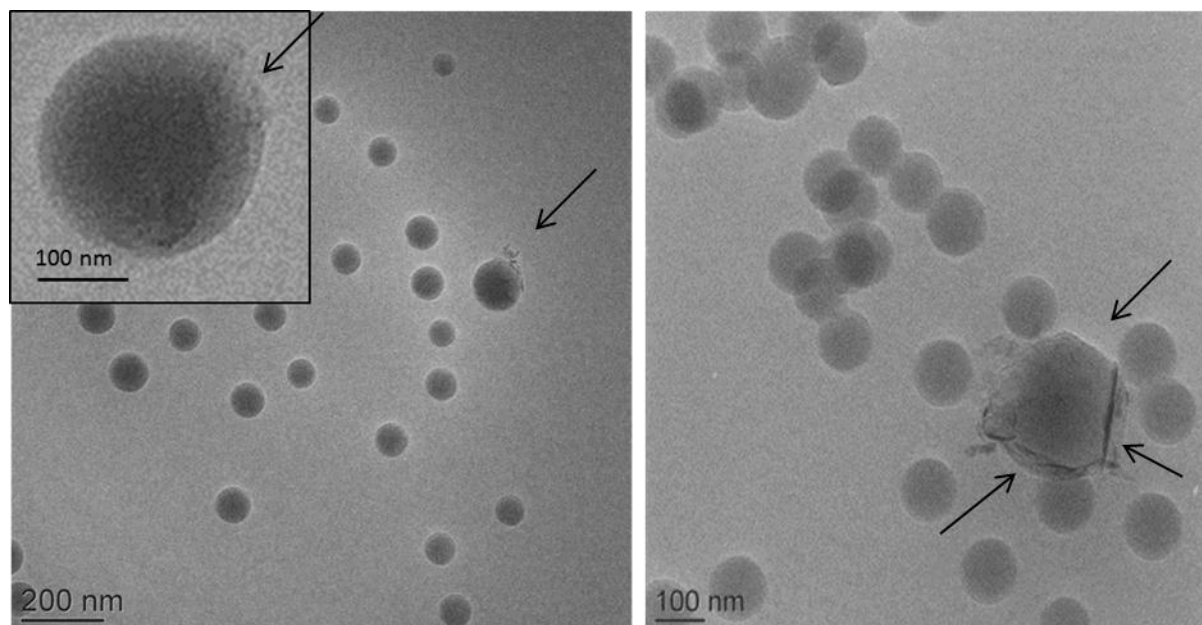


Figure 27. Cryo-TEM images of the nanocomposite latexes mE-NMG/SDBS-0.3 (left) and mE-NMG/SBDS-2.7 (right). [KPS]=2 wt%/monomers and [Hexadecane]=4 wt%/monomers

The number of NMG platelets seems larger for the mE-NMG/SDBS-1.7 sample (Figure 28), which is consistent with the fact that a higher concentration of NMG platelets was used in this experiment.

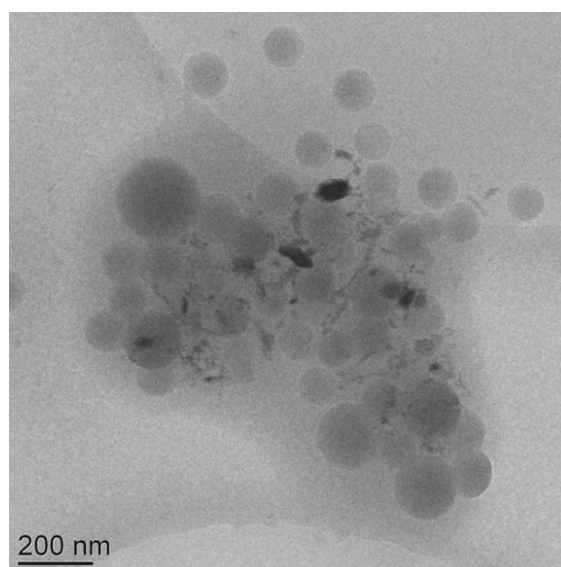


Figure 28. Cryo-TEM images of the nanocomposite latex mE-NMG/SBDS-1.7. [KPS]=2 wt%/monomers and [Hexadecane]=4 wt%/monomers

The droplet size, the polymer particles size and the theoretical surface coverage of this series of experiments are reported in Table 13.

As said above, stable miniemulsion droplets were obtained in all cases. They were larger than in the blank experiment without graphene but their mean DLS diameter was not influenced by the NMG or surfactant concentrations. For all the experiments, the polymer particle diameter

was lower than the monomer droplet diameter. This decrease of the polymer particle diameter suggests the occurrence of secondary nucleation leading to a decrease of the polymer particle size. This decrease in size is larger in the presence of NMG platelets. Moreover, the mean polymer particle diameter is of the same order of magnitude as that of the composite latexes obtained by *in situ* emulsion polymerization under similar conditions.

The theoretical surfaces coverages reported in Table 13 indicate that only the mE-NMG/SDBS-1.7 nanocomposite latex should exhibit conductive properties after film-formation. In this case, the number of NMG platelets is higher than the number of latex particles in agreement with the cryo-TEM micrograph of Figure 28 and the surface coverage is high (i.e., 37%).

Table 13. Polymer particle diameter, monomer conversion, particle number and theoretical surface coverage for blank and *in situ* miniemulsion polymerizations performed using SDBS as surfactant.

Experiment name	Droplets diameter (nm)	DLS		TEM	Conversion (%)	NMG (g L ⁻¹)	N _{NMG}	N _{latex}	$\tau_{coverage}$
		D _h (nm)	Poly	D _{TEM} (nm)					
mE-B/SDBS-2	132	104	0.01	-	100	0	0	-	-
mE-NMG/SDBS-0.3	214	134	0.03	112	65	0.8	5.4 10 ¹⁴	8.7 10 ¹⁴	6.2
mE-NMG/SDBS-1.7	205	127	0.08	140	50	3.9	2.6 10 ¹⁵	7.9 10 ¹⁴	37.1
mE-NMG/SDBS-2.7	204	90	0.06	105	85	2.4	1.6 10 ¹⁵	3.8 10 ¹⁵	9.5

The stability of these composite latexes was also studied (Figure 29).

After five days, a small dark deposit is visible at the bottom of the tube for all composite samples and a slightly lighter grey suspension is also visible at the top of the tube. The change in grey shade is stronger when the NMG content increases, however the supernatant remains grey, which means that some NMG platelets remain in this phase. The nanocomposite mE-NMG/SDBS-1.7 seems to be less stable due to a stronger change in gray shade of the supernatant. This observation would be consistent with the fact that this sample contains a high concentration of NMG but a low concentration of surfactant.

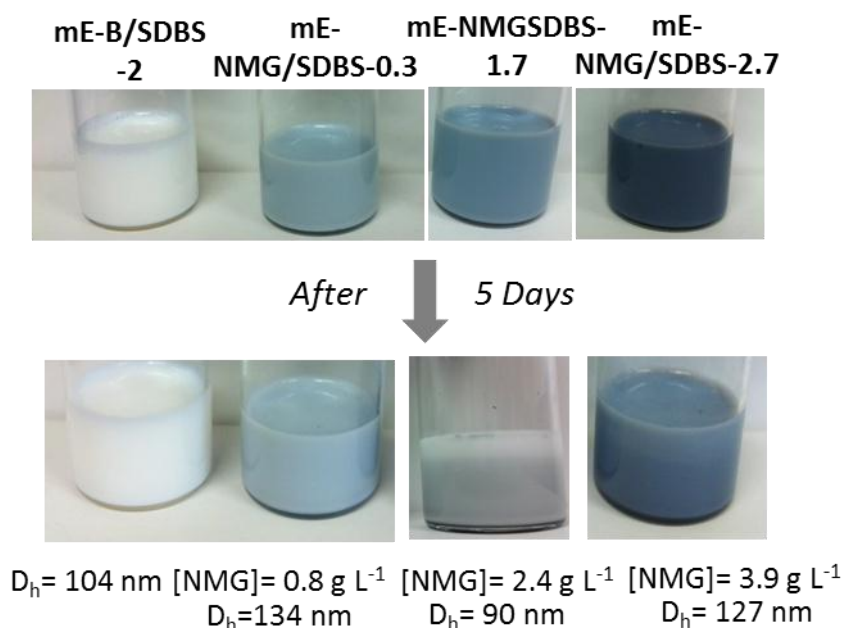


Figure 29. Pictures showing the stability of the blank latex mE-B/SDBS-2 and nanocomposite latexes mE-NMG/SDBS-0.3, mE-NMG/SDBS-1.7 and mE-NMG/SDBS-2.7, with time.

The results of the Turbiscan® experiments are plotted in Figure 30. As expected, the blank sample is stable over time (Figure 30a). For nanocomposite latexes samples, a decrease of the backscattering intensity at the bottom of the samples is visible which can be attributed to sedimentation. Note that sample mE-NMG/SDBS-0.3 in Figure 30b, shows very low variations in the backscattering signal. This may be due to the fact that this sample comprises very low content of NMG. An increase of the backscattering signal at the middle and at the top of the tubes can be explained by a different sedimentation rate of each particle present in the samples (Figures 30c, 30d). The free latex particles do not sediment while some of the NMG platelets fall down (light absorbers) as well as latex particles (partially) covered with platelets. As a consequence, the top of the cylinder absorbs less and thus scatters more. In addition, the particles fall down at different rates depending on their density, which account for variations in the slopes of the curves.

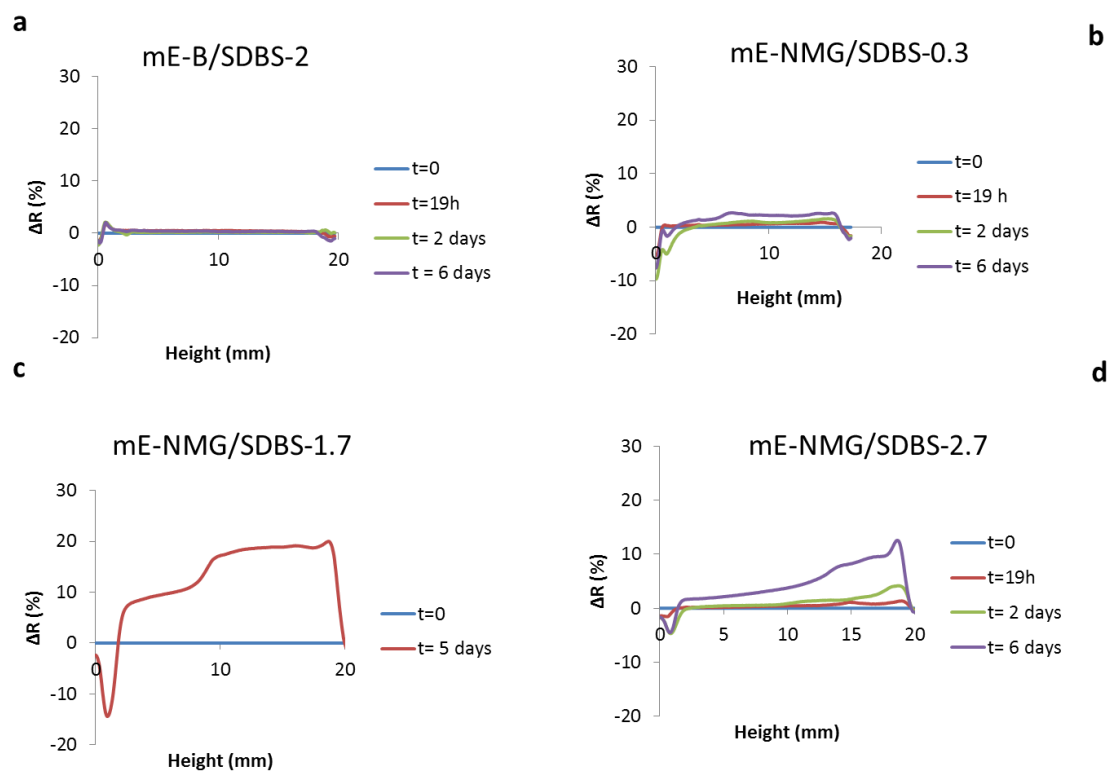


Figure 30. Turbiscan® stability analyses of the nanocomposite latexes synthesized by *in situ* miniemulsion polymerization using SDBS as surfactant.

To conclude on *in situ* miniemulsion polymerizations with NMG/SDBS suspensions, a decrease of the surfactant concentration allowed an increase of the mean polymer particle diameter. But it also induced a sharp decrease of the total conversion, which is likely related to both the surfactant and the NMG concentration. Compared to *in situ* emulsion polymerization, there is no increase of the mean polymer particle diameter and no improvement of shelf stability; however less NMG destabilization during polymerization is visible. The sample mE-NMG/SDBS-1.7 shows a theoretical surface coverage that should be large enough to exhibit conductive properties after film formation.

In order to increase the mean latex diameter, *in situ* miniemulsion polymerization was performed with NMG/PS*b*PEO 1030 suspensions. As already mentioned, no miniemulsion polymerization experiments were carried out with the NMG/PSSNa suspension due to their low NMG concentration.

4. *In situ* miniemulsion with NMG/PS*b*PEO 1030 suspensions

PS*b*PEO block copolymers can also be used as stabilizers in miniemulsion polymerization. Such copolymers enable forming larger polymer particles, compared with surfactants. In fact, it is well known that steric stabilizers (PS*b*PEO) induce the formation of bigger polymer particles than electrostatic stabilizers (SDBS). Moreover, because of their larger mass, polymeric stabilizers diffuse much slower than low molar mass surfactants, and are consequently less prone to desorb from interfaces, which may favor droplets formation and stabilization.

In situ miniemulsion polymerization was carried out using the same NMG/PS*b*PEO1030-10 suspension utilized in the emulsion polymerization part (section II.5), and compared to a blank polymerization performed under similar conditions using 7 g L^{-1} of stabilizer (see Table 12). Once again, no destabilization of the NMG platelets was observed during droplet formation or in the course of polymerization, which points to the specific nucleation mechanism of this *in situ* miniemulsion polymerization process.

The polymerization kinetics of the blank experiment mE-B/PS*b*PEO-7 and mE-NMG/PS*b*PEO-7 are plotted in Figure 31. For the blank experiment, a total conversion is reached. On the contrary, the addition of NMG platelets induces a decrease of the polymerization rate after one hour of polymerization resulting in a maximal conversion of 50% after 7 hours. As for *in situ* emulsion polymerization this sharp decrease of the total conversion might be due to the trapping of part of the radicals by the NMG platelets. This radical capture will be favored in miniemulsion, compared with emulsion polymerization, because the NMG platelets are located at the monomer/water interface since the beginning of the polymerization, and are thus highly accessible to waterborne radicals. In other words, the NMG armor can act as a physical barrier for radical entry, limiting thereby the monomer conversion. Using an organosoluble initiator which will generate radicals inside the droplets can be an alternative to minimize radical trapping by the NMG platelets and increase monomer conversion.

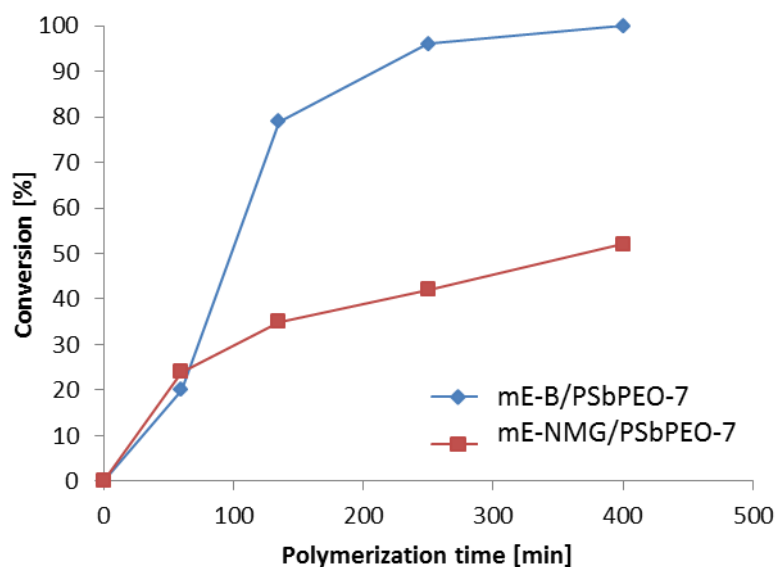


Figure 31. Polymerization kinetics for the blank experiment mE-B/PS*b*PEO-7 and for the nanocomposite latex mE-NMG/PS*b*PEO-7.

Figure 32 shows two cryo-TEM pictures of the nanocomposite latex. In these images, many NMG platelets (pointed to by arrows) are visible around the polymer particles. The polymer particles formed seems larger than the particles formed by *in situ* miniemulsion polymerization with NMG/SDBS suspensions.

Similar light grey spots as those observed during *in situ* emulsion polymerization with NMG/PS*b*PEO 1030, are also visible on the cryo-TEM pictures. These spots correspond to

embedded water pool [32] domains subsequently to PEO chains entrapment in the polymer beads (see Section II.5).

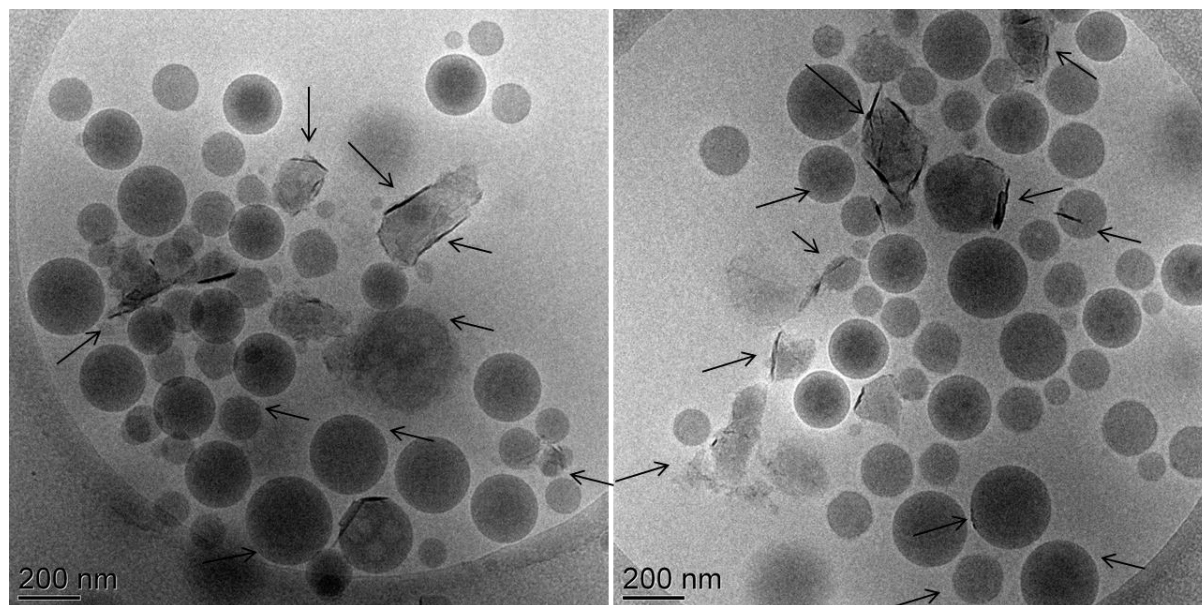


Figure 32. Cryo-TEM pictures of the nanocomposite latex *mE-NMG/PSbPEO-7*.

The mean particle diameter and particle size distribution were characterized by DLS and TEM, which allowed determining the numbers of NMG and polymer particles and the theoretical surface coverage (Table 14).

For the blank experiment, a small increase of the latex diameter is observed between the beginning and the end of the polymerization. It demonstrates that the PS*b*PEO copolymer did not manage to efficiently stabilize the droplets during polymerization. In addition, the particle size distribution is broad (as indicated by the high Poly value), which confirms that PS*b*PEO 1030 is not a good stabilizer for miniemulsion polymerization. Similarly, *in situ* miniemulsion polymerization with PS*b*PEO polymeric stabilizer provides final polymer particles with diameters larger than the monomer droplet diameters, meaning that PS*b*PEO provided poor stabilization. Even if the polymerization process was not fully following a miniemulsion polymerization mechanism, the poor stabilization provided by PS*b*PEO can turn into an advantage because it allows the formation of larger polymer particles, as needed to favor fully armored latex particles. Finally, *in situ* miniemulsion with NMG/PS*b*PEO1030 resulted in a final particle diameter of around 300 nm and a high NMG weight percentage. Hence, the number of NMG platelets was ten times larger than the number of latex particles, which is consistent with the high number of NMG visible on the TEM images. A theoretical surface coverage of 62% was reached, that should lead to conductive properties after film-formation.

Table 14. Polymer particle diameter, monomer conversion, particle number and theoretical surface coverage for blank and in situ miniemulsion polymerizations performed using PSbPEO as stabilizer.

Experiment name	Droplets diameter (nm)	DLS		TEM	Conversion (%)	NMG (g L ⁻¹)	N _{NMG}	N _{latex}	$\tau_{coverage}$
		D _h (nm)	Poly	D _{TEM} (nm)					
mE-B/PSbPEO-7	255	460	0.4	-	100	0	0	-	-
mE-NMG/PSbPEO-7	250	300	0.3	285	50	2.2	5.4 10 ¹⁴	6 10 ¹³	62

Figure 33 shows digital photographs of the blank and of the composite latex right after polymerization and five days later.

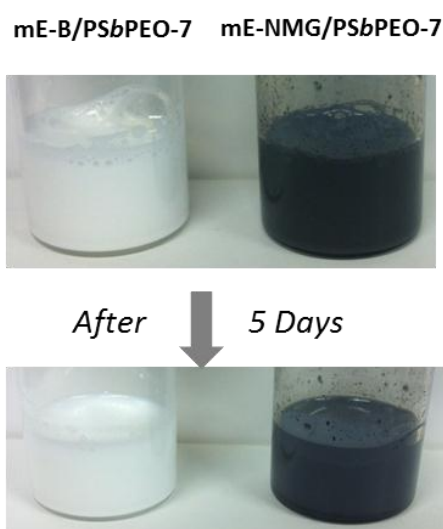


Figure 33. Pictures showing the stability of the blank latex mE-B/PSbPEO-7 and of the nanocomposite latex mE-NMG/PSbPEO-7 synthesized by miniemulsion polymerization, as a function of time.

No destabilization of the blank latex is visible on these pictures. A slight change of grey shade is observed for the composite sample but no sedimentation could be identified by the naked eye. These visual observations were confirmed by Turbiscan® measurements (Figure 34). For the blank latex, a sedimentation phenomenon is clearly visible on the left hand side of Figure 33. This sedimentation can be due to the size of the polymer particles, which will naturally form a sediment. For the composite latex, the decrease of the backscattering intensity in the bottom of the cylinder indicates the formation of a small sediment.

It is noteworthy mentioning that the stability of the composite latex obtained using PSbPEO as stabilizer is higher than that of the latexes formed with NMG/SDBS suspensions, as evidenced by the lower backscattering variations, ΔR (%), in the bottom of the cylinder. Indeed the latter reached only -5% while it reached up to - 15 % for SDBS (see Figure 30c).

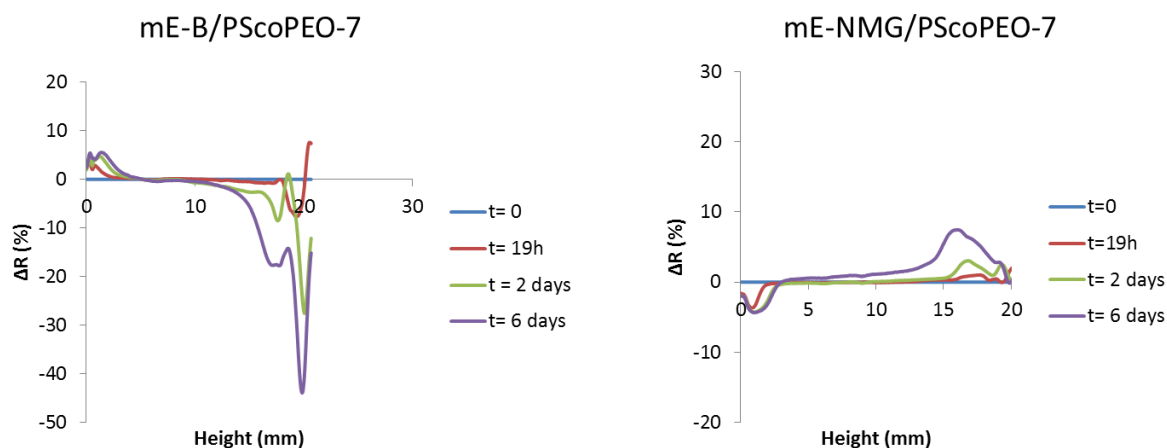


Figure 34. Turbiscan® stability analyses with time of the blank and nanocomposite latexes synthesized by *in situ* miniemulsion polymerization using PSbPEO 1030 as stabilizer.

To sum up, *in situ* miniemulsion polymerization in the presence of NMG/PSbPEO suspensions allowed forming large polymer particles, with a mean diameter of 300 nm. Unfortunately the final conversion was limited to c.a. 50% after 7 hours. The composite latex presents a better stability than the composite latex obtained with NMG/SDBS suspensions and a high theoretical surface coverage, which should give rise to conductive properties after film-formation.

5. Conclusions

To conclude, *in situ* miniemulsion polymerizations were performed in the presence of NMG suspensions stabilized by SDBS, or by PSbPEO1030 block copolymer. Compared to conventional emulsion polymerization, the advantage of the miniemulsion polymerization mechanism is to avoid destabilization of the NMG platelets during the polymerization process. The polymer particles formed in the presence of NMG/SDBS suspensions have a small diameter and the polymerization showed limiting conversions. The mE-NMG/SDBS-1.7 latex presents a high theoretical surface coverage and can induce conductive properties after film formation. As an alternative, *in situ* miniemulsion polymerization was also realized in the presence of NMG/PSbPEO suspensions. This polymeric stabilizer does not stabilize well the miniemulsion and as a consequence creates larger polymer particles. The composite latex formed presents larger polymer particles diameter, 300 nm, and a good stability but again a full conversion was not reached. The surface coverage of this nanocomposite is theoretically sufficient to obtain electrical properties. In order to solve the problem of limiting conversion, organosoluble initiators might be used as a perspective of this work.

As an alternative to emulsion and miniemulsion polymerizations, we used dispersion polymerization. Dispersion polymerization is known to produce polymer particles with rather large diameters between hundreds of nanometers to several microns. The specific experimental conditions of dispersion polymerization process are described hereafter. Then *in situ* dispersion polymerizations in the presence of NMG suspensions are presented. A careful examination of the literature shows that there is no report on *in situ* dispersion polymerization in the presence of graphene particles.

IV. Dispersion polymerization in the presence of NMG

1. Generalities on dispersion polymerization

Dispersion polymerization was first developed by Osmond *et al.* in the 1960's. This process was originally dedicated to the paint industry. The mechanism of dispersion polymerization has been studied by two main authors, Lock *et al.* and Paine *et al.* [46]. In dispersion polymerization, the monomer and the initiator are both soluble in the polymerization medium; the medium is chosen to be a poor solvent for the resulting polymer. Accordingly, the reaction mixture is homogeneous at the onset, and the polymerization is initiated in homogeneous solution. Depending on the solvency of the medium for the resulting macroradicals and macromolecules, phase separation occurs at early stage. This leads to nucleation and the formation of primary particles. Primary particles thus formed in dispersion polymerization are swollen by the polymerization medium and/or the monomer.

Dispersion polymerization requires generally four components: a solvent (for monomer but precipitating the polymer), monomers, an organosoluble initiator and a steric stabilizer. The initial medium formed by these components is homogeneous. The stabilizer is generally a graft copolymer adsorbed at the particle surface and that prevents their aggregation. The particle stabilization in dispersion polymerization is usually referred to as “steric stabilization”, as compared with ionic emulsifiers or charge stabilization in emulsion polymerization. Good stabilizers for dispersion polymerization are polymers and oligomeric compounds with a low solubility in the polymerization medium and a moderate affinity for the polymer particles. For dispersion polymerization in alcohols and other polar solvents, a wide range of polar organic polymers such as polyvinylpyrrolidone (PVP), poly (vinyl alcohol) (PVA) and cellulose derivatives, have been used [47] [48]. In many examples [49], the stabilizer is grafted onto the surface of the polymer particles *in situ* during the polymerization process.

The dispersion polymerization mechanism is detailed in Figure 35. First, the decomposition of the initiator generates primary radicals. These radicals grow in the continuous phase by the addition of monomers units until they reach a critical chain length where they precipitate to form nuclei. These nuclei or primary particles aggregate with each other and adsorb stabilizer at the same time to finally obtain stable mature particles. As long as enough mature particles are formed to capture all the oligo-radicals and nuclei, new particles will not be formed. The existing particles continue to grow by capturing nuclei and the oligo-radicals, which will either continue to polymerize inside the particles or terminate with other radicals. At the end of the polymerization, sterically stabilized particles with a mean diameter comprised between 500 nm and 20 μm , are obtained. [50]

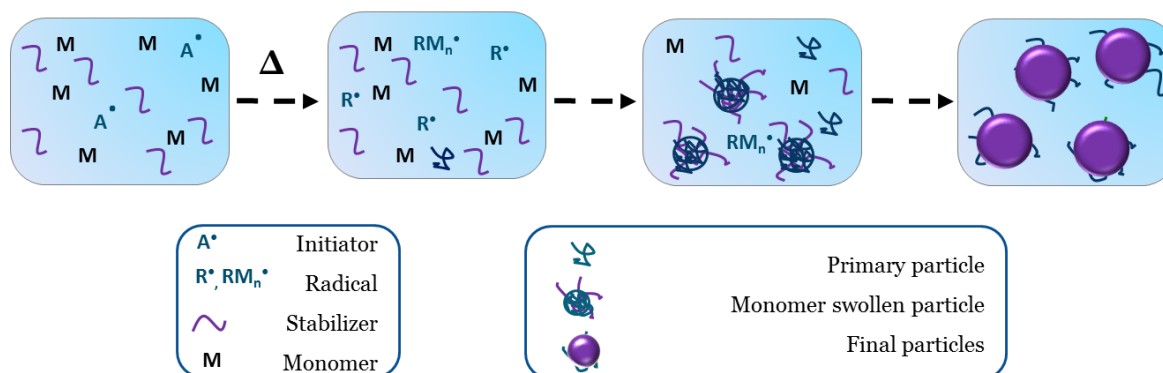


Figure 35. Scheme of the dispersion polymerization mechanism.

Dispersion polymerization in either polar or non-polar solvents has been widely studied. Polymerization in polar media usually involves alcohol/water mixtures, which allows the polymerization of various monomers in the presence of steric stabilizers such as hydroxypropyl cellulose, poly(acrylic acid), poly(vinylmethylether) or poly(vinylpyrrolidone) (PVP) [49]. Among them, PVP has been extensively reported [51]. This stabilizer allows forming polymer particles with diameters in the range 1-10 μm depending on the monomer and solvent polarity. Table 15 summarizes the range of particle diameter obtained (depending on the solvent polarity) for the three main monomers used in this thesis.

Table 15. Range of polymer particles size obtained during dispersion polymerization of styrene, butyl acrylate or a 50/50 (wt/wt) mixture of styrene and butyl acrylate using PVP as a steric stabilizer in polar media of various polarities.

Reference	Monomer	Polymer particle diameter
[46]	Styrene	1.2-7.4 μm
[52]	Butyl acrylate	0.3-9.7 μm
[53][54]	Styrene and butyl acrylate (50/50 wt/wt)	0.6-4.9 μm

Many parameters can influence the size and size distribution of latex particles synthesized by dispersion polymerization. The solvent polarity can have a strong influence on the particle diameter, size distribution, the polymerization kinetics and the molar mass of the latex particles [55]. The monomer concentration, stabilizer concentration and its molar mass can also influence the size and size distribution of the particles [46][56]. For instance, Bamnolker *et al.* showed that increasing the PVP chain length from 10,000 to 360,000 g mol^{-1} , resulted in an increase of the particle size distribution during dispersion polymerization of styrene in a 70/30 wt/wt ethanol/methoxyethanol mixture [57].

Given the large number of parameters that can influence the particle size and the size distribution in dispersion polymerization, we have conducted a preliminary study in order to determine the optimized parameters (temperature, solvent composition, stabilizer

concentration and proportion of each monomers) leading to the formation of polymer particles with a mean diameter around 1 μm . Then, using these optimized conditions, *in situ* dispersion polymerization will be performed in the presence of the NMG/PVP suspensions presented in Chapter 2. As previously described in Chapter 2, PVP allows the formation of highly concentrated NMG suspensions and is therefore a good stabilizer of multilayered graphene in water or in ethanolic solutions, as we shall discuss later.

2. Preliminary study

a. Experimental procedure

In a typical blank experiment, the stabilizer (PVPk30) is dissolved in a mixture of ethanol and water (20 g) and the solution is degassed under N_2 . In parallel, a mixture of styrene (1g), butyl acrylate (1g) and the organosoluble initiator (AIBN, 0.04 g, 2%/M) is degassed under N_2 . The two solutions are introduced in a 50 mL polymerization reactor equipped with a condenser, a nitrogen purging tube and a mechanical stirrer. The polymerization is performed at a temperature of 70°C or 80°C with a rotation speed of 200 rpm for 24 hours.

The experimental conditions of all blank emulsion polymerization experiments are summarized in Table 16. The samples were named according to the following convention with each segment of information separated by a slash or a dash. Segment 1: type of polymerization process (D for dispersion), segment 2: composition of the ethanol/water mixture, segment 3: polymerization temperature, segment 4: type of polymerization (B for blank experiment), segment 5: type of surfactant or stabilizer and segment 6: initial surfactant concentration (g L^{-1}). This nomenclature will be used only for the blank experiments.

Table 16. Experimental conditions of all blank dispersion polymerizations performed in this study using PVPk30 or PSbPEO 1030 as steric stabilizers.

Experiment name	Ethanol/water (wt/wt)	Temperature (°C)	Type of stabilizer	[Stabilizer] (g L^{-1})
D-90/10-80°C-B/PVP-10	90/10	80	PVPk30	10
D-80/20-80°C-B/PVP-10	80/20	80	PVPk30	10
D-70/30-80°C-B/PVP-10	70/30	80	PVPk30	10
D-80/20-70°C-B/PVP-10	80/20	70	PVPk30	10
D-80/20-80°C-B/PVP-15	80/20	80	PVPk30	15
D-80/20-80°C-B/PVP-25	80/20	80	PVPk30	25
D-80/20-80°C-B/PSbPEO-15	80/20	80	PSbPEO 1030	15

In the following, the influence of solvent polarity, polymerization temperature and nature and concentration of stabilizer on the polymerization kinetics and on the final polymer particle size will be successively studied. The monomer to polymer conversion was determined by gravimetric analysis whereas the particle size and particle size distribution were determined using the Mastersizer 3000 instrument from Malvern. This instrument uses the technique of

laser diffraction which is based on the principle that particles passing through a laser beam will scatter light at an angle that is directly related to their size: large particles scatter at low angles, whereas small particles scatter at high angles. The laser diffraction is accurately described by the Fraunhofer Approximation and the Mie theory, with the assumption of spherical particle morphology. The measurable size ranges from 50 nm to 1000 μm .

b. Influence of solvent composition

The nature of the solvent, and particularly its polarity, can affect the critical degree of oligomer precipitation and adsorption rate and consequently influence the particle diameter, size distribution, polymerization kinetics and molar mass of the latex particles [55]. In this section, the effect of the ethanol/water composition was studied by varying the water content from 10 to 30 wt% using the experimental conditions detailed in Table 16 ($[\text{PVPk30}]=10 \text{ g L}^{-1}$ and $T=80^\circ\text{C}$). The conversion versus time curves of Figure 35 show that the polymerization rates increases with increasing water content. The final conversion was not impacted and reached 80% independently of the solvent composition. Increasing the water content also decreased the polymer particle diameter and the particle size distribution. These effects are due to the influence of the solvent polarity on the precipitation rate of oligomers [50]. In fact, increasing the water content leads to a decrease of the length of the critical chain j_{crit} for oligomer precipitation. So, the number of nuclei formed is higher and the final particles smaller [58]. In order to obtain polymer particles with a mean diameter around $1 \mu\text{m}$ and a narrow particle size distribution, a 80/20 (wt/wt) ethanol/water mixture will be used in the following dispersion polymerization experiments.

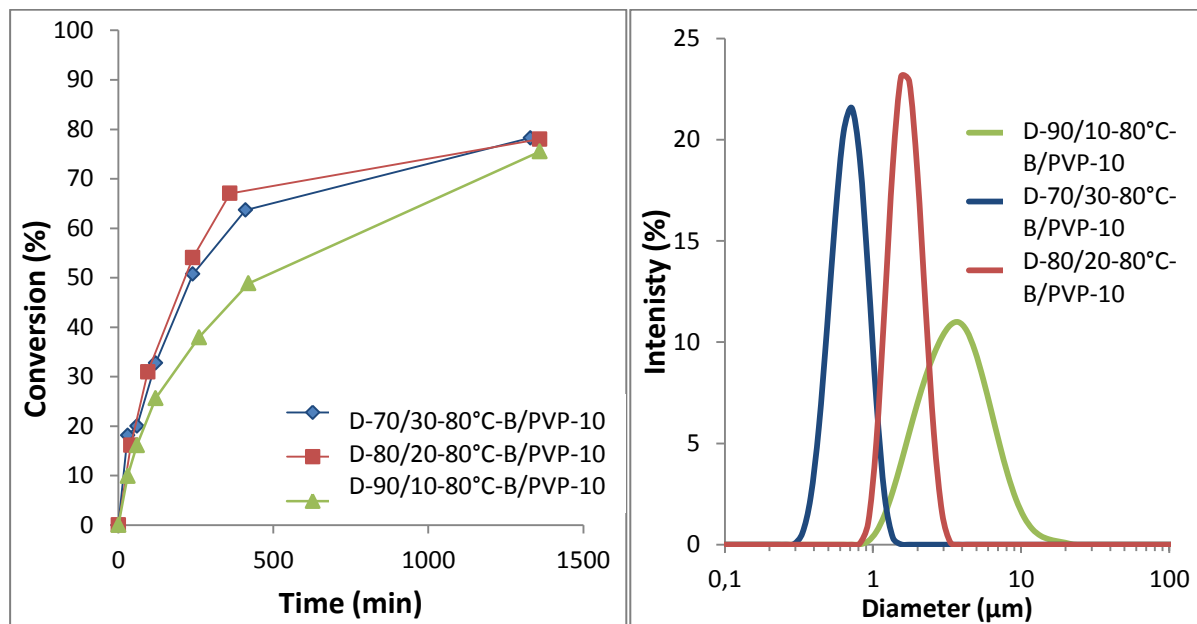


Figure 36. Effect of solvent composition on the polymerization kinetics and polymer particle diameter for blank dispersion polymerization experiments D-70/30-80°C-B/PVP-10, D-80/20-80°C-B/PVP-10 and D-90/10-80°C-B/PVP-10.

c. Influence of temperature

The temperature of polymerization affects the decomposition rate of the initiator, the propagation rate and solvent polarity. Two reaction temperatures, 70°C and 80°C , were

compared for a fixed ethanol/water composition of 80/20 (wt/wt) under otherwise the same experimental conditions as those used in the previous section. Figure 37 shows that the polymerization rate increases with increasing temperature, as expected. Indeed, increasing temperature leads to an increase of the initiator decomposition rate and to an increase of the solvency of the reaction medium. This last effect will induce an increase of the critical chain length for oligomer precipitation, and thus a decrease in the concentration of precipitated chains. As a result, the particle size increases with increasing temperature [59] as shown on the right side of Figure 37.

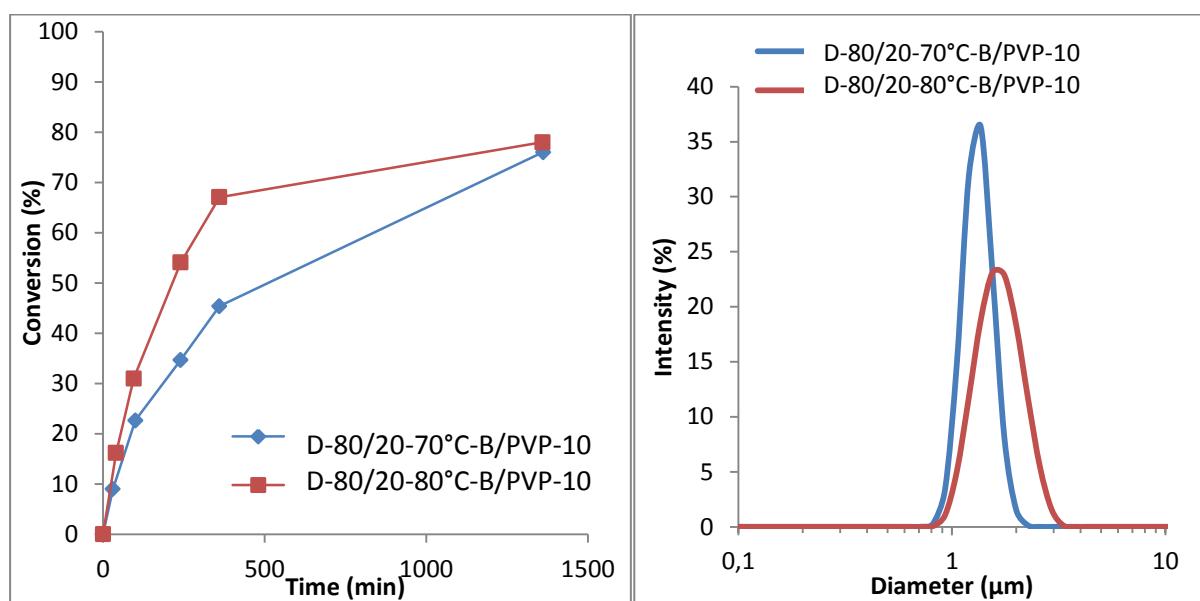


Figure 37. Effect on temperature on the polymerization kinetics and particle diameter for blank dispersion polymerization experiments D-80/20-70°C-B/PVP-10 and D-80/20-80°C-B/PVP-10.

Despite a small increase of the particle size and size distribution with increasing temperature, all following dispersion polymerization experiments will be carried out at 80°C as it allows increasing the reaction rate.

d. Influence of the stabilizer concentration

The nature of the stabilizer and its concentration can have an effect on the polymer particle diameter and the polymerization kinetics [50]. According to the literature, the effect of the stabilizer concentration on particle size is not very important. For instance, Shen *et al.* [60] reported that increasing the PVP concentration increases the viscosity of the continuous phase and the rate of PVP adsorption which should reduce aggregation and decrease particle size.

We have plotted in Figure 38 the polymerization kinetics and the final particle size of three dispersion polymerization experiments performed using three different PVPk30 concentrations under otherwise identical polymerization conditions (i.e. 80°C and ethanol/water 80/20 wt/wt). It clearly appears that there is no effect of the PVP concentration on the polymerization kinetics and the polymer particle diameter.

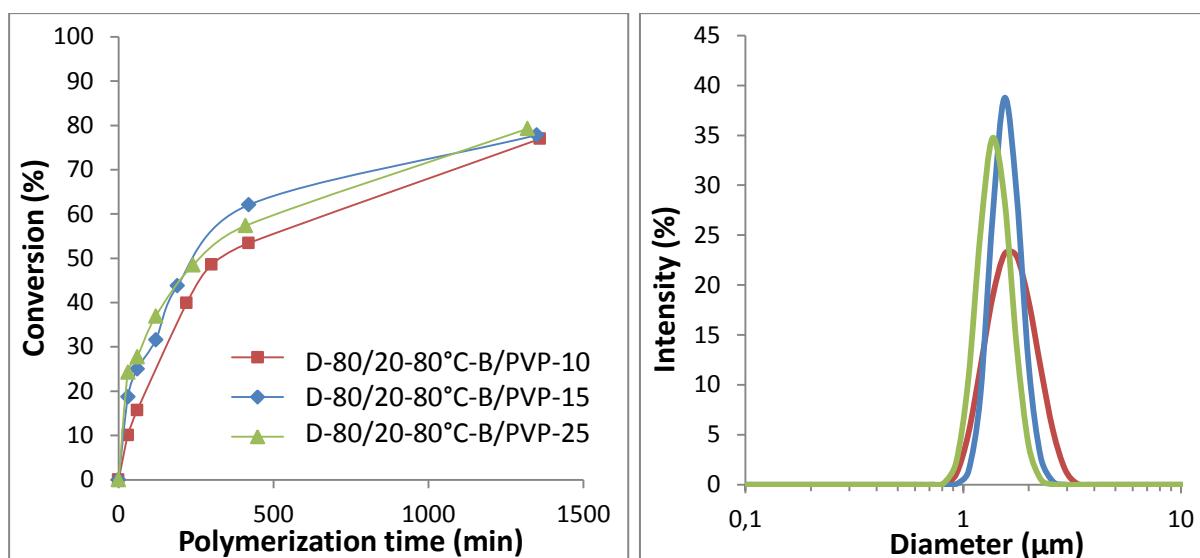


Figure 38. Effect of PVPk30 concentration on the polymerization kinetics and particle diameter for blank dispersion polymerization experiments D-80/20-80°C-B/PVP-10, D-80/20-80°C-B/PVP-15 and D-80/20-80°C-B/PVP-25.

To conclude, the PVPk30 concentration, which will vary between each NMG suspensions in further experiments, should not significantly influence the polymerization kinetics and the polymer particle size.

e. Influence of the type of stabilizer

In this section, PVPk30 was compared to PSbPEO1030 block copolymer. To do so, two dispersion polymerization experiments were carried out under exactly the same conditions, at 80°C in a 80/20 (wt/wt) ethanol/water mixture. The stabilizer concentration was fixed at 15 g L⁻¹. Figure 39 shows the polymerization kinetics and polymer particle diameter for both experiments.

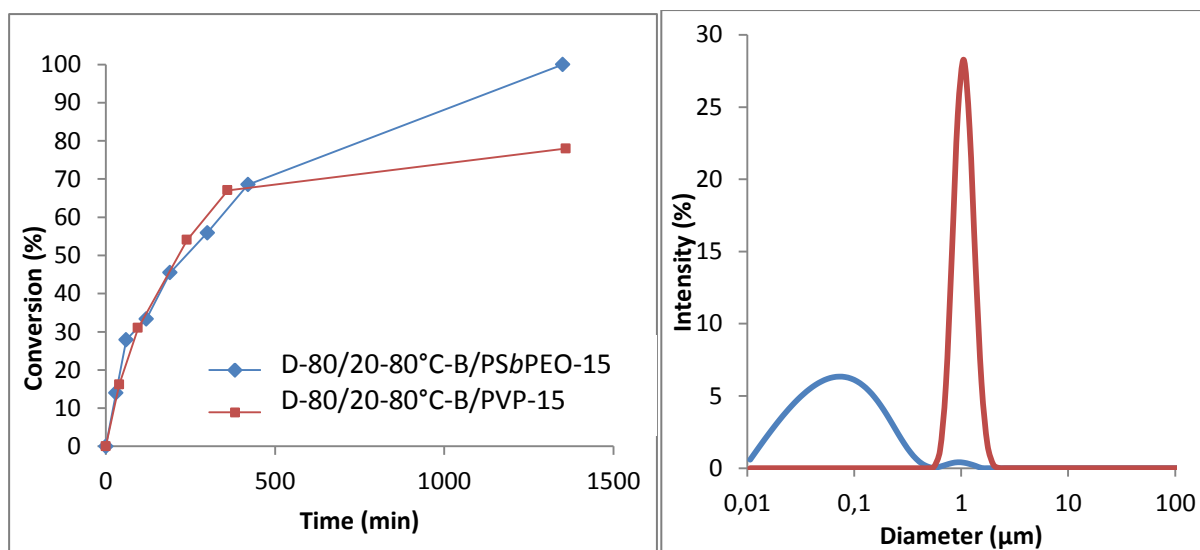


Figure 39. Effect of the nature of the stabilizer on the polymerization kinetics and particle diameter for blank dispersion polymerization experiments D-80/20-80°C-B/PSbPEO-15 and D-80-80°C-B/PVP-15.

While there is almost no effect of the nature of the stabilizer on the polymerization kinetics, the PS*b*PEO1030 block copolymer gives much smaller polymer particle sizes than PVPk30 under the same conditions. The final particle diameter (i.e. around 100 nm) is in agreement with the literature [61].

In conclusion, based on this preliminary study, a 80/20 (wt/wt) ethanol/water mixture and a polymerization temperature of 80°C will be used in the further experiments in order to obtain polymer particles with a mean diameter around 1 µm. Moreover, it was demonstrated that the stabilizer concentration should not influence the polymer particle diameter and that the PS*b*PEO block copolymer is not adapted to form large latex particles under dispersion polymerization conditions.

3. NMG suspensions stabilized by PVPk30

a. Experimental procedure

Two NMG/PVPk30 suspensions with different PVPk30 concentrations (NMG/PVPk30-5 and NMG/PVPk30-10) have been prepared by mechanical delamination in water (see chapter 2) and will be used for *in situ* dispersion polymerization in this section. As the solvent of these suspensions was water, a solvent exchange must be performed first in order to disperse the NMG platelets in a mixture of ethanol and water before *in situ* dispersion polymerization. To do so, the suspensions were introduced in a dialysis tubing which was immersed in a large volume of ethanol (95 vol%). The solvent was changed every day until the volume of the suspension inside the dialysis tube remained constant. The final ethanol/water composition was adjusted to 80/20 (wt/wt) by adding the required amount of water.

This solvent exchange induced an increase of the concentration of the NMG/PVPk30 suspensions but more interestingly, there were no destabilization of the NMG platelets when water was replaced by ethanol/water 80/20 (wt/wt) indicating that PVPk30 is an efficient stabilizer of NMG suspensions in hydro-alcoholic media. The PVPk30 and NMG concentrations before and after solvent exchange, determined by elemental analysis, are reported in Table 17 for both NMG/PVP suspensions.

Table 17. NMG and PVPk30 concentrations of the NMG-PVPk30 suspensions before and after solvent exchange from water to ethanol, as determined by elemental analysis.

NMG suspensions		[PVPk30] (g L ⁻¹)	[NMG] (g L ⁻¹)
Before solvent exchange	NMG-PVPk30-5	2.2	2.3
	NMG-PVPk30-10	4.5	1.3
After solvent exchange	NMG-PVPk30-5	6	9.6
	NMG-PVPk30-10	15.8	4.7

In situ dispersion polymerizations were then carried out using the hydro-alcoholic NMG/PVPk30-5 and NMG/PVPk30-10 suspensions.

In a typical *in situ* dispersion polymerization experiment, 20g of the ethanol/water (80/20 wt/wt) NMG/PVP suspension (NMG/PVPk30-5 or NMG/PVPk30-10) are degased under N₂ for 30 minutes. In parallel, 2 g of a mixture of styrene and butyl acrylate monomers (50/50%wt) and 0.04g of initiator (AIBN, 2wt%/M) are degased under N₂. The monomer solution is added to the NMG suspension and the mixture is introduced in a 50 mL polymerization reactor rotating at 200 rpm. The polymerization starts when the temperature reaches 80°C. Table 18 summarizes the polymerization conditions for these syntheses.

Each polymerization sample was named according to the convention defined in section II.2 with an additional segment indicating the composition of the monomer mixture (Sty/BA 40/60 or 50/50).

Table 18. Experimental conditions for *in situ* dispersion polymerizations with NMG/PVPk30 suspensions. Ethanol/water=80/20 (wt/wt) and T=80°C

Experiment name	NMG suspension	[NMG] (g L ⁻¹)	[PVPk30] (g L ⁻¹)	Sty/BA (wt/wt)
D-NMG/PVPk30-1.2-50/50	NMG/PVPk30-5	2.6	1.2	50/50
D-NMG/PVPk30-1.7-50/50	NMG/PVPk30-5	3.3	1.7	50/50
D-NMG/PVPk30-9-50/50	NMG/PVPk30-10	3.6	9	50/50
D-NMG/PVPk30-22-50/50	NMG/PVPk30-10	3.2	22	50/50
D-NMG/PVPk30-7.5-40/60	NMG/PVPk30-10	3	7.5	40/60

In the following, we studied the influence of the NMG and stabilizer concentration and the monomer composition on the conversion, the polymer particle diameter and the polymerization kinetics. At the end of the polymerization, the nanocomposite latexes were characterized using the same techniques as before. Cryo-SEM was used in addition to the other techniques in order to characterize the morphology of the composite particles.

b. Influence of NMG concentration

We first compared two experiments performed using similar PVPk30 concentrations and slightly different NMG contents (D-NMG/PVPk30-1.2-50/50 and D-NMG/PVPk30-1.7-50/50 in Table 18).

As shown on Figure 40, increasing the NMG weight percentage induces an increase of the polymerization rate and final conversion. For D-NMG/PVPk30-1.7-50/50, two families of particle sizes are clearly visible on the particle size curves, one centered around 3.3 μm and another around 22 μm. For D-NMG/PVPk30-1.2-50/50, three populations of particles are identified at 0.85 μm, 4.3 μm and 25.6 μm, respectively.

In dispersion polymerization, a large particle size distribution is indicative of a long nucleation period. The stabilizer plays an important role during nucleation and controls both the particle number and stability. Stabilization is ensured by *in situ* formation of graft copolymers (via chain transfer reactions), which are the true stabilizer of the system. In the

present study, chain transfer to PVP may not be as efficient as in the blank experiments. Indeed, adsorbed PVP chains located at the NMG surface may be less accessible to radicals than free PVP, which would decrease the effective amount of stabilizer formed. In addition, the formed stabilizer is immobilized on the NMG platelets, which may decrease the anchoring adsorption rate of the resulting PVP/NMG complex on the nucleated particles, and thus increase both particle size and size distribution. The formation of the small population of particles can also be interpreted by a secondary nucleation mechanism promoted by the formation of the very large particles that cannot ensure efficient capture of primary nucleated particles.

The increase of final conversion and polymerization rate with increasing NMG content seems to contradict previous observations. Indeed, the increase of NMG platelets induced a decrease of the polymerization rate and conversion in the previous emulsion or miniemulsion polymerization experiments. This illustrates the high complexity of the reaction mechanism in the presence of NMG, and further investigations would be necessary to explain these unexpected results.

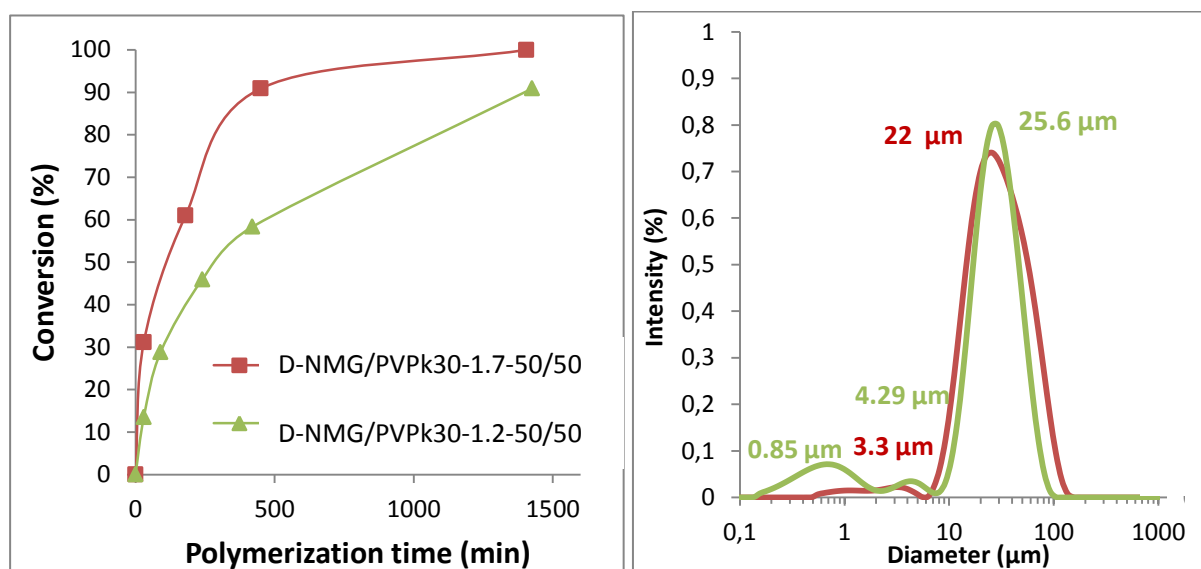


Figure 40. Polymerization kinetics and particle diameter for the nanocomposite latexes D-NMG/PVPk30-1.2-50/50 and D-NMG/PVPk30-1.7-50/50

In order to visualize the presence of NMG platelets around the polymer particles, we performed cryo-SEM analysis. This characterization technique is more adequate than classical SEM to observe low glass transition temperature nanocomposites. In a typical analysis, the nanocomposite latex is first frozen in a metallic preform in nitrogen. This preform containing the sample is inserted in the cryo-chamber of the SEM. Prior to the observation a clean cross sectional fracture of the frozen sample is made *in situ* using a manipulator holding a razor blade. A constraint is to minimize the presence of ice on the sample. Figure 40 represents the pictures of the two nanocomposite latexes D-NMG/PVPk30-1.2-50/50 and D-NMG/PVPk30-1.7-50/50 imaged by this technique.

Each picture shows a latex particle of around 10 μm diameter surrounded with a heterogeneous background that can be attributed to ice or frozen ethanol. The latex particle exhibits a rough surface. This texture can be attributed to NMG platelets covering the particle surface. As a comparison, cryo-SEM image of a blank latex particle is shown in Figure 43: the particle surface shows no texture.

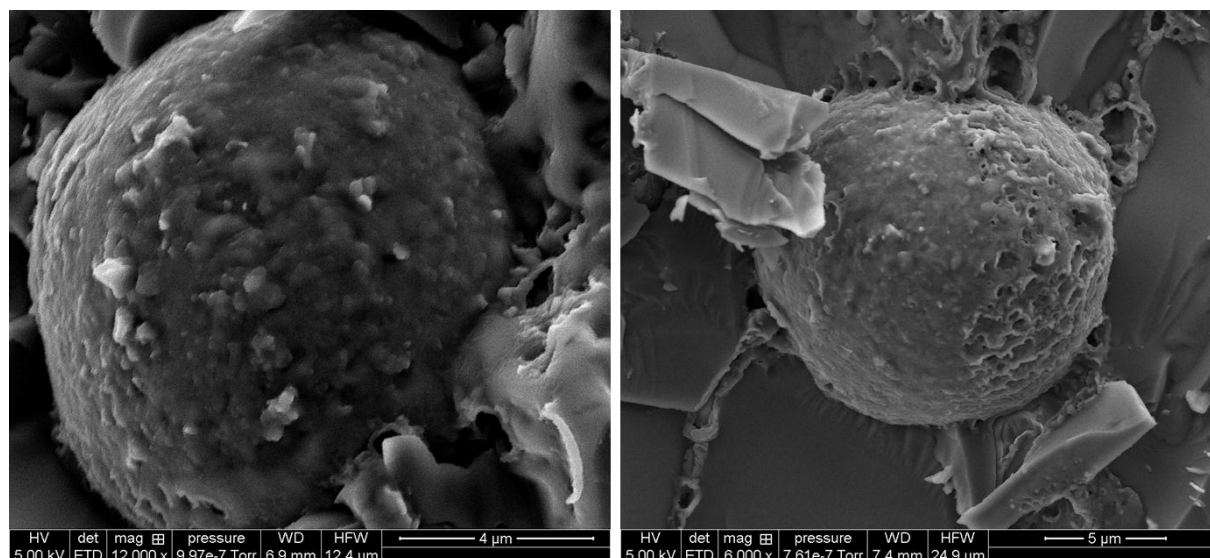


Figure 41. Cryo-SEM pictures of the nanocomposite latexes D-NMG/PVPk30-1.2-50/50 and D-NMG/PVPk30-1.7-50/50.

Table 19 summarizes the characterizations of the two nanocomposites formed after polymerization including the number of NMG and polymer particles and the theoretical surface coverage. To calculate the number of polymer particles, we used 4.3 μm and 3.3 μm , as particle diameters, respectively. These large polymer particle sizes led to a theoretical surface coverage of more than 100% for both polymerizations. In consequence, both of the nanocomposites should possess electrical properties after film formation.

Table 19. Polymer particle diameter, monomer conversion, particle number and theoretical surface coverage for in situ dispersion polymerizations performed using PVPk30 as stabilizer and different amounts of NMG.

Experiment name	DLS	Conversion (%)	NMG (g L^{-1})	N_{NMG}	N_{latex}	τ_{coverage}
	D_h (nm)					
D-NMG /PVPk30-1.2-50/50	0.85-4.3-25.6	90	2.6	$3.9 \cdot 10^{13}$	$3.7 \cdot 10^{10}$	291
D-NMG /PVPk30-1.7-50/50	3.3-22	100	3.3	$4.9 \cdot 10^{13}$	$9.0 \cdot 10^{10}$	255

The influence of the stabilizer concentration is investigated in the following paragraph.

c. Influence of stabilizer concentration

The influence of stabilizer concentration was described as negligible for blank polymerizations. However the amount of stabilizer used in the previous experiments was very low, which encouraged us to study the effect of stabilizer concentration with the aim to decrease particle size. A series of *in situ* dispersion polymerizations with similar NMG contents but different stabilizer concentrations were thus carried out using the hydro-alcoholic NMG/PVPk30-5 and NMG/PVPk30-10 suspensions (see Table 17) in which the required amount of PVPk30 was introduced prior to polymerization.

The polymerization kinetics and the polymer particles diameters are presented in Figure 42.

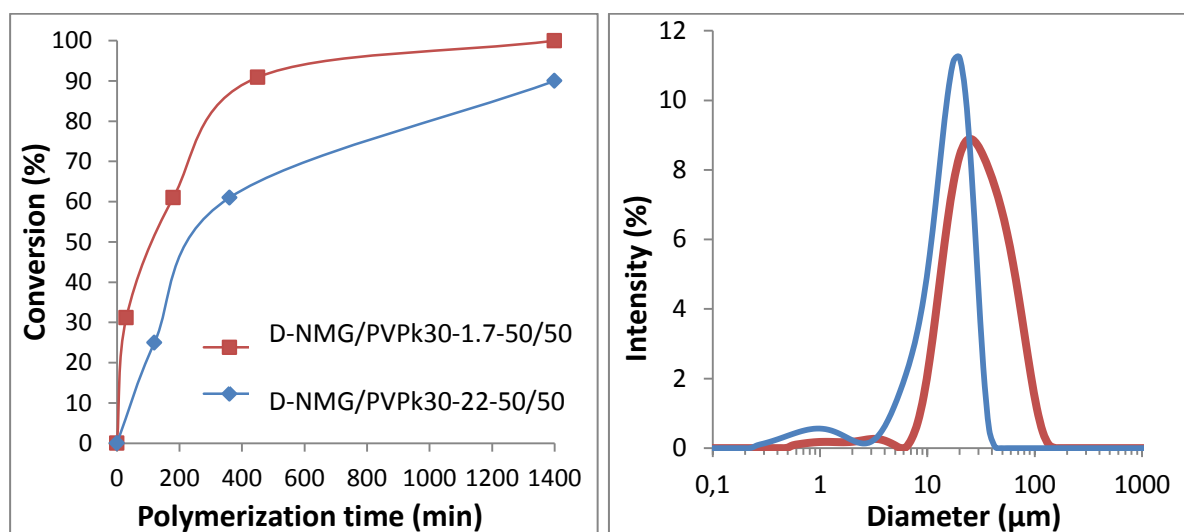


Figure 42. Polymerization kinetics and particle diameter for the nanocomposite latexes D-NMG/PVPk30-1.7-50/50 and D-NMG/PVPk30-22-50/50.

Figure 42 shows that the polymerization rate and total conversion decreases with increasing the stabilizer concentration. Increasing the PVPk30 concentration also leads to a small decrease of the latex diameter. This result is different from the blank experiments in section IV.2.d, and supports the assumption that the stabilization efficiency of PVPk30 is strongly influenced by the presence of NMG.

Cryo-SEM analysis of sample D-NMG/PVPk30-22-50/50 is shown in Figure 43b and compared to the cryo-SEM picture of a blank experiment, D-80/20-80°C-B/PVP-25 (Figure 43a). Compared to the image of the blank latex, the cryo-SEM pictures of sample D-NMG/PVPk30-22-50/50 show NMG platelets around the polymer particles.

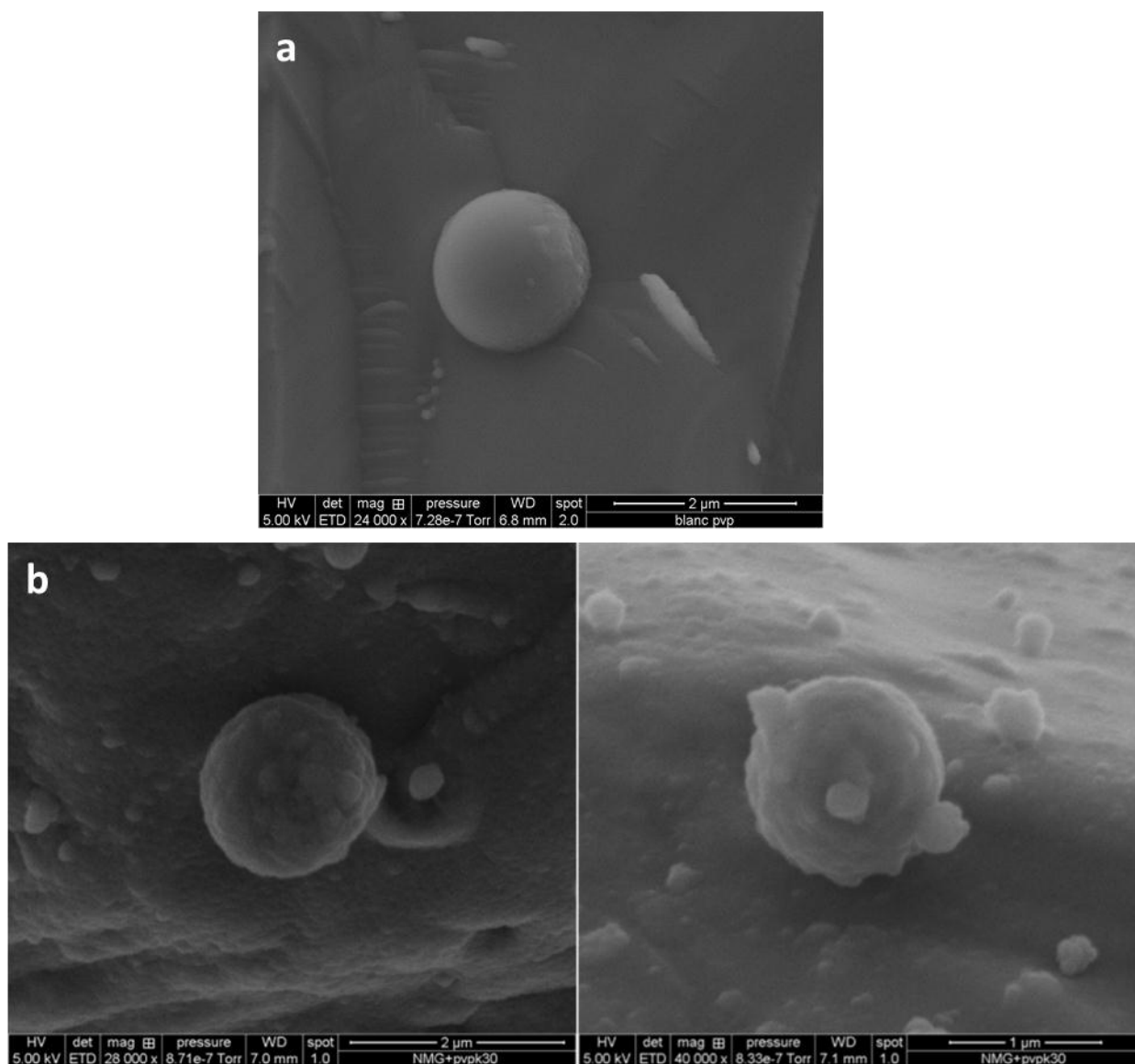


Figure 43. Cryo-SEM pictures of a) the blank experiment D-80/20-80°C-B/PVP-25, and b) the nanocomposite latex D-NMG/PVPk30-22-50/50.

To complete this study, the mean polymer particle diameter, the conversion and the number of NMG and polymer particles are summarized in Table 20. The theoretical surface coverage was also calculated. The number of polymer particles of the nanocomposite latex D-NMG/PVPk30-22-50/50 was calculated by taking 1.05 μm as particle diameter. The theoretical surface coverage is still higher than 100% despite the small decrease of particles size.

The high surface coverage obtained for both syntheses should induce electrical conductivities of the nanocomposites after film formation.

Table 20. Polymer particle diameter, monomer conversion, particle number and theoretical surface coverage for in situ dispersion polymerizations performed using increasing amounts of PVPk30.

Experiment name	DLS	Conversion (%)	NMG (g L ⁻¹)	N _{NMG}	N _{latex}	$\tau_{coverage}$
	D _h (nm)					
D-NMG /PVPk30-1.7-50/50	3.3-22	100	3.3	4.9 10 ¹³	9.0 10 ¹⁰	255
D-NMG /PVPk30-22-50/50	1.05-19	80	3.2	1.8 10 ¹⁴	2.2 10 ¹²	157

The nanocomposite latexes formed in this part, D-NMG/PVPk30-1.2-50/50, D-NMG/PVPk30-1.7-50/50 and D-NMG/PVPk30-22-50/50, were also visually inspected to study their stability as a function of time (Figure 44). They are all darker than the nanocomposite latexes previously synthesized by *in situ* emulsion or miniemulsion polymerization. No destabilization is visible on the pictures. However, a closer look at the suspension by gently shaking the vials to observe the bottom of the tubes, reveals the presence of a sediment for each sample in the bottom of the cylinder which is due to natural sedimentation of the large polymer beads. After a simple agitation, the polymer particles can be re-dispersed in the solvent.

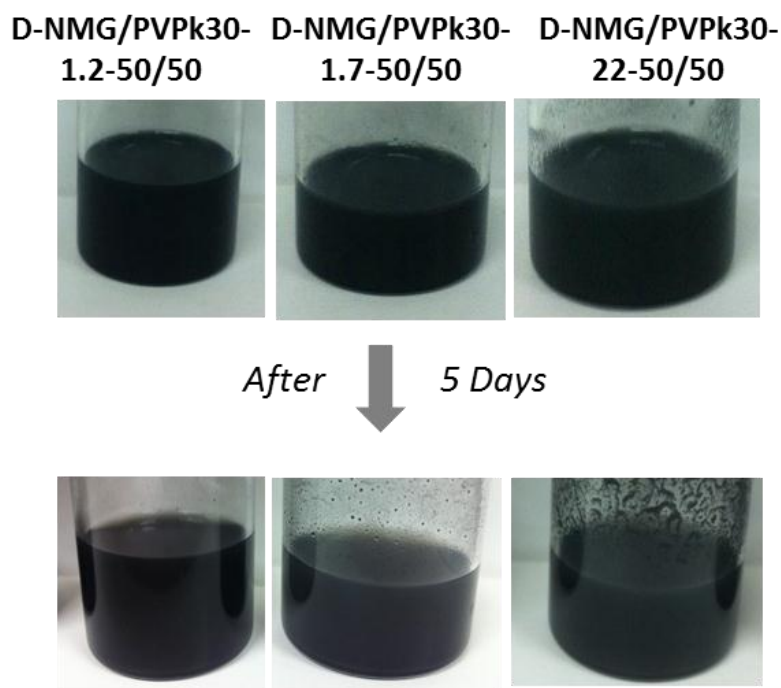


Figure 44. Pictures showing the stability of the nanocomposite latexes D-NMG/PVPk30-1.2-50/50, D-NMG/PVPk30-1.7-50/50 and D-NMG/PVPk30-22-50/50, with time.

To complete these stability measurements, we also performed Turbiscan® analysis. The results are presented in Figure 45.

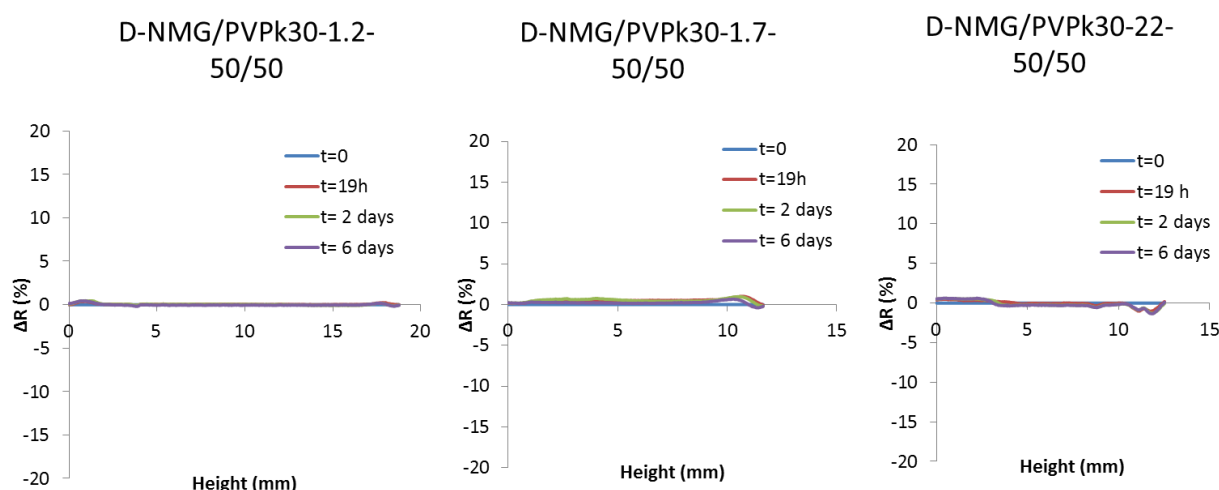


Figure 45. Turbiscan® stability analysis of the nanocomposite latexes D-NMG/PVPk30-1.2-50/50, D-NMG/PVPk30-1.7-50/50 and D-NMG/PVPk30-22-50/50, with time.

No sedimentation of the samples is visible on Turbiscan measurements. Given their high theoretical surface coverage, all the polymer particles are covered by NMG platelets and consequently, all the samples display the same backscattering adsorption. Therefore, their sedimentation is not visible on the Turbiscan measurements and cannot be quantified.

d. Influence of the comonomer composition

The impact of the proportion of each monomers has been studied. In fact, the proportion of each monomer will influence the composition of the copolymer chains, and hence the final glass transition temperature of the nanocomposite. For our application, a T_g around room temperature is needed and is achieved for a 50/50 (wt/wt) Sty/BA composition in the case of submicronic polymer particles. However, in dispersion polymerization, the latex particles are much larger. Such polymer particles with a large diameter are hard to deform. Consequently their T_g needs to be decreased, compared to smaller particles, to allow film formation.

In the subsequent experiments, the proportion of BA was increased to 60%wt to reduce the glass transition temperature of the copolymer. *In situ* dispersion polymerization was performed under otherwise exactly the same polymerization conditions as in section IV.3.a.

The effect of the comonomer composition on the diameter and particle size distributions of the nanocomposite latex particles is shown in Figure 46. D-NMG/PVPk30-9-50/50 and D-NMG/PVPk30-7.5-40/60 contain approximately the same amounts of stabilizer and NMG but have different BA contents. Increasing the proportion of BA induces an increase of the mean polymer particle diameter. This result is in agreement with literature and can be reasonably attributed to an increase of the solvent polarity when changing the comonomer composition, leading to the formation of larger particles.

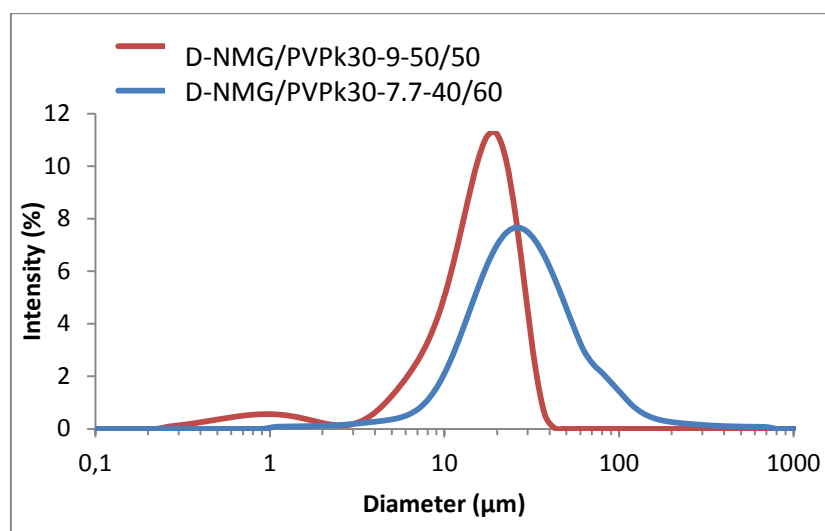


Figure 46. Particle diameters for the nanocomposite latexes D-NMG/PVPk30-9-50/50 and D-NMG/PVPk30-7.5-40/60.

TEM and cryo-SEM are presented in Figure 49 and Figure 50. Due to the low glass transition temperature of the nanocomposite D-NMG/PVPk30-7.5-40/60, TEM could not be performed in this case.

Figure 47 compare the TEM image of the blank experiment, D-80/20-80°C-B/PVP-10 (Figure 47a) with that of the nanocomposite latex D-NMG/PVPk30-9-50/50 (Figure 47b). The polymer particles of the nanocomposite latex seem covered of NMG platelets.

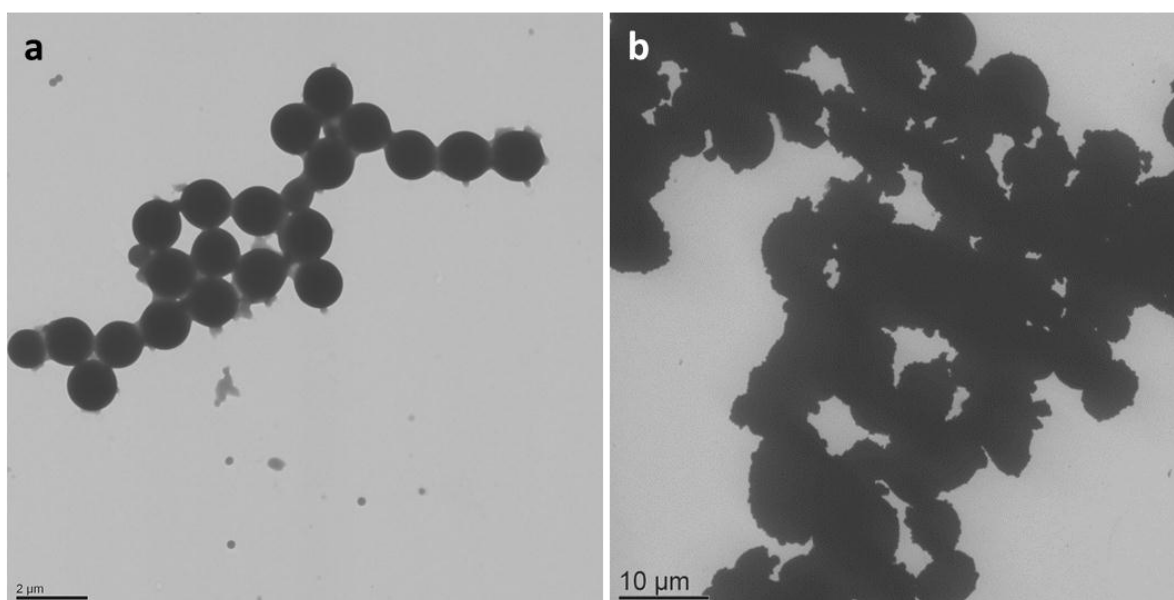


Figure 47. TEM picture of a) the blank experiment D-80/20-80°C-B/PVP-10 and b) the nanocomposite latex D-NMG/PVPk30-9-50/50.

Figure 48 shows cryo-SEM pictures of the nanocomposite latexes D-NMG/PVPk30-9-50/50 and D-NMG/PVPk30-7.5-40/60 after a transversal cut (with the razor blade) of the frozen samples.

For the D-NMG/PVPk30-9-50/50 sample, the NMG platelets are arranged all around the latex beads and the polymer particle distribution seems large. Regarding the nanocomposite latex D-NMG/PVPk30-7.5-40/60, which has a lower T_g , the polymer particles appear deformed. The larger latex particles seem to be surrounded by smaller polymer particles. For both nanocomposites, NMG platelets are clearly visible around the latex particles.

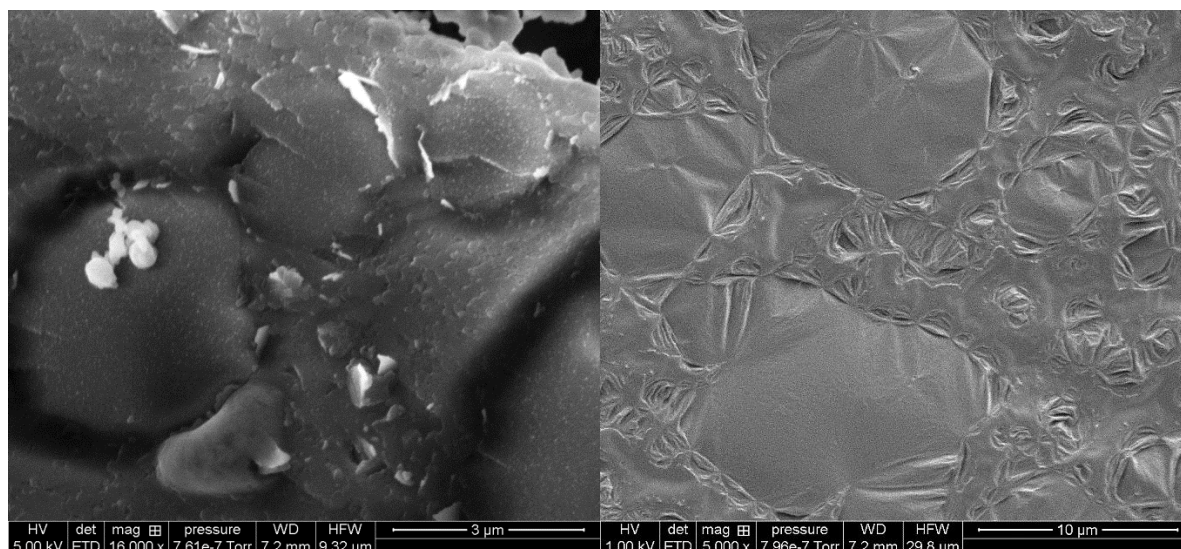


Figure 48. Cryo-SEM pictures of the nanocomposite latexes D-NMG/PVPk30-9-50/50 and D-NMG/PVPk30-7.5-40/60.

The main characteristics of the nanocomposite latexes D-NMG/PVPk30-9-50/50 and D-NMG/PVPk30-7.5-40/60 are summarized in Table 21. The number of polymer particles was calculated considering the smallest particles of 0.92 μm and 2.5 μm respectively.

Table 21. Effect of comonomer composition on the polymer particle diameter, monomer conversion, particle number and theoretical surface coverage of composite latex particles obtained by in situ dispersion polymerization using PVPk30 as stabilizer.

Experiment name	DLS	Conversion (%)	NMG (wt%)	N_{NMG}	N_{latex}	τ_{coverage}
	D_h (nm)					
D-NMG/PVPk30-9-50/50	0.92-19	80	3.6	$2.0 \cdot 10^{14}$	$3.3 \cdot 10^{12}$	155
D-NMG/PVPk30-7.5-40/60	2.5-25	80	3	$1.7 \cdot 10^{14}$	$1.6 \cdot 10^{11}$	351

As already mentioned, the comonomer composition has an influence on the mean polymer particle diameter, which increases with increasing BA content. Both nanocomposite latexes have a high theoretical surface coverage, and should therefore lead to conductive nanocomposites after film formation.

4. Conclusions

To conclude, a series of *in situ* dispersion polymerization experiments have been carried out using NMG/PVPk30 suspensions of varying PVP concentrations. These NMG suspensions were obtained by solvent exchange of the NMG/PVP water dispersions prepared by mechanical delamination. This solvent exchange resulted in a significant increase of both the NMG and PVPk30 concentrations in the suspension. This high NMG content allowed synthesizing nanocomposite latexes with higher NMG weight percentages compared to *in situ* emulsion or miniemulsion polymerizations. For all the nanocomposite latex, the theoretical surface coverage, $t_{coverage}$, exceeds 100 % due to the high polymer particle diameter and the high NMG content: conductive nanocomposites should be obtained after film formation.

In order to establish whether covalent bonds have been created between the NMG platelets and the polymer during *in situ* polymerization, a solubility test was carried out. The film obtained by *in situ* dispersion polymerization in the presence of NMG (D-NMG/PVPk30-9-50/50, 3.6 %vol. NMG) was immersed in THF and its behaviour was compared to that of the nanocomposite film prepared by physical blending of NMG platelets and 650 nm diameter latex particles (D650-WG/S-2, 2 %vol. NMG) (Figure 49). The poly(Sty-co-BA)/NMG blend is fully soluble in THF, indicating that there is no covalent bonding between NMG and the polymer particles. The film is indeed totally destroyed after one day under agitation. In contrast, the film obtained from the nanocomposite latex made by *in situ* dispersion polymerization is not completely soluble in THF, suggesting the existence of covalent bonds (or strong physical interactions) between the NMG platelets and the polymer particles. The solvent resistance of the nanocomposite film made by *in situ* polymerization is a clear benefit for textile applications.

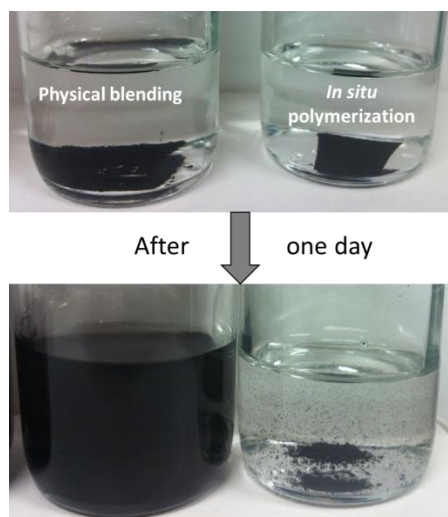


Figure 49. Solubility tests in THF of films made through physical blending (D650-WG/S-2) and *in situ* dispersion polymerization (D-NMG/PVPk30-9-50/50).

V. Electrical properties of the nanocomposites synthesized by *in situ* polymerization

Various NMG/polymer nanocomposite latexes with different particle diameters have been synthesized in this chapter. As the aim was to form conductive suspensions, the electrical properties of these nanocomposites were tested in this section. Each nanocomposite was film-formed in a silicon mold at 40°C during a night. The films were then washed in a water bath during 24h to remove the surfactant or stabilizer present on the surface of the film. Electrical measurements were performed on both sides of each films and the electrical conductivity, σ , (in $S m^{-1}$) was calculated using equations 5 and 6 of Annexe I. Table 22 summarizes the electrical conductivities obtained. Only the electrically conductive films are presented.

For *in situ* emulsion and miniemulsion polymerization, the only conductive films are those made with the NMG/SDBS-5-U.C suspension. The nanocomposites synthesized with PSbPEO 1030 are not conducting despite their high theoretical surface coverage. This polymeric stabilizer, which is insulating might inhibit the electrical conductivity of these films.

The exact weight and volume percentages of NMG in the nanocomposite films were determined by TGA. In fact, knowing the NMG weight percentage and the thermal decomposition profiles of the physical blends (TGA curves shown in Chapter 3) it is easy to determine the weight percentage of the *in situ* nanocomposite films by a simple proportional calculation.

Table 22. Electrical conductivity as a function of the volume percentage of NMG for the different nanocomposites produced by *in situ* polymerization in the presence of NMG suspensions.

<i>In situ</i> polymerization process	Experiment name	Electrical conductivity ($S m^{-1}$)	NMG (vol%)
Emulsion	E-NMG/SDBS U.C	$6.6 \cdot 10^{-6}$	1.2
Miniemulsion	mE-NMG/SDBS U.C	$1.1 \cdot 10^{-4}$	2.1
Dispersion	D-NMG/PVPk30-9-50/50	$1.6 \cdot 10^{-5}$	2
	D-NMG/PVPk30-0.1-50/50	$1.6 \cdot 10^{-4}$	0.3
	D-NMG/PVPk30-22-50/50	$2.9 \cdot 10^{-5}$	1.7
	D-NMG/PVPk30-7.5-60/40	$8 \cdot 10^{-3}$	1.5
	D-NMG/PVPk30-1.7-50/50	$6 \cdot 10^{-3}$	1.8
	D-NMG/PVPk30-1.2-50/50	$1 \cdot 10^{-4}$	1.4

The nanocomposite latex D/NMG/PVPk30-0.1-50/50 was not presented before due to its low NMG percentage and low stability. It was however film-formed and its electrical conductivity was measured.

Figure 50 represents the electrical conductivities of the nanocomposites synthesized through *in situ* emulsion and miniemulsion polymerization, in function of the NMG volume fraction. A theoretical model (3D electrical percolation model) for both polymer particle diameters was calculated and introduced in the Figure.

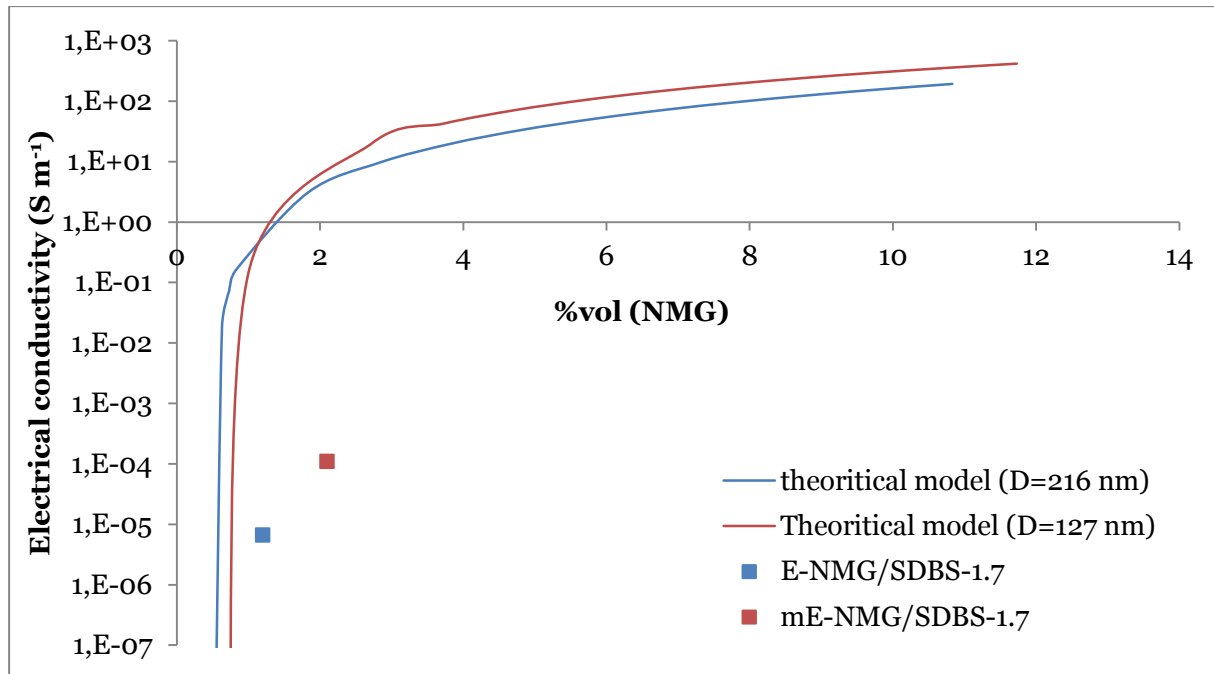


Figure 50. Electrical conductivity of the nanocomposites formed by *in situ* emulsion and miniemulsion polymerizations and comparison with the theoretical model

Both electrical conductivities measured are below the values of conductivities for the theoretical model. This discrepancy between the experimental and theoretical values can be due to the large size distribution of the polymer particles.

Electrical conductivities for the nanocomposites realized by *in situ* dispersion polymerization are represented on Figure 51.

Electrical conductivities are again lower than theoretical models for physical blends with polymer particles of 1 μm or more than 20 μm in diameter, respectively. But, as mentioned above, the large polymer particle size distribution can affect the values of electrical conductivities.

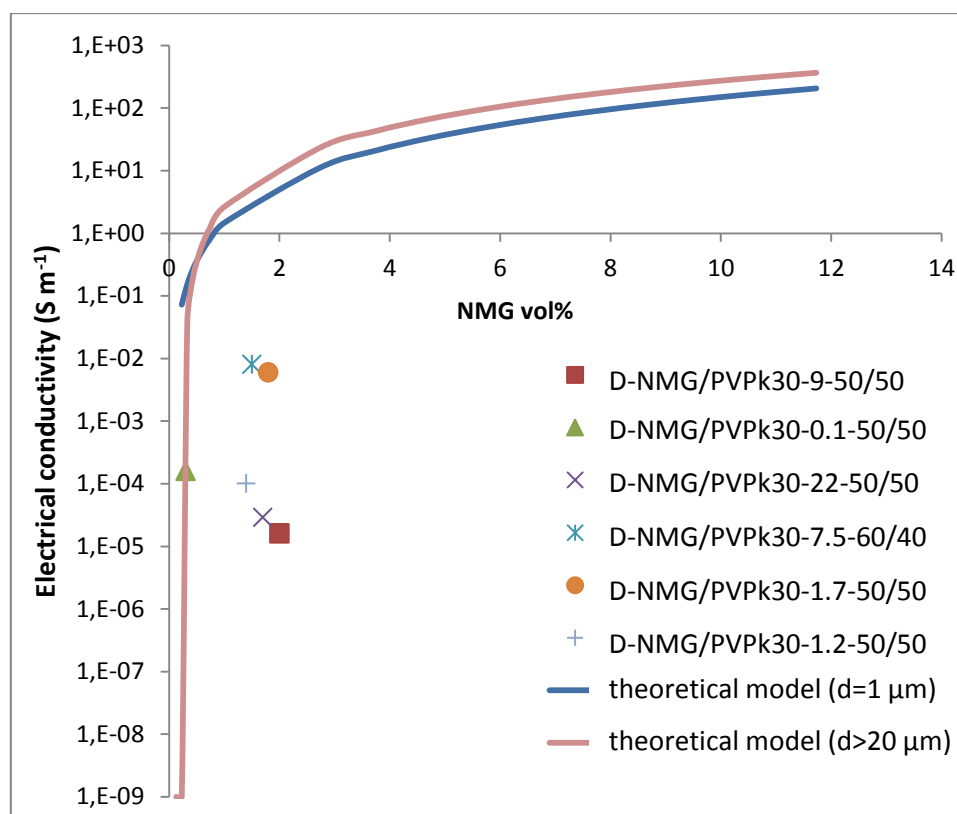


Figure 51. Electrical conductivity of the nanocomposites formed by *in situ* dispersion polymerization.

Conclusions

In this chapter, NMG-based conductive nanocomposite suspensions were synthesized by *in situ* emulsion, miniemulsion and dispersion polymerizations.

Firstly, *in situ* emulsion polymerization was realized with NMG/SDBS suspensions. Decreasing the surfactant concentration induced an increase of the latex diameter. However, it also induced a destabilization of the NMG platelets during the polymerization. This phenomenon is likely due to the high mobility of SDBS. A small decrease of SDBS concentration, just below the CMC_{app} , allowed forming NMG-armored polymer latex particles with a diameter of 200 nm without destabilization of the NMG platelets during the polymerization.

Then, two polymeric stabilizers were investigated PSSNa and PS*b*PEO1030, respectively. Increasing the molar mass of the stabilizer reduced their molecular mobility, which increased the stability of NMG during polymerization. *In situ* emulsion polymerization with NMG/PSSNa led to the formation of stable nanocomposite latexes. No sedimentation was noticeable on the Turbiscan® analysis but the NMG concentration was too low to obtain conductive films. The NMG/PS*b*PEO1030 suspensions were more concentrated in NMG platelets and stable polymer latex particles with 200 nm diameter were successfully obtained in this case. But unfortunately, for obscure reasons, the monomer conversion was limited to only 50% and did not increase with increasing initiator concentration.

To increase the mean polymer particle diameter without NMG destabilization during polymerization, *in situ* miniemulsion polymerizations were performed with NMG/SDBS and NMG/PS*b*PEO1030 suspensions. Latex particles with a mean diameter of 127 nm and 250 nm were obtained for mE-NMG/SDBS-1.7 and mE-NMG/PS*b*PEO-7, respectively with however limiting conversions. Limiting conversions might be due to the trapping of part of radicals by surface oxygen-groups on the NMG platelets. Among all the latex synthesized, only two were electrically conductive (E-2%-NMG/SDBS-1.7 and mE-NMG/SDBS-1.7). Even if their conductivity is lower than the theoretical model, these two nanocomposite latexes are stable in suspension.

As an alternative to emulsion and miniemulsion polymerizations, *in situ* dispersion polymerization using PVPk30 as stabilizer was performed to decrease the number of latex particles, and increase consequently the particle diameter and theoretical surface coverage. Composite latexes with very large particle diameters were indeed obtained in this case. However the particle size distribution was very broad. The large increase in particle size compared to the blank experiment and the broadening of the particle size distribution both indicate that the nucleation was strongly perturbed by the presence of NMG. Increasing the PVPk30 concentrations allowed decreasing the particle size but not in a too significant manner. In both cases, the latex surface coverage was much higher than 100 %.

Electrical conductivity measurements showed that the nanocomposite latex D-NMG/PVPk30-9-50/50, which has smaller polymer particles size but a high NMG content, is the best of the series. The other nanocomposites also present reasonable electrical conductivities. However, these conductivities cannot be compared with the literature as this is to our knowledge the first report on *in situ* dispersion polymerization in the presence of NMG platelets.

References

- [1] S.U. Pickering, *J. Chem. Soc. Trans.* 91 (1907) 2001.
- [2] J.-C. DANIEL, C. PICHOT, *Les latex synthétiques*, Tec & Doc Lavoisier, Paris, 2006.
- [3] F. Banhart, J. Kotakoski, A.V. Krasheninnikov, *ACS Nano* 5 (2011) 26.
- [4] M. Quintana, E. Vazquez, M. Prato, *Acc. Chem. Res.* 46 (2013) 138.
- [5] L. Yan, Y.B. Zheng, F. Zhao, S. Li, X. Gao, B. Xu, P.S. Weiss, Y. Zhao, *Chem. Soc. Rev.* 41 (2011) 97.
- [6] D.W. Boukhvalov, M.I. Katsnelson, *Nano Lett.* 8 (2008) 4373.
- [7] X. Peng, R. Ahuja, *Nano Lett.* 8 (2008) 4464.
- [8] K.P. Loh, Q. Bao, P.K. Ang, J. Yang, *J. Mater. Chem.* 20 (2010) 2277.
- [9] M. Levy, M. Szwarc, *J. Am. Chem. Soc.* 77 (1955) 1949.
- [10] D.H. Hey, G.H. Williams, *Discuss. Faraday Soc.* 14 (1953) 216.
- [11] S. Hayashi, S. Handa, Y. Oshibe, T. Yamamoto, N. Tsubokawa, *Polym. J.* 27 (1995) 623.
- [12] H. Wakai, T. Shinno, T. Yamauchi, N. Tsubokawa, *Polymer* 48 (2007) 1972.
- [13] I. Cha, Y. Yagi, T. Kawahara, K. Hashimoto, K. Fujiki, S. Tamesue, T. Yamauchi, N. Tsubokawa, *Colloids Surf. Physicochem. Eng. Asp.* 441 (2014) 474.
- [14] F. Beckert, A.M. Rostas, R. Thomann, S. Weber, E. Schleicher, C. Friedrich, R. Mülhaupt, *Macromolecules* 46 (2013) 5488.
- [15] K. Ohkita, N. Tsubokawa, E. Saitoh, *Carbon* 16 (1978) 41.
- [16] R. Pecora, *Dynamic Light Scattering: Applications of Photon Correlation Spectroscopy*, Springer Science & Business Media, 1985.
- [17] Formulaction, http://www.formulaction.com/stability_CNT_fuel-cell_CMP-slurries.html, n.d.
- [18] Formulaction, *Formulaction Appl. Pap.* (2009) 1.
- [19] S.A.F. Bon, P.J. Colver, *Langmuir* 23 (2007) 8316.
- [20] W.D. HARKINS, *J. Am. Chem. Soc.* 69 (1947) 1428.
- [21] C.P. Roe, *Ind. Eng. Chem.* 60 (1968) 20.
- [22] J. Ugelstad, M.S. El-Aasser, J.W. Vanderhoff, *J. Polym. Sci. Polym. Lett. Ed.* 11 (1973) 503.
- [23] R.M. Casado, P.A. Lovell, P. Navabpour, J.L. Stanford, *Polymer* 48 (2007) 2554.
- [24] G. Wang, B. Wang, J. Park, Y. Wang, B. Sun, J. Yao, *Carbon* 47 (2009) 3242.
- [25] J.-L. Mura, G. Riess, *Polym. Adv. Technol.* 6 (1995) 497.
- [26] G. Riess, *Colloids Surf. Physicochem. Eng. Asp.* 153 (1999) 99.
- [27] M. Berger, W. Richtering, R. Mülhaupt, *Polym. Bull.* 33 (1994) 521.
- [28] L.M. Bronstein, D.M. Chernyshov, G.I. Timofeeva, L.V. Dubrovina, P.M. Valetsky, E.S. Obolonkova, A.R. Khokhlov, *Langmuir* 16 (2000) 3626.
- [29] J.-L. Mura, *Polymerisation En Émulsion En Présence de Tensioactifs Macromoléculaires*, Haute alsace, 1991.
- [30] A. Durand, E. Marie, *Adv. Colloid Interface Sci.* 150 (2009) 90.
- [31] W.-D. Hergeth, P. Bloß, F. Biedenweg, P. Abendroth, K. Schmutzler, S. Wartewig, *Makromol. Chem.* 191 (1990) 2949.

- [32] T.R. Guimarães, T. de C. Chaparro, F. D'Agosto, M. Lansalot, A.M.D. Santos, E. Bourgeat-Lami, *Polym. Chem.* (2014).
- [33] M. Antonietti, K. Landfester, *Prog. Polym. Sci.* 27 (2002) 689.
- [34] J.L. Reimers, F.J. Schork, *J. Appl. Polym. Sci.* 60 (1996) 251.
- [35] K. Landfester, *Macromol. Rapid Commun.* 22 (2001) 896.
- [36] J.M. Asua, *Prog. Polym. Sci.* 27 (2002) 1283.
- [37] M.-S. Lim, H. Chen, *J. Polym. Sci. Part Polym. Chem.* 38 (2000) 1818.
- [38] Y.T. Choi, M.S. El-Aasser, E.D. Sudol, J.W. Vanderhoff, *J. Polym. Sci. Polym. Chem. Ed.* 23 (1985) 2973.
- [39] P. Taylor, *Adv. Colloid Interface Sci.* 75 (1998).
- [40] M. Barrère, K. Landfester, *Polymer* 44 (2003) 2833.
- [41] C.-S. Chern, Y.-C. Liou, *Polymer* 40 (1999) 3763.
- [42] K. Landfester, *Macromol. Symp.* 150 (2000) 171.
- [43] M.M. Gudarzi, F. Sharif, *Soft Matter* 7 (2011) 3432.
- [44] A.S. Patole, S.P. Patole, H. Kang, J.-B. Yoo, T.-H. Kim, J.-H. Ahn, *J. Colloid Interface Sci.* 350 (2010) 530.
- [45] X. Song, Y. Yang, J. Liu, H. Zhao, *Langmuir* 27 (2011) 1186.
- [46] A.J. Paine, *Macromolecules* 23 (1990) 3109.
- [47] Y. Almog, S. Reich, M. Levy, *Br. Polym. J.* 14 (1982) 131.
- [48] C.M. Tseng, Y.Y. Lu, M.S. El-Aasser, J.W. Vanderhoff, *J. Polym. Sci. Part Polym. Chem.* 24 (1986) 2995.
- [49] D. Coleman, *J. Polym. Sci. Polym. Lett. Ed.* 13 (1975) 575.
- [50] P. Lacroix-Desmazes, *Latex Synthétiques Élabor. Appl.* (2006) 259.
- [51] C.M. Tseng, Y.Y. Lu, M.S. El-Aasser, J.W. Vanderhoff, *J. Polym. Sci. Part Polym. Chem.* 24 (1986) 2995.
- [52] D. Wang, V.L. Dimonie, E.D. Sudol, M.S. El-Aasser, *J. Appl. Polym. Sci.* 84 (2002) 2692.
- [53] S. Kiatkamjornwong, C. Kongsupapsiri, *Polym. Int.* 49 (2000) 1395.
- [54] J.M.A. José M. Sáenz, *Macromolecules* 31 (1998).
- [55] A. Filet, J. Guillot, T. Hamaide, A. Guyot, *Polym. Adv. Technol.* 6 (1995) 465.
- [56] M.-Q. Chen, T. Serizawa, A. Kishida, M. Akashi, *J. Polym. Sci. Part Polym. Chem.* 37 (1999) 2155.
- [57] H. Bamnolker, S. Margel, *J. Polym. Sci. Part Polym. Chem.* 34 (1996) 1857.
- [58] P. Lacroix-Desmazes, A. Guyot, *Macromolecules* 29 (1996) 4508.
- [59] S. Shen, E.D. Sudol, M.S. El-Aasser, *J. Polym. Sci. Part Polym. Chem.* 32 (1994) 1087.
- [60] S. Shen, E.D. Sudol, M.S. El-Aasser, *J. Polym. Sci. Part Polym. Chem.* 31 (1993) 1393.
- [61] C.L. Winzor, Z. Mrázek, M.A. Winnik, M.D. Croucher, G. Riess, *Eur. Polym. J.* 30 (1994) 121.

General conclusions

In this thesis, we aimed to produce conductive latex based on a graphene/polymer nanocomposite material for textiles application. The main challenge was the synthesis of nanocomposites comprising polymer latex particles which can film-form at room temperature (low T_g) and graphene platelets for the electrical properties. The latex route was preferred among other ways to favor the creation of segregated networks leading to a drastic decrease of fillers needed for efficient conductive properties.

The analysis of literature demonstrated that carbon suspensions are an adequate choice due to their low cost. Moreover, the shape and aspect ratio of the graphene fillers can favor the built-up of armored nanocomposite latex, and lead to excellent conductive properties at low filler content. The production of graphene throughout a mechanical delamination of graphite was demonstrated as an appropriate way to obtain Nanosize Multilayered Graphene (NMG) in water suspensions using a low cost and few steps process.

The second chapter described the production of the Nanosize Multilayered Graphene stabilized in water phase by a surfactant or a polymeric stabilizer. Mechanical delamination in water was used to produce NMG with a small lateral size combining wet grinding and sonication. Stable suspensions containing NMG with lateral size of 50 to 300 nm and counting 5 to 10 graphene layers were successfully produced. The concentration of the produced NMG suspensions, in this preliminary study, was 2 mg mL^{-1} which is twice as high as common concentrations of graphene oxide suspensions obtained through chemical methods and for a much shorter process duration (only 4 hours).

Nanocomposites have been produced via two latex routes: physical blending and *in situ* polymerization in the presence of multilayered graphene.

For physical blending route, the NMG suspensions were blend with acrylic latexes. The nanocomposites obtained exhibit a good stability in suspension and were film-formed at room temperature. The influence of the size ratio between the conductive filler and the latex nanosphere drove the study. The final composite materials exhibit micrometer-scale domain size with filler paths running throughout the material. The conductivity behavior was described using a percolation approach and the mechanical reinforcement obtained with increasing NMG content was also consistent with a percolation behavior. The mechanical and electrical percolation thresholds are fairly consistent with the geometrical percolation threshold for both sample series.

Moreover, highly conductive graphene-based composite materials have been produced through a latex route (solvent-free procedure). The composite-latex blend was based on acrylate copolymers that are already mature in the ink and paint industry: they can form continuous and deformable films without neither high temperature curing nor additional hot-

pressing, which is adequate for flexible and textile substrates. The nanocomposite materials exhibited good electrical properties (10^2 S m^{-1} comparable to commercial carbon-based conductive inks) with low filler content: less than 10 wt.% compared to 20-40 wt.% in existing conductive inks. This elaboration route based on blends of NMG platelets and polymer latex particles provides a promising candidate for conductive inks for printed electronics and functional conductive materials.

In the last chapter, NMG-based conductive nanocomposites suspensions were synthesized by *in situ* emulsion, miniemulsion or dispersion polymerization. The main challenge was to synthesize large polymer particles in presence of surfactant or stabilizer, meaning a polymer particle diameter larger than the NMG lateral size. Moreover, an armored nanocomposite, with latex particles surrounded by NMG platelets, with only non-covalent bonding was another challenge. The synthesis of graphene-based nanocomposites by *in situ* polymerization in the presence of NMG suspensions and the resulting electrical properties were performed. For these polymerizations, polymeric stabilizers, such as PPSNa, PSbPEO and PVPk30, were used to produce of NMG suspensions and were demonstrated as good NMG platelets stabilizers with the same or higher yield than SDBS.

A short state-of-the-art on graphene defects has reported the existence of few oxygen-containing groups and structure defects on the graphene structure, according to the synthesis method. These defects act as radical trapping and can interact with the initiators and the growing polymer chains during the polymerization. Three different surfactant (SDBS) or polymeric stabilizers (PSSNa, PSbPEO) were used for *in situ* emulsion polymerizations. Their selection depended on their ability to produce high content and stable NMG suspensions during the NMG mechanical delamination and their mobility in water phase which is a critical parameter during polymerization. SDBS presented a high mobility in the aqueous phase and induces a destabilization of some part of the NMG platelets during the polymerization process. But by decreasing the SDBS content just below the CMC_{app} , almost full polymerization conversion (90%) is reached and composite latex particles of 228 nm mean diameter with high theoretical surface coverage ($\tau_{\text{cov average}} = 19.3$) are produced. Unfortunately NMG/SDBS latexes exhibited low stability and sedimentation was observed within five days. Later on, latexes obtained from NMG/PSSNa presented a low NMG weight percentage and the polymer particles diameter produced did not favor the creation of armored structures. Another polymeric stabilizer, PSbPEO 1030, was used and the final composite latexes obtained had a high NMG content and no destabilization either during polymerization process or within five days was observed. It was determined that mobility of stabilizer and reactivity of initiator was key parameters to efficiently conduct the polymerization process.

To reduce the surfactant mobility in the aqueous phase and the destabilization of the NMG platelets during the polymerization, miniemulsion polymerization can be adequate. *In situ* miniemulsion polymerizations were performed with suspensions of NMG stabilized by SDBS and PSbPEO 1030. Latex particles with a mean diameter of 127 nm and 250 nm were obtained respectively for the nanocomposites latexes with low concentration of SDBS or PSbPEO (mE-NMG/SDBS-1.7, mE-NMG/PSbPEO-7). But, as for *in situ* emulsion

polymerization, a total conversion was not reached, which might be due to the trapping of part of radicals by surface oxygen-groups on the NMG platelets. The electrical properties of the nanocomposites synthesized by *in situ* emulsion and miniemulsion polymerizations showed that only the nanocomposites latex with low concentrations of SBDS as a stabilizer (E-2%-NMG/SDBS-1.7 and mE-NMG/SDBS-1.7) were electrically conductive.

As an alternative to these two polymerizations, *in situ* dispersion polymerizations were performed with the suspensions NMG/PVPk30 to increase the latex diameter and so raise the surface coverage rate. After the polymerizations, all the nanocomposites had a theoretical surface coverage larger than 100% due to the high polymer particle diameters obtained (more than 1 μm). To form armored polymer particles, the best nanocomposite was composite latex with PVPk30 as a stabilizer (D-NMG/PVPk30-9-50/50) because it was the nanocomposite with the smallest polymer particle diameter but the highest NMG content. All these nanocomposites presented an electrical conductivity and could not be compared with the literature where *in situ* dispersion polymerization with NMG platelets were not described. Thus, it might be interesting to explore the grafting of surfactants or stabilizers directly on the graphene surface in order to obtain graphene platelets with amphiphilic properties.

A solubility test was carried out in tetrahydrofuran (THF) to compare the nanocomposites films prepared by physical blending and *in situ* polymerization in the presence of NMG. The films realized by *in situ* dispersion polymerization were not completely dissolved, suggesting the existence of strong interactions between the NMG platelets and the polymer particles.

Finally, the potential interest for electronics was demonstrated by the use of the nanocomposite materials in replacement of copper wires in a LED setup. A pen was also filled with a conductive NMG suspension and conductive results obtained for a deposit on PET film and fabric are similar to the film-standing films. These conductive nanocomposite suspensions might become a cheaper alternative to silver-based conductive inks for printed electronics and might open more versatile electronic applications due to the deformability of the polymer matrix, for instance, on textile substrates.

Appendix I: Characterization techniques

I. Microscopic characterizations.....	190
1. Transmission Electron Microscopy (TEM).....	190
2. Scanning Electron Microscopy (SEM)	190
3. Atomic Force Microscopy (AFM)	190
II. Mechanical characterization: Dynamic Mechanical Analysis (DMA).....	191
III. Electrical characterization	193
IV. UV-Visible spectroscopy	194
V. Diffusion Light Scattering (DLS)	195
References	196

In this appendix, the major characterization techniques that were used in this work will be presented.

I. Microscopic Characterizations

1. Transmission Electron Microscopy (TEM)

TEM observations of latex and NMG/polymer nanocomposite latexes are performed on formvar/carbon grids by evaporation of a small droplet of the diluted suspension on the grids. For the observations of the nanocomposite films, thin foils TEM-specimens (< 100 nm) of the nanocomposite material were prepared using a diamond knife on cryo-ultramicrotome equipment. These specimens are then observed using a Philips CM120 at an accelerating voltage of 120 keV at the CT μ (Centre Technologique des Microstructures, Lyon 1 University). The mean diameter of the polymer particles (D_{TEM}) was determined using the AnalySIS software (Soft Imaging system).

On the TEM micrographs, the polymer matrix appears in medium grey as a homogeneous background. Due to their very small thickness, the NMG platelets are visible when they are edge up, then they appear as dark sticks or dark aggregates.

The polymer matrix, poly(styrene-co-butyl acrylate) or poly(methyl methacrylate-co-butyl acrylate), has a glass transition temperature near room temperature and the PMMA can react into the microscope due to high energy electron beam. This can induce a degradation of the samples. In order to obtain more accurate observations of our specimens, cryo-TEM needs to be done.

This technique consists in the quick freezing of a thin film of the suspension. The frozen particles are then observed at a temperature of -180°C. A drop of the suspension is deposited on copper grids covered by a carbon membrane (NetMesh, Pelco). Then the sample is freezed in liquid ethane of the work station Leica EM CPC (Leica Microsystems, Austria). The grid is then deposit on a cryo plunge Gatan and transferred in the microscope for the observations.

2. Scanning Electron Microscopy (SEM and cryo-SEM)

SEM observations were realized on a MEB FEI Quanta 250 FEG to characterize the morphology of the NMG suspensions.

Concerning the nanocomposite latexes realized by *in situ* dispersion polymerization, the observations are performed in Cryo-SEM mode, on a MEB FEI Quanta 250 FEG in low vacuum with an acceleration tension of 5 kV with a cryo-transfer Gatan Alto 2500.

3. Atomic Force Microscopy (AFM)

Atomic Force Microscopy observations were performed on Nanowizard 3 Nanoscience AFM from JPK Instruments. This method is a topological analysis of the surface with ultrahigh resolution. A scheme of the AFM is presented on Figure 1.

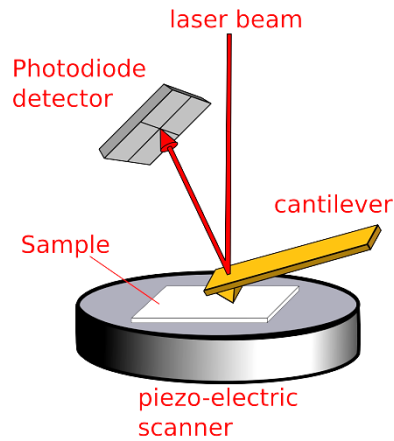


Figure 1. Scheme of the Atomic Force Microscopy equipment

This equipment is used on tapping mode, which consist on the vibration of the cantilever at its own resonance frequency with knowing amplitude. For this mode, the mean position of the tip is near the surface. When the tip interacts with the surface, the amplitude decreases and induces a variation of the oscillation amplitude of the cantilever. This mode is used to characterize the topography of the samples. The micrographs obtained for each samples are treated by Gwyddion software to determine the mean thickness of the graphene platelets. For each specimen, more than 200 platelets are analyzed.

II. Mechanical characterization: Dynamic Mechanical Analysis (DMA)

Dynamic Mechanical Analysis is used to study the viscoelastic properties of a material by measuring its dynamic modulus in function of the temperature or in function of the sollicitation frequency. A sinusoidal stress ($\gamma^* = \gamma_0 \exp(i\omega t)$) is applied and the strain ($\epsilon^* = \epsilon_0 \exp(i(\omega t + \delta))$) in the material is measured, giving the complex modulus ($G^* = \gamma^* / \epsilon^*$). The sollicitations are generally at very low amplitude (between 10^{-4} and 10^{-6}) in order to stay in the linear domain. The complex shear modulus G^* is equal to:

$$G^* = G' + iG'' \quad \text{Equation 1}$$

Where G' represents the storage modulus and G'' the loss modulus. For polymeric materials, the temperature of the maximum of G'' is defined as the mechanical main relaxation temperature of the material determined at a given frequency.

The DMA equipment used is a custom-made equipment developed in MATEIS department at INSA Lyon [1]. A schematic representation of this equipment is presented on Figure 2. The measurements were performed in torsion mode at a fixed frequency (1 Hz) from 200 K to 380 K with a heating rate of 1 K/min.

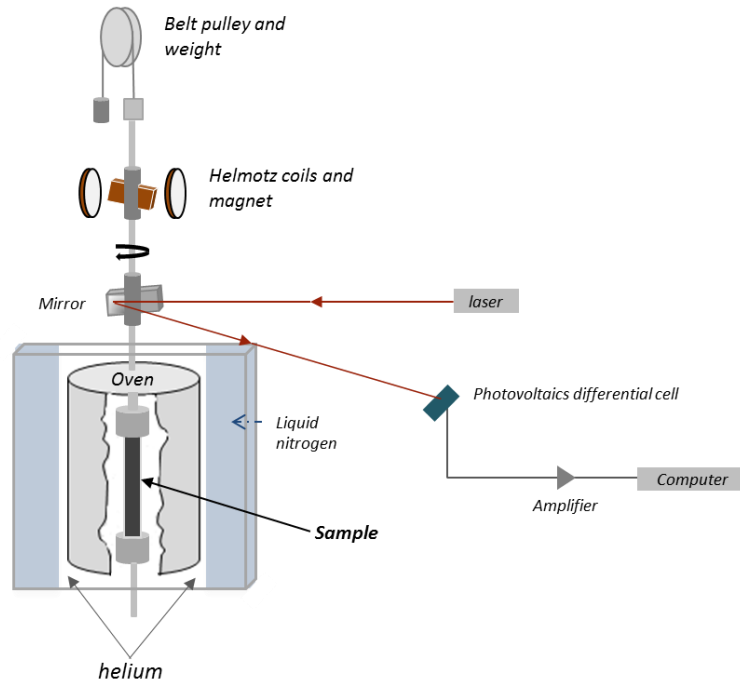


Figure 2. Scheme of DMA equipment used in torsion mode

The samples are rectangle cut out of the films with the following dimensions:

$$6 \text{ mm} < L < 11 \text{ mm}$$

$$2 \text{ mm} < l < 4 \text{ mm}$$

$$0.1 \text{ mm} < e < 0.3 \text{ mm}$$

where L, l and e are respectively the distance between the grips, the width and the thickness of the samples.

The shear modulus G^* is calculated using the following equation:

$$G^* = \frac{1}{f} \cdot \frac{\Gamma^*}{\Theta^*} \quad \text{Equation 2}$$

Where Γ^* is the torque force and Θ^* is the angular deformation. f is a form factor of the sample and is given by the equation :

$$f = \frac{\beta e^3 l}{L} \quad \text{and} \quad \beta \propto \frac{e}{l} \quad \text{Equation 3}$$

The storage modulus G' plots have been normalized so that the glassy plateau is set at 1 GPa. For nanocomposites, this normalization implies that the reinforcement of fillers in glassy polymer matrix has been neglected for the filler volume contents considered. The value of G' in the glassy plateau is calculated based on the dimensions of the samples measured at room temperature.

III. Electrical characterization

The electrical conductivity was measured using a four-point probe setup (with gold contacts and 3.48 mm of distance (s) between each probe) equipped with a galvanometer (Keithley 2400).



Figure 3. Four-probe galvanometer equipment

A galvanometer is used to inject the measurement current in the end pair of leads. The second lead pair is used to measure the potential drop across the device. Assuming that the leads resistance is smaller, four-point probe is more accurate than two point's measurements. For each specimen, five measurements are done on each side of the nanocomposites films. Each measurement allows the calculation of the resistivity through the following equation [2]:

$$\rho = \frac{\pi}{\ln(2)} t \left(\frac{U}{I} \right) f_1 f_2 \quad \text{Equation 4}$$

where t , f_1 and f_2 represent respectively the thickness of the sample and two form factors depending of the shape and thickness of the specimens [3]. The form factor f_1 depends of the thickness of the sample (Figure XX).

The form factor f_2 depends of the shape of the samples (Figure 4).[4]

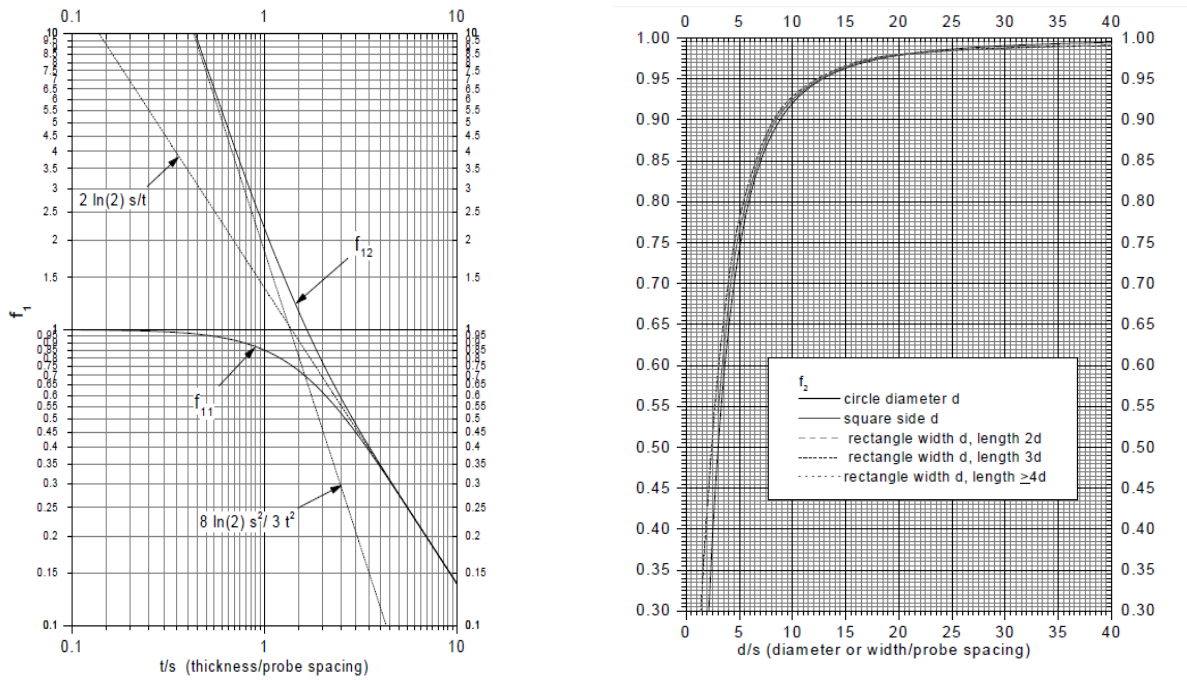


Figure 4. graphics for the calculation of the form factors (f_1 and f_2)

The resistivity measurement allows the calculation of the electrical conductivity using the following equation.

$$\sigma = \frac{1}{\rho} \tag{Equation 5}$$

IV. UV-Visible spectroscopy

UV-visible analyses are realized on a spectrometer UV/VIS (JASCO V-530) with quartz cells at a length of 660 nm. First, the calibration of the spectrometer is realized with SDS or SDBS/graphene suspensions at different concentrations to calculate α coefficient using the Beer-Lambert law's (Equation 2).

$$Abs = \alpha l C \tag{Equation 6}$$

Figure 5 represents the calibration curves for both surfactants.

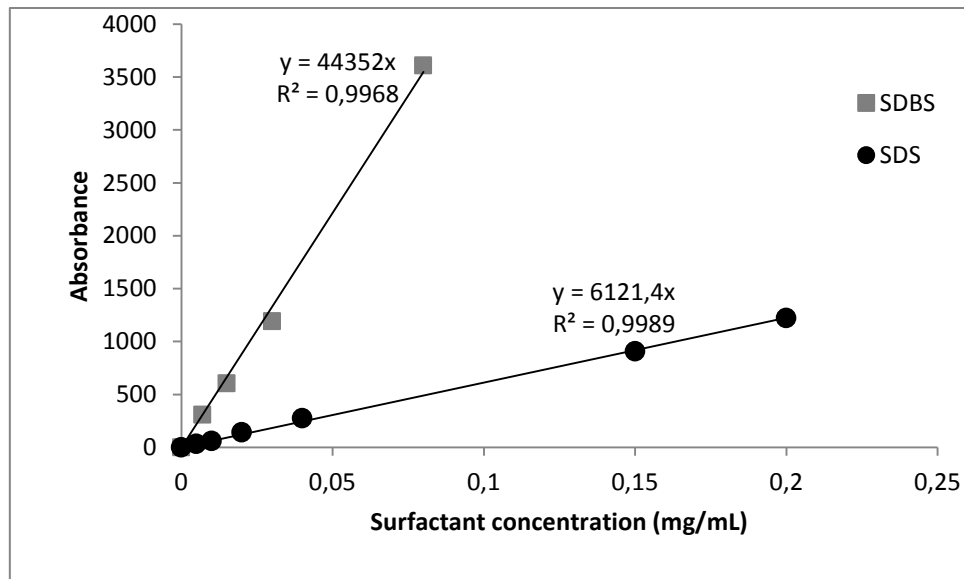


Figure 5. UV-visible calibration for NMG suspensions using SDS or SDBS as a surfactant

UV response of SDS is known to be lower than SDBS response, due to the presence of aromatic groups for SDBS [5].

V. Dynamic Light Scattering (DLS)

Measurements of dynamic Light Scattering allow the determination of the hydrodynamic diameter of nanoparticles in a solvent. The principle is based on the intensity fluctuation of the diffuse light in function of time. These fluctuations reveal the Brownian motion of the objects. Quick diffused intensity fluctuations are attributed to small particles and slow fluctuations are characterized by the presence of large particles.

Using these fluctuations, a diffusion coefficient is calculated and allows the measurement of the hydrodynamic diameter of the nanoparticles based of Stokes-Einstein equation:

$$R = -\frac{k_B T}{6\pi\eta D} \quad \text{Equation 7}$$

With D, the diffusion coefficient, k_B the Boltzmann constant, T the temperature and η the solvent density. These measurements are realized on the NanoZS (Malvern) with an angle of 90° à 20°C .

References

- [1] S. Etienne, J.Y. Cavaille, J. Perez, R. Point, M. Salvia, *Rev. Sci. Instrum.* 53 (1982) 1261.
- [2] L.I. Maissel, R. Glang, *Handbook of Thin Film Technology*, McGraw-Hill, 1970.
- [3] D.K. Schroder, *Semiconductor Material and Device Characterization*, John Wiley & Sons, 2006.
- [4] F.M. Smits, *Bell Syst. Tech. J.* 37 (1958) 711.
- [5] M.J. Fernández-Merino, J.I. Paredes, S. Villar-Rodil, L. Guardia, P. Solís-Fernández, D. Salinas-Torres, D. Cazorla-Amorós, E. Morallón, A. Martínez-Alonso, J.M.D. Tascón, *Carbon* 50 (2012) 3184.

Appendix II: Uniaxial tensile tests for nanocomposite latexes deposit on PET films

The electrical properties of nanocomposites suspensions deposited on PET substrates after a small deformation of the substrate were studied in this appendix. Nanocomposite latexes with 650 nm latex beads diameter and a concentration of NMG from 2 to 4 vol.% have been deposit on a PET film using the procedure of Chapter 3.V.2. (for the electrical measurements on various substrates). The PET film with the nanocomposite was then cut to fit the dimensions and shape of the typical specimens used for tensile uniaxial testing according to standards (Figure 1).

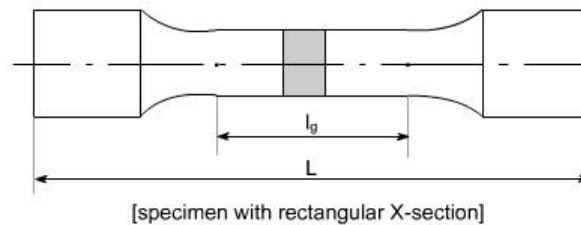


Figure 1. Dimensions of the specimen for uniaxial tensile test, with l_g the length of the specimen on which the mechanical properties are determined.

First, a uniaxial tensile test was realized on a deposit-free PET film in order to determine the maximum of elongation allowed by this substrate without any deformation. The device (Instron 3345-K7349) used a load cell of 500N. Figure 2 illustrated the tensile test curve which represents the loading in function of the displacement for the neat PET film. The maximum deformation allowed by this substrate in the elastic domain will be fixed at 4% for the next experiments in the presence of the nanocomposite.

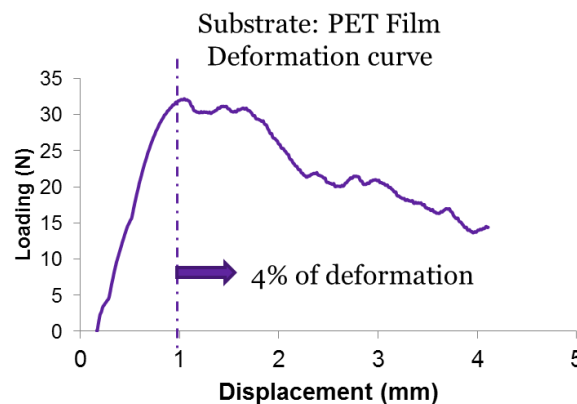


Figure 2. Tensile test curve for deposit-free PET film and determination of the maximum deformation allowed in the elastic domain.

The electrical conductivity of the nanocomposites containing 2, 3 or 4% vol of NMG was measured before and after a tensile test in the elastic domain of the substrate. The results of these electrical measurements are added in Figure 3.

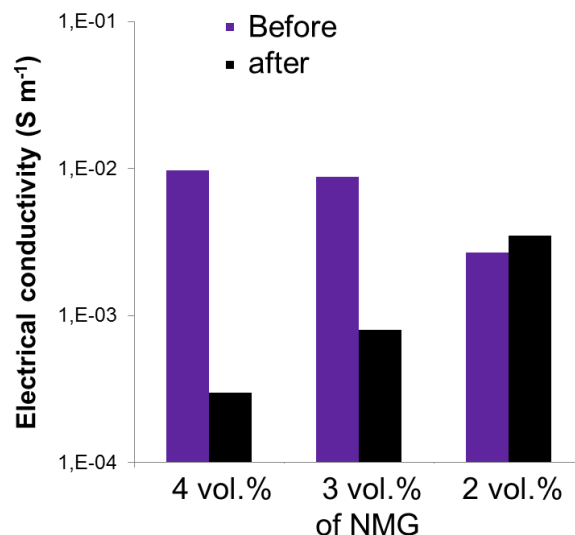


Figure 3. Electrical conductivities for the nanocomposites deposited on PET film substrates with various concentrations of NMG before and after a deformation of the substrate in its elastic domain.

The electrical properties for the nanocomposite containing 2% vol of NMG are identical before and after the deformation of the substrate. Whereas, a decrease of the electrical properties is observed for higher NMG concentrations (3 and 4 vol.%) after the substrate deformation. The nanocomposite latex with the lower concentration of NMG contains a higher concentration of acrylic latex. Consequently, a minimum amount of polymer matrix will be needed to maintain the electrical properties after the deformation of the substrate.

NNT : 2014 EMSE 0767

Amélie NOËL

ELECTRICAL PROPERTIES OF FILM-FORMING POLYMER/GRAPHENE NANOCOMPOSITES: ELABORATION THROUGH LATEX ROUTE AND CHARACTERIZATION

Speciality : Science et Génie des Matériaux

Keywords : Nanocomposites, Graphene, Latex, Electrical properties, ink

Abstract :

Printed electronics, particularly on flexible and textile substrates, raised a strong interest during the past decades opening new applications in electronics. This project presents a procedure that provides a complete and consistent candidate for conductive inks based on a graphene/polymer nanocomposite material. It consists in the synthesis of conductive inks nanocomposites comprising polymer particles (latex) with low glass transition temperature, T_g , to obtain films at room temperature, and graphene platelets, for the conductive properties. The conductive particles, named Nanosize Multilayered Graphene (NMG), are prepared by wet grinding delamination of micro-graphite (1-10 μm diameter) suspensions stabilized by various surfactants and/or polymeric stabilizers. This solvent-free procedure allows the formation of NMG suspensions with low thickness (1 to 10 sheets). Polymer particles are synthesized by surfactant-free emulsion polymerization with acrylate monomers and possess a glass transition temperature around room temperature.

Physical blending of latex particles and NMG platelets are performed to obtain conductive nanocomposite inks. Adding NMG induces a low percolation threshold and a sharp increase of the electrical and mechanical properties of the nanocomposites. Moreover, the polymer particles diameter have an impact on these properties.

To increase the formation of a well-defined cellular microstructure, the nanocomposites are also synthesized by *in situ* polymerization in the presence of NMG platelets, using emulsion, miniemulsion or dispersion polymerization. The excellent electrical properties of these nanocomposites associated to their flexibility make these materials suitable candidates for the production of conductive inks for textile printing applications.

NNT : 2014 EMSE 0767

Amélie NOËL

PROPRIETES ELECTRIQUES DE NANOCOMPOSITES SOUPLES POLYMERE/GRAPHENE : ELABORATION PAR VOIE LATEX ET CARACTERISATION

Spécialité: Science et Génie des Matériaux

Mots clefs : Nanocomposite, graphene, latex, encre, propriétés électriques

Résumé :

Les dispersions de nanocomposite à base aqueuse (aussi appelées nanocomposites latex) sont produites pour des applications diverses telles que les adhésifs, les revêtements et plus récemment les encres.

Ce projet consiste à réaliser des encres conductrices nanocomposites comprenant des particules de polymère (latex) à basse température de transition vitreuse, T_g , pour la formation de films à température ambiante, et des plaquettes de graphène, en raison de leurs excellentes propriétés conductrices.

Les charges conductrices, appelées multi-feuillets de graphène, sont réalisées par broyage en voie aqueuse de graphite (1-10 μm) stabilisées par différents tensio-actifs et/ou stabilisants. Cette méthode sans solvant et à bas coût permet de produire des suspensions de multi-feuillets (1 à 10 feuillets) de graphène. Les particules de polymères utilisées sont synthétisées par polymérisation en émulsion de monomères acrylates. Ce latex possède une température de transition vitreuse proche de la température ambiante.

Dans un second temps, des mélanges physiques de suspensions de graphène et de latex acrylates ont permis d'obtenir des encres nanocomposites. L'ajout de graphène permet l'obtention d'un seuil de percolation à bas taux de charge et une nette amélioration des propriétés électriques et du renfort. Le diamètre des billes de latex a une influence importante sur ces propriétés et a également été étudié.

Afin d'augmenter la stabilité des suspensions et les interactions graphène/latex, des nanocomposites structurés ont été synthétisés par polymérisation *in situ* en émulsion, miniémulsion ou dispersion en présence de graphène. Les excellentes propriétés électriques associées à leur flexibilité font de ces matériaux des candidats adaptés pour la réalisation d'encres conductrices pour impression sur textile.